DEVELOPMENT OF PINCER IRIDIUM CATALYSTS

FOR ALKANE DEHYDROGENATION

by

MICHAEL JOHN BLESSENT

A dissertation submitted to the

Graduate School-New Brunswick

Rutgers, The State University of New Jersey

In partial fulfillment of the requirements

For the degree of

Doctor of Philosophy

Graduate Program in Chemistry and Chemical Biology

Written under the direction of

Professor Alan S. Goldman

And approved by

_____

_____

_____

_____

New Brunswick, New Jersey

January 2016

ABSTRACT OF THE DISSERTATION

DEVELOPMENT OF PINCER IRIDIUM CATALYSTS

FOR ALKANE DEHYDROGENATION

By

MICHAEL JOHN BLESSENT

Dissertation Director:

Professor Alan S. Goldman

Catalysis is a technology of vital importance, enabling the production of many goods which are essential to the modern lifestyle. As such, the continued development of catalysis is of great importance, helping to reduce the costs and environment harm associated with the modern economy.

This thesis describes the study and design of pincer iridium complexes, a type of organometallic complex which can catalyze multiple reactions, including alkane dehydrogenation. If these catalysts are developed sufficiently, in the future they may have commercial applications for the production of fuels and commodity chemicals.

The research described in this thesis focused upon catalytic activity and selectivity, two aspects of a catalytic performance, for study and improvement. Understanding the steric and electronic properties which determine activity and selectivity, from a

mechanistic viewpoint, should allowed for the rational and effective design of new, higher-performing catalysts.

First, the regioselectivity of dehydrogenation was examined through a combination of experimental and computational methods. The influence of each steric and electronic factor was both identified and quantified. Next, catalytic activity was investigated using a similar approach, showing that massive changes in activity (orders of magnitude) could be attributed to a single electronic factor.

With these mechanistic insights in hand, the rational design of new catalysts was begun. Computational studies suggested that cationic catalysts would be several hundred fold more active than their neutral counterparts, and synthetic progress was made in that direction.

Carefully considering the mechanism of dehydrogenation also allowed for process chemistry improvements which increased activity significantly. Lastly, the role of additives to dehydrogenation was also investigated, showing that certain Brønsted bases improved catalytic activity significantly.

Acknowledgements

First and foremost, I would like to thank my advisor Professor Alan Goldman for his years of guidance and support. He urged me to think independently about each problem, giving me the intellectual space to develop my own theories and strategies. But when times were tough, he provided the technical advice to solve each issue and the reassurance to keep me going.

I am also grateful to Professors Heinz Roth, Fuat Celik, and Ralf Warmuth for serving on my thesis committee. Professor Karsten Krogh-Jespersen was actively involved with the research described in this thesis, aiding with the Density Functional Theory calculations which enabled many of the mechanistic discoveries. I would also like to thank that staff who maintained the facilities at Rutgers University, especially Dr. Murali Nagarajan and Dr. Seho Kim for their upkeep of the NMR instruments. My undergraduate advisor Professor Susan Kauzlarich also deserves recognition for introducing me to the world of chemical research, and for encouraging me to pursue graduate school.

I am also very grateful for the advice and support from current and former members of the Goldman Group. They helped me to learn the skills necessary for completing this thesis, while also making our laboratory a fun and enjoyable place to work. In particular I would like to thank Dr. Michael Haibach, Dr. Akshai Kumar, Dr. Thomas Dugan, Dr. David Wang, Dr. Jason Hackenberg, Dr. Kathleen Field, Dr. Andrew Steffens, and Nicholas Lease for fruitful discussions about chemistry. In addition, this

thesis would not have been possible without Tian Zhou, who performed the computational work which was essential to several of the projects described herein.

Lastly, I would like to thank my friends and family for their unwavering love and support. Although the ups-and-downs of graduate school made it hard to remain positive at times, they always inspired me to continue moving forward.

Dedication

To mom, dad, Christina, and David

For always being there

Table of Contents

List of Figures

List of Schemes

List of Tables

List of Equations

Chapter 1

Introduction

1.1 Catalysis: major themes and importance to modern life

Catalysis is a chemical phenomenon which is essential to many aspects of modern life. Technically, a catalyst is a substance which accelerates the rate of a chemical reaction without being consumed during that reaction.[1] Therefore, catalysts can help convert raw materials, such as petroleum, into valuable consumer products which enable the modern lifestyle, such as gasoline for automobiles.[2] Since approximately 90% of all commercialized chemical processes employ catalysts,[3] the continued development of this field is of great importance.

Some of the largest sectors of the chemical industry include fuels, commodity chemicals, fine chemicals, and pharmaceuticals. Generating the products from these industries would be exceedingly more expensive and difficult, if not impossible, without catalysts. In the fuels sector, catalysts are used to perform the reactions (hydrocracking, hydrotreating, reforming, isomerization, and alkylation) required for converting petroleum into gasoline and diesel.[2] Similarly, the production of fertilizer, an extremely important commodity chemical, also relies on catalysis. Without the (catalytic) Haber-Bosch process, creating enough fertilizer to adequately feed the world's population would be very difficult or impossible.[4] Many similar examples of catalysis's importance also exist in the fine chemical and pharmaceutical industries. Therefore, advances in catalysis will also help the chemical industry create products which benefit and improve the modern lifestyle.

With the significance of catalysis well-established, it is important to consider the objectives of catalyst design. In other words, which are the most important properties that a catalyst should have? On one hand, the features which should be increased are catalytic activity, selectivity, recyclability, functional-group and impurity tolerance, and resistance to decomposition.[5-7] In contrast, the undesirable aspects which should be minimized include toxicity, harm to the environment, and cost.[2] As will described in great detail later, this thesis focuses on increasing the activity and selectivity of a particular type of catalyst for a certain set of reactions.

In addition to understanding the performance of a catalyst, there are various methods for classifying a given catalyst. First, catalysts can either originate from a biological system (enzymes)[8] or from a non-biological basis. The catalysts described in this thesis, and most catalysts employed commercially, are of non-biological origins.[2] Next, catalysts can also be classified by the type of "molecular architecture" on which they are based. Major groupings, which partially overlap with one another, include zeolites, metals, metal-containing inorganic compounds, organometallic complexes, organic molecules, metal-organic frameworks, Brønsted acids, Brønsted bases, Lewis acids, and Lewis bases.[2,5] The catalysts described in this thesis are homogeneous organometallic complexes.

Lastly, the energy required for catalysis can be obtained from one of three sources: thermal energy (thermochemical reactions), photon energy (photochemical reactions), and electric potential energy (electrochemical reactions).[5] Like most catalysts employed academically and commercially,[2,5] the catalyst systems described in this thesis employ thermochemical reactions.

Therefore, after establishing the major themes of catalysis and how the field benefits modern life, it is possible to examine specifics relating to the research covered in this thesis. Namely, this thesis describes research on pincer iridium complexes, a type of organometallic compound, and their ability to incorporate the dehydrogenation of alkanes into catalytic cycles. (Scheme 1.1) While there are many aspects of these catalysts which can be improved, the current work focused on understanding and improving catalytic activity and selectivity. If sufficiently developed, pincer iridium catalysts have potential commercial applications relating to the fuels and commodity chemicals industries.

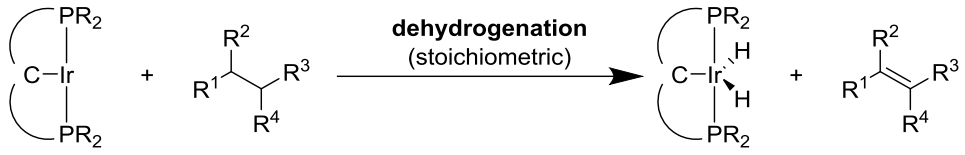

Scheme 1.1 Stoichiometric dehydrogenation by a pincer iridium complex

While the main objective of this research was to understand dehydrogenation reactions, it is noteworthy that these results may have applications for other catalytic reactions as well. Although pincer iridium complexes were originally synthesized for dehydrogenation reactions,[9] they have also been shown to catalyze hydroaryloxylation,[10] as well as a multitude of stoichiometric reactions. Therefore, examining the history leading to pincer iridium catalysts will help demonstrate the broader context of how these complexes can be useful.

1.2 History of H-H activations, C-H activations, and related catalytic reactions by organometallic complexes

As a field, the synthesis of organometallic complexes began in 1757 with the synthesis of cacodyl by Louis Claude Cadet de Gassicourt, a French chemist and pharmacist.[11] (Scheme 1.2)

Although Cadet did not fully understand the significance of his findings, he did complete the first synthesis of an organometallic complex.

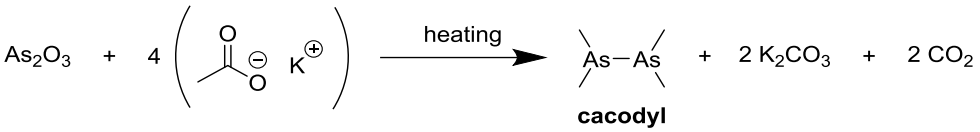

Scheme 1.2 Synthesis of cacodyl by Cadet

During the 19th century, the field of organometallics progressed with the discovery of other organometallic compounds such as Zeise's salt and diethylzinc.[12,13] (Figure 1.1) Zeise's salt carries the distinction of being the first transition metal complex to containing a metal-alkene coordination. Diethylzinc, despite its discovery over 150 years ago, is still employed today, primarily as a source of the ethyl carbanion in organic synthesis.

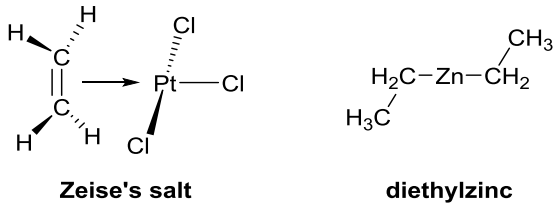

Figure 1.1 Zeise's salt and diethylzinc

In the 20th century the field of transition metal chemistry grew in importance by demonstrating the ability to act as *catalysts* in reactions, instead of simply as stoichiometric reagents. In 1938, Calvin reported cuprous acetate, Cu(OAc), as the first homogeneous hydrogenation catalyst.[14,15] While this complex is not technically organometallic, since it did not contain any metal-carbon bonds, it was still a homogenous transition metal complex. In that report, quinone was hydrogenated in the presence of the cuprous acetate catalyst with molecular hydrogen gas. Similarly, in the mid-1950s Halpern showed that *cupric* acetate, $Cu(OAc)_2$, (not to

be confused with cuprous) catalyzed the hydrogenation of the dichromate anion ($Cr_2O_7^{2-}$) to the Cr^{3+} cation through activation of the H-H bond.[14,16,17] (Scheme 1.3)

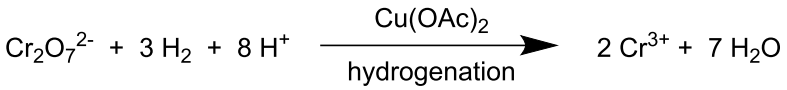

Scheme 1.3 Catalytic hydrogenation of chromate anion by cupric acetate

Similarly, in the early-1960s Vaska reported the synthesis of *trans*-IrX(CO)(PPh_3)$_2$ (where X = Cl, Br, and I) and related compounds.[18] Later, *trans*-Ir(Cl)(CO)(PPh_3)$_2$ would be named as Vaska's complex. Vaska's complex was found to perform the stoichiometric activation and oxidative addition of molecular hydrogen,[19,20] as well as catalyze the hydrogenation of carbon-carbon double bonds and carbon-carbon triple bonds.[21-23]

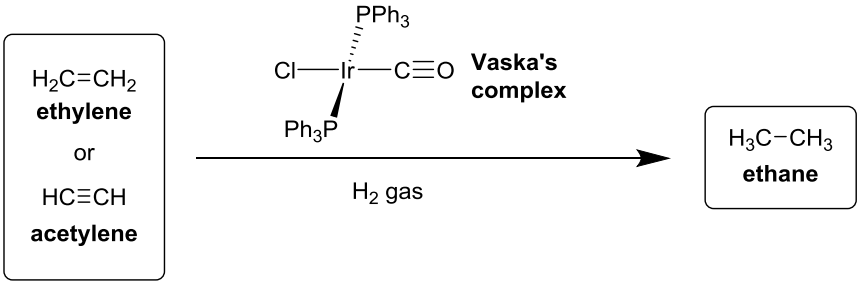

Scheme 1.4 Catalytic hydrogenation of ethylene and acetylene by Vaska's complex

Also in the 1960s, Wilkinson reported the synthesis of Rh(Cl)(PPh_3)$_3$, and subsequently that it also acted as a catalyst for hydrogenation of many different types of olefins.[24-26] While this catalyst was not technically organometallic, it did represent a transition metal catalyst which functioned very similar to a truly organometallic one. In addition, the mechanism likely involved a coordination, or possibly covelant, interaction between the rhodium metal center and a carbon on the substrate, which would represent an organometallic intermediate.

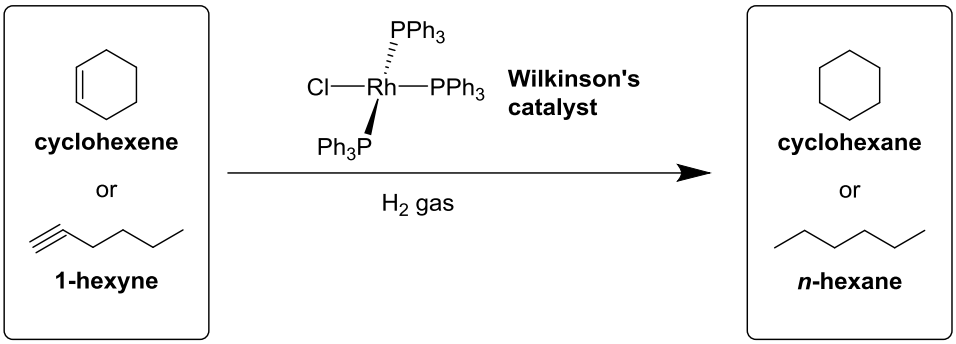

Scheme 1.5 Catalytic hydrogenation of olefins and alkynes by Wilkinson's catalyst

While many other examples exist, it is clear that organometallic complexes were capable of oxidatively adding molecular hydrogen, and subsequently acting as hydrogenation catalysts. With this level of success achieved, focus was directed at activating other types of bonds (in addition to H-H bonds), with the hope of catalyzing other reactions.

One of the major directions that was undertaken was the activation of C-H bonds. In 1965, Chatt reported that stoichiometrically reacting *trans*-$RuCl_2$(dmpe) (where dmpe = 1,2-bis(dimethylphosphino)ethane) with various arenes gave the corresponding 4-coordinate C_{aryl}-H activation products in the form *cis*-Ru(H)(Ar)(dmpe).[27] Although the starting complex was not organometallic itself, the Ru-Ar bond in the products obviously made those complexes organometallic.

In addition, many examples of stoichiometric C-H activations with *alkyl* groups were also reported. In 1982 Graham reported that the irradiation of $Cp^*Ir(CO)_2$ in the presence of neopentane generated the $Cp^*Ir(CO)(H)$(neopentyl) complex, indicating C-H activation.[28] Similarly, in 1983 Jones and Feher demonstrated that irradiation of $Cp^*Rh(PMe_3)_2(H)_2$ at -55 °C in the presence of propane generated the propyl complex $Cp^*Rh(PMe_3)_2(H)$(propyl), with the presumed loss of H_2 gas.[29] Even more interestingly, in the early 1980s Bergman showed that irradiation of the complex $Cp^*Ir(PPh_3)(H)_2$ could not only cause *intermolecular* C-H activations, but

also *intramolecular* C-H activations as well.[30,31] (Scheme 1.6) If the reaction was conducted in acetonitrile, then cyclometalation (which, by definition, is *intramolecular*) of the PPh_3 ligand was observed *via* C-H activation of one of the phenyl groups. In contrast, if the reaction was conducted in benzene solvent then *both* the cyclometalated product *and* $Cp^*Ir(PPh_3)(H)(Ph)$ were obtained. This second product could only be generated by *intermolecular* C-H activation of one molecule of the benzene solvent by the iridium complex.

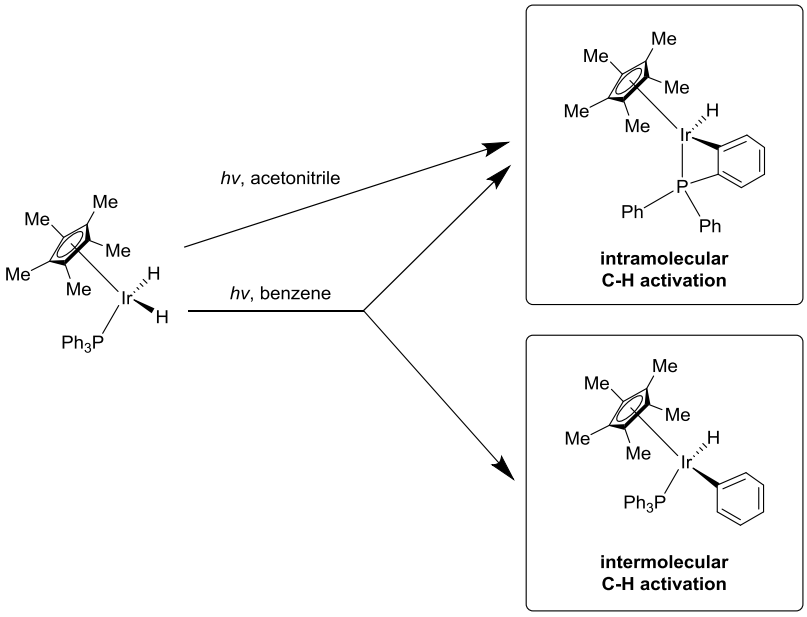

Scheme 1.6 Intramolecular and intermolecular C(sp^2)-H activations by a Cp^*Ir complex

Hence, whereas the above reports demonstrated many examples of the *stoichiometric* activation of C-H bonds involving organometallic complexes, *catalytic* reactions involving C-H activations have also been reported. In 1969, Shilov reported that the inorganic complex K_2PtCl_4 was capable of catalyzing H/D exchange between various substrates.[32] In particular, fully-proteo methane and ethane were found to H/D exchange with the deuterated solvent, which was a mixture of D_2O and acetic acid-d_1. (Scheme 1.7) These studies were continued with other catalytic

H/D exchange experiments, as well as stoichiometric reactions, which suggested that an organometallic platinum complex was involved with the H/D exchange reaction.[33,34]

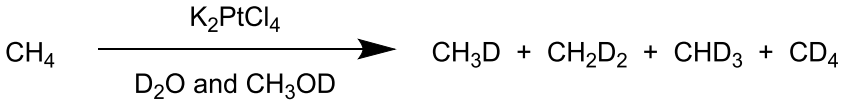

Scheme 1.7 H/D exchange catalyzed by K_2PtCl_4

Thus, many of the same transformations had been observed with different organometallic complexes: oxidative addition of the H-H bond, oxidative addition of C-H bonds, hydrogenation of C-C multiple bonds, and the photochemical loss of H_2 from the metal center. The next advances in this field, stoichiometric and catalytic alkane dehydrogenation, built upon many of these previous transformations.

In 1979 Crabtree reported the first example of *dehydrogenation* by an organometallic complex. It was reported that heating *trans*-$[Ir(cyclooctene)_2(PPh_3)_2]^+[BF_4]^-$ resulted in the appearance of $[Ir(cylooctadiene)(PPh_3)_2]^+[BF_4]^-$.[35] (Scheme 1.8) Presumably, the two hydrogens removed from the first cyclooctene were either lost as hydrogen gas, or employed to hydrogenate the second cyclooctene to cyclooctane. Further investigation confirmed that the stoichiometric intramolecular dehydrogenation of similar monoenes to dienes was also achieved.

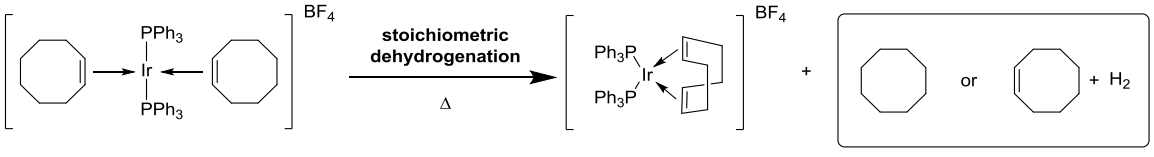

Scheme 1.8 Stoichiometric dehydrogenation by an iridium complex

In addition, during the 1980s several groups reported the first examples of *catalytic* dehydrogenation. Felkin employed $(Ar_3P)_2ReH_7$ complexes (Ar = p-F-C_6H_4, Ph, and p-Me-C_6H_4) as thermochemical catalysts for the catalytic transfer dehydrogenation.[36] (Scheme 1.9) In this process, one substrate (i.e. methylcyclohexane) was dehydrogenated to an olefin. However, this leaves the metal with two extra hydrogen atoms. To account for this, a secondary substrate (the "hydrogen acceptor," which was typically an olefin) was also added to the reaction mixture. After dehydrogenation, statistics dictated that the two hydrogen atoms were bonded to the hydrogen acceptor (i.e. *tert*-butyl ethylene), hydrogenating it to an alkane and regenerating the organometallic complex that is capable of dehydrogenating another molecule of substrate.

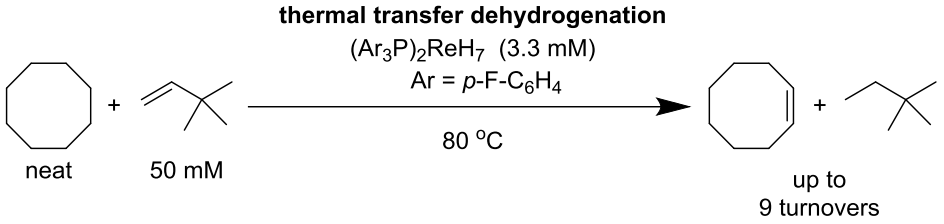

Scheme 1.9 Thermal catalytic transfer dehydrogenation by a rhenium complex

In addition, Crabtree reported that similar complexes of the type $IrH_2(\eta^2\text{-}O_2CCF_3)(PR_3)_2$ were capable of catalyzing both thermal *and* photochemical catalytic dehydrogenation reactions.[37] Up to 32 turnovers were observed. Notably, in the photochemical reactions employed a different process, *acceptorless dehydrogenation*, than in the thermal *transfer* dehydrogenation reaction. (Scheme 1.10) In acceptorless dehydrogenation the dehydrogenation step proceeds in the same manner as with transfer dehydrogenation. However, the two hydrides are not removed from the metal center by bonding to a hydrogen acceptor, but instead reductively eliminate to form H_2 gas that leaves the solution.

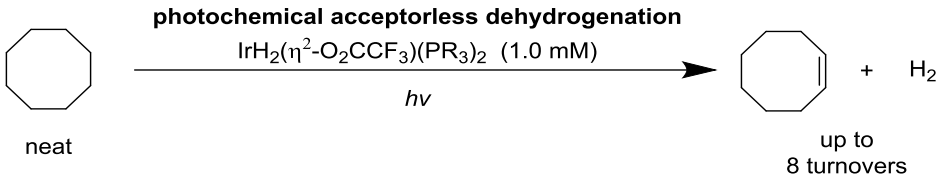

Scheme 1.10 Photochemical catalytic acceptorless dehydrogenation by an iridium complex.

Despite these successes, turnovers in catalytic dehydrogenation reactions remained relatively low. However, in 1989 Goldman reported that irradiation of a solution of *trans*-$Rh(PMe_3)_2(CO)Cl$ in an alkane yielded up to 5,000 turnovers of catalytic acceptorless dehydrogenation.[38,39]

1.3 Pincer iridium complexes for thermochemical alkane dehydrogenation

Unfortunately, however, several aspects limited the practical utility of both the thermochemical and photochemical dehydrogenation catalysts described above. While scaling-up photochemical reactions would prove difficult, the thermochemical catalysts developed by Felkin and Crabtree achieved relatively low turnover numbers, amongst other limitations.

Therefore, in 1996 Jensen reported that a new type of dehydrogenation catalyst, employing a single pincer ligand, was synthesized and showed to be highly active for thermal transfer dehydrogenation.[9] (Scheme 1.11) This complex was named (^{tBu4}PCP)Ir. While the process of transfer dehydrogenation employed by Jensen were functionally identical to those reported by Felkin in the early-1980s, the pincer iridium catalyst used by Jensen was very different. First reported in 1976 by Moulton and Shaw, a pincer ligand is one which adopts a tridentate bonding/coordination mode to the metal center while maintaining a meridional geometry.[40] Jensen found that by attaching the ^{tBu4}PCP ligand (the first pincer ligand reported) to an iridium

atom, the resulting dehydrogenation catalyst maintained activity and resisted decomposition even at 200 °C.

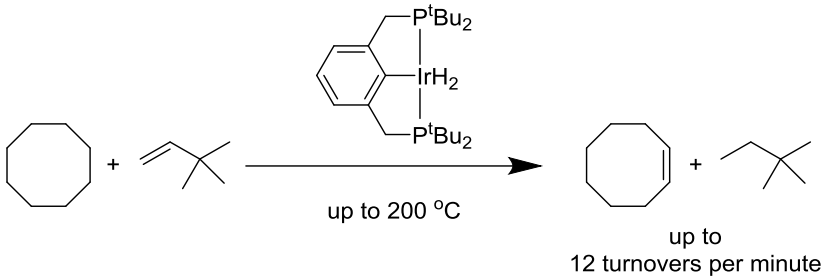

Scheme 1.11 Catalytic thermochemical transfer dehydrogenation by (^{tBu4}PCP)Ir

Hence, since that time the majority of investigations into transfer dehydrogenation have employed pincer iridium complexes in thermochemical reactions. In order to design and synthesize better catalysts, with one or more of the desirable properties described earlier, a multitude of new pincer ligands have been synthesized, attached to the metal, and their catalytic performance measured. (Figure 1.2) While many pincer ligands and metal complexes have been synthesized for many different purposes, only the ones intended for dehydrogenation-related reactions have been described below.

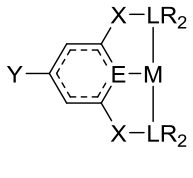

M = Ir, Rh, Ru
L = P, N, carbene
R = ^{t}Bu, ^{i}Pr, Ad, CF_3, Me
X = CH_2, O, S
E = C(sp^2), C(sp^3), Si, O, amine, amido
Y = H, OMe, NMe_2, CO_2Me, Me

Figure 1.2 Variety of organometallic pincer complex for dehydrogenation

First, different metals have been employed, such as Ir, Rh,[41] and Ru.[42] the two ends of the pincer ligand, which where phosphorous atoms in Jensen's (^{tBu4}PCP)Ir catalyst, have also been modified to amine[43] and carbene[44] groups. Next, the groups attached those ends have included ^{t}Bu, ^{i}Pr,[45] Ad,[46] CF_3,[42] and Me[47] groups. In addition, the linkages between the end groups (i.e. P^{t}Bu$_2$

in (^{tBu4}PCP)Ir) have included CH_2, oxygen,[48] and sulfur groups.[49] Next, the middle attachment point between the ligand and the metal center has been an sp^2 carbon, and sp^3 carbon,[50] amine groups,[51] amido groups,[52] O,[41] and Si.[53] Lastly, if the backbone contains an arene ring, then the group in the Y position has included H, OMe,[54] NMe_2,[54] CO_2Me,[54] and Me.[55]

Thus, since Jensen's first report in 1996 there has been a vast array of pincer complexes which have been synthesized and tested in the hope of creating better thermochemical alkane dehydrogenation catalysts. A representative sample of these are shown in Figure 1.3.

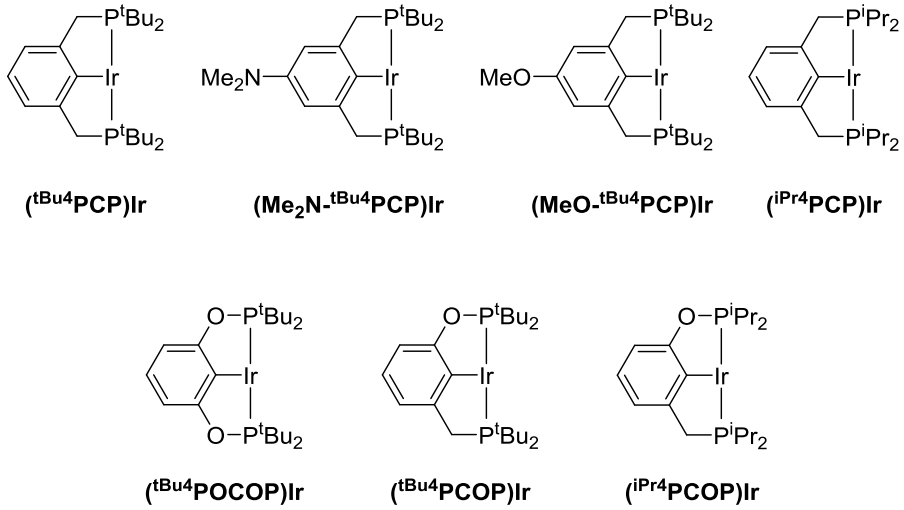

Figure 1.3 Selected pincer iridium catalysts

In addition to simply catalyzing alkane dehydrogenation as an academic exercise, several processes have been developed which employ this reaction to generate useful fuels and commodity chemicals. (Figure 1.4) In the future, further catalyst developments might even allow for applications of alkane dehydrogenation in the fine chemical or pharmaceutical industries.

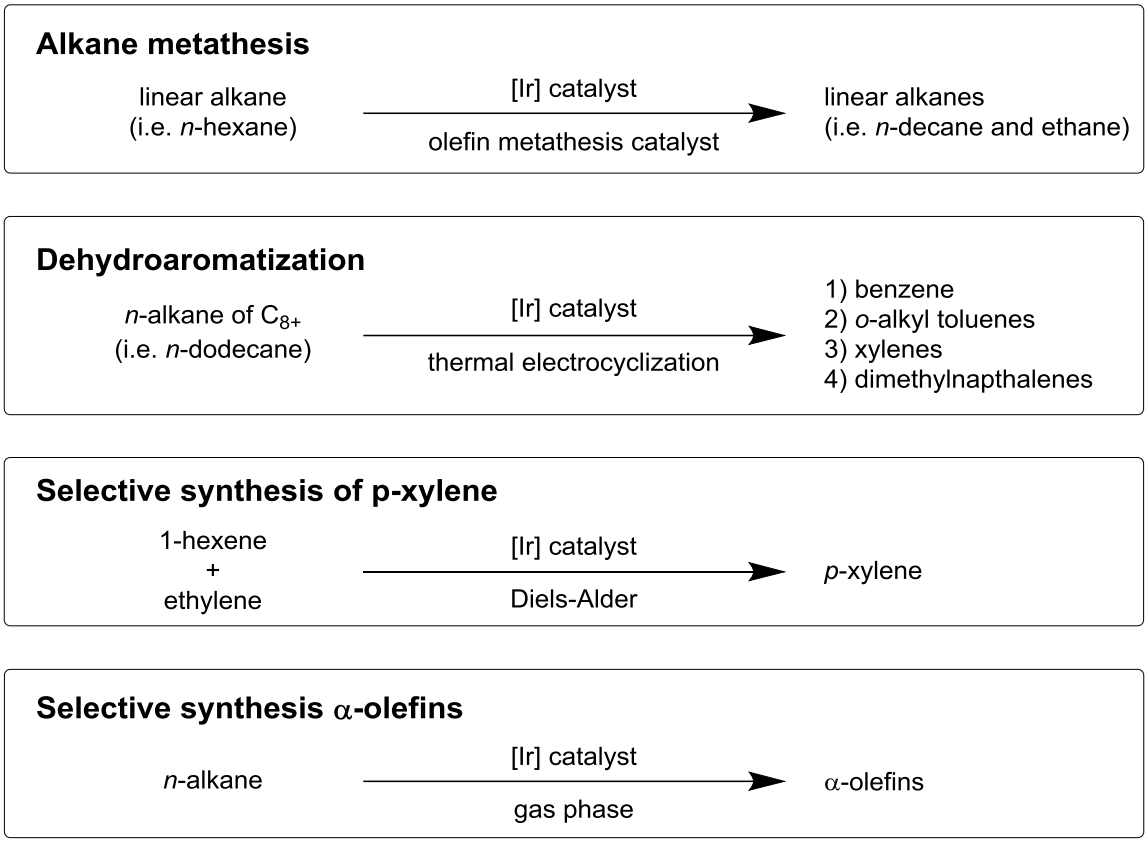

Figure 1.4 Applications of pincer iridium catalyzed dehydrogenation reactions to the fuels and commodity chemicals industries

Alkane metathesis, the first process, employs tandem alkane dehydrogenation and olefin metathesis in order to redistribute the molecular weights of alkanes.[56,57] In the first report, alkane metathesis was shown to convert *n*-hexane into *n*-decane, along with several side products. Because the value of *n*-hexane is relatively low, whereas *n*-decane is an important component of diesel fuel, this process can upgrade lower-value feedstocks into higher-value ones.

Next, dehydroaromatization affects the conversion of longer linear alkanes (C_{8+}) into a range of valuable aromatic products including benzene, *ortho*-alkyl toluenes, xylenes, and dimethylnapthalene.[58,59] This transformation is accomplished by performing multiple dehydrogenations on substrate, eventually leading to a triene, which then undergoes thermal

electrocyclization. In addition, thermal Diels-Alder reactions also occur between some of the monoenes and dienes before they are dehydrogenated to trienes, generating other products.

Similarly, the selective one-pot conversion of 1-hexene into p-xylene has been accomplished through the use of pincer iridium catalysts.[60] Specifically, 1-hexene can be catalytically dehydrogenated and isomerized into 2,4-hexadiene, which then undergoes a Diels-Alder reaction with ethylene to form p-xylene. Analogous reactions with *n*-pentane have been shown to give toluene and piperylene.[61]

The last class of products, α-olefins or 1-olefins, have been obtained using gas-phase transfer dehydrogenation reactions with solid-supported pincer iridium catalysts.[62] Although 1-olefins can also be generated with solution-phase reactions, the conversions and selectivities achieved with gas-phase reactions are vastly higher.

1.4 Research themes of this thesis

Therefore, since catalytic alkane dehydrogenation by pincer iridium catalysts have many potential applications, then mechanistic studies and improvements to the catalysts themselves could benefit each of these processes. Hence, the research projects described in this thesis were aimed at understanding and improving the selectivity and activity of pincer iridium catalysts during dehydrogenation reactions.

In Chapter 2 the regioselectivity of several pincer iridium catalysts when dehydrogenating *n*-alkanes was measured experimentally. Specifically, regioselectivity was quantified as the amount of 1-olefins produced as a percentage of all olefins produced (i.e. also 2-olefins, 3-olefins, etc.). Two model reactions, referred to as direct determination and competitive

dehydrogenation, were used to estimate regioselectivity. It was found that while all (PCP)Ir catalysts had very high regioselectivity (≥ 91%), the (PCOP)Ir and (POCOP)Ir catalysts studied had much lower regioselectivity (closer to 50%). In addition, regioselectivity varied slightly within the (PCP)Ir category, with the stericly open (^{iPr4}PCP)Ir catalyst having only 91% regioselectivity while the more crowded catalysts with four ^{t}Bu groups showing 96% regioselectivity.

Chapter 3 describes the Density Functional Theory (DFT) calculations used to identify the steric and electronic factors which determined the experimental regioselectivity observed in Chapter 2. Namely, this investigation began with the finding that if the rate-determining step of dehydrogenation was either C-H activation or β-H elimination, then regioselectivity would be high due to steric crowding. However, if olefin dissociation was the rate-determining step then lower amounts of steric crowding would permit both 1-olefins and 2-olefins to be generated at similar rates. Next, it was found that all (PCP)Ir catalysts had β-H elimination as their rate-determining steps, corroborating the experimental results. Similarly, (PCOP)Ir and (POCOP)Ir catalysts had a rate-determining step of olefin dissociation, confirming why they had low experimental regioselectivity. Finally, additional DFT calculations showed that two electronic factors, σ-donation and π-donation of electron density from the aryl ring, were the main determinants of the rate-determining step and therefore regioselectivity.

Chapter 4 presents a DFT-based project which was launched to understand how electronic factors affect the activity of pincer iridium dehydrogenation catalysts. Comparisons between experimental data collected in Chapter 2 and DFT calculations from Chapter 3 showed that aryl electronics seemed to be the major factor determining catalytic activity. In particular, a ligand with a slightly weaker π-donating aryl ring might give the most active catalysts. DFT-based

catalyst screening was conducted, suggesting that (PCP-pyridinium)Ir, a new of type iridium complex, would be several hundred fold more active than any previous catalyst.

Chapter 5 describes attempts to increase the activity and selectivity of alkane metathesis by modifying its experimental conditions. Specifically, it was found that optimizing the steady-state concentration of free olefin led to a 110% increase in apparent rate. Employing two different pincer iridium catalysts was also tested in an effort to balance the rates of the dehydrogenation and hydrogenation halves of the transfer dehydrogenation cycle. However, no improvements were achieved.

Chapter 6 discusses how catalytic activity seemed to increase when small quantities of sodium *tert*-butoxide were added to transfer dehydrogenation reaction mixtures. Several initial experiments suggested that a mechanistic effect might be occurring, such as the additive co-catalyzing the dehydrogenation reaction. However, the effect stopped being reproducible and the observations remain unexplained.

Finally, Chapter 7 describes synthetic progress towards (PONC)Ir, a new type of pincer iridium complex. The objective was to create a catalyst with novel electronic properties by retaining the bonding motif of traditional pincer ligands (2 dative bonds and 1 covelant bond), but by arranging them in a different order around iridium. Initial studies showed that the hydride and ethylene complexes can be synthesized, raising the possibility of a successful dehydrogenation catalyst.

1.5 References

(1) International Union of Pure and Applied Chemistry, "Catalyst" in *Compendium of Chemical Terminology*, 2nd ed. (the "Gold Book"), compiled by A. D. McNaught and A. Wilkinson. Blackwell Scientific Publications: Oxford, 1997.

(2) Wittcoff, H. A.; Reuben, B. G.; Plotkin, J. S. *Industrial Organic Chemicals*; 2nd ed.; Wiley-IEEE, 2005.

(3) Rutherford, A.; Bell, A. T.; Boudart, M.; Chen, N. Y.; Gates, B. C.; Haag, W. O.; Somorjai, G. A.; Wei, J.; Hegedus, L. S. *Catalyst Design: Progress and Perspectives*; Wiley: New York, 1987.

(4) Appl, M. "Ammonia" in *Ullmann's Encyclopedia of Industrial Chemistry*; Wiley-VCH: Weinheim, Germany, 2006.

(5) Hartwig, J. F. *Organotransition Metal Chemistry*; University Science Books: Sausalito, CA, 2010.

(6) Benaglia, M. *Recoverable and Recyclable Catalysts*; John Wiley and Sons: Chichester, UK, 2009.

(7) Bartholomew, C. H. *Appl. Catal., A* **2001**, *212*, 17-60.

(8) Stryer, L.; Berg, J. M.; Tymoczko, J. L.; *Biochemistry*, 5th ed., W. H. Freeman: San Francisco, CA, 2002.

(9) Gupta, M.; Hagen, C.; Flesher, R. J.; Kaska, W. C.; Jensen, C. M. *Chem. Commun.* **1996**, 2083.

(10) Haibach, M. C.; Guan, C.; Wang, D. Y.; Li, B.; Lease, N.; Steffens, A. M.; Krogh-Jespersen, K.; Goldman, A. S. *J. Am. Chem. Soc.* **2013**, *135*, 15062.

(11) Seyferth, D. *Organometallics* **2001**, *20*, 1488.

(12) Zeise, W. C. *Annalen der Physik und Chemie* **1831**, *97*, 497.

(13) Frankland, E. *Q. J. Chem. Soc.* **1850**, *2*, 263.

(14) Halpern, J. D., R. G. *J. Chem. Phys.* **1954**, *22*, 1272.

(15) Calvin, M. *Trans. Faraday. Soc.* **1938**, *34*, 1181.

(16) Halpern, J.; Peters, E. *J. Chem. Phys.* **1955**, *23*, 605.

(17) Halpern, J.; MacGregor, E. R.; Peters, E. *J. Phys. Chem.* **1956**, *60*, 1455.

(18) Vaska, L.; DiLuzio, J. W. *J. Am. Chem. Soc. FIELD Full Journal Title:Journal of the American Chemical Society* **1961**, *83*, 2784.

(19) Vaska, L.; DiLuzio, J. W. *J. Am. Chem. Soc.* **1962**, *84*, 679.

(20) Chock, P. B.; Halpern, J. *J. Am. Chem. Soc.* **1966**, *88*, 3511.

(21) Vaska, L.; Rhodes, R. E. *J. Am. Chem. Soc. FIELD Full Journal Title:Journal of the American Chemical Society* **1965**, *87*, 4970.

(22) James, B. R.; Memon, N. A. *Can J. Chem.* **1968**, *46*, 217.

(23) Eberhardt, G.; Vaska, L. *J. Catal.* **1967**, *8*, 183.

(24) Osborn, J. A.; Jardine, F. H.; Young, J. F.; Wilkinson, G. *J. Chem. Soc., A* **1966**, 1711.

(25) Young, J. F.; Osborn, J. A.; Jardine, F. H.; Wilkinson, G. *Chem. Commun.* **1965**, 131.

(26) Gillard, R. D.; Osborn, J. A.; Stockwell, P. B.; Wilkinson, G. *Proc. Chem. Soc.* **1964**, 284.

(27) Chatt, J.; Davidson, J. M. *J. Chem. Soc.* **1965**, 843.

(28) Hoyano, J. K.; Graham, W. A. G. *J. Am. Chem. Soc.* **1982**, *104*, 3723.

(29) Jones, W. D.; Feher, F. J. *Organometallics* **1983**, *2*, 562.

(30) Janowicz, A. H.; Bergman, R. G. *J. Am. Chem. Soc.* **1983**, *105*, 3929.

(31) Janowicz, A. H.; Bergman, R. G. *J. Am. Chem. Soc.* **1982**, *104*, 352.

(32) Gol'dshleger, N. F.; Tyabin, M. B.; Shilov, A. E.; Shteinman, A. A. *Zhurnal Fizicheskoi Khimii* **1969**, *43*, 2174.

(33) Khrushch, A. P.; Tokina, L. A.; Shilov, A. E. *Kinetika i Kataliz* **1966**, *7*, 901.

(34) Gol'dshleger, N. F.; Es'kova, V. V.; Shilov, A. E.; Shteinman, A. A. *Zhurnal Fizicheskoi Khimii* **1972**, *46*, 1353.

(35) Crabtree, R. H.; Mihelcic, J. M.; Quirk, J. M. *J. Am. Chem. Soc.* **1979**, *101*, 7738.

(36) Baudry, D.; Ephritikhine, M.; Felkin, H.; Holmes-Smith, R. *J. Chem. Soc., Chem. Comm.* **1983**, 788.

(37) Burk, M. J.; Crabtree, R. H. *J. Am. Chem. Soc.* **1987**, *109*, 8025.

(38) Maguire, J. A.; Boese, W. T.; Goldman, A. S. *J. Am. Chem. Soc.* **1989**, *111*, 7088.

(39) Rosini, G. P.; Soubra, S.; Wang, S.; Vixamar, M.; Goldman, A. S. *J. Organomet. Chem.* **1998**, *554*, 41.

(40) Moulton, C. J.; Shaw, B. L. *J. Chem. Soc., Dalton Trans.* **1976**, 1020.

(41) Haibach, M. C.; Wang, D. Y.; Emge, T. J.; Krogh-Jespersen, K.; Goldman, A. S. *Chem. Sci.* **2013**, *4*, 3683.

(42) Gruver, B. C.; Adams, J. J.; Warner, S. J.; Arulsamy, N.; Roddick, D. M. *Organometallics* **2011**, *30*, 5133.

(43) Gandelman, M.; Vigalok, A.; Shimon, L. J. W.; Milstein, D. *Organometallics* **1997**, *16*, 3981.

(44) Chianese, A. R.; Mo, A.; Lampland, N. L.; Swartz, R. L.; Bremer, P. T. *Organometallics* **2010**, *29*, 3019.

(45) Liu, F.; Goldman, A. S. *Chem. Commun.* **1999**, 655.

(46) Punji, B.; Emge, T. J.; Goldman, A. S. *Abstracts of Papers, 236th ACS National Meeting, Philadelphia, PA, United States, August 17-21, 2008* **2008**, INOR.

(47) Kundu, S.; Choliy, Y.; Zhuo, G.; Ahuja, R.; Emge, T. J.; Warmuth, R.; Brookhart, M.; Krogh-Jespersen, K.; Goldman, A. S. *Organometallics* **2009**, *28*, 5432.

(48) Göttker-Schnetmann, I.; White, P.; Brookhart, M. *J. Am. Chem. Soc.* **2004**, *126*, 1804

(49) Yao, W.; Zhang, Y.; Jia, X.; Huang, Z. *Angew Chem Int Ed Engl* **2014**, *53*, 1390.

(50) Arunachalampillai, A.; Olsson, D.; Wendt, O. F. *Dalton Trans.* **2009**, 8626.

(51) Fryzuk, M. D.; MacNeil, P. A. *Organometallics* **1983**, *2*, 355.

(52) Gruendemann, S.; Albrecht, M.; Loch, J. A.; Faller, J. W.; Crabtree, R. H. *Organometallics* **2001**, *20*, 5485.

(53) MacLean, D. F.; McDonald, R.; Ferguson, M. J.; Caddell, A. J.; Turculet, L. *Chem. Commun. (Cambridge, U. K.)* **2008**, 5146.

(54) Huang, Z.; Brookhart, M.; Goldman, A. S.; Kundu, S.; Ray, A.; Scott, S. L.; Vicente, B. C. *Adv. Synth. Catal.* **2009**, *351*, 188.

(55) Field, K., Rutgers, the State University of New Jersey, 2014.

(56) Goldman, A. S.; Roy, A. H.; Huang, Z.; Ahuja, R.; Schinski, W.; Brookhart, M. *Science* **2006**, *312*, 257.

(57) Ahuja, R.; Kundu, S.; Goldman, A. S.; Brookhart, M.; Vicente, B. C.; Scott, S. L. *Chem. Commun.* **2008**, 253.

(58) Ahuja, R.; Punji, B.; Findlater, M.; Supplee, C.; Schinski, W.; Brookhart, M.; Goldman, A. S. *Nature Chem.* **2011**, *3*, 167.

(59) Steffens, A. M., Rutgers, The State University of New Jersey, 2015.

(60) Lyons, T. W.; Guironnet, D.; Findlater, M.; Brookhart, M. *J. Am. Chem. Soc.* **2012**, *134*, 15708.

(61) Kundu, S.; Lyons, T. W.; Brookhart, M. *ACS Catal.* **2013**, *3*, 1768.

(62) Kumar, A.; Zhou, T.; Emge, T. J.; Mironov, O.; Saxon, R.; Krogh-Jespersen, K.; Goldman, A. S. *J. Am. Chem. Soc.* **2015**, *137*, 9894.

Chapter 2

Experimentally determining the regioselectivity of dehydrogenation by pincer iridium catalysts

Abstract

The regioselectivity of dehydrogenation by pincer iridium catalysts was investigated by experimental methods. In particular, whether the dehydrogenation of linear alkanes gave 1-, 2-, 3-, or 4-olefins was investigated. Two experimental methods, direct determination and competitive dehydrogenation, were developed to study regioselectivity. These tests showed that > 91% of the olefins generated by (PCP)Ir catalysts were 1-olefins, with the remainder being 2-olefins. In contrast, (PCOP)Ir catalysts and (^{tBu4}POCOP)Ir showed much lower selectivity for 1-olefins (40% to 65%) with the remainder being 2-olefins. Although 3- and 4-olefins were observed at later times of the reaction, their appearance was attributed to C=C bond isomerization of existing olefins and not to the dehydrogenation of alkanes.

2.1 Introduction

With reports that pincer iridium complexes can catalyze alkane dehydrogenation since the early 1990s,[1] it would be advantageous to understand and increase the selectivity of these dehydrogenation reactions. While the dehydrogenation and regioselectivity of branched alkanes[2]

and heteroatom-containing substrates had been examined previously, the current study focused on the dehydrogenation of unfunctionalized, linear *n*-alkanes.

The ability of (^{iPr4}PCP)Ir to dehydrogenation *n*-octane was investigated in the late-1990s, and it was reported to have high (> 90%) regioselectivity for producing 1-octene over other octenes. (Scheme 2.1) Similarly, the regioselectivity of (^{tBu4}PCP)Ir and (^{tBu4}POCOP)Ir had been investigated recently.[2] While the (^{tBu4}PCP)Ir appeared to have high (> 90%) regioselectivity for 1-olefins, (^{tBu4}POCOP)Ir had much lower regioselectivity, possibly even being selective for generating internal olefins instead of 1-olefins.

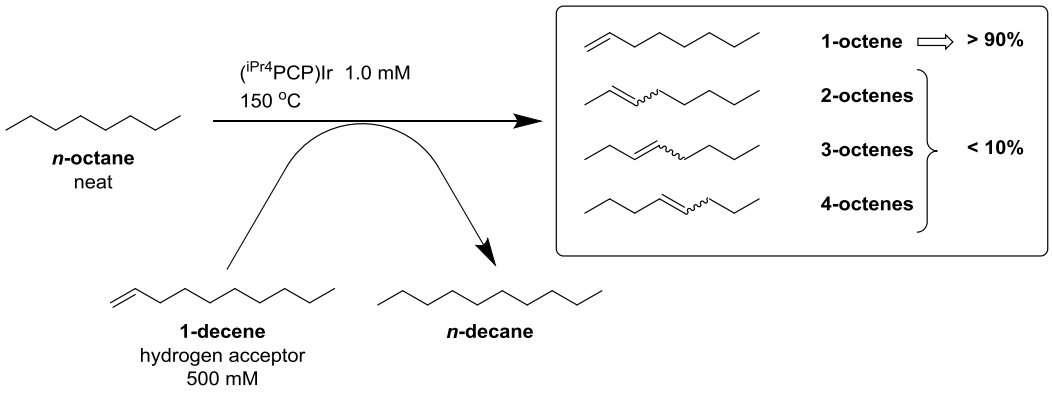

Scheme 2.1 Regioselectivity of dehydrogenation by (^{iPr4}PCP)Ir

Therefore, the study of additional pincer iridium catalysts was conducted in order to reveal general trends about all pincer iridium catalysts, instead of simply knowing the regioselectivity of three individual catalysts.

Before beginning the study of dehydrogenation regioselectivity, however, it is important to recognize the importance of this aspect of pincer iridium catalysts. Namely, regioselectivity has a large effect on processes which might become commercially viable in the future. Three of such processes have been recently reported for the conversion of simple *n*-alkanes into valuable products (α-olefins, benzene, *ortho*-alkyl toluenes, bicyclic products such as 1,5-

dimethylnapthalene, and *n*-alkanes suitable for diesel fuel).[3-5] As will be discussed below, α-olefins (also known as alpha-olefins, 1-olefins, or 1-alkenes) are not only desirable as end products, but they are also intermediates in the production of the valuable aromatic products and diesel discussed above. Therefore, the regioselectivity of dehydrogenation for 1-olefins is of great importance.

Notably, catalytic dehydrogenation (and regioselectivity) are *not* the only factors which influence the viability of these potentially-commerical processes. In addition, all pincer iridium catalysts also catalyze the isomerization of olefins. (Scheme 2.2) This reaction is completely distinct and separate from dehydrogenation (and therefore hydrogenation). Hence, when an alkane is dehydrogenated to an olefin it also becomes a substrate for catalytic isomerization. Similarly, the hydrogen acceptors (which are olefins themselves) are not only hydrogenated to alkanes during transfer dehydrogenation, but they can also be isomerized before being hydrogenated. All of these interrelated reactions are the determinants of transfer dehydrogenation reactions.

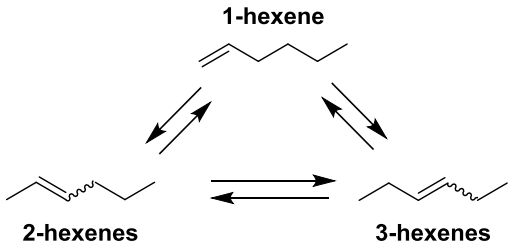

Scheme 2.2 Isomerization of 1-hexene, 2-hexenes, and 3-hexenes

In dehydroaromatization, and application of dehydrogenation, an *n*-alkane with 8 or more carbons is heated at ca. 170 °C for several hours or days with a pincer iridium catalyst and several equivalents (typically 4-10) of a hydrogen acceptor (such as *tert*-butyl ethylene).[4] The products of this reaction fall into four categories: *ortho*-alkyl toluenes, benzene, shorter alkanes/olefins as

side products of benzene formation, and bicyclic products (such as 1,5-dimethylnapthalene) if the starting alkane has at least 12 carbons. (Scheme 2.3) Mechanistic investigations were used to propose probably pathways by which each class of compounds was formed.[6] Since the pathway for generating benzene and the shorter alkanes/olefins begins with a 1-olefin, then pincer iridium catalysts with high regioselectivity for generating 1-olefins would be expected to produce greater quantities of benzene and shorter alkanes/olefins than catalysts with low regioselectivity for giving 1-olefins. Likewise, catalysts with relatively slow isomerization of 1-olefins to 2-olefins would also be predicted to generate more benzene. Or, if *ortho*-alkyl toluenes and bicyclics were preferred, then catalysts with low regioselectivity for 1-olefins and fast isomerization would be preferred. Thus, a thorough understanding of the fundamental factors governing isomerization (which has been previously studied)[7] and the regioselectivity of dehydrogenation (the current study) could help design new catalysts with desirable selectivity patterns.

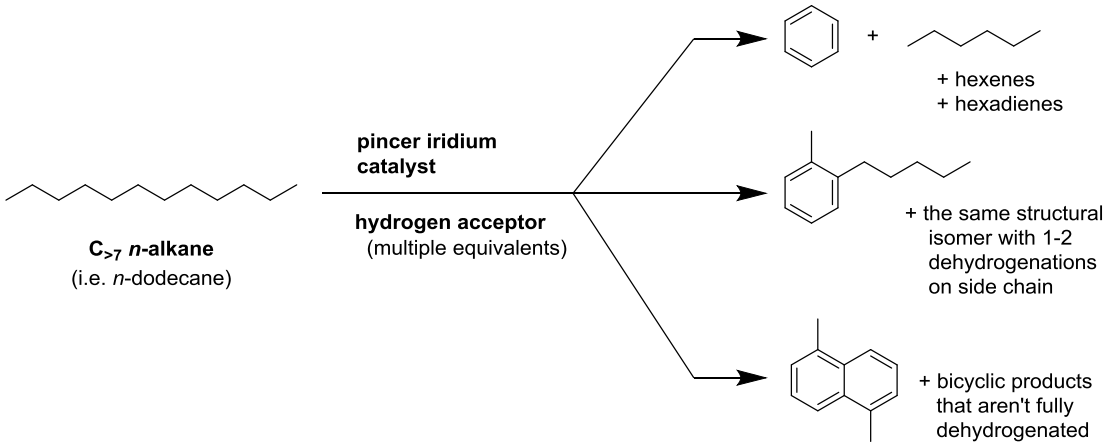

Scheme 2.3 Dehydroaromatization of linear alkanes of $C_{>7}$ into aromatic products

The second reaction, gas phase transfer dehydrogenation, employs solid-supported pincer iridium catalysts in an attempt to convert light linear alkanes (i.e. *n*-pentane, *n*-hexane) into their corresponding α-olefins (1-pentene, 1-hexene, etc.).[3] (Scheme 2.4) These compounds

are valuable in industrial applications, but are typically difficult to generate since their corresponding 2- and 3-olefins are more thermodynamically stable. Although the yields and selectivities for α-olefins with this method are relatively good, a study of dehydrogenation regioselectivity might yield ways to improve selectivity.

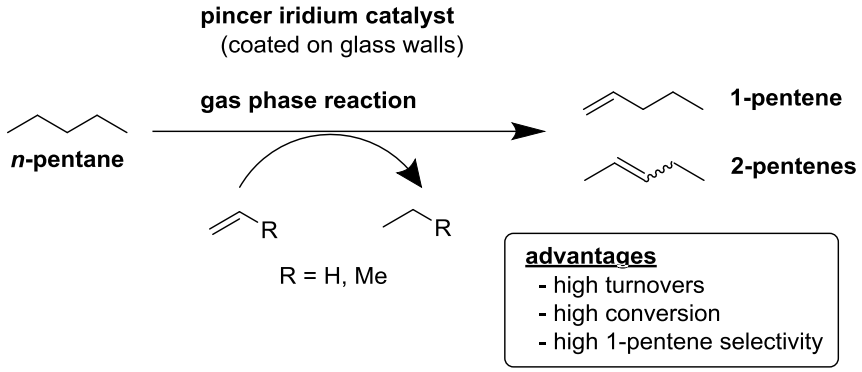

Scheme 2.4 Dehydrogenation of *n*-pentane in the gas phase by solid-supported pincer iridium catalysts

Lastly, alkane metathesis is a reaction which employs tandem transfer dehydrogenation and olefin metathesis catalysts in order to redistribute the molecular weight of a set of linear alkanes.[5] (Scheme 2.5) The original report detailed the conversion of *n*-hexane into a range of linear alkanes (C_2 to C_{12}), of which some ($C_{\geq 10}$) are valuable components of diesel fuel.

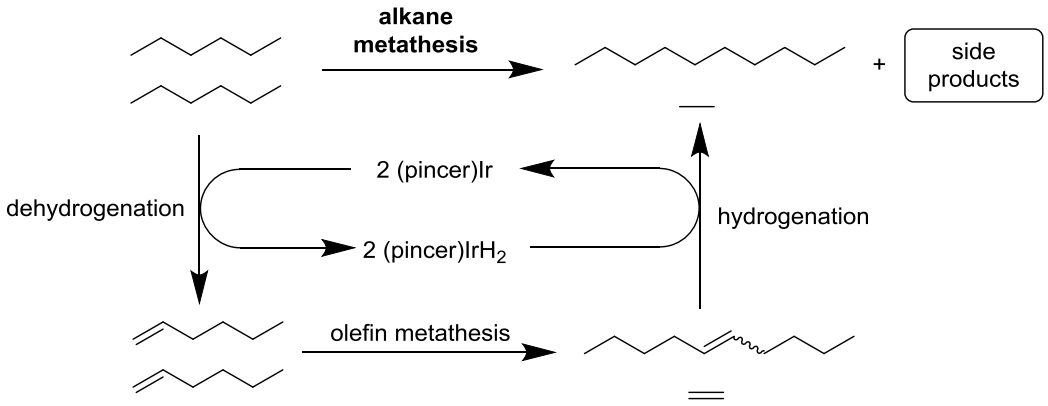

Scheme 2.5 Alkane metathesis of *n*-hexane

Critically, examination of the reaction's mechanism shows that the ability to generate the longest chains (i.e. C_{10}) depends on both the regioselectivity of dehydrogenation and the rate of isomerization. (Scheme 2.6) Like the production of benzene in dehydroaromatization, the generation of C_{10} requires that the regioselectivity of dehydrogenation provides high selectivity for the 1-olefin, and that isomerization of the C=C bond is relatively slow. Thus, elucidating the factors which determine the regioselectivity of dehydrogenation could improve the selectivity for diesel-range *n*-alkanes in alkane metathesis.

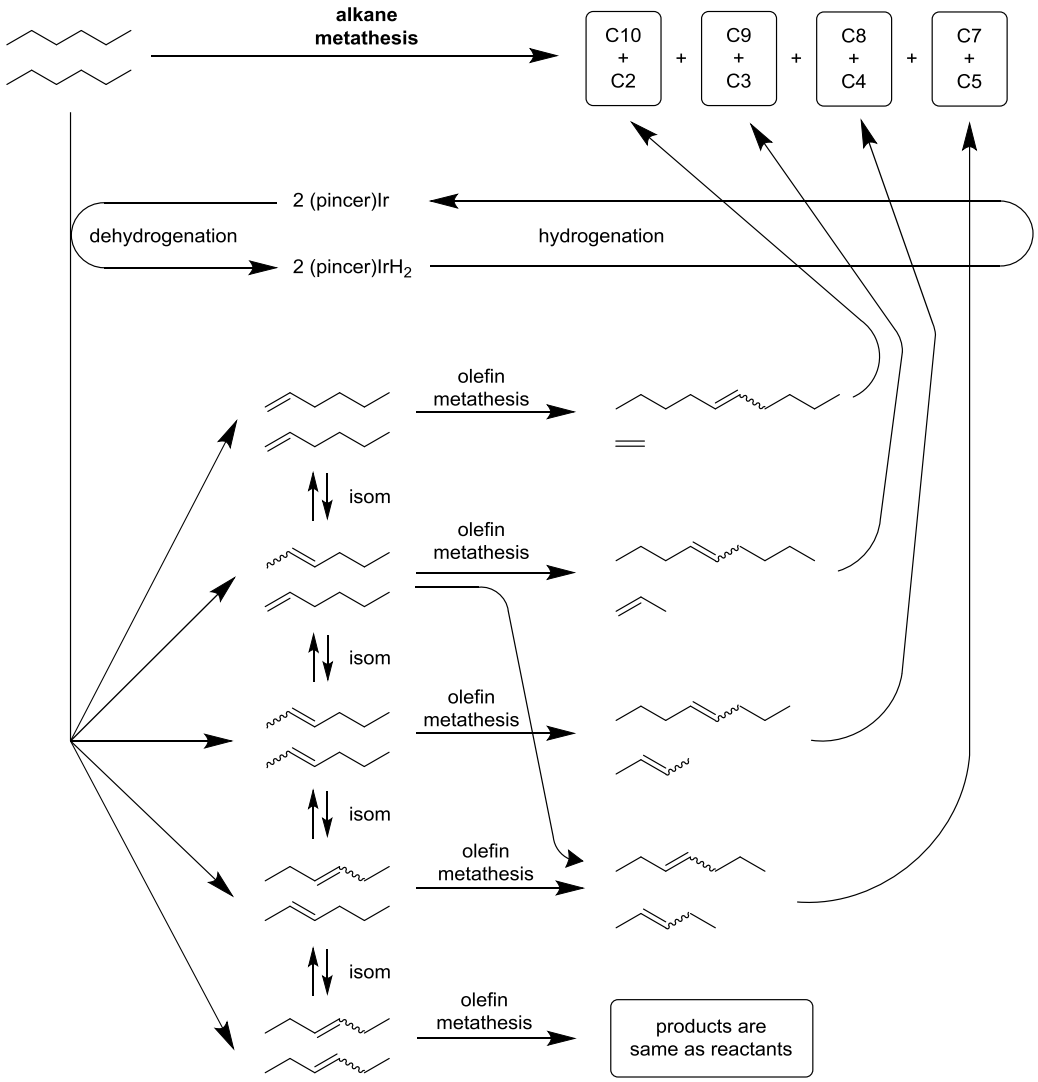

Scheme 2.6 Pathways to desired products and side products during alkane metathesis

In fact, it has been observed that different pincer iridium catalysts have vastly different selectivities for *n*-decane, the desired product and a component of diesel fuel.[8] (Table 2.1) In particular, alkane metathesis selectivity was defined as the ratio of C_{10} products over the sum of C_7 through C_{10} products after 1 hour of reaction time at 125 °C. (Equation 2.1) The overall trend shows that the (PCP)Ir catalysts have the highest selectivity, whereas (PCOP)Ir and (POCOP)Ir catalysts have the lowest selectivity. There were also differences within each category (i.e. (^{tBu4}PCP)Ir has 55% selectivity while (^{iPr4}PCP)Ir gave 30% selectivity. As shown in Scheme 2.6 above, the possible causes of these alkane metathesis selectivity differences are known. On one hand, this could be due to (PCOP)Ir/(POCOP)Ir having lower regioselectivity for 1-olefins during dehydrogenation than (PCP)Ir catalysts. In addition, the low selectivity for (PCOP)Ir/(POCOP)Ir could be caused by relatively faster rates of isomerization (relative to dehydrogenation) with (PCOP)Ir/(POCOP)Ir catalysts than with (PCP)Ir catalysts. Or, lastly, the selectivity differences could be due to both factors.

$$Alkane\ metathesis\ selectivity = \frac{C_{10}}{C_7 + C_8 + C_9 + C_{10}}$$

Equation 2.1 Definition of selectivity during alkane metathesis

Catalyst	Selectivity
(^{tBu4}PCP)Ir	55%
(MeO-^{tBu4}PCP)Ir	50%
(^{tBu3Me}PCP)Ir	39%
(^{iPr4}PCP)Ir	30%
(^{tBu4}PCOP)Ir	16%
(^{tBu2}PCOP^{iPr2})Ir	25%
(^{iPr4}PCOP)Ir	23%
(^{tBu4}POCOP)Ir	22%

Table 2.1 Experimentally-observed selectivity during alkane metathesis[8]

Hence, with importance of regioselectivity to these potentially-commercializable processes in hand, focus was directed towards the technical aspects of *measuring* regioselectivity.

If regioselectivity for all known pincer iridium catalysts could be accurately assessed, then trends could be observed. In turn, this would help direct the design of new pincer iridium catalysts. Unfortunately, however, the situation is much more complex. In most organic reactions, measuring selectivity is as simple as integrating data from an NMR or gas chromatogram. However, this is not the case with pincer iridium catalysts and dehydrogenation. The complicating aspect is that pincer iridium catalysts, which are responsible for dehydrogenation, are *also* proficient at catalytically *isomerizing* the location of C=C double bonds within a molecule. (Scheme 2.7) Hence, if a given catalyst were to give exclusively 1-octenes, then that iridium complex would *also* catalyze the isomerization of 1-octene to 2-, 3-, and 4-octenes. In fact, this phenomenon was observed during the study of (^{iPr4}PCP)Ir: while regioselectivity for 1-octene with 500 mM of 1-decene as the acceptor was > 90% after 15 minutes, regioselectivity decreased to 45% and then 8% after 30 and 60 minutes, respectively. Presumably, most of the 1-octene generated was being isomerized to 2- or 3- or 4-octenes.

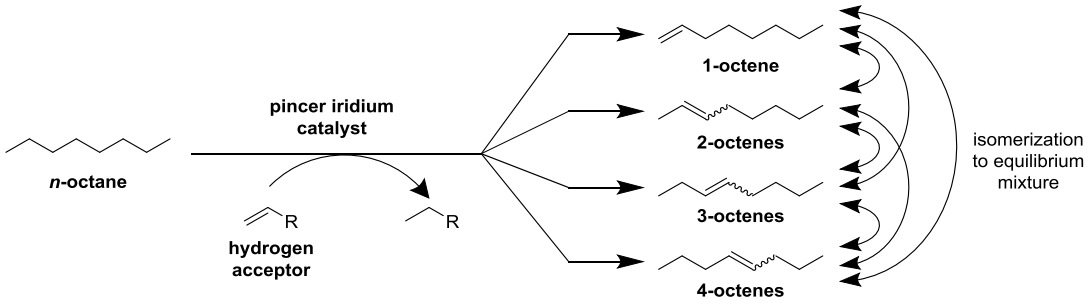

Scheme 2.7 1-hexene/*n*-octane transfer dehydrogenation

Therefore, in reality the *observed* selectivity of dehydrogenation (i.e. by gas chromatography) depends upon *both* the regioselectivity of the actual dehydrogenation *and* the rate by which the pincer iridium catalysts subsequently isomerize the location of the C=C bond within the olefin. To understand this isomerization process, it is necessary to consider the changes in thermodynamic stability that occur upon C=C bond isomerization.

It is known well known that hyperconjugation between the π-electrons in the C=C bond and neighboring C-H bonds creates significant stabilization.[9] This effect can be illustrated by considering the equilibrium between 1-butene, *cis*-2-butene, and *trans*-2-butene. (Scheme 2.8) This equilibrium can be fully described by finding the two equilibrium constants (K_{eq}) for the isomerization of 1-butene into *cis*-2-butene and from *cis*-2-butene into *trans*-2-butene.

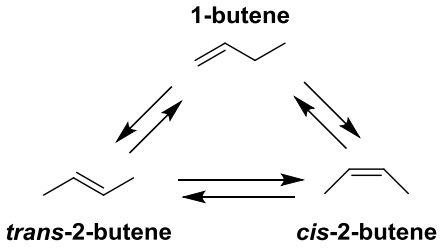

Scheme 2.8 Isomerization of 1-butene and 2-butenes

Although the equilibrium itself is defined by the standard state energy change (ΔG°) (Equation 2.2), experimentally observed calorimetric data regarding the gas phase heat of formation ($\Delta_f H°_{gas}$) can be used as a good approximation for $\Delta_r G°$. (Table 2.2) This data gives ΔG° approximations for the isomerization of 1-butene into *cis*-2-butene as 1.68 kcal/mol and from *cis*-2-butene into *trans*-2-butene as 0.75 kcal/mol.[10] Using these values and a temperature of 293 K, the equilibrium constant equation gives K_{eq} = 17.8 for the isomerization to *cis*-2-butene and K_{eq} = 3.6 for the isomerization to *trans*-2-butene. Hence, the overall equilibrium for 1-butene : *cis*-2-butene : *trans*-2-butene is predicted to be approximately 1 : 18 : 64.

$$K_{eq} = e^{\frac{\Delta_r G°}{RT}}$$

Equation 2.2 Equation relating equilibrium constant to standard state energy change and temperature

Compound	$\Delta_f H°_{gas}$ (kcal/mol)	Relative concentration at equilibrium
1-butene	-0.15 ± 0.19	1
***cis*-2-butene**	-1.83 ± 0.30	18
***trans*-2-butene**	-2.58 ± 0.24	64

Table 2.2 Heats of formation and equilibrium constants for 1-butene and 2-butenes

It is important to distinguish this consideration of *thermodynamics* from that of *kinetics*. Kinetics is represented by the rate constant for a reaction, which is related to the kinetic barrier of that reaction ($\Delta G^{\ddagger}$) through the Eyring equation. (Equation 2.3)

$$k = \frac{k_B T}{h} e^{-\frac{\Delta G^{\ddagger}}{RT}}$$

Equation 2.3 Eyring equation

The key finding of this analysis is *not* any specifics regarding butene, but rather that (given enough time) pincer iridium catalyzed isomerization will always change the distribution of olefins into their equilibrium-defined ratios. Barring any extremely unlikely coincidences, this *thermodynamic* distribution will be at least somewhat different, if not very very different, from the *kinetic* distribution (the regioselectivity) produced directly from dehydrogenation. Therefore, the *experimentally observed* selectivity depends both upon the regioselectivity of the catalyst and how far olefin isomerization has taken the distribution towards its equilibrium.

With the three types of selectivity clearly defined (kinetic/regioselectivity, equilibrium/thermodynamic, and observed), it is now possible to begin experimentally measuring the true regioselectivity of pincer iridium catalysts.

2.2 Estimation of regioselectivity through direct determination reactions

2.2.1 Introduction to the direct determination reaction

The most straightforward method of determining the regioselectivity of a catalyst would be to measure the production of various the olefins over time. Notably, resolving the various olefins from one another, and from the remaining n-alkane from which they came, is not trivial. ^{1}H NMR could theoretically be used to identify the appropriate vinylic and allylic protons in a sample, but in practice this could prove to be difficult. Next, gas chromatography (GC) could also theoretically be used to separate the various components of a reaction mixture. However, the stationary phase in typical GC columns causes separation primary regarding boiling point, which would not necessarily be sufficient for the current endeavor. Upon analysis of a mixture of *n*-octane, 1-octene, and trans-2-octene using a standard boiling point GC column, all of the peaks overlapped with each other and were not resolved. Thus, standard boiling point columns could not be used either to solve this analytical issue.

Lastly, a specialty GC column was purchased (Agilent J&W GS-GasPro column, 60 m x 0.32 mm) which contains a proprietary stationary phase which adsorbs olefins more strongly than simple alkanes. This results in olefins (i.e. 1-octene) which elute at retention times of ca. 1 minute longer than their corresponding alkanes (i.e. *n*-octane). In addition, since the π-bond is coordinating to the stationary phase, various olefin isomers will elute at different retention times. In practice, small quantities (ca. 50 mM) of various octenes were added to a sample of *n*-octane and injected into a Varian 430 GC equipped with the GasPro column. The results indicated that while 1-octene and *trans*-4-octene overlapped, each of the other octenes were clearly resolved from each other *and* from the large and broad *n*-octane peak. Specifically, the order of elution (from first to last) was *n*-octane, 1-octene and *trans*-4-octene, *trans*-3-octene, *trans*-2-octene, *cis*-

4-octene, *cis*-3-octene, and *cis*-2-octene. Similarly, the order of elution of *n*-hexane and the hexenes were found to be *n*-hexane, 1-hexene, *trans*-3-hexene, *trans*-2-hexene, *cis*-3-hexene, and *cis*-2-hexene. Likewise, cycloalkenes and branched olefins were also found to elute ca. 1 minute after their corresponding alkanes, and the various cis/trans isomers (i.e. *cis*-cyclododecene and *trans*-cyclododecene) could usually be resolved from one another.

With the analytical method established, an experiment needed to be designed to measure regioselectivity. The most straightforward method, which has been termed "direct determination," was to simply observe the kinetic products of transfer dehydrogenation and quantify them. The reaction mixture would consist of an *n*-alkane, an olefin, and the pincer iridium catalyst. (Scheme 2.9)

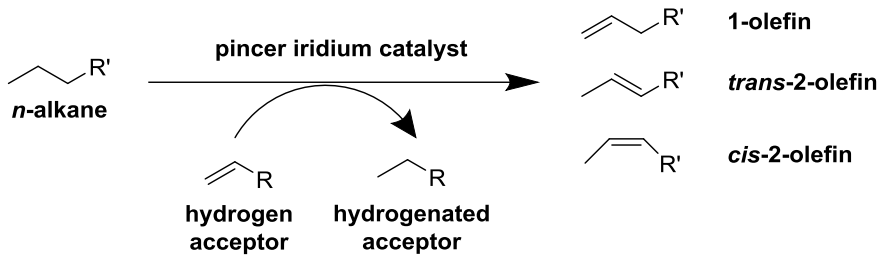

Scheme 2.9 Generalized form of direct determination method for estimating regioselectivity

Previous studies indicated that a reaction mixture of neat *n*-alkane (~ 6 M), olefin hydrogen-acceptor (~ 200 mM), and pincer iridium catalyst (~5 mM) gave observable quantities of the different dehydrogenation products after several minutes.[2] Therefore, these experimental conditions would allow the relatively easy study of many pincer iridium catalysts. Notably, however, the initial studies showed that the choice of hydrogen acceptor influenced the observed regioselectivity. Although the various reactions were not perfectly comparable to one another (upon changing the hydrogen acceptor, the reaction temperature or concentration of components were also changed), the highest regioselectivity observed with (^{tBu4}PCP)Ir using TBE

as the acceptor was 71%, whereas the highest value with 1-hexene as the acceptor was 96%. In addition, isomerization appeared to become a more problematic confounding variable with TBE as the hydrogen acceptor than with 1-hexene. This is because ratio of the rate of isomerization (from 1-octene to 2-octenes) to the rate of transfer dehydrogenation was higher with TBE than with 1-hexene. Therefore, quantification of the true kinetic regioselectivity should be more accurate with 1-hexene as the acceptor than with TBE.

Thus, the current studies always employed 1-hexene as the hydrogen acceptor. To standardize the analysis for all catalysts, the reaction mixture was always composed of neat *n*-octane, 200 mM of 1-hexene, 2.5 mM of the catalyst, and the reaction was monitored at 125 °C. (Scheme 2.10)

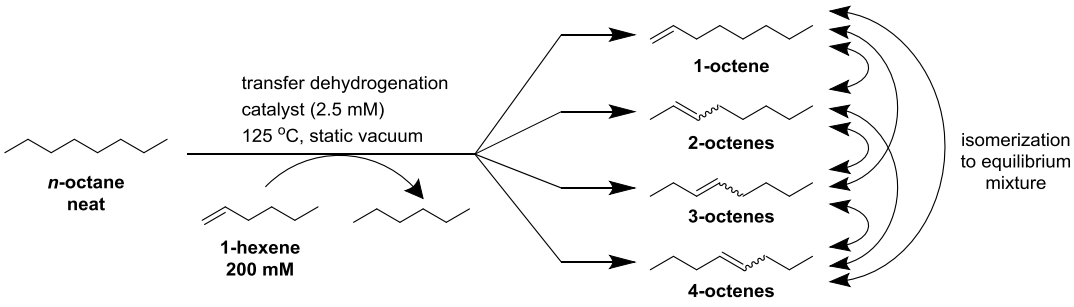

Scheme 2.10 Experimental conditions used during direct determination

Given this experimental procedure, the regioselectivity for generating 1-olefins (in general) could be approximated by the rate for producing 1-octene versus the rate for producing the other possible octa-monoenes (2-, 3-, and 4-octenes). As will be discussed later, the experimental concentrations of 3- and 4-octenes were always found to be very low or close to zero. In combination with DFT calculations which will be presented later, it seems that >> 99% of all octenes produced will be either 1-octene or 2-octenes. Therefore, the regioselectivity for 1-octene can be expressed as a function of the rate for generating 1-octene (k_{dh1}), the rate for *cis*-

2-octene (k_{dhcis2}), and the rate for *trans*-2-octene ($k_{dhtrans2}$). (Equation 2.4) Notably, the numerical values for these rate constants only are only accurate for the specific reaction conditions specified.

$$Regioselectivity = \frac{k_{dh1}}{k_{dh1} + k_{dhcis2} + k_{dhtrans2}}$$

Equation 2.4 Definition of regioselectivity for 1-olefins during dehydrogenation

2.2.2 Mathematical foundation of the direct determination analysis

However, a proper kinetic analysis of transfer dehydrogenation requires more in-depth equations because it is unlike most other stoichiometric or catalytic reactions. For a typical reaction like hydration of an olefin, the reagents (i.e. water and propylene) are converted into a mixture of products (i.e. 1-propanol and 2-propanol) and the reaction finishes, yielding a stable ratio of the two products. However, in transfer dehydrogenation the products (i.e. 1-octene) can readily undergo further reactions: isomerization (i.e. to 2-octenes), another dehydrogenation (i.e. to 1,3-octadiene), or hydrogenation (i.e. to *n*-octane). Therefore, the change in the concentration of a given olefin depends not-only on dehydrogenation but also on isomerization, hydrogenation, and further dehydrogenation to a diene. (Equation 2.5) Notably, the sign of "change by isomerization" can be either positive or negative, depending on circumstances. As the experimental results will show, the sign for 1-octene during these reactions is always negative because it is being isomerized to 2-octenes. Conversely, the sign for isomerization for *trans*-2-octene is positive in the beginning of the reaction (when lots of 1-octene is being isomerized to *trans*-2-octene), but changes to negative towards later time periods of the reaction (little 1-octene is present to isomerize to *trans*-2-octene, whereas plentiful *trans*-2-octene starts being isomerized to 3-octenes). Although Scheme 2.10 was drawn to represent the possibility of chain-

walking isomerization, wherein the C=C bond is moved by two or more carbons in a single step (i.e. 1-octene directly to *trans*-3-octene, without formation of either 2-octene), experimental results suggest that most (if not all) isomerization happens one carbon at a time (i.e. 1-octene to *cis*-2-octenes).

$$\frac{d[olefin]}{dt} = dehydrogenation + (change\ by\ isomerization) - hydrogenation - (further\ dehydrogenation\ to\ diene)$$

Equation 2.5 Factors determining the rate of change in concentration of an olefin

Because of the interrelated nature of transfer dehydrogenation, the rate of each individual transformation depends upon multiple rate constants (which are constant over the course of the reaction) and the concentration of many different species (which *vary* considerable during the reaction). Thus, a simple spreadsheet software program would not be sufficient for accurate kinetic modeling of the reaction. Instead, a specialized software program called Copasi was used to perform the kinetic modeling.[11] Copasi will employ the user-inputted information (what type of rate law for each reaction) to accurately model the experimental data (concentrations of each alkane/olefin over time from GC analysis). Specifically, Copasi will vary the *rate constants* for each rate law equation in order to obtain the best fit between the computer model and the kinetic data.

Therefore, the rates and behaviors of isomerization, hydrogenation, and further dehydrogenation(s) must be understood before Copasi can accurately model dehydrogenation. Previous studies demonstrated that isomerization of 1-hexene by (^{tBu4}PCP)Ir was zero-order in 1-hexene, whereas isomerization by (^{tBu4}POCOP)Ir was first-order in 1-hexene. Thus, those orders were used in kinetic modeling of isomerization during the transfer dehydrogenation studies of (^{tBu4}PCP)Ir and (^{tBu4}POCOP)Ir. However, the orders of the isomerization reaction had not been

established for the other catalysts investigated. Therefore, three different Copasi models were made regarding the rate law of isomerization:

1. Rate of isomerization of 1-hexene to 2-hexenes was zero-order in all olefins
2. Rate of isomerization of 1-hexene to 2-hexenes was first order in [1-hexene]
3. Rate of isomerization of 1-hexene to 2-hexenes was first order in [1-hexene] but inverse first order in [1-hexene + 1-octene]

In general, each rate law caused the overall fit of the model to change, but not by an appreciable amount. While the first rate law sometimes gave the best fit for a given catalyst, other times the second rate law gave a better fit. And, in other circumstances, the third rate law gave the best fit. Therefore, no conclusive evidence could be obtained about which rate law was the most accurate. Likewise, the desired outcome of this project (numerical estimates of regioselectivity) changed only by insignificant amounts when switching between isomerization rate laws. To explain it another way, the error created by possibly selecting the incorrect isomerization rate law appeared to be *less* than the random error from other sources (i.e. accuracy of GC integrations). Therefore, all isomerizations were assumed to be and modeled as first-order in the olefin being isomerized. (Equations 2.6 and 2.7) Note that since there are two 2-octenes, the rate constant $k_{isom\text{-}oct}$ is actually equal to the sum of $k_{isom\text{-}oct\text{-}cis}$ and $k_{isom\text{-}oct\text{-}trans}$. The same property also holds for isomerization of 1-hexene.

$$rate\ of\ isom\ 1hex\ to\ 2hex = k_{isom-hex} * [1hex]$$

$$rate\ of\ isom\ 1oct\ to\ 2oct = k_{isom-oct} * [1oct]$$

Equations 2.6 and 2.7 Rate laws for isomerization of 1-olefins to 2-olefins

The values of $k_{isom\text{-}oct}$ and $k_{isom\text{-}hex}$ were assumed to be equal, and Copasi was forced to keep them equal, for multiple reasons. First, examination of DFT-optimized dehydrogenation/hydrogenation structures shows that the tails of the substrate molecules, which could be considered R = H with *n*-hexane or R = Et with *n*-octane, are quite far away from the PR_2 groups of the catalysts. Therefore, their influence on the energetics of the rate-determining step *via* sterics could be considered very low or negligible. Likewise, the electronic changes due to R = H versus R = Et were reasonably assumed to be exceedingly small. Lastly, during studies of the KIE of dehydrogenation it was shown that the rate for dehydrogenating *n*-octane versus the rate for *n*-decane were equal within +/- 10% error, further suggesting that the alkyl tail had negligibly small effects on dehydrogenation (or isomerization). Therefore, two new rate constants, $k_{isom\text{-}cis}$ and $k_{isom\text{-}trans}$, will be used to represent the isomerization of a 1-olefin to either a *cis*-2-olefin or a *trans*-2-olefin, regardless of the tail length. (Equations 2.8 and 2.9)

$$rate\ of\ isomerize\ 1olefin\ to\ cis2olefin = k_{isom-cis} * [1olefin]$$

$$rate\ of\ isomerize\ 1olefin\ to\ trans2olefin = k_{isom-trans} * [1olefin]$$

Equations 2.8 and 2.9 Rate laws for isomerization of 1-olefins to *cis*-2-olefins and *trans*-2-olefins

Next, the role of hydrogenation in changing in concentrations of the various olefins was considered. First, 1-octene can be considered. Since the tail of the substrate is unlikely to noticeably affect the rate of its reaction at iridium, the *rate constant* for hydrogenation of 1-octene to *n*-octane will likely be very similar to the rate constant for hydrogenation of 1-hexene to *n*-hexane. (Equations 2.10 through 2.12)

$$rate\ of\ hydrogenating\ 1octene = k_{1octene} * [1octene]$$

$$rate\ of\ hydrogenating\ 1hexene = k_{1hexene} * [1hexene]$$

$$k_{1octene} \approx k_{1hexene}$$

Equations 2.10 through 2.12 Rate constants for dehydrogenation to give 1-hexene and 1-octene should be very similar

Thus, if [1-octene] is equal to 10% of [1-hexene], then the overall rate of hydrogenation of 1-octene will likely be about 10% of the rate for 1-hexene. (Equations 2.13 and 2.14)

$$[1octene] \approx 10\% * [1hexene]$$

$$rate\ of\ hydrogenating\ 1octene \approx 10\% * (rate\ of\ hydrogenating\ 1octene)$$

Equations 2.13 and 2.14 Rate of hydrogenating 1-octene will be slow compared to hydrogenating 1-hexene

To put it another way, if [1-octene] is significantly smaller than [1-hexene], then the amount of [1-octene] that is hydrogenated *back* to *n*-octane is likely to be very small. Therefore, collecting GC data at "early" reaction times (when [1-octene] << [1-hexene]) allows the Copasi kinetic analysis to ignore the hydrogenation of 1-octene back to *n*-octane, greatly simplifying the analysis. In reality, GC data *was* collected at time points where [1-octene] << [1-hexene] for this reason (see later sections).

Likewise, the hydrogenation of 2-octenes to *n*-octane would likely have rate constants very similar to those for the hydrogenation of 2-hexenes to *n*-hexane. As the experimental data will show, [2-hexenes] was always vastly larger than [2-octenes] (at least 10-fold), so the hydrogenation of 2-octenes to *n*-octane can also be omitted from the Copasi kinetic analysis without incurring any noticeable error. (Equations 2.15 through 2.19)

$$rate\ of\ hydrogenating\ 2octenes = k_{2octenes} * [2octenes]$$

$$rate\ of\ hydrogenating\ 2hexenes = k_{2hexenes} * [2hexenes]$$

$$k_{2octenes} \approx k_{2hexenes}$$

$$[2octenes] < 10\% * [2hexenes]$$

$$rate\ of\ hydrogenating\ 2octenes < 10\% * (rate\ of\ hydrogenating\ 2hexenes)$$

Equations 2.15 through 2.19 Hydrogenation of 2-octenes is slow compared to other reactions during transfer dehydrogenation

Lastly, the role of further dehydrogenation from a monoene to a diene also needed to be considered. Fortunately, the specialized column (GS-Gaspro) used for GC analysis clearly resolved the dienes from the monoenes (monoenes eluted about 1 minute before dienes) and the alkanes (about 2 minutes before dienes) of the same carbon number. Initial experiments showed that production of dienes by any examined catalyst was extremely slow compared to both transfer dehydrogenation and isomerization, and therefore diene production would not cause any noticeable error in the Copasi kinetic analysis or estimates of regioselectivity.

Thus, since the impact of hydrogenation and further dehydrogenation on the concentration of an olefin are extremely small, the formal definition for change in concentration of an olefin can be safely and accurately simplified. (Equation 2.20)

$$\frac{d[olefin]}{dt} \approx dehydrogenation + (change\ by\ isomerization)$$

Equation 2.20 Approximation for the rate of change in concentration of an olefin

Thus, the GC data collected could be used to find the rate of change of each olefin (d[olefin]/dt), and those values could be related to other known quantities ([1-octene] and [Ir]) in order to solve for the unknown rate constants. (Equations 2.21 through 2.23)

$$\frac{d[1oct]}{dt} \approx \{k_{dh1} - k_{isom-cis} * [1oct]^X - k_{isom-trans} * [1oct]^X\} * [Ir]$$

$$\frac{d[cis2oct]}{dt} \approx \{k_{dhcis2} + k_{isom-cis} * [1oct]^X\} * [Ir]$$

$$\frac{d[trans2oct]}{dt} \approx \{k_{dhtrans2} + k_{isom-trans} * [1oct]^X\} * [Ir]$$

Equations 2.21 through 2.23 Rate laws used during kinetic modeling of experimental data from direct determination experiments

2.2.3 Direct determination of regioselectivity for known (PCP)Ir catalysts

With a comprehensive data analysis plan in place, the collection of experimental data with the reaction conditions specified in Scheme 2.10 was begun. The first catalyst studied was (^{tBu4}PCP)Ir (see Figure 1.3 for molecular structure). In a previous report (^{tBu4}PCP)Ir was found to have high regioselectivity for producing 1-octene over 2-octenes.[2] In the current study, the initial samples collected at early time points showed strong production of 1-octene and small amounts of 2-octenes, but no detectable 3-octenes or 4-octenes. (Figure 2.1) At later time points, the increase in 1-octene began to slow and the quantity of 2-octenes began to increase more rapidly. Notably, very small or undetectable quantities of 3-octenes or 4-octenes were observed. When viewed in total, this confirms the previous report that (^{tBu4}PCP)Ir had high regioselectivity for generating 1-octene. It also suggests that essentially no 3-octenes or 4-octenes are kinetically

produced, and their appearance must come from isomerization of 1-octene or 2-octenes. Notably, visual inspection of Figure 2.1 cannot determine the regioselectivity for 2-octenes since they could be generated by dehydrogenation, isomerization, and/or both processes.

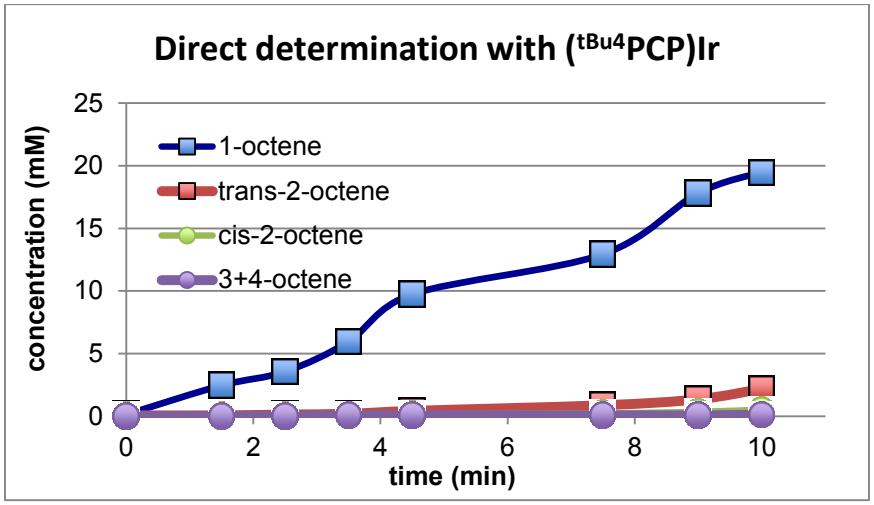

Figure 2.1 Direct determination with (^{tBu4}PCP)Ir

However, kinetic modeling with the Copasi software package was used to more accurately quantify the regioselectivity of dehydrogenation. Since isomerization of olefins by (^{tBu4}PCP)Ir was known to be zero-order in the given olefin,[7] this information was used during Copasi modeling. Given the accuracy of the GC data, an exact numerical value for regioselectivity could not be established. However, a lower-bound of ≥ 96% selectivity for 1-olefins could be estimated. Likewise, the selectivity for producing 2-olefins was estimated at ≤ 4% with selectivity for 3-olefins and 4-olefins near 0%.

Moving forward, the regioselectivity of (^{iPr4}PCP)Ir was investigated next (see Figure 1.3 for molecular structure). Since its PCP backbone was identical to that of (^{tBu4}PCP)Ir, presumably the electronic differences between the two catalysts would be negligibly small. However, the much smaller ^{i}Pr groups (relative to ^{t}Bu groups) on (^{iPr4}PCP)Ir would allow a much more open steric environment for dehydrogenation to take place. By isolating one of the variables in the

steric/electronic pair, it might be possible to elucidate information of the role of each variable on regioselectivity.

Like its more stericly crowded counterpart, (^{iPr4}PCP)Ir also showed fast initial production of 1-octene and relatively slower generation of 2-octenes. However, the quantities of 2-octenes seemed to be larger in the current (^{iPr4}PCP)Ir study than with the previous (^{tBu4}PCP)Ir tests. As discussed previously, this could be caused by either faster isomerization of 1-octene to 2-octenes by (^{iPr4}PCP)Ir, or by a lower regioselectivity for dehydrogenating to give 1-octene (and therefore higher relative quantities of 2-octenes), or both. Kinetic modeling with Copasi was also slightly limited by the imperfections of the GC data, but the best fit was obtained with regioselectivity for 1-octene of 91% (and 9% regioselectivity for 2-octenes). As with (^{tBu4}PCP)Ir, the regioselectivity for generating 3-octenes and 4-octenes appeared to be very close to 0%.

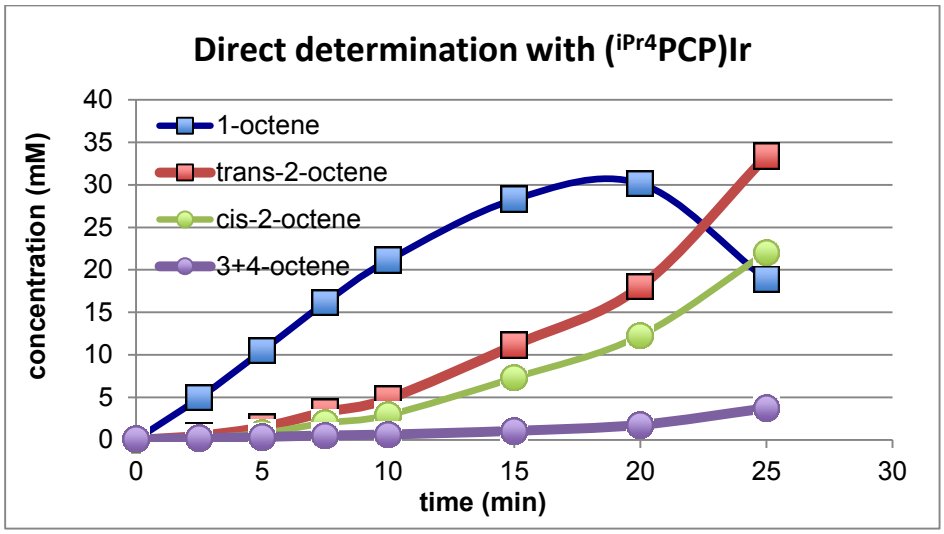

Figure 2.2 Direct determination with (^{iPr4}PCP)Ir

At this stage, it appeared that steric differences between (^{tBu4}PCP)Ir and (^{iPr4}PCP)Ir could alter the regioselectivity of dehydrogenation by a small but noticeable amount. Whereas (^{tBu4}PCP)Ir has a regioselectivity of ≥ 96%, the regioselectivity for (^{iPr4}PCP)Ir was closer to 91%.

To examine whether electronic differences could also affect the regioselectivity, two catalysts in the (*para*-X-^{tBu4}PCP)Ir family were studied, (MeO-^{tBu4}PCP)Ir and (Me_2N-^{tBu4}PCP)Ir-^{tBu4}PCP)Ir (see Figure 1.3 for molecular structure). While the steric environment around the iridium center in these two catalysts was essentially identical to that of (^{tBu4}PCP)Ir, the electronic properties the ligands were markedly different. Based on Hammet parameters, both the *para*-NMe_2 and *para*-OMe groups would make the ipso carbon less electron-donating based on inductive effects (i.e. nitrogen and oxygen are more electronegative than hydrogen) than with the *para*-H of (^{tBu4}PCP)Ir, but *more* electron-donating based on resonance structures. While it is known that the *net* effect of the NMe_2 and OMe groups in the para position is electron *donation*, it was unknown whether any influence on regioselectivity would happen through the *individual* effects or the *net* effect.

Catalytic experiments with (MeO-^{tBu4}PCP)Ir and (Me_2N-^{tBu4}PCP)Ir showed similar regioselectivity values to those of the parent (^{tBu4}PCP)Ir catalyst. (Figures 2.3 and 2.4) Namely, there was strong production of 1-octene while the quantities of 2-octenes were quite small. Kinetic modeling with the Copasi software package approximated regioselectivity values of ≥ 96% for both the (MeO-^{tBu4}PCP)Ir and (Me_2N-^{tBu4}PCP)Ir catalysts.

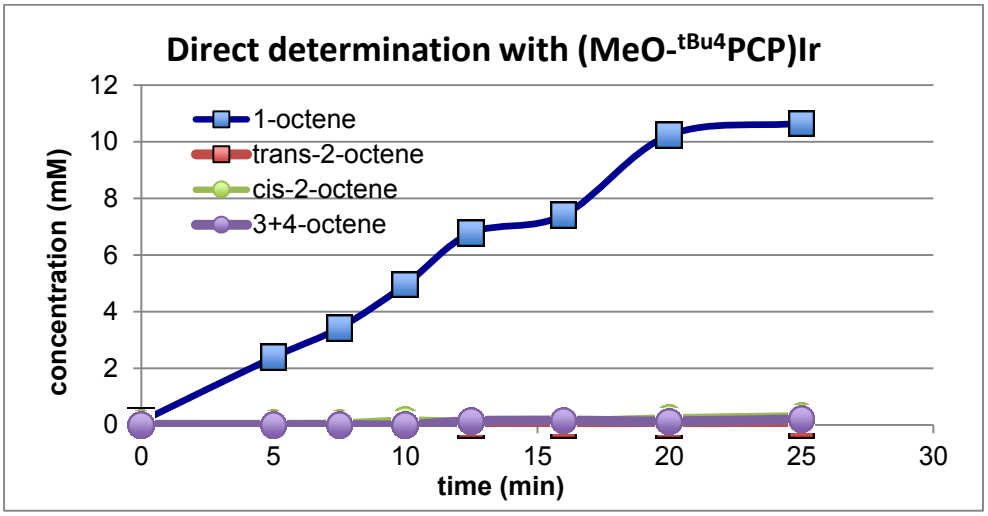

Figure 2.3 Direct determination with (MeO-^{tBu4}PCP)Ir

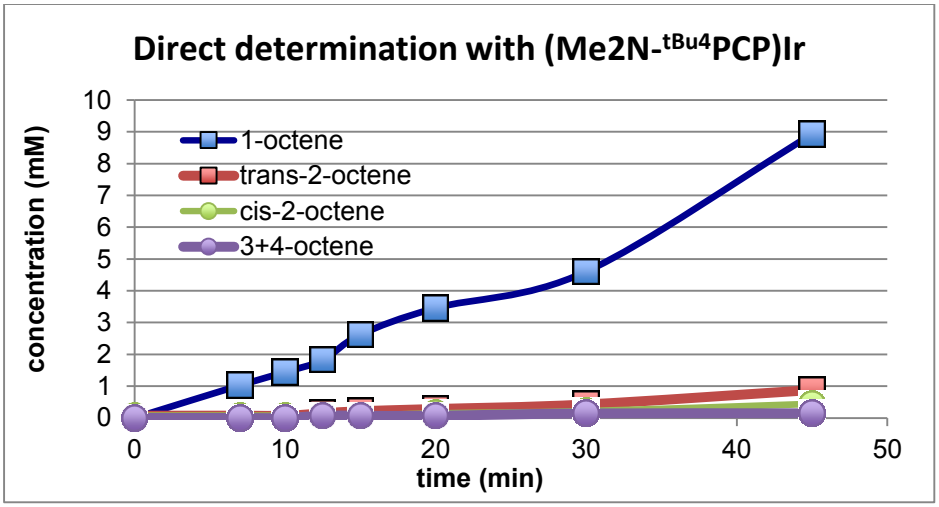

Figure 2.4 Direct determination with (Me_2N-^{tBu4}PCP)Ir

Thus, the regioselectivity for producing 1-olefins by PCP catalysts was estimated as ≥ 96% for the three catalysts with ^{t}Bu groups, but was approximately 91% for (^{iPr4}PCP)Ir. Moving forward, more pincer iridium catalysts would need to be examined to elucidate the mechanism which determined regioselectivity. To further probe the role of sterics, a new catalyst with a steric profile between that of (^{tBu4}PCP)Ir and (^{iPr4}PCP)Ir could be synthesized and tested. As described in

the next section, the catalyst (^{tBu2}PCP^{iPr2})Ir with two ^{t}Bu groups on one phosphorous and two ^{i}Pr groups on the other phosphorous was synthesized and tested. In addition, three known catalysts (^{iPr4}PCOP)Ir and (^{tBu4}PCOP)Ir and (^{tBu4}POCOP)Ir with at least one oxygen-linked arm were also examined (see later section). These oxygen-included catalysts would have both different steric profiles *and* different electronic properties than PCP catalysts.

2.2.4 Synthesis of the (^{tBu2}PCP^{iPr2})Ir catalyst

While most pincer iridium catalysts reported in literature have been symmetrical, in the sense that the alkyl groups attached to each phosphorous are identical, catalytic improvements have been observed by employing unsymmetrical catalysts. Namely, the (^{tBu3Me}PCP)Ir catalyst was synthesized and shown to be more active for transfer dehydrogenation than both the (^{tBu4}PCP)Ir and (^{iPr4}PCP)Ir catalysts. However, the reported synthesis of (^{tBu3Me}PCP)Ir required the difficult mono-phospination of the 1,3-bis(bromomethyl)benzene starting material, and an even more tedious series of purification steps (crystalize from diethyl ether six times in sequence).

Therefore, the planned synthesis of the (^{tBu2}PCP^{iPr2})Ir catalyst utilized a different type of synthetic strategy that had previously been used to synthesize the ^{Ph2}PCP^{tBu2} ligand.[12]

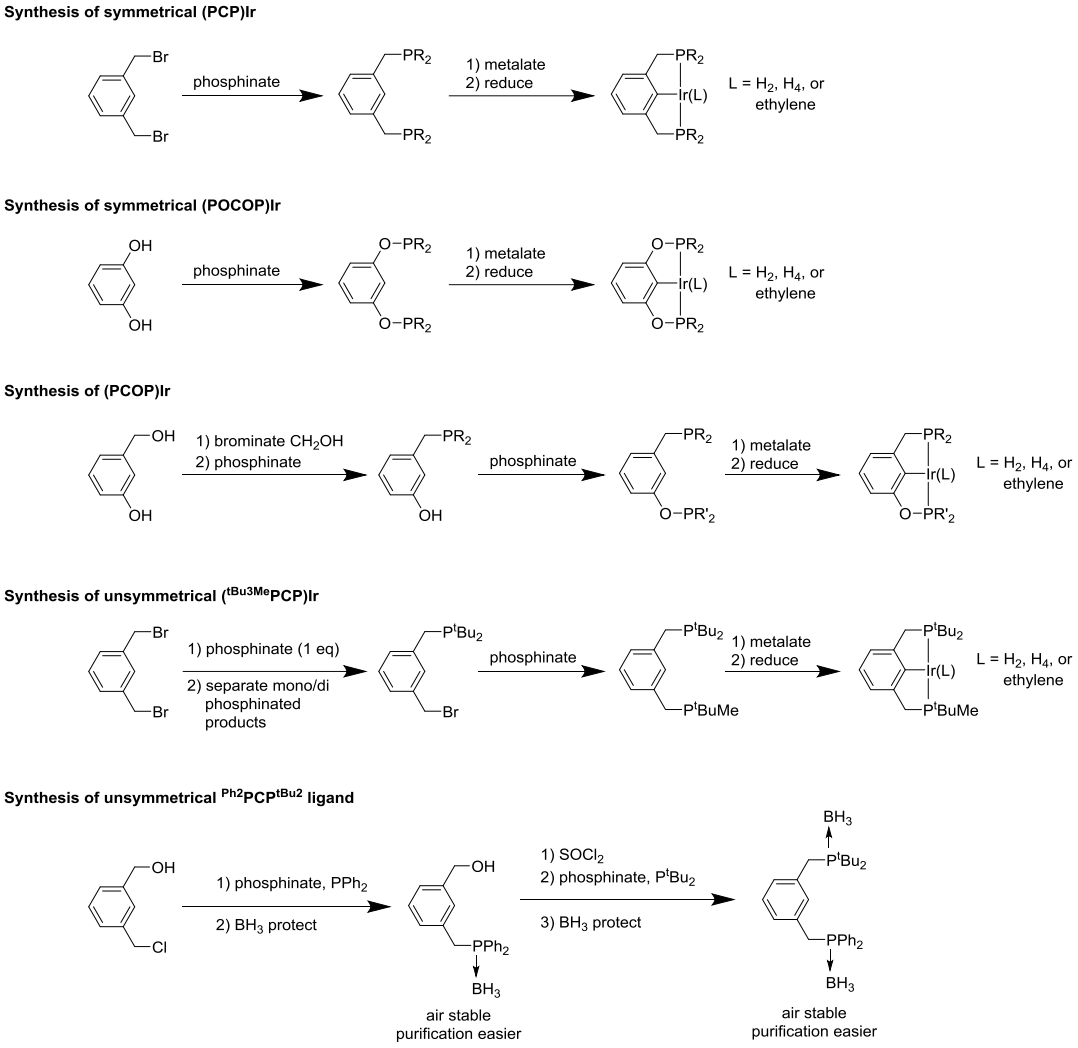

Figure 2.5 Synthetic strategies used for constructing symmetrical and asymmetrical pincer ligands[1,12-16]

In particular, the new strategy began with an asymmetrical starting aryl compound (methyl 3-(bromomethyl)benzoate , with a bromomethyl group on one side and a methyl ester on the other) which allowed for each phosphorous group to be added separately. However, unlike the synthesis of the unsymmetrical PCOP ligands which also began with an unsymmetrical aryl compound, the current strategy with methyl 3-(bromomethyl)benzoate allowed the construction

of the PCP backbone. (Scheme 2.11) Notably, this synthetic strategy also required the protection of the lone pair on the phosphorous atoms with Lewis acidic BH_3 groups.

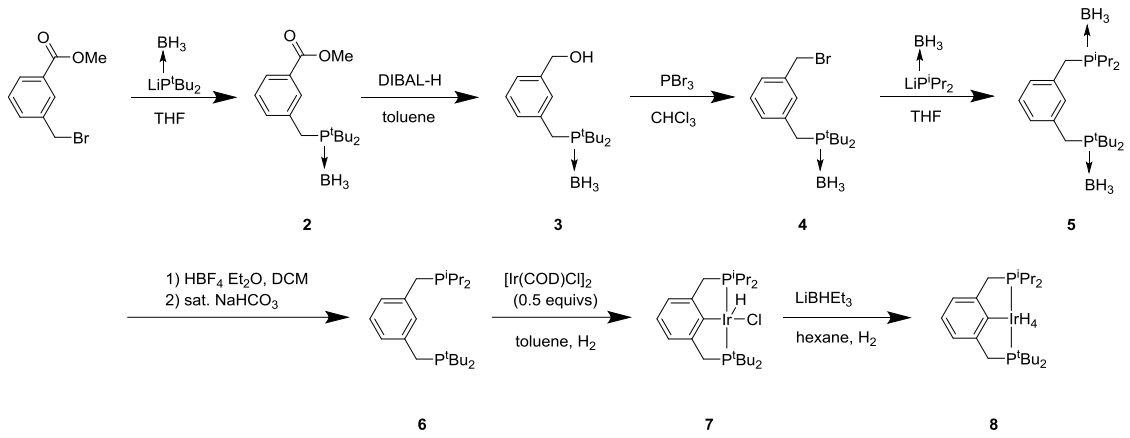

Scheme 2.11 Synthesis of (^{tBu2}PCP^{iPr2})Ir

First, the methyl 3-(bromomethyl)benzoate starting material was reacted with deprotonated (*via* ^{n}BuLi) and BH_3-protected di-tert-butyl phospine, giving the monophosphinated product. Column chromatography afforded the pure product in 91% yield. Next, the methyl ester was reduced to an alcohol moiety with DIBAL-H in toluene in 88% yield. Afterwards, the hydroxy group was transformed into a bromo group with phosphorous tribromide in 83% yield. Notably, the success of this reaction depended upon the purity of the phosphorous tribromide. Attempting the reaction with previously-opened bottles of phosphorous tribromide caused the reaction to fail, presumably due to decomposition of the reagent.

Next, the bromide was replaced with the second phosphorous group by reacting the aryl with deprotonated (*via* ^{n}BuLi) and BH_3-protected di-isopropyl phospine. Although the crude product was of relatively low purity, the BH_3 groups (by design) rendered the product air-stable. Thus, flash column chromatography was used to purify the compound, obtaining the desired product in 65% yield. The final step of the ligand synthesis was then to remove the BH_3 groups (deprotection) so that the phosphorous lone pairs could be used to attach to iridium. Reacting

the protected ligand with 10 equivalents of the tetrafluoroboric acid diethyl ether complex (HBF_4 – Et_2O) and an air-free aqueous workup gave the desired ligand in 68% yield. Notably, the careful measurement of volume for each workup solution (i.e. saturated sodium bicarbonate) was very important, as too much or too little liquid would prevent the proper separation of the aqueous and organic layers. In addition, saturated sodium chloride solutions were not used in the optimized procedure because they caused difficulties in separating the layers; although two layers were visible (not simply one layer), the boundary was not sharp, and removing only one layer was difficult.

Next, the $^{tBu2}PCP^{iPr2}$ ligand was metalated onto iridium in the typical manner for PCP compounds (reflux in toluene for 3 days under H_2 atmosphere). Pentane extraction and recrystallization gave pure ($^{tBu2}PCP^{iPr2}$)Ir(H)(Cl). Finally, the tetrahydride compound ($^{tBu2}PCP^{iPr2}$)IrH_4 was obtained by reducing the hydridochloride complex with $LiBHEt_3$ under a H_2 atmosphere. Notably, only the tetrahydride compound was observed by NMR despite the parent (^{tBu4}PCP)Ir compound always being a mixture of dihydride and tetrahydride compounds.

2.2.5 Direct determination of regioselectivity for ($^{tBu2}PCP^{iPr2}$)Ir

After synthesizing the ($^{tBu2}PCP^{iPr2}$)Ir catalyst, its regioselectivity for the dehydrogenation of a linear alkane (*n*-octane) was examined in the same manner as (^{tBu4}PCP)Ir and (^{iPr4}PCP)Ir were tested. Like all of the other PCP catalysts, it showed fast production of 1-octene and much slower generation of 2-octenes. Kinetic analysis with Copasi estimated a regioselectivity of approximately 95% for 1-octene, with the remaining 5% for 2-octenes and <<1% for 3-octenes or 4-octenes.

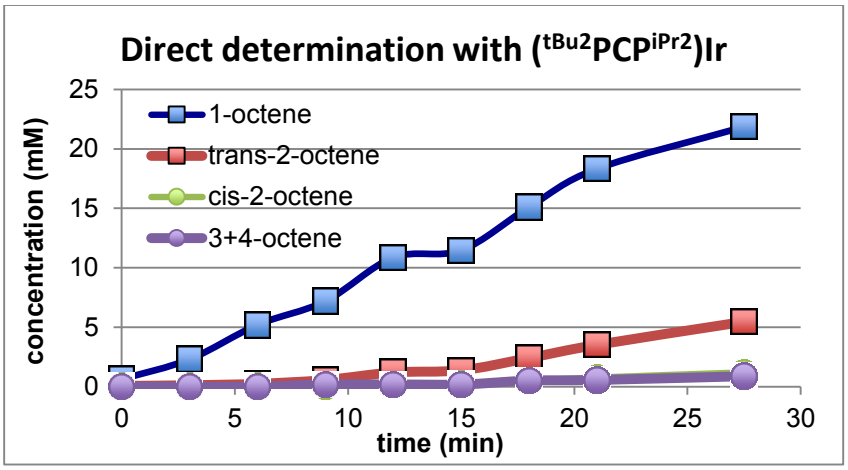

Figure 2.6 Direct determination with (^{tBu2}PCP^{iPr2})Ir

At this stage, all five different PCP catalysts showed high (≥ 91%) regioselectivity for 1-olefins, undetectable regioselectivity for 3-olefins or 4-olefins, and the remaining 4% to 9% for producing 2-olefins. (Table 2.3)

Catalyst	Regioselectivity for 1-olefins by direct determination
(^{tBu4}PCP)Ir	96%
(^{iPr4}PCP)Ir	91%
(MeO-^{tBu4}PCP)Ir	96%
(Me_2N-^{tBu4}PCP)Ir	96%
(^{tBu2}PCP^{iPr2})Ir	95%

Table 2.3 Regioselectivity estimates of (PCP)Ir catalysts by direct determination

By comparing the results of (^{tBu4}PCP)Ir with those of (^{tBu2}PCP^{iPr2})Ir and (^{iPr4}PCP)Ir, it seemed apparent that sterics had a measurable but small effect on regioselectivity for 1-olefins. This is unsurprising given that the transition state to give a 2-olefins would be more stericly crowded than the transition state for a 1-olefins. On the other hand, comparison of (^{tBu4}PCP)Ir with (MeO-^{tBu4}PCP)Ir and (Me_2N-^{tBu4}PCP)Ir suggested that electronic factors had no influence on the regioselectivity.

2.2.6 Direct determination of regioselectivity for (PCOP)Ir catalysts and (^{tBu4}POCOP)Ir

Despite the importance of the results described above, PCP catalysts comprise only a portion of known pincer iridium catalysts. Therefore, the study of PCOP and POCOP catalysts would be warranted because it would provide a survey of a wider range of steric and electronic properties than PCP catalysts could give alone.

The first catalyst examined for the 1-hexene/*n*-octane transfer dehydrogenation reaction was (^{tBu4}PCOP)Ir (see Figure 1.3 for molecular structure). Upon initial inspection, it appeared that the regioselectivity of (^{tBu4}PCOP)Ir for 1-olefins was drastically lower than that of the (PCP)Ir catalysts. (Figure 2.7) For example the observed selectivity for 1-octene at the earliest time points of 2.5 and 5 minutes is approximately 50%. At longer time points that observed selectivity drops noticeably (38% at 45 minutes), most likely due to the effects of isomerization of 1-octene to 2-octenes.

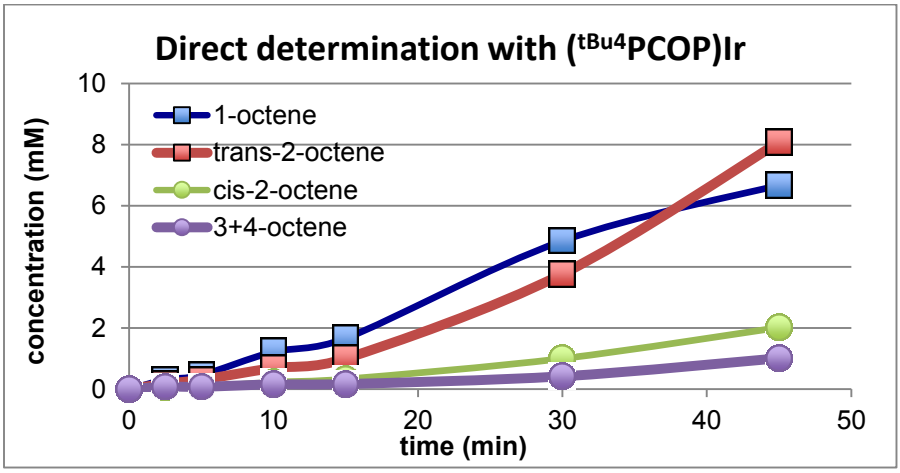

Figure 2.7 Direct determination with (^{tBu4}PCOP)Ir

In fact, the importance of olefin isomerization can be observed by examining the isomerization of the 1-hexene acceptor to 2-hexenes. (Figure 2.8). Compared with (^{tBu4}PCP)Ir, the dehydrogenation of *n*-octane is noticeable *slower* with (^{tBu4}PCOP)Ir but the isomerization of 1-

hexene to 2-hexenes is much *faster*. (Figures 2.1 and 2.9) Therefore, olefin isomerization might have played a large role in the low (~ 50%) *observed* selectivity for 1-octene by (^{tBu4}PCOP)Ir.

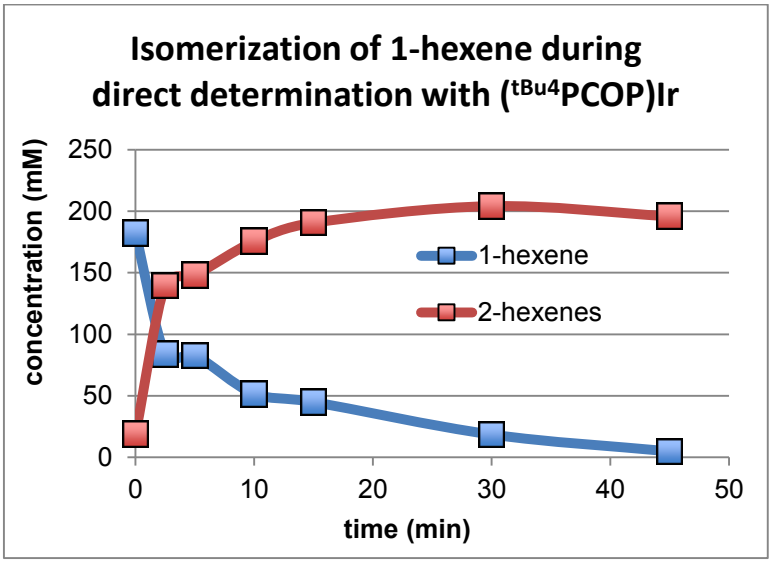

Figure 2.8 Isomerization of 1-hexene by (^{tBu4}PCOP)Ir during transfer dehydrogenation

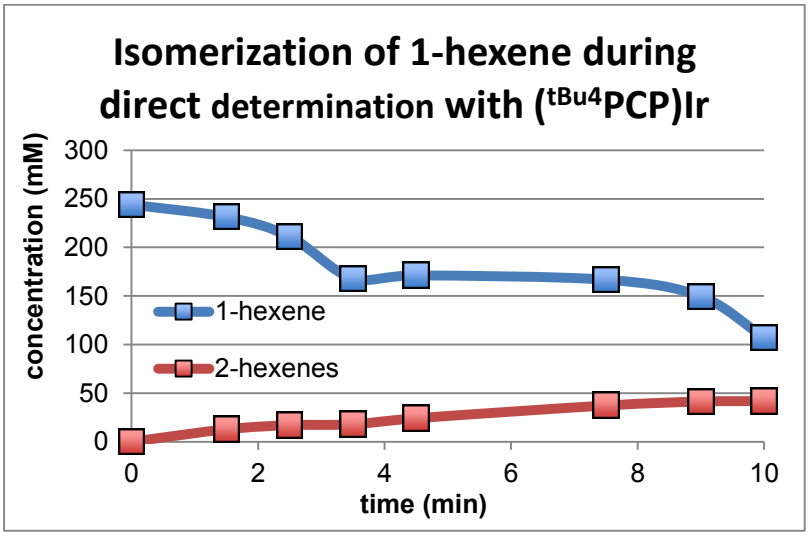

Figure 2.9 Isomerization of 1-hexene by (^{tBu4}PCP)Ir during transfer dehydrogenation

Attempts at using Copasi kinetic modeling to unravel this issue (whether the low observed selectivity was due to low regioselectivity during dehydrogenation or simply due to fast isomerization of 1-octene to 2-octenes) were unsuccessful. The fast rate of isomerization caused

a poor fit between the model and the experimental data. Hence, although a definitive conclusion could not be drawn, it did appear that the regioselectivity of (^{tBu4}PCOP)Ir was unequivocally *much* less than any of the PCP catalysts.

Since the difference in regioselectivity between (^{tBu4}PCP)Ir and (^{tBu4}PCOP)Ir was so large, this suggested that possibly some mechanistic aspect of the dehydrogenation pathways might have changed in a discrete way, as opposed to a gradual shift along a continuous spectrum. To make an analog, the Schrödinger equation predicts that the electron in a hydrogen atom will exist at a single, discrete energy level depending on which shell it inhabits (n = 1, 2, 3, etc.) whereas other aspects of physics (say, the wavelength of a photon) can fall anywhere along a continuous spectrum. The regioselectivity differences amongst the PCP catalysts ((^{tBu4}PCP)Ir at 96%, (^{iPr4}PCP)Ir at 91%) might be due to a gradual shift in sterics, whereas the difference between (^{tBu4}PCP)Ir and (^{tBu4}PCOP)Ir might come from an abrupt change due to so-far unidentified steric and/or electronic factors.

Hence, the mechanistic investigation into regioselectivity continued by examining the regioselectivity of (^{iPr4}PCOP)Ir (see Figure 1.3 for molecular structure) (Figure 2.10). The earliest time point of 2.5 minutes had an observed selectivity for 1-octene of 76% whereas the last time point of 60 minutes showed 47% selectivity. As a reminder, the initial selectivity of (^{tBu4}PCOP)Ir appeared much closer to 50%.

Using Copasi, the isomerization of 1-octene to 2-octenes was taken into account, giving an estimated true regioselectivity of 79% for (^{iPr4}PCOP)Ir. Notably, this regioselectivity is both significantly less than that of the (PCP)Ir catalysts (≥ 91%) but also much higher than (^{tBu4}PCOP)Ir (~ 50%). In general, it appears that changing from the PCP to PCOP ligand backbone causes significant steric and/or electronic changes which fundamentally alter how the dehydrogenation

transformation proceeds. Therefore, it would be worthwhile to continue this investigation and examine the regioselectivity of (POCOP)Ir catalysts.

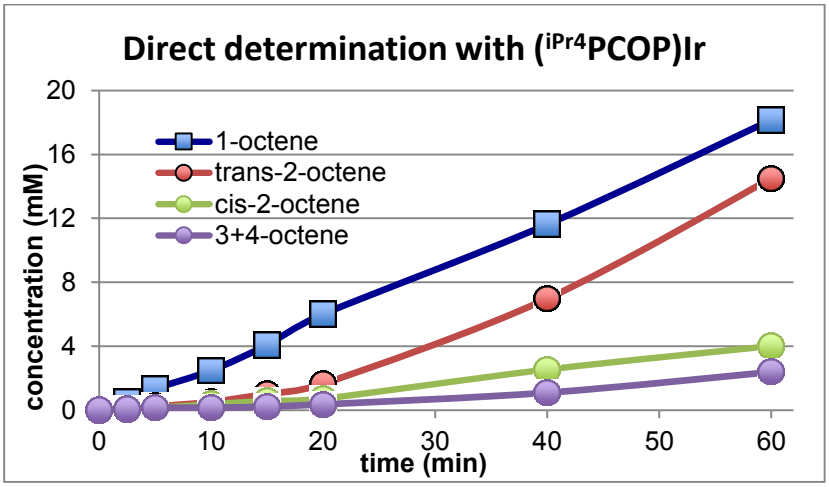

Figure 2.10 Direct determination with (^{iPr4}PCOP)Ir

In fact, the regioselectivity of (^{tBu4}POCOP)Ir had previously been investigated using the same 1-hexene/*n*-octane transfer dehydrogenation as in the current study (see Figure 1.3 for molecular structure).[2] Unfortunately, however, the results proved to be inconclusive. First, the observed selectivity for 1-octene over other octenes appeared to be roughly 50%. However, the transfer dehydrogenation reaction proceeded extremely slowly compared to reactions with PCP and PCOP catalysts, accomplishing less than one turnover after 210 minutes. Therefore, the actual concentrations measured by GC (up to 1.0 mM after 210 minutes) would have been relatively close to the detection limit of the GC (roughly 0.1 mM), making those values less reliable. In addition, examination of the isomerization of 1-hexene to 2-hexenes (roughly 190 mM over 200 minutes) demonstrated that catalytic isomerization was much faster than dehydrogenation. Therefore, it was very unclear whether the observed 2-octenes came from the dehydrogenation of *n*-octane or whether it came from isomerization of 1-octene. Thus, the 1-

hexene/*n*-octane transfer dehydrogenation with (^{tBu4}POCOP)Ir did not provide any conclusive evidence, or even any usable estimates, about its regioselectivity.

In conclusion, expansion of the regioselectivity studies from (PCP)Ir catalysts to (^{tBu4}PCOP)Ir and (^{iPr4}PCOP)Ir demonstrated that the (PCOP)Ir catalysts do have lower regioselectivity (< 91%), and that the change appears quite abrupt, possibly signifying a discrete mechanistic change. (Table 2.4) However, examination of (^{tBu4}POCOP)Ir did not lend additional insights because its rate of isomerization was *much* faster than its rate of transfer dehydrogenation, prohibiting any reliable estimations of its regioselectivity.

Catalyst	Regioselectivity for 1-olefins by direct determination
(^{tBu4}PCP)Ir	96%
(^{iPr4}PCP)Ir	91%
(MeO-^{tBu4}PCP)Ir	96%
(Me_2N-^{tBu4}PCP)Ir	96%
(^{tBu2}PCP^{iPr2})Ir	95%
(^{tBu4}PCOP)Ir	~ 50%
(^{iPr4}PCOP)Ir	79%
(^{tBu4}POCOP)Ir	inconclusive

Table 2.4 Regioselectivity estimates by direct determination

2.2.7 Attempted synthesis of (^{iPr4}POCOP)Ir

Since (^{tBu4}POCOP)Ir was too slow at transfer dehydrogenation to permit analysis of its regioselectivity, a search for another suitable (POCOP)Ir catalyst was conducted. Since (^{iPr4}PCP)Ir was faster at transfer dehydrogenation than its ^{t}Bu analog (^{tBu4}PCP)Ir, then (^{iPr4}POCOP)Ir might be more active for transfer dehydrogenation than (^{tBu4}POCOP)Ir. Thus, attempts were made at synthesizing (^{iPr4}POCOP)Ir.

The ligand was constructed in a single synthetic step with sodium hydride and diisopropylchlorophosphine in 93% yield.[13] (Scheme 2.12)

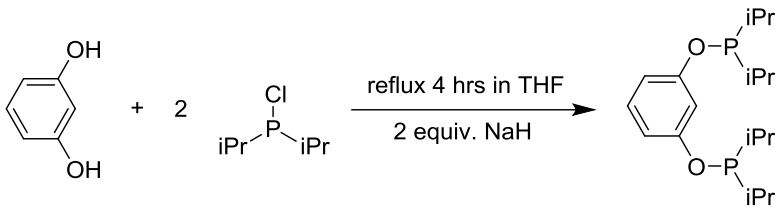

Scheme 2.12 Synthesis of ^{iPr4}POCOP ligand

However, successful metalation of the iridium complex proved to be significantly more difficult. Previously, it had been reported that the complex (^{iPr4}POCOP)IrH_4 had been successfully synthesized by metalation of the ligand by $[Ir(COE)_2Cl]_2$ (where COE = cyclooctene) and subsequent reduction by lithium triethylborohydride ($LiBHEt_3$).[17] However, attempts to follow this a dimeric hydridochloride product instead of the monomeric one reported in literature. (Scheme 2.13) In fact, repeating the experiment with $[Ir(COD)Cl]_2$ (where COD = cyclooctadiene) gave the same result. Notably, these reactions were conducted under an argon atmosphere. Attempts to form the hydride or ethylene complexes, using either $LiBHEt_3$ or NaO^tBu, paired with either hydrogen gas or ethylene, resulted in decomposition products and the disappearance of all peaks from the ^{31}P NMR spectrum.

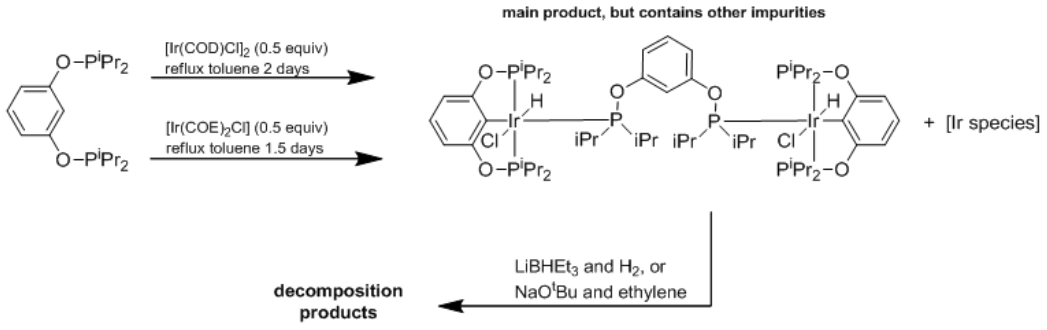

Scheme 2.13 Dimeric hydrodridochloride complex obtained upon metalation of ^{iPr4}POCOP ligand

Next, it was hypothesized that the kinetic product of metalation was actually the desired monomeric hydridochloride, but that high temperatures (i.e. refluxing toluene) and long reaction times allowed for the (undesirable) generation of the bridged dimer. Therefore, several metalation reactions were conducted at room temperature under argon with either $[Ir(COE)_2Cl]_2$, $[Ir(COE)_2Cl]_2$, or $[Ir(C_2H_4)_2Cl]_2$ (which was generated *in-situ*[18]) and the solvent was removed after 30 minutes to prevent further reaction. (Scheme 2.14) Interesting, reactions with different iridium precursors gave different metalation products. With $[Ir(COD)Cl]_2$, the ^{31}P NMR spectrum showed large peaks at 148.8 (free ligand), 143.2, and 140.9 ppm of similar intensities, possibly representing a dimeric complex (two iridium atoms, one ligand, inequivalent phosphorous atoms, possibly COD still coordinated) and free ligand. However, all attempts to obtain the ethylene or hydride complexes resulted in decomposition (as evidenced by blurred ^{1}H NMR spectra and the absence of all peaks in the ^{31}P NMR spectra).

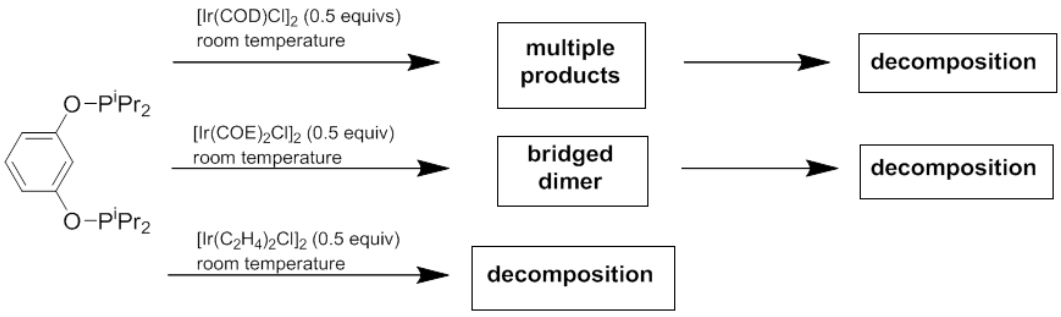

Scheme 2.14 Metalation of ^{iPr4}POCOP ligand at room temperature under argon

Metalation reactions were also conducted under H_2 in the hope that hydrogenating the COE/COD initially attached to the iridium might help obtain the desired monomeric hydridochloride complex. (Scheme 2.15) Experimentally, the ligand was dissolved in toluene in one flask while the iridium precursor was dissolved in toluene in another. Next, both flasks were placed under a hydrogen atmosphere for 10 minutes before the ligand solution was transferred

to the iridium-containing flask. Unexpectedly, however, after about 5 minutes under hydrogen the $[Ir(COE)_2Cl]_2$ solution changed color from clear and orangish-red to clear with black solids. Presumably, the $[Ir(COE)_2Cl]_2$ decomposed by hydrogenation of the COE moiety. Thus, that reaction was not conducted.

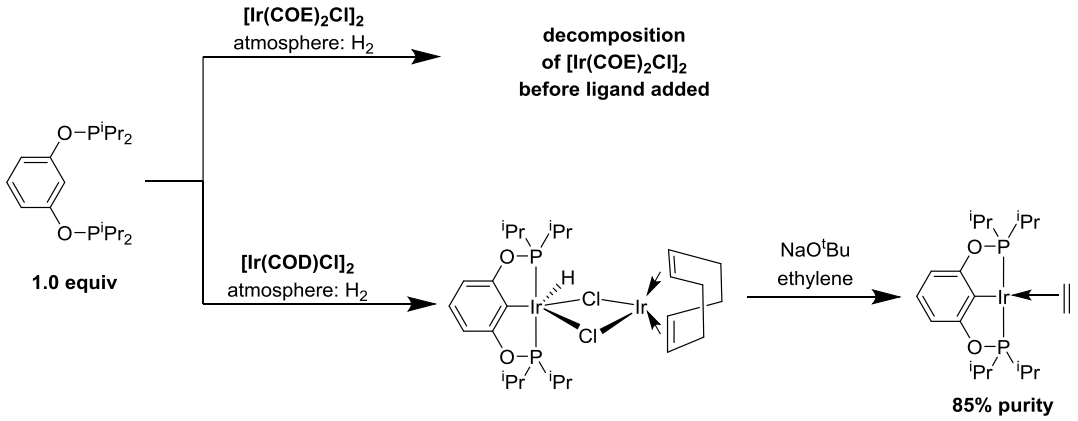

Scheme 2.15 Metalation of ^{iPr4}POCOP ligand under a hydrogen atmosphere

On the other hand, the reaction with $[Ir(COD)Cl]_2$ gave a single product with a ^{31}P NMR chemical shift of 153.3 ppm and a hydride in the ^{1}H NMR spectrum at -25 ppm (triplet). Although the structure of this complex could not be definitively identified, the presence of several peaks in the allylic and vinylic regions of the ^{1}H NMR spectra suggested that an additional COD molecule was present. Reaction of this complex with NaO^tBu and ethylene gave a new complex with a ^{31}P NMR shift of 183.9 ppm which appeared to be the desired ethylene complex. However, purity was only approximately 85%.

Alternate reduction strategies were also attempted, but decomposition resulted in each case. (Scheme 2.16) Reactions with ethylene gas and either lithium *tert*-butoxide or potassium *tert*-butoxide were completed, but decomposition resulted. Similarly, attempts to obtain the hydride complexes by reaction with $LiBHEt_3$ or $LiBH_4$ under hydrogen gas also gave decomposition products.

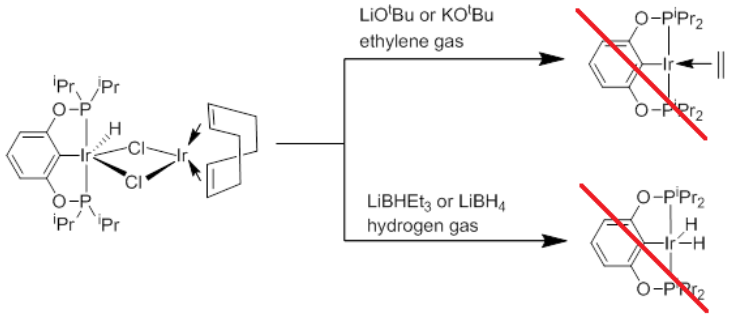

Scheme 2.16 Alternate strategies for reduction of monomeric (^{iPr4}POCOP)Ir hydridochloride complex

Lastly, attempts to purify the product obtained from Scheme 2.15 were made, but none were successful. Recrystallization experiments resulted in the formation of a thick gel instead of precipitating the desired solid. Column chromatography in an air-free environment resulted in decomposition, as seen by NMR. Thus, it appeared that a (^{iPr4}POCOP)Ir catalyst suitable for experimental testing could not be obtained.

2.2.8 Attempts at determining the regioselectivity for (^{iPr4}POCOP)Ir

Although the current attempt at synthesizing pure (^{iPr4}POCOP)Ir was unsuccessful, Chen Cheng of Professor Maurice Brookhart's group at the University of North Carolina also undertook the challenge of synthesizing (^{iPr4}POCOP)Ir.[19] They employed a strategy where the ^{iPr4}POCOP ligand was metalated on to iridium in the presence of a *secondary* ligand in order to form a stable 6-coordinate hydridochloride species. By performing the metalation reaction *in* pyridine, they successfully obtained the 6-coordinate hydridochloride pyridine species (^{iPr4}POCOP)Ir(H)(Cl)(pyridine). (Scheme 2.17) Then, reduction to the ethylene complex using the standard procedure (sodium *tert*-butoxide and ethylene) afforded pure (^{iPr4}POCOP)Ir(ethylene).

Afterwards, the *para*-methoxy analog (MeO-^{iPr4}POCOP)Ir(ethylene) was also synthesized through an identical procedure.

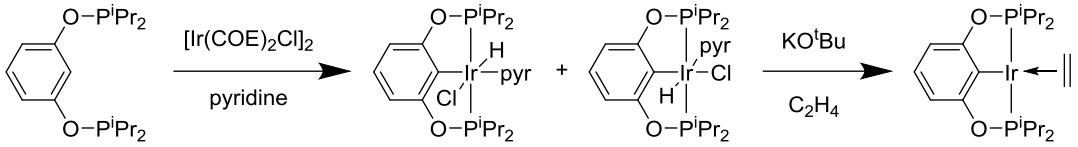

Scheme 2.17 Successful synthesis of (^{iPr4}POCOP)Ir(ethylene) complex[19]

After completing these syntheses, samples of both compounds were sent to Rutgers University for use in the regioselectivity project. Due to more mass of the *para*-MeO compound being available, the 1-hexene/*n*-octane transfer dehydrogenation study was conducted using (MeO-^{iPr4}POCOP)Ir(ethylene). Unfortunately, however, the results of these tests were inconclusive for the same reasons as with (^{tBu4}POCOP)Ir. Namely, while olefin isomerization proceeded well (roughly 100 mM of 1-hexene isomerized to 2-hexenes over 150 minutes), the rate of transfer dehydrogenation was undetectably slow (less than the GC's detection limit, 0.1 mM, over 150 minutes). Therefore, without the appearance of *any* octenes, assessing regioselectivity would obviously be impossible.

However, even if the reaction was heated at a higher temperature and/or for longer time periods, in order to obtain detectable quantities of octenes, then the results would not be useful for assessing regioselectivity. Many more turnovers of olefin isomerization would occur compared to alkane dehydrogenation, making it unclear whether any 2-octenes came from olefin isomerization or directly from dehydrogenation. Attempts to remedy this issue were made by conducting transfer dehydrogenation reactions with norbornene as the hydrogen acceptor, but isomerization was still much too fast compared to transfer dehydrogenation. Therefore, the regioselectivity of (^{iPr4}POCOP)Ir could not be determined through direct determination reactions.

Thus, the overall assessment of the regioselectivity of pincer iridium catalysts stood as it did before: (PCP)Ir catalysts had high regioselectivity (≥ 91%), the two (PCOP)Ir catalysts had markedly lower regioselectivity, and the two (POCOP)Ir catalysts studied continue to have unknown regioselectivity due to inconclusive results. (Table 2.5)

Catalyst	Regioselectivity for 1-olefins by direct determination
(^{tBu4}PCP)Ir	96%
(^{iPr4}PCP)Ir	91%
(MeO-^{tBu4}PCP)Ir	96%
(Me_2N-^{tBu4}PCP)Ir	96%
(^{tBu2}PCP^{iPr2})Ir	95%
(^{tBu4}PCOP)Ir	~ 50%
(^{iPr4}PCOP)Ir	79%
(^{tBu4}POCOP)Ir	inconclusive
(MeO-^{iPr4}POCOP)Ir	inconclusive

Table 2.5 Complete list of regioselectivity estimates by direct determination

2.3 Estimation of regioselectivity through competitive dehydrogenation reactions

2.3.1 Introduction to competitive dehydrogenation reactions

Since the utility of the 1-olefin/*n*-alkane reaction for assessing regioselectivity had been reached, another method of determining regioselectivity was required. Previous studies employed the competitive dehydrogenation reaction as a method of qualitatively examining the 1-olefins regioselectivity of (^{tBu4}PCP)Ir and (^{tBu4}POCOP)Ir.[2] Therefore, the current study aimed to employ the competitive dehydrogenation reaction to *quantitatively* assess the regioselectivity a wide range of pincer iridium catalysts, and thereby hopefully help elucidate the mechanism by which regioselectivity is determined.

The utility of competitive dehydrogenation relies on the fact that (unlike in direct determination) olefin isomerization does not interfere with the manner by which regioselectivity is estimated. Experimentally, a 1-olefin such as 1-hexene is used as the hydrogen acceptor while two different alkanes (one *n*-alkane and one cycloalkane) are also added to the reaction mixture. The term "competitive" refers to the fact that the 14 electron complex (pincer)Ir can either dehydrogenation the *n*-alkane or the cycloalkane, and therefore these two alkanes are "competing" against one another.

The estimation of regioselectivity relies on the fact that the *n*-alkane can be dehydrogenated either at the terminal position (with a methyl group) or internally (without a methyl group), whereas the cycloalkane can only be dehydrogenated at an internal position (without a methyl group). (Scheme 2.18)

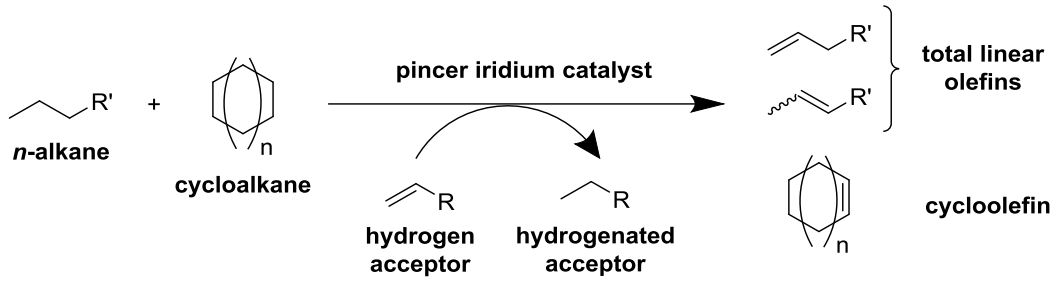

Scheme 2.18 Generalized form of competitive dehydrogenation reactions

Qualitatively, if a catalyst has high regioselectivity for generating 1-olefins, then it will only dehydrogenate the *n*-alkane giving a 1-olefins (which might then isomerization to 2-olefins). However, critically, the positions of the cycloalkane will appear similar to the internal position of the *n*-alkane). Therefore, a catalyst with high regioselectivity will be *much* slower at dehydrogenating the cycloalkane to give a cycloalkene than it will be at dehydrogenating the *n*-alkane into a linear olefin. (Figure 2.11) This logic can also be reversed: a catalyst which produces

much more linear olefins than cycloalkenes will most likely do so because of high regioselectivity for 1-olefins.

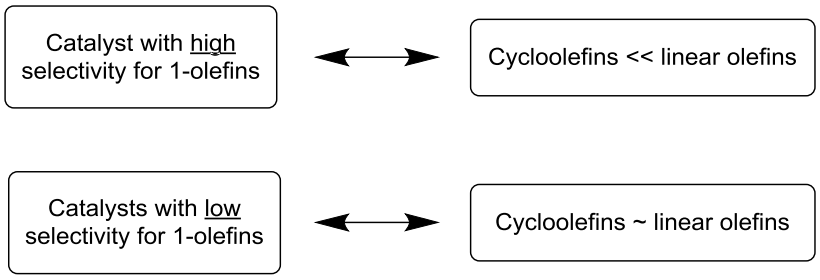

Figure 2.11 Relationship between regioselectivity and competitive dehydrogenation

In contrast, a catalyst with low regioselectivity for generating 1-olefins will perform all three types of dehydrogenations at relatively similar rates (1-olefins, 2-olefins, cycloalkenes). Thus, in this case the concentration of cycloalkenes generated will be fairly similar to the concentration of linear olefins.

2.3.2 Mathematical foundation of the competitive dehydrogenation analysis

However, this analysis is only *qualitative*, and can only roughly distinguish catalysts with high regioselectivity from those with low regioselectivity. Hence, a mathematical derivation can be used to provide *quantitative* estimations of regioselectivity.

First, the definition of regioselectivity for 1-olefins can be expressed mathematically as the ratio of the rate constant for production of the 1-olefins (k_{dh1}) to the sum of rate constants for all possible olefins. (Equation 2.4) Due to the experimental observation that only 1-olefins and 2-olefins were produced, and to simplify the analysis, only the rate constants for production of *cis*-2-olefins (k_{dhcis2}) and *trans*-2-olefins ($k_{dhtrans2}$) were included in the equation and not 3- or 4- or n-olefins.

Next, the rate of change of the *n-olefins* can also be expressed mathematically as their increase due to dehydrogenation of the *n*-alkane, and decrease due to hydrogenation back to the *n*-alkane or due to further dehydrogenation to a diene. (Equation 2.24)

$$\frac{d[pentenes]}{dt} = dehydrogenation - hydrogenation - (further\ dehydrogenation\ to\ diene)$$

Equation 2.24 Change in concentration of pentenes

Experimentally, the direct dehydrogenation reactions showed that both hydrogenation and diene formation were very slow compared to the dehydrogenation of the *n*-alkane, so the change in *n*-olefins can be approximated as the changes due to dehydrogenation. (Equations 2.25 through 2.28) Rearrangement of this equation gives an expression for k_{dh1}.

$$\frac{d[pentenes]}{dt} \approx dehydrogenation$$

$$\frac{d[pentenes]}{dt} \approx \{k_{dh1} + k_{dhcis2} + k_{dhtrans2}\} * [Ir] * [pentane]$$

$$k_{dh1} * [Ir] * [pentane] \approx \frac{d[pentenes]}{dt} - \{k_{dhcis2} + k_{dhtrans2}\} * [Ir] * [pentane]$$

$$k_{dh1} \approx \frac{\frac{d[pentenes]}{dt}}{[Ir] * [pentane]} - \{k_{dhcis2} + k_{dhtrans2}\}$$

Equations 2.25 through 2.28 Expression for rate constant k_{dh1}

Next, the definition of regioselectivity (Equation 2.3) and the expression for k_{dh1} can be combined to give a new expression for regioselectivity. (Equations 2.29 and 2.30) The objective

is to remove rate constants that cannot be measured directly (such as k_{dh1} due to olefin isomerization) from the equation for regioselectivity.

$$Regioselectivity \approx \frac{\frac{\frac{d[pentenes]}{dt}}{[Ir]*[pentane]} - \{k_{dhcis2} + k_{dhtrans2}\}}{\frac{\frac{d[pentenes]}{dt}}{[Ir]*[pentane]} - \{k_{dhcis2} + k_{dhtrans2}\} + k_{dhcis2} + k_{dhtrans2}}$$

$$Regioselectivity \approx \frac{\frac{\frac{d[pentenes]}{dt}}{[Ir]*[pentane]} - \{k_{dhcis2} + k_{dhtrans2}\}}{\frac{\frac{d[pentenes]}{dt}}{[Ir]*[pentane]}}$$

Equations 2.29 and 2.30 Rearranged expression for regioselectivity

Moving forward, the change in concentration of cyclododecenes can also be expressed using the rate constants for generation of *cis*-cyclododecene and *trans*-cyclododecene. (Equation 2.31)

$$\frac{d[cyclododecene]}{dt} \approx \{k_{dhciscyclododecene} + k_{dhtranscyclododecene}\} * [Ir] * [cyclododecane]$$

Equation 2.31 Rate of change in concentration of cyclododecenes

Notably, these rate constants for the generation of *cyclic* olefins, which are obviously not the same as the *linear* olefins involved with the regioselectivity equation. Hence, they must also be removed from the expression. Fortunately, since the transition state (and therefore rate constant) for generating a *cis*-2-olefins would be expected to be very similar (steric and electronically) to that for generating a *cis*-cycloolefins, then the rate constants for those two reactions can be assumed to be very similar. (Equations 2.32 through 2.35) Likewise, the same

can be safely assumed for *trans*-2-olefins and *trans*-cycloolefins. Hence, the change in cyclododecenes concentration can be expressed as a function of the rate constants for generating *linear* 2-olefins. Rearranging the equation can also express the sum of the two rate constants as a function of the change in cyclododecenes, the concentration of iridium catalyst, and the concentration of cyclododecane.

$$k_{dhcis2} \approx k_{dhciscyclododecene}$$

$$k_{dhtrans2} \approx k_{dhtranscyclododecene}$$

$$\frac{d[cyclododecene]}{dt} \approx \{k_{dhcis2} + k_{dhtrans2}\} * [Ir] * [cyclododecane]$$

$$k_{dhcis2} + k_{dhtrans2} \approx \frac{\frac{d[cyclododecene]}{dt}}{[Ir] * [cyclododecane]}$$

Equations 2.32 through 2.35 Relating production of 2-olefins to generation of cycloolefins

Finally, this equation can inserted into the previous (Equation 2.30) to thereby *remove all rate constants from the regioselectivity equation*. (Equation 2.36) This is the critical step because none of the rate constants related to *n*-olefins can be accurately determined if olefin isomerization happens at a significant rate (which *was* indeed happening with (PCOP)Ir and (POCOP)Ir catalysts during the direct determination experiments).

$$Regioselectivity \approx \frac{\frac{d[pentenes]}{dt}}{[Ir] * [pentane]} - \frac{\frac{d[cyclododecene]}{dt}}{[Ir] * [cyclododecane]}}{\frac{\frac{d[pentenes]}{dt}}{[Ir] * [pentane]}}$$

Equation 2.36 Estimation of regioselectivity using competitive dehydrogenation

While the above equation may look complex and intimidating at first, its simplification is trivial. First, the concentration of the pincer iridium catalyst can be cancelled from each of the three denominators. Next, since the GC instrument used has a detection limit of ~ 0.1 mM then high quality kinetics data can be collected at conversions of ≤ 50 mM. Therefore, since no more than 50 mM of a given alkane is lost (to dehydrogenation), then the concentration of each alkane never drops below 0.95 M, or 5% of its starting value. Hence, within experimental error the concentration of both *n*-pentane and cyclododecane can be assumed to be 1.0 M. Therefore, the final equation expresses regioselectivity in terms of only the rate of change in pentenes and the rate of change in cyclododecenes, both of which are readily and directly measured by GC. (Equations 2.37 through 2.39)

$$[pentane] \approx 1.0\ M$$

$$[cyclododecane] \approx 1.0\ M$$

$$Regioselectivity \approx \frac{\frac{d[pentenes]}{dt} - \frac{d[cyclododecene]}{dt}}{\frac{d[pentenes]}{dt}}$$

Equation 2.37 through 2.39 Simplified estimation of regioselectivity using competitive dehydrogenation

Therefore, Equation 2.39 provides a *quantitative* method for estimating the regioselectivity for 1-olefins of a given pincer iridium catalyst. In addition, evaluation of Equation 2.39 verifies the *qualitative* analyses mentioned above. If the rate of cyclododecenes production is very low (i.e. 10% of the pentene rate), then the estimated regioselectivity is very high (i.e. 90%). In contrast, if the rate of cyclododecenes generation is much higher (i.e. 60% of pentenes rate), then the estimated regioselectivity is much lower (i.e. 40%).

In effect, this is very similar to the way that enantiomeric excess is expressed through the variable "ee." If two enantiomers are generated in equimolar amounts (i.e. the mixture is racemic), then it is said that ee = 0%. With regioselectivity, if 1-olefins and 2-olefins are present in equimolar amounts then regioselectivity = 0%. Notably, ee values are always either zero or positive (due to taking an absolute value) whereas this regioselectivity estimation could technically return a negative value if the rate for cyclododecenes production was *greater* than that of pentenes generation. However, this could only ever happen if dehydrogenation of cyclododecane to form cyclododecenes was *easier and faster* that the dehydrogenation to give either 1-pentene or 2-pentenes.

2.3.3 Competitive dehydrogenation with (PCP)Ir catalysts

With a firmly established mathematical description about how competitive dehydrogenation can be used to estimate the regioselectivity of dehydrogenation for 1-olefins, actual competitive dehydrogenation reactions were begun. First, the five (PCP)Ir catalysts studied during the direct determination section were also analyzed in competitive dehydrogenation. (Scheme 2.19) Cyclododecane was selected as the cycloalkane due its large size, and the good separation on the GS-GASPRO column between cyclododecane and its corresponding cyclododecene isomers (cis and trans). The large size of cyclododecane was important due to the effects of ring strain. Presumably, the many possible conformers would cause it to have lower ring strain than smaller cycloalkanes such a cyclohexane. While the ring strain of the cycloalkane is not important by itself, it was the *change* in ring strain upon dehydrogenating it to a cycloolefin that is important. According to the Hammond postulate, release (or increase) of too much ring strain during dehydrogenation would make the kinetic barrier to dehydrogenation of the

cycloalkane artificially low (or high) relative to the barrier for the *n*-alkane. Thus, this could invalidate the approximation of Equation 2.39, thereby skewing the regioselectivity estimate of Equation 2.39.

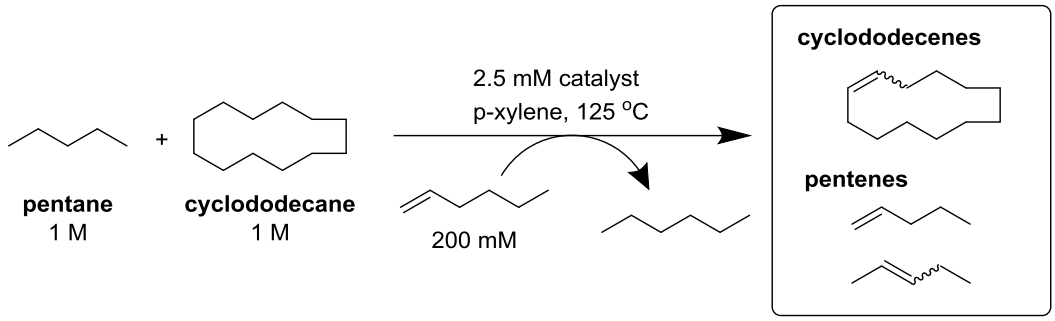

Scheme 2.19 Experimental conditions used during competitive dehydrogenation

(^{tBu4}PCP)Ir, the first pincer iridium catalyst to be examined, strong production of pentenes and much slower generation of cyclododecenes. (Figure 2.12) Although not listed in Figure 2.12, most of the pentenes generated at the earlier time points were in-fact 1-pentenes. Regardless, qualitatively the low quantity of cyclododecenes suggests high regioselectivity for (^{tBu4}PCP)Ir. Linear regressions gave rates were 0.0676 and 0.0070 mM/min for the pentenes and cyclododecenes, respectively. This gave an estimated regioselectivity estimate of 90%.

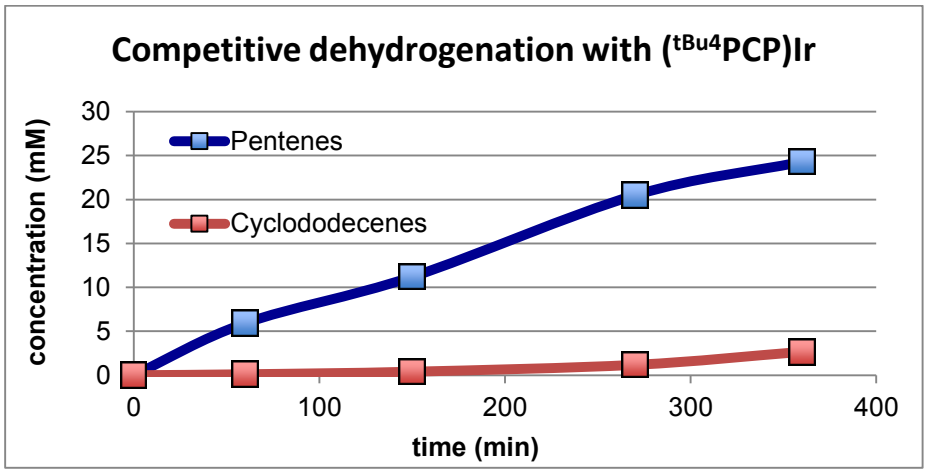

Figure 2.12 Competitive dehydrogenation with (^{tBu4}PCP)Ir

However, closer inspection showed that the production of cyclododecenes was not linear. (Figures 2.13 and 2.14) Using a linear regression with only the first few data points, the new regioselectivity estimate was 96%, in strong agreement with the direct determination results.

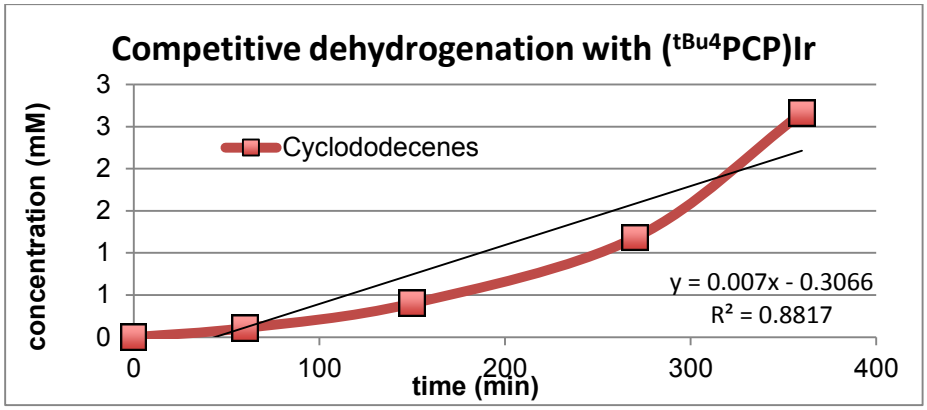

Figure 2.13 Cyclododecene production by (^{tBu4}PCP)Ir over 360 minutes

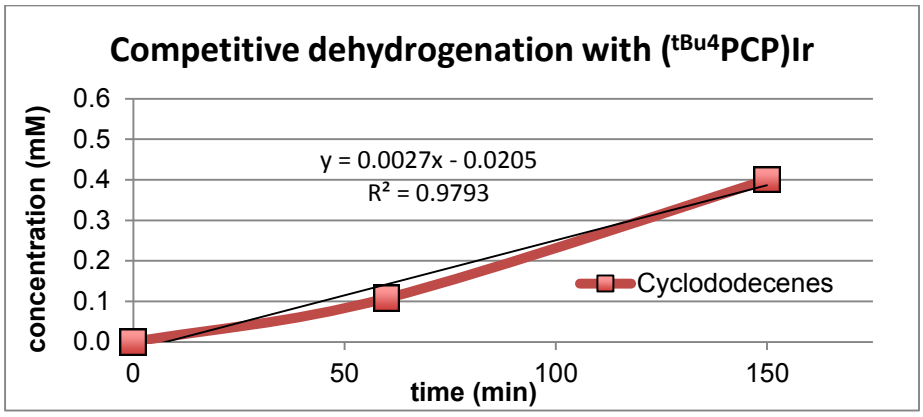

Figure 2.14 Cyclododecene production by (^{tBu4}PCP)Ir over 150 minutes

Next, the *para*-functionalized catalysts (MeO-^{tBu4}PCP)Ir and (Me_2N-^{tBu4}PCP)Ir were examined for their regioselectivity in the competitive dehydrogenation reaction. As previously described above, these *para*-functionalized catalysts would be expected to have nearly identical sterics to that of the parent catalyst (^{tBu4}PCP)Ir, but the electronics in their aryl rings would be

decidedly different. Thus, assessing their regioselectivity might help identify whether that electronic factor was important in determining regioselectivity.

Like the parent catalyst (^{tBu4}PCP)Ir, (MeO-^{tBu4}PCP)Ir showed strong production of pentenes and very slow generation of cyclododecenes. (Figure 2.15) Linear regressions estimated rates of 0.0319 and 0.0008 mM/min for pentenes and cyclododecenes, respectively, giving an estimated regioselectivity of 97%, in excellent agreement with the 96% estimation of (MeO-^{tBu4}PCP)Ir from the direct determination experiment.

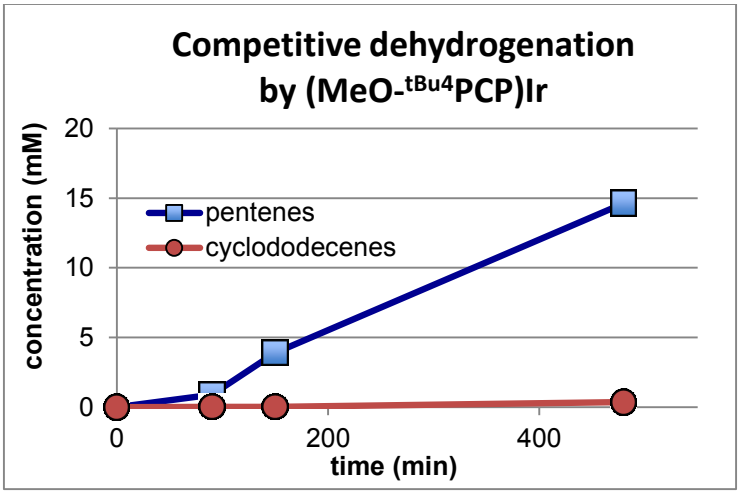

Figure 2.15 Competitive dehydrogenation with (MeO-^{tBu4}PCP)Ir

Moving onwards, (Me_2N-^{tBu4}PCP)Ir was also examined with the competitive dehydrogenation reaction. The linear regressions were a good fit for the GC data, giving rates of 0.0485 and 0.0018 mM/min for pentenes and cyclododecenes, respectively. The estimated regioselectivity for (Me_2N-^{tBu4}PCP)Ir was 96%, in perfect agreement with the 96% estimated with the direct determination method.

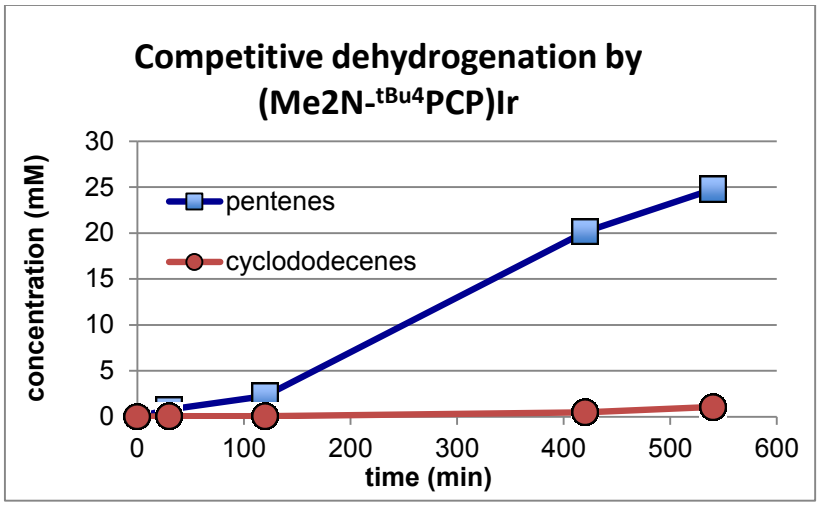

Figure 2.16 Competitive dehydrogenation with (Me_2N-^{tBu4}PCP)Ir

Hence, comparison of the estimated regioselectivities of (^{tBu4}PCP)Ir, (MeO-^{tBu4}PCP)Ir, and (Me_2N-^{tBu4}PCP)Ir show that all three catalysts have nearly identical regioselectivity values (given experimental error) in the ~96% region. Chemically, this suggested that either the effects of electronics from the aryl ring are not a factor which determines regioselectivity.

Next, the role of sterics in determining regioselectivity was investigated by examining the (^{tBu2}PCP^{iPr2})Ir and (^{iPr4}PCP)Ir catalysts for their behavior during competitive dehydrogenation. With (^{tBu2}PCP^{iPr2})Ir, production of pentenes was once again much faster than cyclododecenes, suggesting high regioselectivity. (Figure 2.17) Linear regressions gave rates of 0.516 and 0.039 mM/min, for pentenes and cyclododecenes, respectively, and a regioselectivity estimated of 93%. For comparison, regioselectivity estimate from the direct determination experiments was 95%.

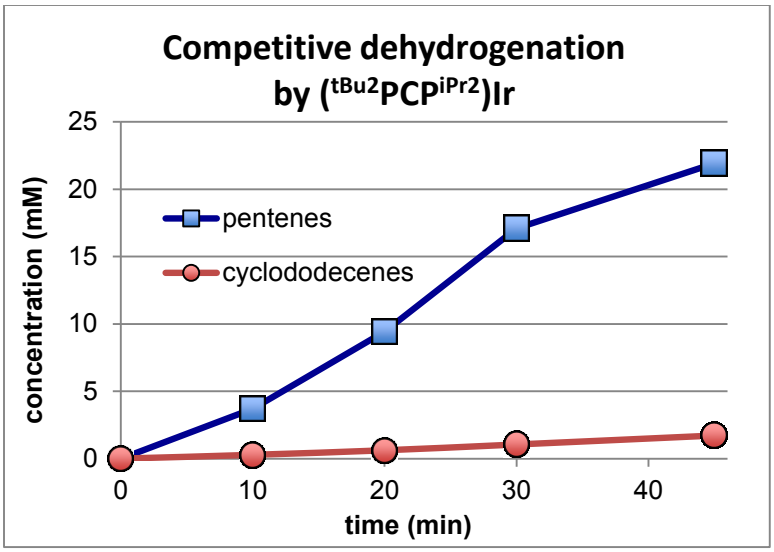

Figure 2.17 Competitive dehydrogenation with (^{tBu2}PCP^{iPr2})Ir

While the differences between the competitive dehydrogenation result from (^{tBu2}PCP^{iPr2})Ir (93%) and the three (PCP)Ir catalysts with four ^{t}Bu groups (96%) may not seem statistically significant at first, the difference appears to be very real. To put it another way, it appears that this 3% difference represents a true difference in regioselectivity and not simply random error.

Next, competitive dehydrogenation with (^{iPr4}PCP)Ir was performed, showing strong production of pentenes and slow generation of cyclododecenes. (Figure 2.18) Linear regressions gave rates of 0.374 and 0.034 mM/min for pentenes and cyclododecenes, respectively. The estimated regioselectivity was 91%, identical to the 91% obtained from the direct determination experiment.

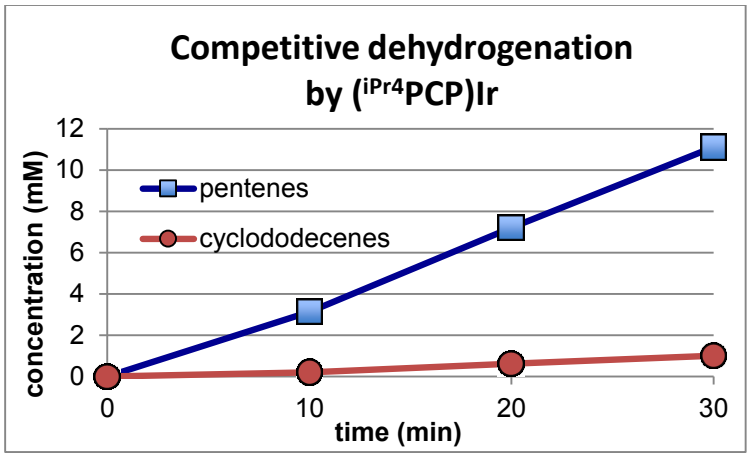

Figure 2.18 Competitive dehydrogenation by (^{iPr4}PCP)Ir

Hence, at this stage five (PCP)Ir catalysts had been examined through the competitive dehydrogenation reaction, yielding estimates of their regioselectivities that were in nearly perfect agreement with the values obtained from the direct determination method. Thus, this confirmed the reliability of the competitive dehydrogenation analysis.

2.3.4 Competitive dehydrogenation with (PCOP)Ir catalysts and (^{tBu4}POCOP)Ir

Next, the competitive dehydrogenation analysis was continued by examining the (PCOP)Ir and (POCOP)Ir catalysts.

In contrast to all (PCP)Ir catalysts studied, the competitive dehydrogenation with (^{tBu4}PCOP)Ir produced large quantities of cyclododecenes. (Figure 2.19) In fact, the quantity of cyclododecenes observed was actually *larger* than that of pentenes. Hence, on a qualitative level, it is clear that (^{tBu4}PCOP)Ir had *much* lower regioselectivity for 1-olefins than the (PCP)Ir catalysts. Numerically, linear regressions gave 0.051 and 0.063 mM/min for the production of pentenes and

cyclododecenes respectively. In turn, this actually gave a regioselectivity estimation of -24% (negative!).

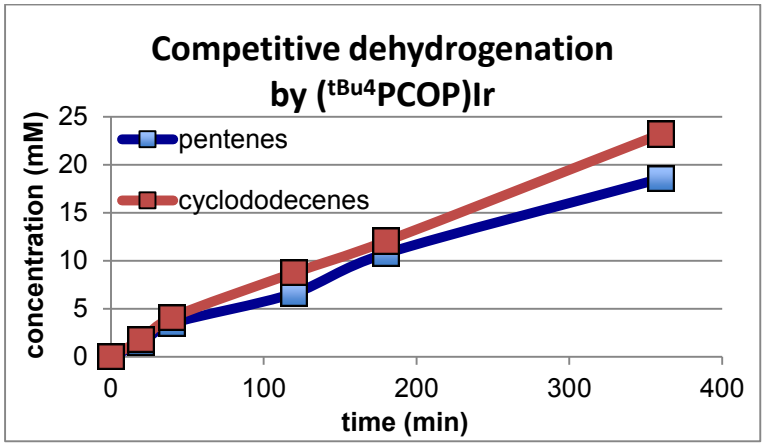

Figure 2.19 Competitive dehydrogenation by (^{tBu4}PCOP)Ir

Understanding this seemingly counterintuitive result of a -24% regioselectivity requires a detailed examination of Equation 2.39 and cyclododecane. First, it is by-definition impossible to have a negative regioselectivity for 1-olefins because that would imply that dehydrogenation is actually *consuming* 1-olefins while also producing 2-olefins. While it is true that *transfer* dehydrogenation is consuming the 1-olefins acceptor of 1-hexene in the 1-hexene/*n*-octane transfer dehydrogenation, this is *not* the same phenomenon as a true negative regioselectivity.

Therefore, it is important to understand which part of the mathematical derivation of Equation 2.39, which began with the very definition of regioselectivity (Equation 2.4), caused this estimating of an impossible result. Based on the direct determination experiments, it seems that ignoring the hydrogenation of newly-produced olefin and their further dehydrogenation to dienes was a reasonable and safe assumption to make. In contrast, it is not known whether the rate of dehydrogenation to give a 2-olefins would be the same as that for giving a cycloolefin. (Equation 2.32 through 2.35)

First, the dehydrogenation to give a 2-olefins versus a cycloolefin should be nearly identical on an electronic level, and therefore electronics should not have caused the observed negative regioselectivity estimate. Next, the steric crowding during dehydrogenation would presumably be *greater* for that of a cycloalkane than that of an *n*-alkane, leading to a smaller rate constant for the cycloalkane (i.e. $k_{dhcis2} > k_{dhciscyclododecene}$). In turn, this should lead to *faster* generation of 2-pentenes (and therefore also total pentenes) than cyclododecenes, which was the *opposite* of what was observed during competitive dehydrogenation with (^{tBu4}PCOP)Ir. Therefore, steric crowding during the dehydrogenation transition state could not account for the negative regioselectivity estimate.

However, the negative regioselectivity estimate could have plausibly been caused by the release of ring strain from cyclododecane upon its dehydrogenation to cyclododecenes. It has been well documented that most cycloalkanes are less thermodynamically stable than they would be based upon the enthalpy of their C-C and C-H bonds alone, and this discrepancy has been attributed to "ring strain."[20] In detail, ring strain refers to two thermodynamically unfavorable aspects of cyclic molecules. In general, these two aspects are caused by the cyclic nature of these molecules putting more geometric constraints on the position of each atom within the molecule than more flexible linear molecules. On one hand, this causes increased steric repulsion between hydrogen atoms which are forced into closer proximity with each other than in linear alkanes. Secondly, "angle strain" is caused when the bonds attaching one atom to other atoms bend away from their most stable VSEPR-predicted geometries in order to limit the steric repulsion mentioned before. For example, a sp^3 carbon with four bonds is predicted by VSEPR theory have 120° angles between each of its bonds. However, if one of those angles decreased to 105° to limit steric repulsion between nearby atoms, then this would cause non-optimal overlap between the

hybridized orbitals of the carbon and its bonding partners, reducing the thermodynamic stability of the molecule.

Hence, removing two hydrogens from a cyclic molecule (such as cyclododecane) would both eliminate the steric repulsions experienced by (and due to) those hydrogens, and it would also change the hybridization of those two carbons (i.e. sp^3 to sp^2) and therefore their optimal VSEPR-predicted geometries. Thermochemical data shows that for all common cycloalkanes, these dehydrogenations cause a net decrease in ring strain (being steric repulsion and angle strain).[21] (Table 2.6)

Cycloalkane	Number of carbon atoms	Ring strain (kcal/mol)
Cyclopropane	3	27.5
Cyclobutane	4	26.3
Cyclopentane	5	6.2
Cyclohexane	6	0.1
Cycloheptane	7	6.2
Cyclooctane	8	9.7
Cyclononane	9	12.6
Cyclodecane	10	12.4
Cycloundecane	11	11.3
Cyclododecane	12	4.1
Cyclotridecane	13	5.2
Cyclotetradecane	14	1.9
Cyclopentadecane	15	1.9
Cyclohexadecane	16	2.0

Table 2.6 Ring strain of common cycloalkanes

Returning to the competitive dehydrogenation with (^{tBu4}PCOP)Ir, the release of angle strain energy upon dehydrogenation of cyclododecane to cyclododecenes could decrease the associated kinetic barrier. In turn, this could make the dehydrogenation of cyclododecane *faster* than the dehydrogenation of *n*-pentane to 2-pentenes (i.e. $k_{dhcis2} > k_{dhciscyclododecene}$), despite the sterics and electronics of those two reactions appearing very similar upon initial inspection.

Therefore, the release of ring strain could account for the impossible estimation of -24% regioselectivity.

It is notable, however, that each of the (PCP)Ir catalysts also faced this same "ring strain bias" which "encouraged" them to dehydrogenation cyclododecane to cyclododecenes. However, the competitive dehydrogenation analysis with PCP catalysts still returned regioselectivity estimates that were nearly identical to the direct determination results, which by definition were measuring regioselectivity directly. Therefore, the ring strain bias experienced by PCP catalysts was not sufficiently strong to skew the results of the competitive dehydrogenation analysis. Thus, although the -24% result obtained for (^{tBu4}PCOP)Ir is obviously not numerically correct, it does strongly suggest that (^{tBu4}PCOP)Ir does have a *much* lower regioselectivity than any of the (PCP)Ir catalysts.

Moving forward, the regioselectivity of (^{iPr4}PCOP)Ir was also estimated through the competitive dehydrogenation reaction. (Figure 2.20) Like (^{tBu4}PCOP)Ir there was significant production of cyclododecenes by (^{iPr4}PCOP)Ir, but unlike (^{tBu4}PCOP)Ir the rate of cyclododecenes generation by (^{iPr4}PCOP)Ir was *less* than that of pentenes. Specifically, rates of 0.047 and 0.029 mM/min were obtained for generation of pentenes and cyclododecenes, respectively. Using Equation 2.39 gave an estimated regioselectivity of 38%.

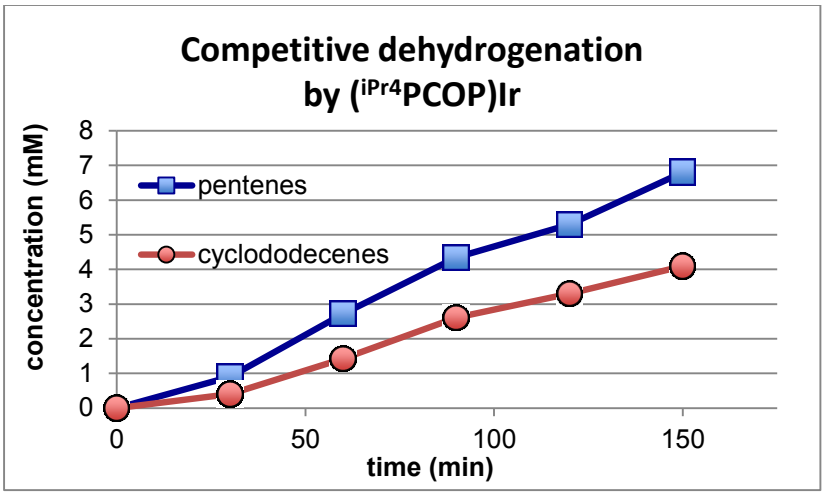

Figure 2.20 Competitive dehydrogenation by (^{iPr4}PCOP)Ir

Notably, the estimated regioselectivity of 38% for (^{iPr4}PCOP)Ir from competitive dehydrogenation was much lower than the 79% measured during direct determination. As was discussed during the results with (^{tBu4}PCOP)Ir, the release of ring strain during dehydrogenation of cyclododecane may account for the unexpectedly faster rate of cyclododecenes generation, and therefore the unexpectedly low regioselectivity estimate.

One the upside, however, these results *do* paint a *qualitatively* consistent picture of the regioselectivity of (PCOP)Ir catalysts. In both analyses (^{iPr4}PCOP)Ir had a noticeably lower regioselectivity than that of all five (PCP)Ir catalysts, and in turn (^{tBu4}PCOP)Ir had a significantly lower regioselectivity than (^{iPr4}PCOP)Ir. Interestingly, the pattern for (PCP)Ir catalysts wherein less steric bulk leads to less regioselectivity ((^{tBu4}PCP)Ir at 96% versus (^{iPr4}PCP)Ir at 91%) does not hold with (PCOP)Ir catalysts, and conversely the less stericly crowded (^{iPr4}PCOP)Ir actually has *higher* regioselectivity than the more crowded (^{tBu4}PCOP)Ir.

Finally, the regioselectivity of (^{tBu4}POCOP)Ir was also examined through the competitive dehydrogenation reaction. (Figure 2.21) Noticeably, the reaction yielded extremely low quantities of both pentenes and cyclododecenes that were barely above the detection limit of the

GC. Presumably, the same mechanistic aspect which had slowed the direct determination reaction with (^{tBu4}POCOP)Ir also slowed the catalyst during the competitive dehydrogenation reaction. As discussed in the section regarding DFT-assisted design of more active dehydrogenation catalysts, this mechanistic aspect was found to be the extremely stable (^{tBu4}POCOP)Ir(1-olefin) catalytic resting state.

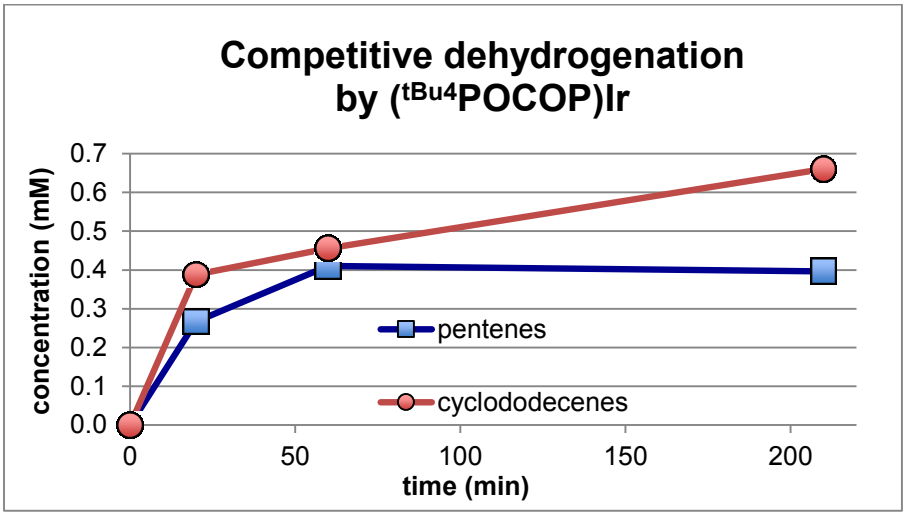

Figure 2.21 Competitive dehydrogenation by (^{tBu4}POCOP)Ir

Regardless of this low conversion, however, the relative rates of pentenes and cyclododecenes production could still be used to estimate regioselectivity. Given that cyclododecenes production was faster than pentenes generation, Equation 2.39 would estimate a negative regioselectivity (similarly to the result with (^{tBu4}PCOP)Ir). As described previously, it appears that the release of ring strain during dehydrogenation of cyclododecane to cyclododecenes caused that reaction to be faster than the one for generating 2-pentenes, skewing the numerical estimate regioselectivity. Regardless, however, this does qualitatively confirm that (^{tBu4}POCOP)Ir has a significantly lower regioselectivity than any of the (PCP)Ir catalysts, and also a lower regioselectivity than (^{iPr4}PCOP)Ir. The current data cannot conclusively determine whether (^{tBu4}PCOP)Ir or (^{tBu4}POCOP)Ir have higher or lower regioselectivities.

Moving forward, the competitive dehydrogenation reaction could have been also applied to (^{iPr4}POCOP)Ir or its *para*-methoxy analog. However, since its rate of transfer dehydrogenation would likely be even slower than with (^{tBu4}POCOP)Ir (based on results during the direct determination experiments), then it was decided that testing (^{iPr4}POCOP)Ir through competitive dehydrogenation would not be worthwhile.

2.4 Summary

Thus, the totality of these experimental studies (both direct determination and competitive dehydrogenation) gave consistent qualitative and, in some cases, quantitative measures of regioselectivity the dehydrogenation for 1-olefins. (Table 2.7) All of the (PCP)Ir catalysts with four ^{t}Bu groups showed 96% or 97% regioselectivity for both of the analysis methods used. Functionalization of (^{tBu4}PCP)Ir with a *para*-methoxy or *para*-dimethylamino group had no discernable effect on observed regioselectivity. However, changing the steric bulkiness of the (PCP)Ir ligand by substituting either two or four ^{i}Pr groups for the ^{t}Bu groups *did* lead to decreases in regioselectivity. However, even those most stericly open (PCP)Ir catalyst still had high regioselectivity of 91%.

Catalyst	Regioselectivity for 1-olefins by direct determination	Regioselectivity for 1-olefins by competitive dehydrogenation
(^{tBu4}PCP)Ir	96%	96%
(^{iPr4}PCP)Ir	91%	91%
(MeO-^{tBu4}PCP)Ir	96%	97%
(Me_2N-^{tBu4}PCP)Ir	96%	96%
(^{tBu2}PCP^{iPr2})Ir	95%	93%
(^{tBu4}PCOP)Ir	~ 50%	"-24%" or very low
(^{iPr4}PCOP)Ir	79%	"38%" or low
(^{tBu4}POCOP)Ir	inconclusive	very low
(MeO-^{iPr4}POCOP)Ir	inconclusive	not examined

Table 2.7 Regioselectivity estimates by both direct determination and competitive dehydrogenation

Due to fast olefin isomerization, the regioselectivity of (PCOP)Ir catalysts was more difficult to measure through the direct determination method than for (PCP)Ir catalysts. However, estimated regioselectivities of ~50% for (^{tBu4}PCOP)Ir and 79% for (^{iPr4}PCOP)Ir were found. Analysis with competitive dehydrogenation reactions was complicated by the fact that one of the underlying assumptions (dehydrogenation to give cyclododecenes would proceed at same rate as to give 2-pentenes) proved to be incorrect. However, qualitative analysis still showed that (^{iPr4}PCOP)Ir had significantly lower regioselectivity than the (PCP)Ir catalysts, and (^{tBu4}PCOP)Ir had an even lower regioselectivity than (^{iPr4}PCOP)Ir.

Lastly, analysis of the regioselectivity of (POCOP)Ir catalysts proved to be even more difficult than with (PCOP)Ir catalysts, primary because of the extremely slow transfer dehydrogenation rate (and moderately fast olefin isomerization) of these catalysts in reactions with 1-olefin hydrogen acceptors. In particular, the direct determination experiments for (^{tBu4}POCOP)Ir and (MeO-^{iPr4}POCOP)Ir were inconclusive. Next, analysis with the competitive dehydrogenation reaction proved to be equally problematic due to extremely slow

dehydrogenation rates. However, enough conversion for (^{tBu4}POCOP)Ir during competitive dehydrogenation was obtained to show that its regioselectivity was very low and similar to that of (^{tBu4}PCOP)Ir.

2.5 Experimental

2.5.1 General considerations

All manipulations were performed either in a glovebox or on a Schlenk line under an inert atmosphere of dry argon. Except for $^{i}Pr_2PCl$ and $^{t}Bu_2PCl$, which were purchased from Strem Chemicals, all reagents and solvents were obtained from Aldrich. For catalytic experiments, all solvents and liquid reagents were degassed by three freeze-pump-thaw cycles, dried by stirring over either sodium-potassium alloy (NaK) or activated alumina for 12 h, and finally distilled under vacuum using Schlenk techniques. For synthetic reactions, all solvents and liquid reagents were degassed by bubbling argon through the liquid for 20 min. (^{tBu4}PCP)Ir$H_{2/4}$,[1] (^{tBu4}POCOP)Ir$H_{2/4}$,[13,22,23] (^{iPr4}PCP)Ir(ethylene),[24] (^{iPr4}PCOP)Ir(ethylene),[25] (^{tBu4}PCOP)IrH_4[25] were synthesized according to literature methods. NMR spectra were recorded on either a Bruker DRX-400, Bruker Avance-400, or Bruker DRX-500 spectrometer at 298 K.

Gas chromatography: Gas chromatography was performed with a Varian 430 gas chromatograph that was equipped with either a Supelco column (100 m x 0.25 mm) or an Agilent J&W GS-GasPro column (60 m x 0.32 mm) using the following parameters:

- Starting temperature: 40 ^{o}C
- Time at starting temperature: 1.4 min
- Ramp: 20 ^{o}C/min to 260 ^{o}C, hold for 50 min
- Flow rate: 1.4 mL/min of N_2

- Split ratio: 25
- Injector temperature: 250 ^{o}C
- Detector temperature: 260 ^{o}C
- Detector: flame ionization

Response factors: GC response factors for the alkanes (n-pentane, n-hexane, n-octane, cyclododecane) and several olefins (1-pentene, 1-hexene, 2-hexenes, 1-octene, 2-octenes, cyclododecenes) were obtained experimentally by injecting known concentrations of the alkane or olefin, along with mesitylene, into the GC. Each response factor was calculated as the average of three independent runs. The response factors for the 2-pentenes, 3-hexenes, 3-octenes, and 4-octenes were extrapolated from their corresponding 1- and 2-olefins.

Direct determination: A 4-mL vial was charged with the pincer iridium catalyst [0.0025 mmol; 2.5 mM; (^{tBu2}PCP^{iPr2})IrH_4, 1.4 mg; (^{iPr4}PCP)Ir(C_2H_4), 1.4 mg; (^{iPr4}PCOP)Ir(C_2H_4), 1.4 mg; (^{tBu4}PCOP)IrH_4, 1.5 mg], 1-hexene (25 μL , 0.20 mmol, 0.20 M), mestitylene (10 μL, 0.072 mmol, 72 mM), and *n*-octane (0.97 mL, 6.0 mmol, 6.0 M) to make a total volume of 1.0 mL. The mixture was shaken until all solids dissolved. Ten aliquots of this stock solution (0.10 mL each) were syringed into glass tubes (5 mm x 140 mm) that had been flame-dried prior to being brought into the glovebox. Vacuum adapters were fitted onto the tubes, and the assemblies were removed from the glovebox. The tubes were then frozen in liquid nitrogen, the headspace was evacuated, and the tubes were flame-sealed to give a headspace:liquid ratio of approximately 1:1. The tubes were immersed into a temperature-calibrated oil bath at the specified temperature. The tubes were then removed at the stated time intervals and cooled with liquid nitrogen. The seal of each tube was carefully broken and capped with a 5 mm septum. Each sample was allowed to return to room temperature and analyzed by GC.

Competitive dehydrogenation: A 4-mL vial was charged with the pincer iridium catalyst [0.0025 mmol; 2.5 mM; (^{tBu4}PCP)IrH_2/H_4, 1.5 mg;(^{tBu2}PCP^{iPr2})IrH_4, 1.4 mg; (^{iPr4}PCP)Ir(C_2H_4), 1.4 mg; (^{tBu4}POCOP)Ir$H_{2/4}$, 1.5 mg; (^{tBu4}PCOP)IrH_4, 1.5 mg; (^{iPr4}PCOP)Ir(C_2H_4), 1.4 mg], 1-hexene (25 μL, 0.20 mmol, 0.20 M), mestitylene (10 μL, 0.072 mmol, 72 mM), cyclododecane (168 mg, 1.00 mmol, 1.0 M), *n*-pentane (114 μL, 1.00 mmol, 1.0 M), and p-xylene (0.72 mL, bringing total volume to 1.0 mL). The mixture was shaken until all solids dissolved. Ten aliquots of this stock solution (0.10 mL each) were syringed into glass tubes (5 mm x 140 mm) that had been flame-dried prior to being brought into the glovebox. Vacuum adapters were fitted onto the tubes, and the assemblies were removed from the glovebox. The tubes were then frozen in liquid nitrogen, the headspace was evacuated, and the tubes were flame-sealed to give a headspace:liquid ratio of approximately 1:1. The tubes were immersed into a temperature-calibrated oil bath at the specified temperature. The tubes were then removed at the stated time intervals and cooled with liquid nitrogen. The seal of each tube was carefully broken and capped with a 5 mm septum. Each sample was allowed to return to room temperature and analyzed by GC.

2.5.2 Synthesis of (^{tBu2}PCP^{iPr2})IrH$_4$

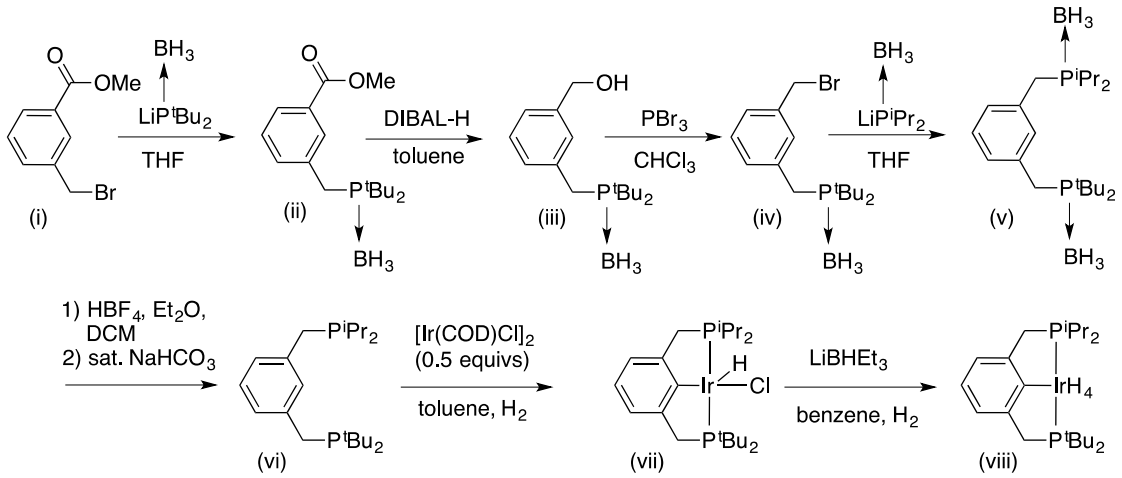

Scheme 2.20 Synthesis of (^{tBu2}PCP^{iPr2})IrH$_4$

Compound (iv). Compound (iv) was synthesized by Dr. David Wang, another member of the Goldman group.[26]

Compound (v). Diisopropylphosphine (1.1 mL, 7.1 mmol) was added to 15 mL of THF at room temperature. Borane dimethylsulfide (0.78 mL, 8.2 mmol) was added to the flask and the solution was stirred for 1 h. Solvent was removed by vacuum, giving a colorless gel. 15 mL of THF was added to the gel, making a colorless solution, and the flask was cooled to 0 °C. *n*-Butyllithium (2.9 mL of 2.5 M in hexanes, 7.1 mmol) was added and the solution was allowed to stir for 30 minutes at 0 °C. In a separate flask, compound (iv) (1.0 g, 7.1 mmol) was dissolved in 10 mL of THF and cooled to 0 °C. A cannula was used to slowly add the solution containing compound (iv) to the flask with the Li^{i}Pr$_2$P·BH$_3$ solution. This solution was allowed to slowly warm to room temperature and let stir for 2 h. The solution was washed with degassed deionized water (1 x 10 mL) and degassed saturated sodium bicarbonate (1 x 10 mL). The aqueous washes were extracted with dichloromethane (3 x 10 mL), and the combined organic layers were dried over magnesium

sulfate, filtered, and the solvent was evaporated. The crude product was dissolved in 2 mL of DCM and purified by column chromatography (10:1 hexanes:ethyl acetate), giving the product as a white solid in 65% yield. NMR (δ/ppm, CD_2Cl_2): $^{31}P\{^1H\}$ (202 MHz) 46.9 (br), 34.4 (br); ^1H (500 MHz) 7.36 (1H, s, aryl), 7.27 – 7.18 (3H, m, aryl), 3.12 (6H, dd, J = 30.6 Hz, J = 12.1, B*H*$_3$), 2.05 (4H, m, C*H*Me_2), 1.29 (18H, d, $^2J_{HP}$ = 12.7 Hz, C(C*H*$_3$)$_3$), 1.21 – 1.12 (12H, m, CH(C*H*$_3$)$_2$).

Compound (vi). Compound (v) (0.20 g, 0.51 mmol) was dissolved in 10 mL of DCM. Tetrafluoroboric acid diethyl ether complex (0.75 mL, 5.1 mmol, 10 equivalents) was slowly added at room temperature, and the solution was stirred at room temperature for 16 h. 10 mL of Et_2O was added to the solution. Two separate solutions (25 mL each of saturated sodium bicarbonate and deionized water) were degassed by freeze-pump-thawing. The sodium bicarbonate solution was slowly added to the reaction mixture, and then the solution was vigorously stirred for 10 min. The organic layer was removed by cannula, washed with the deionized water, and dried over magnesium sulfate. Filtration and evaporation of solvent gave a colorless gel in 68% yield. NMR (δ/ppm, C_6D_6): $^{31}P\{^1H\}$ (202 MHz) 33.2, 9.6; ^1H NMR (500 MHz) 7.55-7.00 (3H, m, aryl), 2.74 (2H, d, $^2J_{HP}$ = 2.5 Hz, Ar-C*H*$_2$-P), 2.68 (2H, br d, Ar-C*H*$_2$-P), 1.58 (2H, d of sept, J = 2.0 Hz, J = 7.1 Hz, C*H*Me_2), 1.06 (18H, d, $^2J_{HP}$ = 10.5 Hz, C(C*H*$_3$)$_3$), 0.93 – 1.02 (12H, J = 1.2 Hz, J = 7.1 Hz, CH(C*H*$_3$)$_2$).

Compound (vii). Compound (vi) (75 mg, 0.20 mmol) and bis(1,5-cyclooctadiene)diiridium(I) dichloride (68 mg, 0.20 mmol) were dissolved in 10 mL of toluene and heated to reflux for 2 days under a hydrogen atmosphere. Solvent was removed by vacuum, and the crude product was extracted with hexane (3 x 25 mL). The product was recrystallized by gently refluxing the solution while flowing argon into the flask and out a needle in the Schlenk flask's septum. After solids became visible, the argon flow was stopped and the solution was slowly cooled to 0 °C. The liquid was removed by cannula filtration and the solids were dried by vacuum, giving a red solid in 63%

yield. $^{31}P\{^{1}H\}$ NMR (C_6D_6, 202 MHz): δ 70.02 ($^{2}J_{PP}$= 335 Hz, $^{2}J_{HP}$ = 9.3 Hz), 57.3 ($^{2}J_{PP}$ = 335 Hz, $^{2}J_{HP}$ = 10.9 Hz). ^{1}H NMR (C_6D_6, 500 MHz) δ 7.05 – 6.90 (3H, m, aryl), 3.20 – 2.60 (4H, m, Ar-CH_2-P), 2.00 (2H, m, CH(CCH_3)$_2$), 1.23 (16H, dd, J = 15.4 Hz, J = 12.6 Hz, C(CH_3)$_3$), 0.92 – 0.76 (12H, m, CH(CH_3)$_2$), -39.91 (1H, dd, $^{2}J_{HP}$ = 11.7 Hz, $^{2}J_{HP}$ = 14.2 Hz).

Compound (viii). Compound (vii) (0.21 g, 0.35 mmol) was dissolved in 10 mL of benzene, giving a reddish-orange solution. Hydrogen gas was bubbled through the solution for 20 min and lithium triethylborohydride (0.42 mL of 1.0 M in THF, 0.42 mmol) was taken into a syringe. The borohydride was added very slowly (2-3 drops per min) until the solution lost all traces of orange and was bright yellow. Solvent was removed by vacuum, the product was extracted with hexane (1 x 40 mL), and the solution was filtered. The hexane was evaporated with vacuum, giving a red solid in 96% yield. NMR (δ/ppm, C_6D_6): $^{31}P\{^{1}H\}$ (202 MHz) 71.9 ($^{2}J_{PP}$ = 318 Hz), 55.0 ($^{2}J_{PP}$ = 318 Hz); ^{1}H (500 MHz) 6.50 – 7.20 (3H, m, Ar-H), 3.29 (2H, d, $^{2}J_{HP}$ = 9.4 Hz, CH_2P^{t}Bu$_2$), 3.13 (2H, d, $^{2}J_{HP}$ = 9.8 Hz, CH_2P^{i}Pr$_2$), 1.51 (2H, d sept, $^{2}J_{HP}$ = 7.0 Hz, $^{3}J_{HH}$ = 1.5 ppm, CHMe$_2$), 1.17 (18H, d, $^{3}J_{HP}$ = 12.6 Hz, C(CH_3)$_3$), 1.02 – 0.88 (12H, m, CH(CH_3)$_2$), -9.19 (4H, t, $^{2}J_{HP}$ = 10.0 Hz, Ir-H); $^{13}C\{^{1}H\}$ (126 MHz) 18 (dd J = 28 Hz, J = 4 Hz, CH(CH_3)$_2$), 26 (d, J = 4.7, CH(CH$_3$)$_2$), 27 (dd, J=29 Hz, J = 4 Hz, CMe$_3$), 29.6 (d, J = 4 Hz, C(CH$_3$)$_3$), 41.0 (d, J = 30 Hz, Ar-CH$_2$-P), 45.5 (d, J = 35 Hz, Ar-CH$_2$-P), 121 (d, J = 16 Hz, aryl), 122 (d, J = 15 Hz, aryl), 124 (s, aryl), 147 (dd, J = 11 Hz, J = 4 Hz, aryl), 149 (dd, J = 11 Hz, J = 4 Hz, aryl), 152 (m, aryl).

2.6 Appendix

2.6.1 Identification of dimeric ^{iPr4}POCOP hydridochloride complex

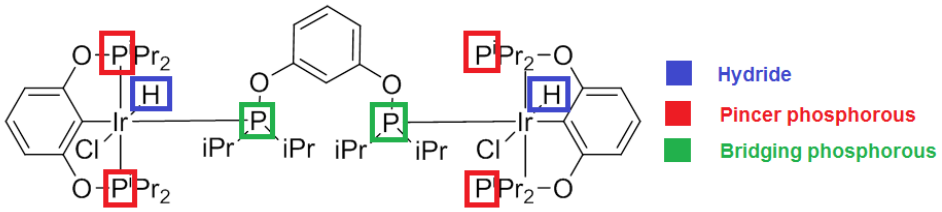

Figure 2.22 Identification of bridged ^{iPr4}POCOP hydridochloride complex

^{1}H-NMR	Splitting	Chemical Shift
Predicted (5-coordinate monomer)	t	-40 ppm
Predicted (6-coordinate dimer)	d of t	-20 ppm
Actual	d of t	-22 ppm

^{31}P-NMR	Pincer	Bridging	Integration Ratio
Predicted (5-coordinate monomer)	d	n/a	n/a
Predicted (6-coordinate dimer)	d of d	d of t	2.0 to 1.0
Actual	d of d	d of t	2.0 to 0.9

Tables 2.8 and 2.9 NMR identification of bridged ^{iPr4}POCOP hydridochloride complex

2.6.2 Direct determination GC data

(^{tBu4}PCP)Ir direct determination										
Time (mins)	*n*-hexane	1-hexene	2-hexenes	1-octene	*trans*-4-octene	*trans*-3-octene	*trans*-2-octene	*cis*-4-octene	*cis*-3-octene	*cis*-2-octene
0.0	0.0	240.0	0.0	0.0	0.0	0.0	0.0	0.0	0.0	0.0
1.5	7.5	231.3	11.4	2.7	0.0	0.0	0.1	0.0	0.0	0.0
2.5	9.2	211.1	15.7	3.6	0.0	0.0	0.1	0.0	0.0	0.0
3.5	10.3	167.9	16.6	5.9	0.0	0.0	0.2	0.0	0.1	0.0
4.5	15.1	171.1	22.8	9.7	0.0	0.0	0.4	0.0	0.1	0.0
7.5	20.4	166.7	36.0	12.9	0.0	0.0	0.9	0.0	0.1	0.1
9.0	26.6	149.5	40.0	17.8	0.0	0.0	1.4	0.0	0.1	0.2
10.0	26.4	107.1	40.5	19.5	0.0	0.1	2.2	0.0	0.1	0.4

Table 2.10 Direct determination with (^{tBu4}PCP)Ir

(^{tBu2}PCP^{iPr2})Ir direct determination												
Time (mins)	*n*-hexane	1-hexene	*trans*-2-hexene	*cis*-2-hexene	hexa-dienes	1-octene	*trans*-4-octene	*trans*-3-octene	*trans*-2-octene	*cis*-4-octene	*cis*-3-octene	*cis*-2-octene
0.0	1.4	208.7	1.8	1.1	0.9	0.6	0.0	0.0	0.1	0.0	0.0	0.1
3.0	2.8	192.9	8.3	2.8	1.9	2.3	0.0	0.0	0.1	0.0	0.0	0.1
6.0	5.9	172.2	14.3	4.2	1.6	5.2	0.0	0.0	0.2	0.0	0.0	0.1
9.0	9.1	164.9	23.5	6.9	3.0	7.2	0.0	0.1	0.6	0.0	0.1	0.1
12.0	13.5	151.0	29.5	8.1	0.8	10.9	0.0	0.1	1.2	0.0	0.1	0.2
15.0	14.8	142.8	36.3	10.2	2.0	11.5	0.0	0.1	1.4	0.0	0.1	0.2
18.0	19.5	128.8	44.9	12.5	2.2	15.1	0.0	0.4	2.4	0.0	0.1	0.5
21.0	25.7	116.9	49.2	13.0	1.5	18.3	0.0	0.5	3.5	0.0	0.1	0.7
27.5	32.2	94.7	58.3	15.4	1.6	21.9	0.0	0.7	5.5	0.0	0.2	1.2

Table 2.11 Direct determination with (^{tBu2}PCP^{iPr2})Ir

(^{iPr4}PCP)Ir direct determination													
Time (mins)	*n*-hexane	1-hexene	*trans*-2-hexene	*cis*-2-hexene	hexa-dienes	1-octene	*trans*-4-octene	*trans*-3-octene	*trans*-2-octene	*cis*-4-octene	*cis*-3-octene	*cis*-2-octene	*octa-dienes*
0.0	0.2	219.2	2.6	2.3	0.0	0.1	0.0	0.1	0.0	0.0	0.0	0.0	0.0
2.5	6.4	196.6	12.0	9.7	0.2	5.0	0.0	0.1	0.5	0.0	0.1	0.2	0.0
5.0	13.5	155.1	24.4	17.5	0.3	10.5	0.0	0.3	1.5	0.0	0.1	0.8	0.0
7.5	23.2	136.7	34.5	27.2	0.5	16.1	0.0	0.5	3.3	0.0	0.1	2.0	0.1
10.0	30.7	109.1	40.3	31.8	0.6	21.1	0.0	0.5	4.8	0.0	0.1	2.9	0.0
15.0	51.0	56.8	57.2	43.3	1.3	28.3	0.0	0.9	11.1	0.0	0.1	7.3	0.1
20.0	66.1	29.9	63.9	49.2	1.9	30.1	0.0	1.4	18.0	0.0	0.4	12.3	0.4
25.0	86.1	2.9	68.4	48.6	3.8	18.9	0.0	3.0	33.4	0.0	0.7	22.0	0.8

Table 2.12 Direct determination with (^{iPr4}PCP)Ir

(MeO-^{tBu4}PCP)Ir direct determination											
Time (mins)	*n*-hexane	1-hexene	2-hexenes	hexa-dienes	1-octene	*trans*-4-octene	*trans*-3-octene	*trans*-2-octene	*cis*-4-octene	*cis*-3-octene	*cis*-2-octene
0.0	0.0	221.4	0.0	0.0	0.0	0.0	0.0	0.0	0.0	0.0	0.0
5.0	1.8	180.7	19.4	0.1	2.4	0.0	0.0	0.1	0.0	0.0	0.1
7.5	3.5	203.3	35.4	0.4	3.4	0.0	0.0	0.3	0.0	0.0	0.1
10.0	6.6	196.0	41.4	0.6	5.0	0.0	0.0	0.2	0.0	0.0	0.2
12.5	7.6	194.5	26.5	0.3	6.8	0.0	0.1	0.3	0.0	0.1	0.1
16.0	7.5	180.7	24.8	0.1	7.4	0.0	0.1	0.4	0.0	0.1	0.2
20.0	10.4	142.0	35.8	-0.1	10.2	0.0	0.1	0.5	0.0	0.1	0.3
25.0	11.2	140.4	37.4	-0.1	10.7	0.0	0.1	0.9	0.0	0.1	0.3
30.0	17.9	165.7	44.7	0.2	15.8	0.0	0.0	0.7	0.0	0.1	0.5
40.0	19.4	140.2	35.7	-0.1	17.9	0.0	0.1	1.3	0.0	0.1	0.5
50.0	21.0	87.1	29.2	-0.5	25.0	0.0	0.3	2.7	0.0	0.1	0.5

Table 2.13 Direct determination with (MeO-^{tBu4}PCP)Ir

(Me_2N-^{tBu4}PCP)Ir direct determination										
Time (mins)	*n*-hexane	1-hexene	2-hexenes	1-octene	*trans*-4-octene	*trans*-3-octene	*trans*-2-octene	*cis*-4-octene	*cis*-3-octene	*cis*-2-octene
0.0	0.0	215.9	0.0	0.0	0.0	0.0	0.1	0.0	0.0	0.1
7.0	0.5	190.7	21.9	1.0	0.0	0.0	0.1	0.0	0.0	0.1
10.0	1.0	170.4	27.7	1.4	0.0	0.0	0.1	0.0	0.0	0.1
12.5	1.4	173.9	34.3	1.8	0.0	0.0	0.1	0.0	0.1	0.1
15.0	2.6	167.7	37.6	2.6	0.0	0.0	0.2	0.0	0.1	0.1
20.0	3.6	156.4	42.1	3.5	0.0	0.0	0.3	0.0	0.1	0.1
30.0	4.9	145.4	54.9	4.6	0.0	0.1	0.4	0.0	0.1	0.2
45.0	10.2	135.6	65.1	8.9	0.0	0.1	0.9	0.0	0.1	0.4
85.0	19.1	106.6	88.8	15.3	0.0	0.1	2.1	0.0	0.1	1.0

Table 2.14 Direct determination with (Me_2N-^{tBu4}PCP)Ir

(^{tBu4}PCOP)Ir direct determination												
Time (mins)	*n*-hexane	1-hexene	*trans*-2-hexene	*cis*-2-hexene	hexa-dienes	1-octene	*trans*-4-octene	*trans*-3-octene	*trans*-2-octene	*cis*-4-octene	*cis*-3-octene	*cis*-2-octene
0.0	0.0	182.2	0.0	0.0	0.0	0.0	0.0	0.0	0.0	0.0	0.0	0.0
2.5	3.4	84.0	72.3	48.6	0.3	0.0	0.1	0.2	0.0	0.0	0.1	2.5
5.0	3.0	82.9	84.8	44.4	0.5	0.0	0.1	0.3	0.0	0.0	0.1	5.0
10.0	4.7	51.5	109.1	47.5	1.2	0.0	0.2	0.7	0.0	0.1	0.2	10.0
15.0	5.9	45.0	122.2	49.5	1.7	0.0	0.2	1.0	0.0	0.1	0.3	15.0
30.0	14.7	18.6	136.8	48.4	4.9	0.0	0.4	3.8	0.0	0.1	1.0	30.0
45.0	23.2	4.9	131.2	45.6	6.7	0.0	1.0	8.1	0.0	0.2	2.0	45.0

Table 2.15 Direct determination with (^{tBu4}PCOP)Ir

(^{iPr4}PCOP)Ir direct determination												
Time (mins)	*n*-hexane	1-hexene	*trans*-2-hexene	*cis*-2-hexene	hexa-dienes	1-octene	*trans*-4-octene	*trans*-3-octene	*trans*-2-octene	*cis*-4-octene	*cis*-3-octene	*cis*-2-octene
0.0	0.0	207.3	0.0	0.0	0.0	0.0	0.0	0.0	0.0	0.0	0.0	0.0
2.5	1.0	156.3	14.1	10.5	0.5	0.0	0.0	0.1	0.0	0.0	0.0	2.5
5.0	2.9	186.9	25.5	14.9	1.3	0.0	0.1	0.2	0.0	0.1	0.1	5.0
10.0	4.4	167.4	35.9	17.3	2.5	0.0	0.1	0.5	0.0	0.1	0.4	10.0
15.0	7.3	143.0	46.3	19.4	4.1	0.0	0.1	1.0	0.0	0.1	0.6	15.0
20.0	9.6	104.3	62.3	29.9	6.0	0.0	0.3	1.6	0.0	0.1	0.7	20.0
40.0	24.9	65.0	92.4	31.6	11.6	0.0	0.9	7.0	0.0	0.2	2.5	40.0
60.0	40.5	45.0	124.6	39.6	18.2	0.0	1.6	14.5	0.0	0.8	4.0	60.0

Table 2.16 Direct determination with (^{iPr4}PCOP)Ir

2.7 References

(1) Gupta, M.; Hagen, C.; Flesher, R. J.; Kaska, W. C.; Jensen, C. M. *Chem. Commun.* **1996**, 2083.

(2) Biswas, S. *Doctoral Thesis, Rutgers, The State University of New Jersey* **2010**.

(3) Kumar, A.; Zhou, T.; Emge, T. J.; Mironov, O.; Saxton, R. J.; Krogh-Jespersen, K.; Goldman, A. S. **2015**, submitted for publication to J. Am. Chem. Soc.

(4) Ahuja, R.; Punji, B.; Findlater, M.; Supplee, C.; Schinski, W.; Brookhart, M.; Goldman, A. S. *Nature Chem.* **2011**, *3*, 167.

(5) Goldman, A. S.; Roy, A. H.; Huang, Z.; Ahuja, R.; Schinski, W.; Brookhart, M. *Science* **2006**, *312*, 257.

(6) Steffens, A. M., Rutgers, The State University of New Jersey, 2015.

(7) Biswas, S.; Huang, Z.; Choliy, Y.; Wang, D. Y.; Brookhart, M.; Krogh-Jespersen, K.; Goldman, A. S. *J. Am. Chem. Soc.* **2012**, *134*, 13276.

(8) Hackenberg, J., Rutger, the State University of New Jersey, 2014.

(9) Mulliken, R. S. *J. Chem. Phys.* **1939**, *7*, 339.

(10) NIST2001.

(11) Hoops, S.; Sahle, S.; Gauges, R.; Lee, C.; Pahle, J.; Simus, N.; Singhal, M.; Xu, L.; Mendes, P.; Kummer, U. *Bioinformatics* **2006**, *22*, 3067.

(12) Naghipour, A.; Ghasemi, Z. H.; Morales-Morales, D.; Serrano-Becerra, J. M.; Jensen, C. M. *Polyhedron FIELD Full Journal Title:Polyhedron* **2008**, *27*, 1947.

(13) Göttker-Schnetmann, I.; White, P.; Brookhart, M. *J. Am. Chem. Soc.* **2004**, *126*, 1804

(14) Nawara-Hultzsch, A. J.; Hackenberg, J. D.; Punji, B.; Supplee, C.; Emge, T. J.; Bailey, B. C.; Schrock, R. R.; Brookhart, M.; Goldman, A. S. *ACS Catal.* **2013**, *3*, 2505.

(15) Kundu, S.; Choliy, Y.; Zhuo, G.; Ahuja, R.; Emge, T. J.; Warmuth, R.; Brookhart, M.; Krogh-Jespersen, K.; Goldman, A. S. *Organometallics* **2009**, *28*, 5432.

(16) Wang, D. Y.-B. Ph. D. thesis, Rutgers University, 2013.

(17) Morales-Morales, D.; Redon, R.; Yung, C.; Jensen, C. M. *Inorg. Chim. Acta.* **2004**, *357*, 2953.

(18) Schultz, K. M.; Goldberg, K. I.; Gusev, D. G.; Heinekey, D. M. *Organometallics* **2011**, *30*, 1429.

(19) Cheng, C.; Brookhart, M. *Unpublished work.*

(20) Wilberg, K. B. *Angew Chem Int Ed Engl* **1986**, *25*, 312.

(21) Anslyn, E. V.; Dougherty, D. A. *Modern Physical Organic Chemistry*; University Science Books: Sausalito, California, 2005.

(22) Göttker-Schnetmann, I.; Brookhart, M. *J. Am. Chem. Soc.* **2004**, *126*, 9330.

(23) Göttker-Schnetmann, I.; White, P. S.; Brookhart, M. *Organometallics* **2004**, *23*, 1766.

(24) Liu, F.; Goldman, A. S. *Chem. Commun.* **1999**, 655.

(25) Nawara-Hultzsch, A. J.; Hackenberg, J. D.; Punji, B.; Supplee, C.; Emge, T. J.; Bailey, B. C.; Schrock, R. R.; Brookhart, M.; Goldman, A. S. *ACS Catalysis* **2013**, *3*, 2505.

(26) Wang, D. Ph. D. Thesis, Rutgers University, 2012.

Chapter 3

Elucidating the factors determining the regioselectivity of dehydrogenation by pincer iridium catalysts *via* DFT calculations

Abstract

DFT calculations were used to elucidate the mechanistic reasons why different pincer iridium catalysts showed different levels of regioselectivity for 1-olefins during transfer dehydrogenation. These results showed that regioselectivity was determined by the rate-determining step of the reaction: if C-H activation or β-H elimination were rate-determining, regioselectivity for 1-olefins would be high (> 90%). In contrast, if olefin dissociation was the rate-determining step then much lower regioselectivity (ca. 50%) would be expected. These same DFT calculations also showed that β-H elimination was the rate-determining step for all (PCP)Ir catalysts, explaining the high experimentally-observed regioselectivity of (PCP)Ir catalysts. It also showed that more stericly crowded (PCP)Ir catalysts would have the highest regioselectivity, in strong agreement with experimental results. Likewise, the rate-determining step with (PCOP)Ir and (POCOP)Ir catalysts was found to be olefin dissociation, explaining the low experimentally-observed regioselectivity for those catalysts. Lastly, whether steric and/or electronic factors caused this change in rate-determining step was also investigated by DFT. Comparing the trends amongst known catalysts with those of (^{tBu4}PBP-pN)Ir and (^{tBu4}PNP-pB)Ir, it was shown that electronic factors acting through the ipso carbon of the aryl ring (C_{ipso}) were the primary factors governing the relative height of the transition states, and therefore the rate-determining step and

regioselectivity. Specifically, it was found that strong π-donation by C_{ipso} reduced the barrier to β-H elimination while strong σ-donation increased the barrier to olefin dissociation.

3.1 Introduction

Based on the data in Chapter 2, the five (PCP)Ir catalysts studied had high regioselectivity (> 91%) whereas the two (PCOP)Ir catalysts and (^{tBu4}POCOP)Ir had low regioselectivity. Hence, it could be reasonably assumed that new (PCP)Ir catalysts would have high regioselectivity, whereas new (PCOP)Ir or (POCOP)Ir catalysts would have low regioselectivity. Therefore, the design and synthesis of new catalysts should employ the (PCP)Ir framework. However, this approach had two main limitations:

1. No information about the regioselectivity of other possible ligand frameworks, such as (PNC)Ir or (PCN)Ir, was available. No methods were available to estimate the regioselectivity of these new catalysts without synthesizing and testing them, a process which would consume considerable time and effort.
2. Even while maintaining the (PCP)Ir framework, it was not known whether all (PCP)Ir catalysts would also have high regioselectivity.

Therefore, elucidating the mechanism which determines regioselectivity would allow for more informed catalyst design. If certain steric or electronic factors were found to influence regioselectivity, then new catalysts could be conceive with those ideas in mind. Employing DFT calculations to aid in catalyst design is a process which has received much attention and success. In 2009 Goldman reported that the most active *n*-alkane transfer dehydrogenation catalyst reported to date, (^{tBu3Me}PCP)Ir, had been designed with the aid of DFT calculations.[1] (Figure 3.1)

In particular, that study aimed to maximize catalytic activity by designing a (PCP)Ir catalyst with optimal steric parameters. Eight catalysts were studied by DFT with various combinations of ^{t}Bu, ^{i}Pr, and Me groups attached to the phosphorous atoms. By calculating and comparing the overall kinetic barriers for the dehydrogenation of *n*-butane to 1-butene for all eight catalysts, it was found that (^{tBu3Me}PCP)Ir was predicted to have the lowest barrier. Hence, the considerable effort required to synthesize the unsymmetrical (^{tBu3Me}PCP)Ir catalyst was expended. Upon measuring the kinetics of transfer dehydrogenation by (^{tBu3Me}PCP)Ir, this new catalyst was found to be approximately 70% more active than (^{iPr4}PCP)Ir, which had been the most active *n*-alkane transfer dehydrogenation catalyst up until that point.

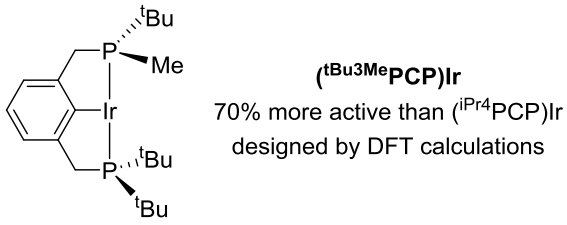

Figure 3.1 (^{tBu3Me}PCP)Ir catalyst

Hence, mechanistic studies employing DFT calculations were instrumental in designing a better pincer iridium catalyst. Notably, the difficult synthesis of (^{tBu3Me}PCP)Ir would have never been performed without the DFT calculations which predicted its high activity. In this way, DFT calculations serve as a more efficient catalyst screening method. Similarly, DFT calculations have also been used to aid the design of (^{dm}Phebox)Ir type complexes for C-H activation and alkane dehydrogenation. In 2013 Goldberg reported that heating (^{dm}Phebox)Ir(OAc)$_2$(OH$_2$) in *n*-octane resulted in the stoichiometric dehydrogenation of *n*-octane, giving (^{dm}Phebox)Ir(OAc)(H), 1-octene, acetic acid, and water.[2] (Scheme 3.1) The original bis-acetate complex could also be regenerated by heating the acetate-hydride complex in the presence of air or oxygen gas, along with acetic acid and water.[3]

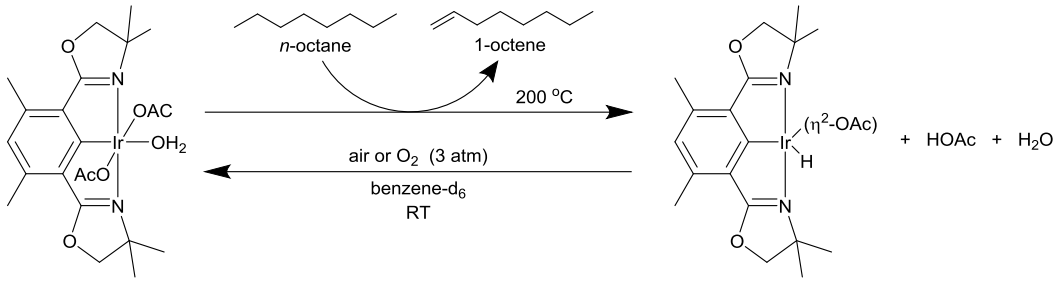

Scheme 3.1 Dehydrogenation of *n*-octane by (^{dm}Phebox)Ir(OAc)$_2$(OH$_2$)

Thus, the Goldberg group has attempted to take the results of these stoichiometric reactions and expand them into catalytic reactions. First, they began by conducting a DFT study of the steric and electronic factors affecting the kinetic barrier to C-H activation, which is one step during the dehydrogenation of *n*-octane to 1-octene.[4] It was found that after the water ligand dissociated from the metal center, C-H activation of the alkane occurred through concerted metalation-deprotonation (CMD) mechanism. Thus, the kinetic barriers to CMD were calculated for many different pincer ligands, as well as ancillary ligands (i.e. the acetate groups). First, it was found that changing the side linkages from a phebox groups to a carbene had almost no effect (30.9 versus 31.5 kcal/mol). Similarly, functionalizing the aryl backbone in the para or meta positions Me, NMe$_2$, or NO$_2$ groups also had almost no effect (total range of 30.7 to 31.6 kcal/mol). Next, varying the identity of the ancillary ligand (i.e. XCO$_2^-$ where X = Me, CF$_3$, ^{t}Bu, or Ph) also had a fairly small effect on the kinetic barrier, giving a range of 30.5 to 32.7 kcal/mol. The lowest barrier of 30.5 kcal/mol, obtained with X = ^{t}Bu, was only 0.4 kcal/mol lower than X = Me. Therefore, since previous experiments were performed with acetic acid (where X = Me), then no viable strategies for improvement were found in any of these modifications.

However, changing the ipso and/or para atoms in the aromatic ring caused massive changes in the calculated barriers. (Figure 3.1) (Table 3.1) Changing the para group from a C-H group to a nitrogen atom, denoted here as L', only increased the barrier 0.4 or 0.5 kcal/mol.

However, changing the ipso group caused a *drastic* change. Whereas the barriers were approximately 32 kcal/mol with an ipso carbon, those same barriers decreased to about 27 kcal/mol with a *nitrogen* in the ipso position.

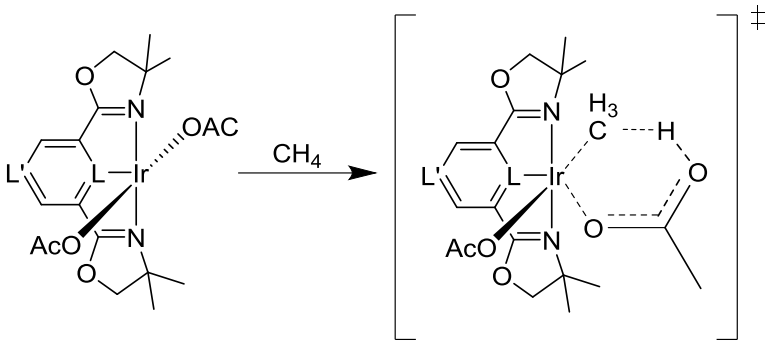

Scheme 3.2 Concerted metalation-deprotonation

Ligand	L'	L	$\Delta G^{\ddagger}$
Phebox	CH	C	31.6
ParaNbox	N	C	32.0
Pybox	CH	N	26.6
Pyzbox	N	N	27.1

Table 3.1 Kinetic barrier for concerted metalation-deprotonation step (in kcal/mol)

Thus, according to the Eyring equation, (Equation 2.3) a decrease in barrier of that magnitude would correspond to an approximately 200-fold (or 20,000%) increase in the rate constant (k) at 200 °C (the reaction temperature used experimentally). And, since the rate law shows that the actual reaction rate is directly proportional to the rate constant, (Equation 3.1) then the experimentally observed reaction rate would also increase approximately 200-fold.

$$rate = k * [A]^X * [B]^Y * [C]^Z$$

Equation 3.1 General form of the rate law

In relation to the current regioselectivity project, this study of (^{dm}Phebox)Ir(OAc)$_2$ by Goldberg shows that DFT calculations can be very powerful for designing better catalysts. Specifically, the DFT study of (^{dm}Phebox)Ir(OAc)$_2$ showed that no significant improvements to the

kinetic barriers of C-H activation could be expected by modifying or changing the ancillary ligand, the phebox end groups, or the meta or para positions on the aryl backbone. However, the study *did* show that changing the ipso atom from a carbon to a nitrogen might *massively* reduce the kinetic barrier. Thus, DFT calculations have directed further experimental work.

Hence, conducting DFT calculations to understand the mechanism behind regioselectivity might also aid in rationally designing and synthesizing new catalysts with high regioselectivity.

3.2 Identifying the possible steric and electronic factors affecting regioselectivity

With firm experimental correlations between catalyst structure and regioselectivity established, DFT calculations were begun with the objective of elucidating the *mechanism* causing these regioselectivity differences. Namely, if (PCP)Ir catalysts have high regioselectivity exclusively for 1-olefins, then the kinetic barrier for that reaction must be significantly lower than those for 2-olefins, 3-olefins, and further internal olefins. Likewise, if (PCOP)Ir and (POCOP)Ir catalysts have low regioselectivity between 1-olefins and 2-olefins, then those dehydrogenation pathways must have relatively similar kinetic barriers. In contrast, the kinetic barriers for 3-olefins and further olefins must higher barriers.

On the highest level of theory, these differences in kinetic barriers must be caused by a combination of steric and/or electronic factors. In particular, the following five factors were brainstormed as possible causes:

1. Steric – changing the identity of the R groups in the PR_2 moieties would cause more or less crowding at the iridium center, in turn prompting more or less regioselectivity, respectively. (Figure 3.2)

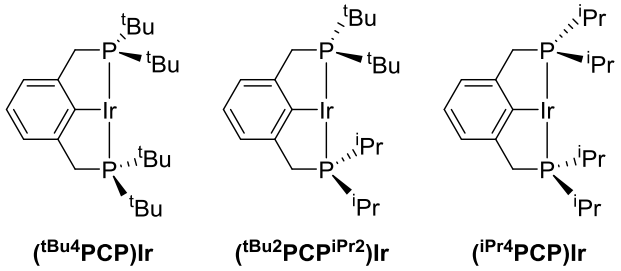

Figure 3.2 Steric crowding at (PCP)Ir catalysts

2. Steric – planarity versus twisting of the PCP versus PCOP/POCOP ligands (at the methylene versus oxygen linkers) could affect the conformations of the PR_2 groups, thereby causing more or less crowding at the iridium center, in turn prompting more or less regioselectivity, respectively.[5] (Figure 3.3)

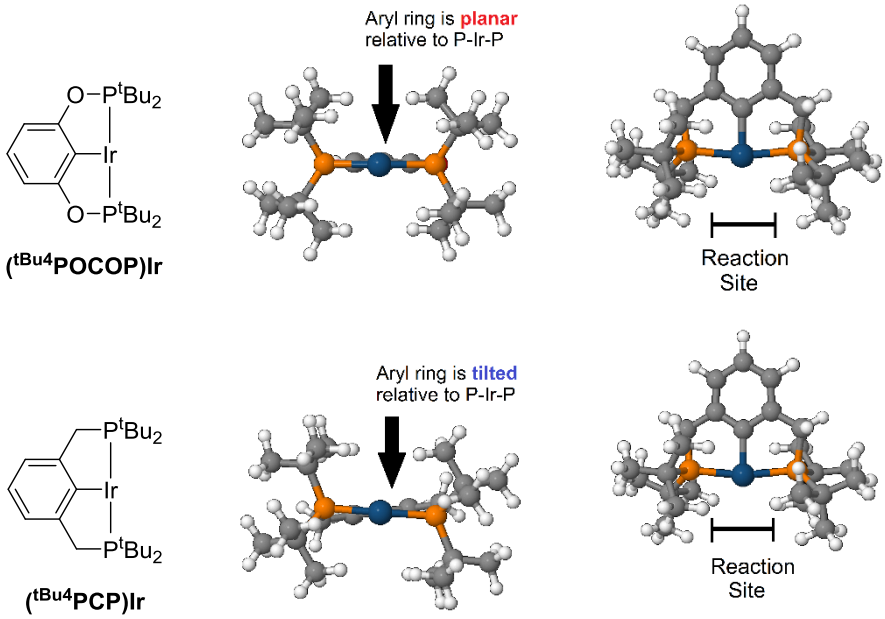

Figure 3.3 DFT-optimized geometries of the 14 electron complexes of (^{tBu4}POCOP)Ir (top row) and (^{tBu4}PCP)Ir (bottom row)

3. Steric – the observation that the PR_2 groups are "pulled backwards" in (PCOP)Ir and (POCOP)Ir catalysts, due to the fact that the C-O and O-P bonds are shorter than their corresponding C-C and C-P bonds,[5] thereby causing less crowding at the iridium center, in turn prompting less regioselectivity. (Table 3.2)

Catalyst	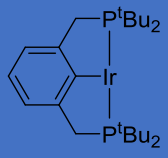 **(^{tBu4}PCP)Ir**	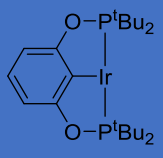 **(^{tBu4}POCOP)Ir**
C(aryl) – C(methylene)	1.515 Å	1.393 Å
C(methylene) - P	1.867 Å	1.707 Å

Table 3.2 Selected bond lengths in DFT-optimized geometries for 14 electron complexes of (^{tBu4}PCP)Ir and (^{tBu4}POCOP)Ir

4. Electronics – the quantity of electron donation through the two phosphorous atoms, which would be different in every catalyst, could affect the energy of the rate-determining step.[6] (Figure 3.4)

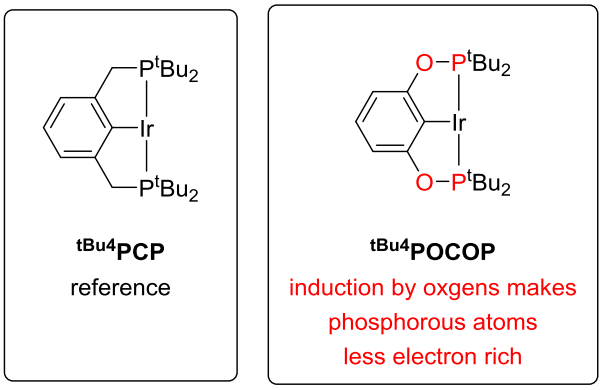

Figure 3.4 Electronic effects relating to phosphorous atoms in pincer iridium catalysts

5. Electronics – the quantity of electron donation through the ipso carbon of the aryl ring, which would be different in every catalyst, could affect the energy of the rate-determining step. Notably, this could either happen due to two distinct events (σ-donation *via* the C-Ir covelant bond, and/or π-donation *via* the aryl ring's π cloud into a *different* orbital on iridium), or simply due to the net donation of electron density into iridium (irrespective of which particular orbitals are involved).[6] (Figure 3.5)

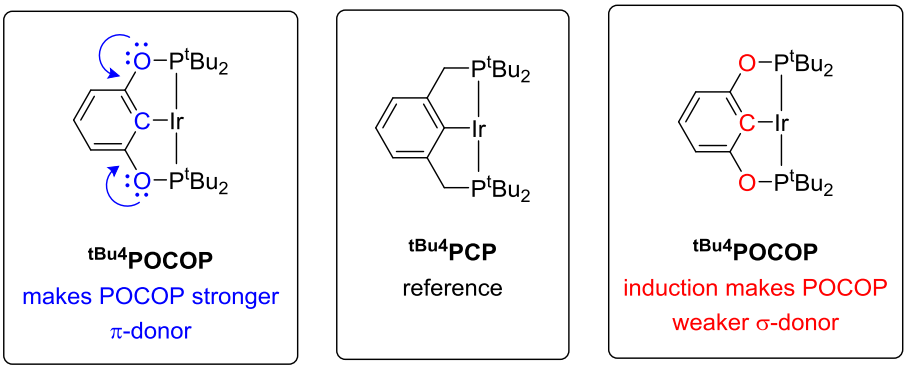

Figure 3.5 Electronic effects relating to C_{ipso} atom in pincer iridium catalysts

Upon initial inspection, the role of steric crowding does offer a plausible explanation for a change in regioselectivity. When generating a 1-olefin, the major (destabilizing) steric interactions will be between the *n*-alkane's tail and the PR_2 groups of the catalyst. (Figure 3.6) However, when a 2-olefin is being generated, both the *n*-alkane tail *and* the methyl group at the first carbon will cause destabilizing steric repulsion with the PR_2 groups. Likewise, generating a further-internal olefin like a 3-olefin or a 4-olefin will involve an ethyl or *n*-propyl group, respectively, which would generate even more steric destabilization than the methyl group involved in producing a 2-olefins. Since the preferred product is 1-olefins, and 3-olefins and 4-olefins are never observed experimentally, then this explanation is at least plausible, although no direct evidence has been yet collected to support it.

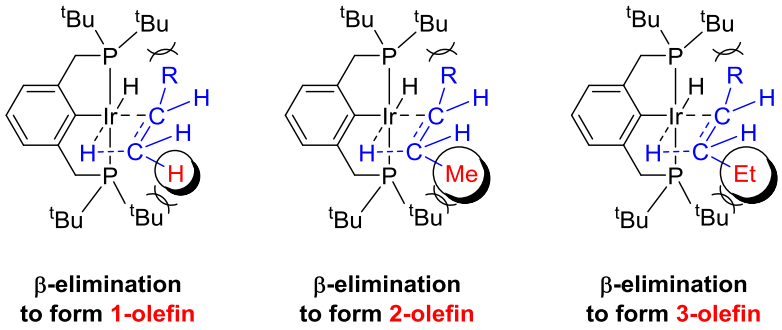

Figure 3.6 Steric crowding during β-H elimination

Furthermore, previous studies have demonstrated that (^{tBu4}POCOP)Ir, with low regioselectivity, is measurably more stericly open than (^{tBu4}PCP)Ir, which has very high regioselectivity.[5]

However, it has also been shown that (^{tBu4}PCP)Ir, (MeO-^{tBu4}PCP)Ir, and (^{tBu4}POCOP)Ir have measurably different electronic structures.[6] In terms of atomic net charges, the phosphorous atoms in (^{tBu4}POCOP)Ir had a much higher net charge (1.255) compared to (^{tBu4}PCP)Ir (0.937) and (MeO-^{tBu4}PCP)Ir (0.937 also). Hence, the oxygen linkages in (^{tBu4}POCOP)Ir most likely withdraw electron density from the phosphorous atoms, giving the more positive net charge, compared to the (PCP)Ir catalysts. Next, the net atomic charges on the ispo carbon were also assessed. Using (^{tBu4}PCP)Ir as a reference, its charge on C_{ipso} was -0.086. In contrast, the value for (MeO-^{tBu4}PCP)Ir was -0.116, indicating more electron density, presumably through resonance structures with the π-system. Simiarly, the net charge for C_{ipso} in (^{tBu4}POCOP)Ir was -0.234, suggesting an even larger increase in electron density. Since the oxygen atom withdraws electron density *inductively*, then the net increase in electron density must come from donation of electron density *via* resonance in the π-system. In fact, the occupancy of actual p-orbital on C_{ipso} was also calculated, supporting the above conclusions. Using (^{tBu4}PCP)Ir as the reference point, moving to (MeO-^{tBu4}PCP)Ir lead to

an increase in occupancy of the C_{ipso} p-orbital from 0.958 to 0.992. Likewise, the corresponding occupancy for (^{tBu4}POCOP)Ir was even higher at 1.059. Therefore, these DFT calculations show that the electronic changes postulated above in Figure 3.4 and 3.5 appear to be true.

Therefore, these electronic differences may account for the observed regioselectivity differences, although the mechanism by which electronics would affect regioselectivity is not immediately apparent.

Hence, with the theoretical framework established for how catalyst structure could affect regioselectivity, DFT calculations were begun to elucidate which factor(s) discussed above caused the observed regioselectivity differences. Tian Zhou, another member of Professor Goldman's research group, performed the actual DFT calculations and reported the calculated energies. Planning which DFT calculations to conduct, and interpreting the results of those calculations, was a collaboration between myself and Tian.

3.3 Considering multiple dehydrogenation pathways

Before conducting any DFT calculations, it is important to consider the mechanism of dehydrogenation, along with each of the possible pathways (or variations of the dehydrogenation sequence) which are possible. To simplify the DFT calculations, as well as shorten the time required to complete each calculation, *n*-hexane was used as the substrate (instead of the *n*-octane used in the direct determination experiments).

As reported previously, the mechanism of dehydrogenation proceeds through C-H activation and then β-H elimination.[7] (Figure 3.7) For clarity, this figure gives a specific example of the dehydrogenation pathway, C1-C2 with a *trans*-(pincer)Ir(H)(H)(1-hexene) intermediate, but

several other variations exist. Each possibility will be described below. Although not explicitly specified in the original report, a third elementary reaction step of olefin dissociation must also occur, completing the dehydrogenation reaction. Notably, the second half of the transfer dehydrogenation reaction is hydrogenation, and is accomplished by simply reversing the sequence of dehydrogenation. Namely, it proceeds through olefin association, insertion of the olefin into the Ir-H bond, and finally reductive elimination.

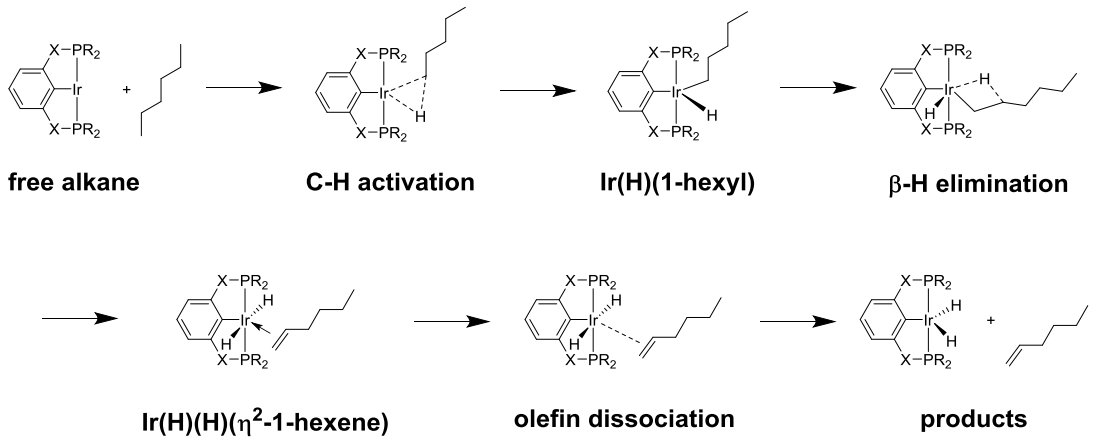

Figure 3.7 Dehydrogenation *via* the C1-C2 pathway and the *trans*-(pincer)Ir(H)(H)(1-hexene) intermediate

The first possible variation on the dehydrogenation sequence involves the "location of C-H activation," and therefore also the location of β-H elimination. (Figure 3.8) For example, generating 1-hexene could proceed through either C-H activation at the terminal/first carbon (C_1) and then through β-H elimination at the second carbon (C_2), or through C-H activation at C_2 and then β-H elimination at C_1. These two pathways will be referred to as C1-C2 and C2-C1, respectively. Similarly, the two possible pathways for generating a 2-hexene will be described as C2-C3 and C3-C2.

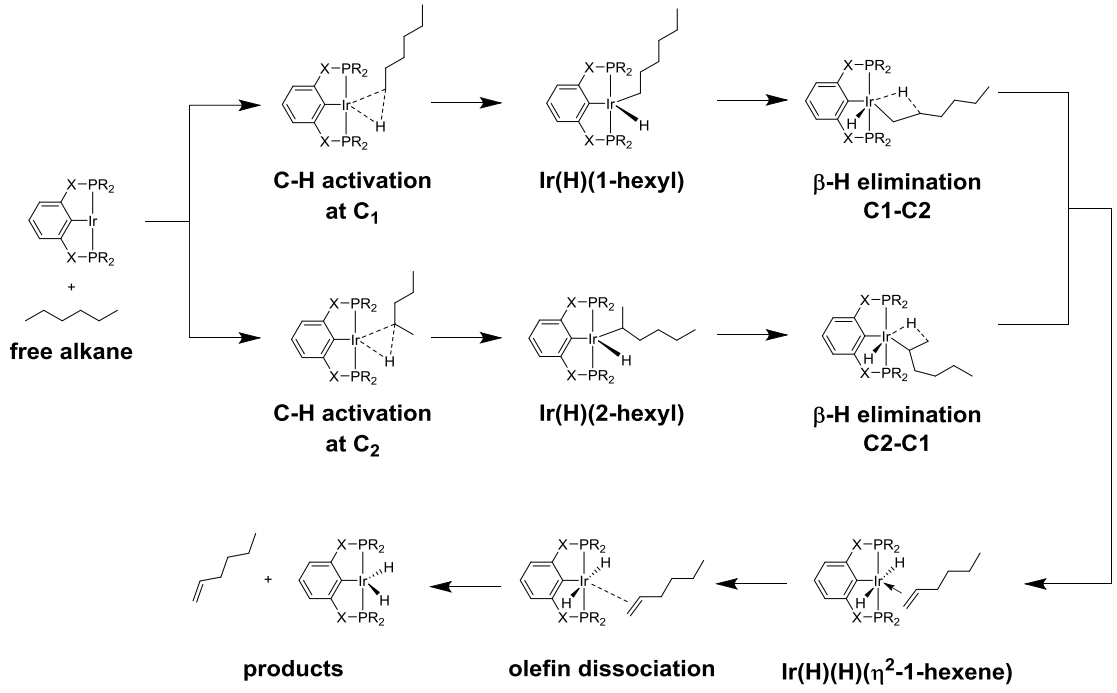

Figure 3.8 Dehydrogenation through either the C1-C2 or C2-C1 pathway

As will be discussed throughout this Chapter (and also in Chapter 4 regarding the DFT-assisted design of new catalysts), the barriers for C1-C2 versus C2-C1 were found to be *quite* different from each other. As a general rule, the barriers could differ from approximately 2 to 8 kcal/mol relative to each other, making one pathway several dozen-fold to several *hundred-fold* faster than the other. Thus, all four possibilities (C1-C2, C2-C1, C2-C3, and C3-C2) were calculated for almost all catalysts investigated.

The next possible variation involves the two possible isomers for the (pincer)Ir(H)(H)(olefin) intermediate. Namely, depending upon the conformation of β-H elimination, the newly-generated olefin could either be located *trans* to the aryl ring (Figures 3.7 and 3.8) (also making the hydrides *trans* to one another), or the olefin could be located *cis* to the aryl ring (Figure 3.9) (also making the hydrides *cis* to one another). Thus, the two different β-H eliminations required for generating the two different (pincer)Ir(H)(H)(olefin) isomers would also

yield different kinetic barriers. Moreover, olefin dissociation from the two isomers would also give different barriers. Therefore, the energies of both the *trans* pathway and the *cis* pathways were considered for the first several catalysts studied. However, it became apparent that the *cis* pathway was always much higher in energy than the *trans* pathway. Thus, all DFT calculations reported in this thesis involve dehydrogenation (and, by proxy, hydrogenation) proceeding through the *trans* pathway.

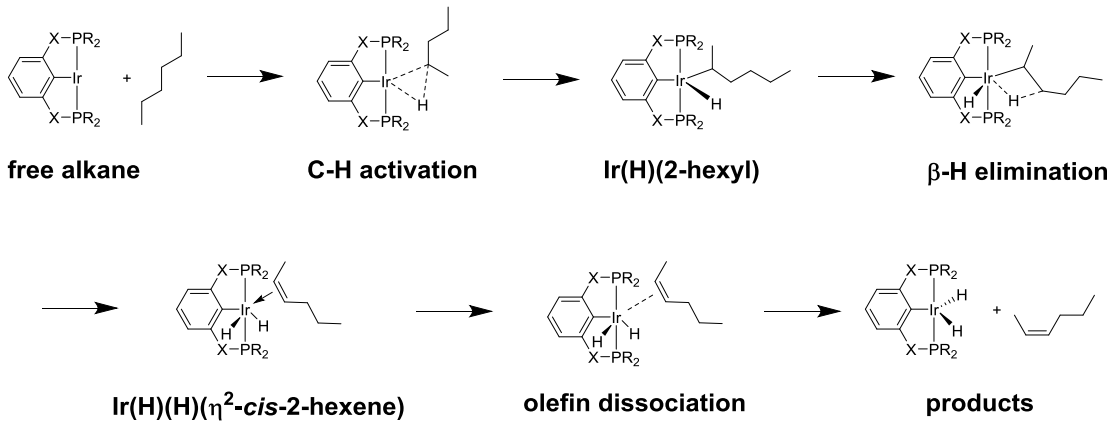

Figure 3.9 Dehydrogenation *via* the *cis*-(pincer)Ir(H)(H)(olefin) intermediate

Lastly, it is important to distinguish the issues surrounding the *cis*/*trans* isomers of (pincer)Ir(H)(H)(olefin) from the generation of *cis*-2-hexene versus *trans*-2-hexene. As specified in the previous paragraph, dehydrogenation/hydrogenation through the *trans*-(pincer)Ir(H)(H)(olefin) complex had a lower barrier than the *cis* pathway. Therefore, for the first few catalysts examined, two possibilities were considered: dehydrogenation of *n*-hexane *via* C2-C3 and *trans*-(pincer)Ir(H)(H)(olefin) to yield *cis*-2-hexene, and dehydrogenation of *n*-hexane *via* C2-C3 and *trans*-(pincer)Ir(H)(H)(olefin) to yield *trans*-2-hexene. In each case, the barriers for producing *cis*-2-hexene (i.e. 31.0 kcal/mol) were extremely similar to those for generating *trans*-2-hexene (i.e. 31.1 kcal/mol). Therefore, for assessing regioselectivity it was unnecessary to calculate both cases.

Thus, for simplicity, all further calculations (and all the DFT calculations reported in this thesis) only examined the generation of *trans*-2-hexene. Thus, the barriers for generating "2-hexene" are actually the barriers for producing *trans*-2-hexene.

Lastly, the dehydrogenation sequence does not formally begin with the first transition state (C-H activation), but actually starts with the formation of an intermediate σ-complex where the to-be-activated C-H bond begins interacting with the iridium center. While these complexes were calculated for most pathways and catalysts, there was essentially no barrier between the σ-complex "intermediate" and either the completely naked 14-electron species and the C-H activation transition state. Therefore, the σ-complex does not play a meaningful role in determining regioselectivity or the mechanism of dehydrogenation. When available, the energies of the σ-complexes will be reported in the data tables of the appendix, but will not be discussed in the main text of this thesis.

3.4 Identifying how the rate-determining step determines regioselectivity

3.4.1 Regioselectivity of (^{tBu4}PCP)Ir and the influence of sterics on each rate-determining step

To begin the DFT investigation, the dehydrogenation of *n*-hexane into either 1-hexene or 2-hexene by (^{tBu4}PCP)Ir was examined. (Table 3.3)

(^{tBu4}PCP)Ir	C1-C2	C2-C1	C2-C3	C3-C2
[Ir](1-hexene)	0.0	0.0	0.0	0.0
[Ir] + hexane	2.4	2.4	2.4	2.4
C-H activation	23.1	28.2	28.0	30.0
[Ir](H)(hexyl)	20.6	24.6	23.5	26.4
β-H elimination	29.3	28.6	34.4	33.7
[Ir](H)(H)(hexene)	14.3	14.3	20.9	20.9
olefin dissociation	24.9	24.9	27.2	27.2
[Ir]H_2 + hexene	4.7	4.7	1.1	1.1

Table 3.3 Kinetic barriers for dehydrogenation by (^{tBu4}PCP)Ir in kcal/mol

However, before examining these results, it is important to consider how the zero-point energy is set for each calculation. While initial calculations referenced the 14 electron complex as the zero point energy, since that is the step where dehydrogenation begins, further analysis showed that it would be more intuitive to reference the (pincer)Ir(1-hexene) complex even though that species is not part of the catalytic dehydrogenation (or hydrogenation) reaction. This is because referencing the (pincer)Ir(1-hexene) complex gives more intuitive comparisons between catalysts (i.e. (^{tBu4}PCP)Ir versus (^{tBu4}PCOP)Ir versus (^{iPr4}PCP)Ir) than would be possible when using the 14 electron complex. For example, comparison of Table 3.3 with Table 3.5 much further below accurately shows that the two catalysts have similar kinetic barriers to dehydrogenation, whereas referencing the 14 electron complex would predict (^{iPr4}PCP)Ir having extremely low kinetic barriers.

With the issue of the zero-point energy resolved, the two pathways for generating 1-hexene (C1-C2 and C2-C1) were considered. Interestingly, C-H activation at C_1 (i.e. C1-C2, 23.1 kcal/mol) occurred at a lower energy than C-H activation at C_2 (i.e. C2-C1, 28.2 kcal/mol). However, somewhat unexpectedly, the barriers for β-H elimination followed a similar trend, where "action" at C_1 yielded a lower kinetic barrier than at C_2 (28.6 versus 29.3 kcal/mol). When

put together, this showed that although C1-C2 appeared more facile during C-H activation, C2-C1 actually occurred at a lower energy overall due to effects during β-H elimination. Examining olefin dissociation, both C1-C2 and C2-C1 yielded the same *trans* isomer of (^{tBu4}PCP)Ir(H)(H)(1-hexene), causing both pathways to have identical olefin dissociation barriers of 24.9 kcal/mol. More accurately, both C1-C2 and C2-C1 *can* involve *cis*-(^{tBu4}PCP)Ir(H)(H)(1-hexene), but (as discussed in the previous section) the *cis* pathways was always higher in energy than the *trans* pathway, and therefore did not need to be examined.

Thus, β-H elimination was the rate-determining step for both the C1-C2 and C2-C1 pathways during the generation of 1-hexene by (^{tBu4}PCP)Ir. Interestingly, although the C1-C2 pathway seemed more facile on the basis of C-H activation, the circumstances of β-H elimination caused the C2-C1 pathway to *actually* have a lower kinetic barrier. For generating 2-hexene, C-H activation at C_3 was higher in energy than at C_2 (30.0 versus 28.0 kcal/mol), presumably due to additional steric crowding at C_3. However, β-H elimination at C_2 (C3-C2, 33.7 kcal/mol) was actually *lower* in energy than β-H elimination at C_3 (C2-C3, 34.4 kcal/mol). Once again, the action at further-internal positions gave higher energies.

However, the *cause* of the difference in energy between either terminal or internal positions could be caused by either steric or electronic effects. As described earlier, the further internal the position, the more negative steric repulsions would be expected. (Figure 3.6) However, this does not preclude the possibility of electronic differences between the C-H bonds at C_1 versus those at C_2 or C_3.

Moving forward, comparing the most facile pathway for 1-hexene generation (C2-C1) with that of 2-hexene (C3-C2) should provide an explanation for the high experimentally observed

regioselectivity of (^{tBu4}PCP)Ir. (Figure 3.10) Hence, the two overall barriers (measured from the (^{tBu4}PCP)Ir(1-hexene) resting state) are 28.6 and 33.7 kcal/mol.

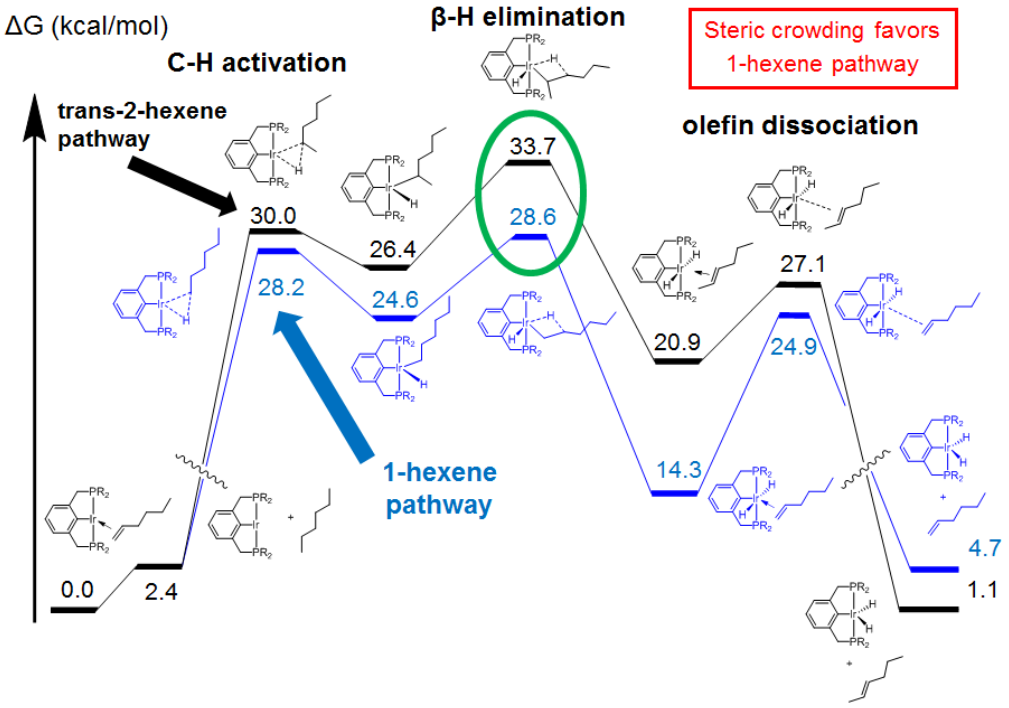

Figure 3.10 Steric crowding during β-H elimination causes high regioselectivity with (^{tBu4}PCP)Ir

Upon initial inspection, this large difference ($\Delta\Delta G^{\ddagger}$) supports the very high regioselectivity. Quantitatively, the Eyring equation can be used to estimate regioselectivity based on the DFT-predicted barriers. Using a temperature of 125 °C (the reaction temperature from direct determination), this gives a rate constant (k) for 1-hexene generation that is approximately 632 times larger than the rate constant for 2-hexene, implying 99.8% regioselectivity for 1-olefins. Notably, this is much higher than the experimental value of 96%.

Thus, DFT calculations show that (^{tBu4}PCP)Ir has high regioselectivity for 1-olefins because the kinetic barriers to dehydrogenation are *much* higher for generating 2-hexene than for 1-hexene. Based on comparisons between pathways, it seems plausible that steric crowding is why

the most facile 1-hexene pathway (C2-C1) has a lower kinetic barrier than the easiest 2-hexene pathway (C3-C2). In both cases the rate-determining step is β-H elimination.

In order to examine whether sterics caused the C3-C2 pathway to have a higher overall barrier than the C2-C1 pathway, another of DFT calculations were conducted. Specifically, the energies for C1-C2 generation of 1-hexene by a series of (^{R4}PCP)Ir catalysts (R = H, Me, Ph, ^{i}Pr, ^{t}Bu) were calculated. In the terminology described in Section 3.2, this analysis examined the first possible factor affecting regioselectivity (changing PR_2 groups) while keep the other four factors constant. (Table 3.4) Technically, changing the PR_2 groups would also influence the electronics of the phosphorous atoms, but those differences are assumed to be negligibly small. Energies were referenced to the 14 electron complex. The (pincer)Ir(1-hexene) catalytic resting state energies were not calculated for the R = Ph, Me, or H complexes.

	R = ^{t}Bu	R = ^{i}Pr	R = Ph	R = Me	R = H
[Ir] + hexane	0.0	0.0	0.0	0.0	0.0
C-H activation	20.8	13.7	9.4	7.5	7.2
[Ir](H)(hexyl)	18.2	11.7	5.6	2.2	2.6
β-H elimination	26.9	14.0	7.4	3.9	3.6
[Ir](H)(H)(hexene)	11.9	0.1	-4.6	-8.8	-8.2
olefin dissociation	22.6	13.7	13.1	12.4	14.4
[Ir]H_2 + hexene	2.4	-0.9	2.1	0.8	1.6

Table 3.4 Kinetic barriers for dehydrogenation by (^{R4}PCP)Ir in kcal/mol *via* C1-C2 pathway

First, this analysis shows that the barrier of C-H activation is drastically affected by sterics, increasing from 7.2 to 20.8 kcal/mol upon modifying R from H to ^{t}Bu, and suggesting a sterically crowded transition state. Likewise, β-H elimination also showed continuous and drastic increase in energy due to sterics (3.6 to 26.9 kcal/mol).

Interestingly, olefin dissociation showed a much different pattern. The barriers for R = H to R = ^{i}Pr were almost identical to one another (when referenced to the 14 electron complex).

However, the barrier for (^{tBu4}PCP)Ir was *much* higher, jumping from 13.7 with (^{iPr4}PCP)Ir to 22.6 kcal/mol. Thus, it appears that olefin dissociation might experience a threshold effect, where no significant steric crowding exists until the PR_2 groups are very large (such as ^{t}Bu).

Hence, this data provides information relevant to regioselectivity. Since both C-H activation and β-H elimination are very sensitive to steric crowding, then the pathways for generating 1-hexene would most likely occur at lower energies than the more crowded pathways for producing 2-hexene. (Figure 3.6) In other words, these DFT calculations predict that if the rate-determining step was C-H activation or β-H elimination, then regioselectivity would be high.

In contrast, since olefin dissociation has much lower sensitivity to sterics, then the energy of the 1-hexene and 2-hexene pathways would be more similar in energy. Hence, if olefin dissociation was the rate-determining step, then regioselectivity for 1-hexene would be lower.

3.4.2 Regioselectivity of other (PCP)Ir catalysts

With an DFT-based explanation of the regioselectivity of (^{tBu4}PCP)Ir in hand, these DFT calculations were extended to other (PCP)Ir catalysts. First, the role of altering the PR_2 groups was examined.

For (^{iPr4}PCP)Ir, the rate-determining step was found to be either β-H elimination or C-H activation. (Table 3.5) Comparing the most facile kinetic barriers for generating 1-hexene versus 2-hexene showed that DFT calculations predicted high regioselectivity for (^{iPr4}PCP)Ir. Specifically, the lowest pathway to 1-hexene was C1-C2 (28.7 kcal/mol relative to the 1-olefin resting state), whereas the most facile path to 2-hexene was C2-C3 at 31.7 kcal/mol. The Eyring equation can

be used to estimate the regioselectivity of (^{iPr4}PCP)Ir at 125 °C. These calculations yield an estimated 98% regioselectivity.

	C1-C2	C2-C1	C2-C3	C3-C2
[Ir](1-hexene)	0.0	0.0	0.0	0.0
[Ir] + hexane	14.7	14.7	14.7	14.7
σ-complex	19.4	20.6	20.6	21.9
C-H activation	28.4	31.3	31.7	32.6
[Ir](H)(hexyl)	26.4	26.2	27.1	27.5
β-H elimination	28.7	27.7	30.9	31.6
[Ir](H)(H)(hexene)	14.8	14.8	17.8	17.8
olefin dissociation	28.4	28.4	29.1	29.1
[Ir]H_2 + hexene	13.8	13.8	10.2	10.2

Table 3.5 Kinetic barriers for dehydrogenation with (^{iPr4}PCP)Ir in kcal/mol

While DFT calculations appears to be overestimating regioselectivity somewhat, the qualitative results are strongly consistent with experiment, and provide a mechanistic rationale for why (^{iPr4}PCP)Ir has lower regioselectivity than (^{tBu4}PCP)Ir. (Table 3.6)

Catalyst	Steric crowing	Experimental regioselectivity	DFT-predicted regioselectivity
(^{tBu4}PCP)Ir	More	96 %	99.8 %
(^{iPr4}PCP)Ir	Less	91 %	98 %

Table 3.6 Comparison of regioselectivity by (^{tBu4}PCP)Ir and (^{iPr4}PCP)Ir

Notably, the C-H activation kinetic barrier in the C2-C1 pathway is *not* the same as the C-H activation barrier in C2-C3 pathway (31.3 versus 31.7 kcal/mol), despite both being C-H activations at C_2. This is because the two intermediates produced by C-H activation, the (^{iPr4}PCP)Ir(H)(2-hexyl) complexes, represent different conformers. Therefore, the specific geometric conformations during C-H activation required to generate these conformers are also not the same. These differences are required because the hexyl chain in (^{iPr4}PCP)Ir(H)(2-hexyl) oriented in a particular direction for β-H elimination to occur at a specific atom. For example, in

order to generate 1-hexene *via* C2-C1, the hexyl chain must be oriented so that β-H elimination can occur at C_1. In contrast, producing 2-hexene *via* C2-C3 requires β-H elimination at C_3. Due to the steric bulkiness of the P^iPr_2 groups, rotation of the hexyl group around the Ir-C bond is not possible. Hence, direct interconversion of the two (^{iPr4}PCP)Ir(H)(2-hexyl) conformers is not energetically possible, and only indirect interconversion (through reductive elimination and a subsequent, second C-H activation) is energetically feasible. This trend was found for all pincer iridium catalysts studied.

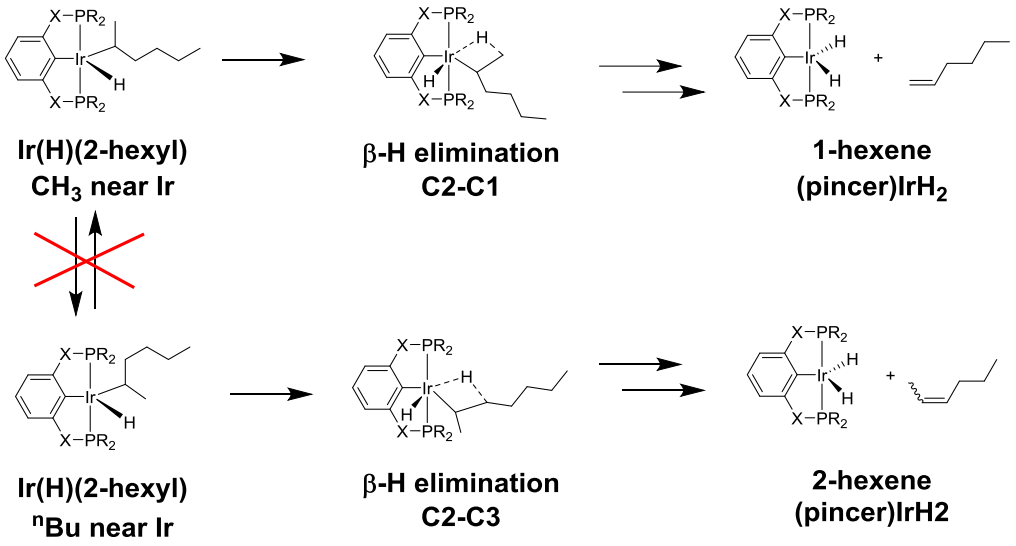

Figure 3.11 Geometric differences between C2-C1 and C2-C3 pathways

Although (^{tBu2}PCP^{iPr2})Ir was not studied by DFT calculations, it is plausible and highly likely that the same steric-based rationales also apply to its observed regioselectivity. With two ^{t}Bu groups but also two ^{i}Pr groups, its steric crowding is intermediate between (^{tBu4}PCP)Ir and (^{iPr4}PCP)Ir. Thus, if DFT calculations had been conducted, they would have most likely provided a DFT-predicted regioselectivity between 94 % and 99.8 % (the values for (^{iPr4}PCP)Ir and (^{tBu4}PCP)Ir). Matched with the experiment-observed regioselectivity of 93% to 95% for (^{tBu2}PCP^{iPr2})Ir, the DFT

calculations would have likely corroborated the proposed explanation for the observed regioselectivity.

Moving forward, (MeO-^{tBu4}PCP)Ir and (Me_2N-^{tBu4}PCP)Ir were also examined by DFT calculations in order to elucidate the possible effect of aryl electronics on regioselectivity. (Section 3.2) (Tables 3.7 and 3.8) In both cases the rate-determining step was always β-H elimination, causing high estimated regioselectivities. In particular, these estimates were 99.8% for (MeO-^{tBu4}PCP)Ir and 99.7% for (Me_2N-^{tBu4}PCP)Ir.

	C1-C2	C2-C1	C2-C3	C3-C2
[Ir](1-hexene)	0.0	0.0	0.0	0.0
[Ir] + hexane	1.9	1.9	1.9	1.9
C-H activation	22.6	26.6	27.0	29.0
[Ir](H)(hexyl)	19.9	23.5	22.9	25.0
β-H elimination	29.2	27.9	34.6	33.0
[Ir](H)(H)(hexene)	15.2	15.2	20.0	20.0
olefin dissociation	27.3	27.3	26.8	26.8
[Ir]H_2 + hexene	2.3	2.3	-1.3	-1.3

Table 3.7 Kinetic barriers to dehydrogenation with (MeO-^{tBu4}PCP)Ir in kcal/mol

	C1-C2	C2-C1	C2-C3	C3-C2
[Ir](1-hexene)	0.0	0.0	0.0	0.0
[Ir] + hexane	2.5	2.5	2.5	2.5
C-H activation	22.1	26.8	26.8	28.8
[Ir](H)(hexyl)	19.8	23.2	22.6	24.8
β-H elimination	29.6	28.9	34.9	33.6
[Ir](H)(H)(hexene)	15.5	15.5	20.3	20.3
olefin dissociation	27.8	27.8	27.8	27.8
[Ir]H_2 + hexene	2.3	2.3	-1.4	-1.4

Table 3.8 Kinetic barriers to dehydrogenation with (Me_2N-^{tBu4}PCP)Ir in kcal/mol

Hence, the combination of experimental and computational results clearly demonstrates that that the *para*-methoxy and *para*-dimethylamino groups have no discernable effect on regioselectivity.

3.4.3 Regioselectivity of (PCOP)Ir and (POCOP)Ir catalysts

With a solid understanding of (PCP)Ir catalysts in hand, the DFT calculations were extended to (PCOP)Ir and (POCOP)Ir catalysts. In addition to explaining why (PCP)Ir catalysts had such high regioselectivities, these new DFT calculations were undertaken to help elucidate why (PCOP)Ir and (POCOP)Ir catalysts had such *low* experimentally-observed regioselectivity.

First, DFT calculations regarding (^{tBu4}POCOP)Ir and (^{iPr4}POCOP)Ir were performed. While the experimental regioselectivity of (^{iPr4}POCOP)Ir could not be determined due to an extremely low rate of transfer dehydrogenation (relative to isomerization), its results could still be employed in understanding the mechanism behind regioselectivity and to corroborate the results from (^{tBu4}POCOP)Ir.

Comparison of the C-H activation and β-H elimination energies of (^{tBu4}POCOP)Ir to (^{tBu4}PCP)Ir revealed familiar trends. (Table 3.9) C-H activation at further internal positions had higher kinetic barriers than at terminal positions. β-H elimination followed the same trend. Due to this steric crowding, as expected, C-H activation and β-H elimination allowed 1-hexene to be formed with a lower kinetic barrier than 2-hexene (30.2 kcal/mol *via* C2-C1 versus 35.3 kcal/mol *via* C2-C3).

	C1-C2	C2-C1	C2-C3	C3-C2
[Ir](1-hexene)	0.0	0.0	0.0	0.0
[Ir] + hexane	13.3	13.3	13.3	13.3
σ-complex	18.7	19.8	19.8	20.2
C-H activation	25.0	28.8	29.4	30.5
[Ir](H)(hexyl)	22.1	24.2	23.4	25.3
β-H elimination	34.6	30.2	35.3	37.2
[Ir](H)(H)(hexene)	22.5	22.5	24.8	24.8
olefin dissociation	36.3	36.3	36.6	36.6
[Ir]H_2 + hexene	10.1	10.1	6.4	6.4

Table 3.9 Kinetic barriers to dehydrogenation by (^{tBu4}POCOP)Ir in kcal/mol

However, of critical importance, this represented only the *formation* of 1-hexene and the creation of the (^{tBu4}POCOP)Ir(H)(H)(hexene) complex. The *dissociation* of that hexene from the iridium center had not yet been considered. So, upon calculation of the olefin dissociation barrier, a very surprising finding was revealed: olefin dissociation had a higher barrier than both C-H activation and β-H elimination! The rate-determining step had changed to olefin dissociation! (Figure 3.12)

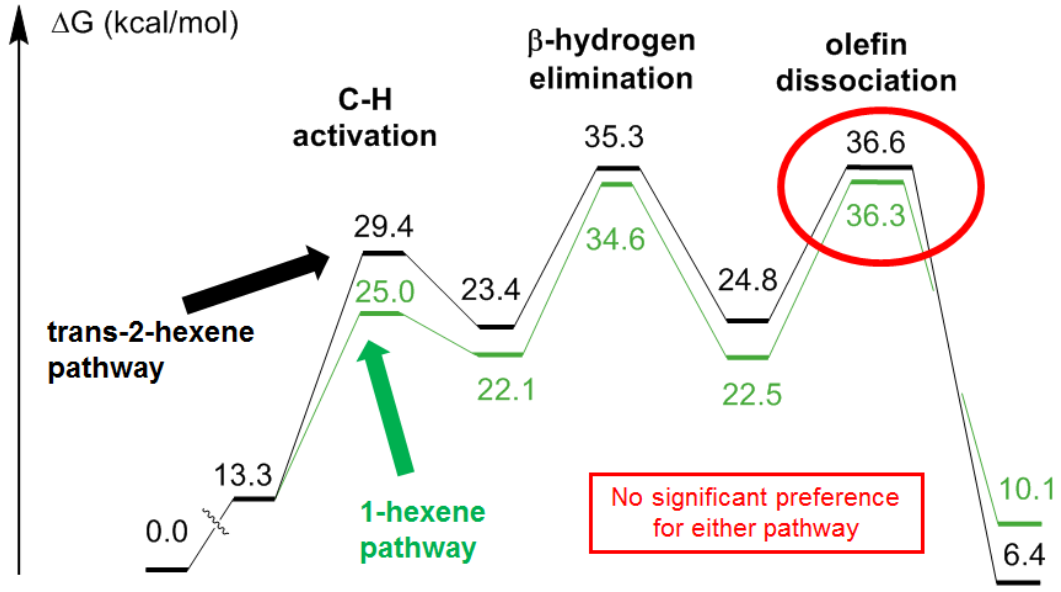

Figure 3.12 Nearly identical kinetic barriers to olefin dissociation with (^{tBu4}POCOP)Ir cause low regioselectivity

While this was a very intriguing finding, by itself this change in rate-determining step did not necessarily affect regioselectivity. However, in the case of (^{tBu4}POCOP)Ir, this change in rate-determining step *does* fundamentally change regioselectivity. As noted in Table 3.9, interestingly the two barriers for olefin dissociation (for 1-hexene or 2-hexene) are essentially identical at 36.3 and 36.6 kcal/mol. Given that the random error of these DFT calculations was approximately 0.5 kcal/mol, these two olefin dissociation barriers are essentially statistically identical. Hence, given

two identical barriers, the quantity of each product generated would also be equal, yielding *much* lower regioselectivity (in the neighborhood of 50%). This is in strong agreement with experiment, which showed that (^{tBu4}POCOP)Ir had *much* lower regioselectivity than any of the (PCP)Ir catalysts.

In essence, the olefin dissociation step in (^{tBu4}POCOP)Ir does not discriminate against producing 2-hexene, unlike the β-H elimination step in the (PCP)Ir catalysts which *favors* the generation of 1-hexene over 2-hexene. This lack of discrimination against 2-hexene by olefin dissociation is unsurprising given that it is less sensitive to sterics than the other two transition states. (Table 3.4) In fact, with (PCP)Ir catalysts olefin dissociation has only a weak or non-existent preference for 1-hexene. In contrast, the β-H elimination step in (^{tBu4}POCOP)Ir *was* discriminatory against 2-hexene, favoring 1-hexene, but it was not the rate-determining step and so it did not influence the actual result.

Therefore, the following working hypothesis was formulated: due to varying sensitivities to steric crowding, catalysts which had C-H activation or β-H elimination as their rate-determining step would likely be highly regioselective, whereas catalysts with olefin dissociation rate-determining steps would probably have much lower regioselectivity.

The next catalyst studied, (^{iPr4}POCOP)Ir, reinforced many of the trends and conclusions found with (^{tBu4}POCOP)Ir. (Table 3.10) In particular, rate-determining step changed to olefin dissociation. Nominally, production of 2-hexene was predicted to have a lower barrier (by 0.3 kcal/mol) than generation of 1-hexene, causing < 50% regioselectivity. However, as described above the random error of these DFT calculations was roughly 0.5 kcal/mol, and so the two olefin dissociation barriers were statistically identical. Hence, although the regioselectivity of (^{iPr4}POCOP)Ir could not be measured experimentally, these DFT calculations suggest that it would be quite low (~ 50%) and similar to that of (^{tBu4}POCOP)Ir.

	C1-C2	C2-C1	C2-C3	C3-C2
[Ir](1-hexene)	0.0	0.0	0.0	0.0
[Ir] + hexane	20.5	20.5	20.5	20.5
σ-complex	20.8	21.7	21.7	23.3
C-H activation	26.1	28.6	29.0	30.3
[Ir](H)(hexyl)	24.1	22.7	22.2	23.6
β-H elimination	25.6	25.0	27.1	29.4
[Ir](H)(H)(hexene)	16.7	16.7	18.1	18.1
olefin dissociation	32.7	32.7	32.4	32.4
[Ir]H_2 + hexene	14.2	14.2	10.6	10.6

Table 3.10 Kinetic barriers to dehydrogenation with (^{iPr4}POCOP)Ir in kcal/mol

Moving forward, the trends observed with DFT calculations on (POCOP)Ir catalysts were further verified and examined by studying (PCOP)Ir catalysts, which also had low regioselectivity during the experimental studies.

First, DFT calculations of the four possible dehydrogenation pathways by (^{tBu4}PCOP)Ir gave results that were different from both the (PCP)Ir catalysts *and* from (POCOP)Ir catalysts. (Table 3.11) In specific, it was unclear which step was the rate-determining step for generation of 1-hexene by (^{tBu4}PCOP)Ir. In the C1-C2 pathway, β-H elimination and olefin dissociation had kinetic barriers that were very similar (31.5 and 31.2 kcal/mol). Moreover, the C2-C1 pathway had a lower kinetic barrier for β-H elimination (28.6 kcal/mol) but the same olefin dissociation barrier (31.2 kcal/mol) as in the C1-C2 pathway. Therefore, on a nominal level, it appeared that the rate-determining step in C1-C2 was β-H elimination at 31.5 kcal/mol, while that of C2-C1 was olefin dissociation at 31.2 kcal/mol. Hence, on a superficial level, it appeared that 1-hexene would be generated mostly *via* C2-C1.

	C1-C2	C2-C1	C2-C3	C3-C2
[Ir](1-hexene)	0.0	0.0	0.0	0.0
[Ir] + hexane	6.3	6.3	6.3	6.3
σ-complex	15.3	15.9	15.9	16.1
C-H activation	23.5	27.5	27.6	29.5
[Ir](H)(hexyl)	20.9	23.4	22.7	24.8
β-H elimination	31.5	28.6	33.3	35.0
[Ir](H)(H)(hexene)	17.8	17.8	22.0	22.0
olefin dissociation	31.2	31.2	31.0	31.0
[Ir]H_2 + hexene	6.6	6.6	3.0	3.0

Table 3.11 Kinetic barriers to dehydrogenation with (^{tBu4}PCOP)Ir in kcal/mol

However, examination of the sources of error for DFT calculations demonstrated that this conclusion is not exactly correct. Before examining these sources of error, it is useful to highlight other aspects of the (^{tBu4}PCOP)Ir calculations which strongly suggest the issues created by these errors.

Moving onto the generation of 2-hexene by (^{tBu4}PCOP)Ir, it appears that β-H elimination is the rate-determining step. The C2-C3 pathway (33.3 kcal/mol) has a lower overall barrier than C3-C2 (35.0 kcal/mol), and the C2-C3 pathway has a rate-determining step of β-H elimination. However, comparison between the 1-hexene generation barrier (31.2 kcal/mol) and that for 2-hexene production (33.3 kcal/mol) suggests that (^{tBu4}PCOP)Ir would have high regioselectivity, in direct contrast to experimental observations. Calculating the Eyring equation with a 125 °C reaction temperature, the ratio of 1-hexene to 2-hexene rate constants would be approximately 14 : 1, yielding a 93% regioselectivity for 1-olefins. Based on direct determination and competitive dehydrogenation tests, (^{tBu4}PCOP)Ir had much lower regioselectivity.

Hence, the stark disagreement between experimentally-observed regioselectivities for (^{tBu4}PCOP)Ir and the predictions from DFT calculations would need to be resolved. In particular, the errors inherent in DFT calculations would need to be assessed in order to ascertain how accurate those calculations were.

3.4.4 Assessing the random and systematic errors in DFT calculations

In general, it is important to recognize the errors and uncertainties in these DFT-calculated energies, both between different pathways (i.e. β-H elimination of C1-C2 versus C2-C3) and between different transition states (i.e. β-H elimination of C1-C2 versus olefin dissociation of C1-C2 also). In particular, the differences between *systematic error* and *random error* must be understood. Depending on the terminology used, this can also be understood as the difference between accuracy (high accuracy requires low systematic error) and precision (high precision requires low random error).

With these type of DFT calculations, the random errors between pathways are generally fairly small (≤ 0.5 kcal/mol). As a fictitious example, assume that for Catalyst A the actual β-H elimination barrier for C1-C2 is 30.0 kcal/mol, and that the β-H elimination barrier for C2-C3 is 40.0 kcal/mol. (Table 3.12) However, also assume that the DFT-predicted values are 32.0 and 42.3 kcal/mol instead. Using C1-C2 as a reference point, the +2.0 kcal/mol difference between the DFT and experimental barriers (30.0 versus 32.0 kcal/mol) represents the *systematic* error in assessing this particular step (β-H elimination) for this particular catalyst (Catalyst A). To understand the *random* error between C1-C2 and C2-C3, the systematic error of 2.0 kcal/mol can be added to the actual C2-C3 barrier of 40.0 kcal/mol, yielding 42.0 kcal/mol. Thus, it is expected that DFT calculations will calculate the C2-C3 barrier as 42.0 kcal/mol. However, when DFT calculations return a value of 42.3 kcal/mol instead, this suggests that the random error between C1-C2 and C2-C1 was 42.3 – 42.0 = +0.3 kcal/mol.

Catalyst A	C1-C2	C2-C3
[Ir](1-hexene)	0.0	0.0
Actual β-H elimination	30.0	40.0
DFT-calculated β-H elimination	32.0	42.3
Systematic error in DFT calculations	If C1-C2 is used as a reference point, DFT calculations underestimate the C-H activation barrier for Catalyst A by +2.0 kcal/mol	
Random error in DFT calculations	Assuming this systematic error of 2.0 kcal/mol, then the expected DFT barrier for C2-C1 would be 37.0 kcal/mol. However, since the value was 37.3, this represents a +0.3 kcal/mol random error between C1-C2 and C2-C1.	

Table 3.12 Hypothetical example using "Catalyst A" to discuss errors in β-H elimination in kcal/mol

Secondly, comparisons between *different* transition states, even while keeping the pathway and catalyst the same, are subject to much larger errors, mainly due to large systematic errors. Expanding upon the previous example, actual olefin dissociation barriers (34.0 and 44.0 kcal/mol) as well as DFT-calculated barriers (31.0 and 40.9 kcal/mol) can be included in the example. (Table 3.13) Thus, the errors originating from two different transition states can be examined.

Following the procedure described above, both the random and systematic errors in olefin dissociation can be calculated. In this fictitious example, the systematic error was -3.0 kcal/mol, while the random error was only -0.1 kcal/mol.

Catalyst A	C1-C2	C2-C3
[Ir](1-hexene)	0.0	0.0
Actual β-H elimination	30.0	40.0
DFT-calculated β-H elimination	32.0	42.3
Systematic error in β-H elimination	As described in Table 3.13, the systematic error was +2.0 kcal/mol	
Random error in β-H elimination	As described in Table 3.13, the random error was +0.3 kcal/mol	
Actual olefin dissociation	34.0	44.0
DFT-calculated olefin dissociation	31.0	40.9
Systematic error in olefin dissociation	Using C1-C2 as the reference point, the systematic error is -3.0 kcal/mol	
Random error in olefin dissociation	Assuming this systematic error of -3.0 kcal/mol, then the expected DFT barrier for C2-C1 would be 41.0 kcal/mol. However, since the value was 41.1, this represents a -0.1 kcal/mol random error between C1-C2 and C2-C1.	

Table 3.13 Hypothetical example using "Catalyst A" to discuss errors in kcal/mol

Returning to the concept of (^{tBu4}PCOP)Ir and regioselectivity, as described previously it is the identity of the rate-determining step that appears to determine regioselectivity. Thus, the calculation of systematic and random errors *within* a certain transition state is not sufficient to understand or validate regioselectivity. Instead, how these errors propagate *between* different transition states must also be examined, since the different in energies of each transition state (i.e. which one has the highest energy) is what determines the rate-determining step and thereby regioselectivity.

Returning to the hypothetical example, rearranging the data from Table 3.13 allows for the calculation of a new parameter, $\Delta\Delta G^{\ddagger}_{\beta H\text{-}OD}$. (Equation 3.2) (Table 3.14) By convention, it is the β-H elimination energy minus the olefin dissociation energy. As expressed, a positive value for $\Delta\Delta G^{\ddagger}_{\beta H\text{-}OD}$ indicates that β-H elimination has a higher energy, and is therefore the rate-determining step. In contrast, a negative value for $\Delta\Delta G^{\ddagger}_{\beta H\text{-}OD}$ signifies that olefin dissociation is the rate-determining step.

$$\Delta\Delta G^{\ddagger}_{\beta H-OD} = \beta H\ elimination - olefin\ dissociation$$

Equation 3.2 Definition of $\Delta\Delta G^{\ddagger}_{\beta H\text{-}OD}$

Catalyst A	C1-C2	C2-C3
[Ir](1-hexene)	0.0	0.0
DFT-calculated β-H elimination	32.0	42.3
DFT-calculated olefin dissociation	31.0	40.9
DFT-calculated $\Delta\Delta G^{\ddagger}_{\beta H\text{-}OD}$	+ 1.0	+ 1.4
DFT conclusion regarding rate-determining step	β-H elimination is rate-determining step	
Actual β-H elimination	30.0	40.0
Actual olefin dissociation	34.0	44.0
Actual $\Delta\Delta G^{\ddagger}_{\beta H\text{-}OD}$	- 4.0	- 4.0
Actual rate-determining step	Olefin dissociation is rate-determining step	
Explanation of how DFT calculations predicted the incorrect rate-determining step	The systematic errors of β-H elimination being too high by 2.0, and olefin dissociation too low by 3.0, changed $\Delta\Delta G^{\ddagger}$ from - 4.0 to + 1.0. Random errors increased this difference to + 1.4 in C2-C3.	

Table 3.14 Employing $\Delta\Delta G^{\ddagger}_{\beta H\text{-}OD}$ to explain errors in hypothetical example in kcal/mol

Given the specific energies in this example, DFT calculations predicts a positive value of + 1.0 kcal/mol for $\Delta\Delta G^{\ddagger}_{\beta H\text{-}OD}$ during C1-C2. In turn, this suggests β-H elimination is the rate-determining step. Notably, this value becomes + 1.4 kcal/mol when considering C2-C3, also signifying β-H elimination as the rate-determining step. This difference originates from the combination of the +0.3 and -0.1 kcal/mol random errors between C1-C2 and C2-C3 during β-H elimination and olefin dissociation, respectively.

Moving forward, the same calculation of $\Delta\Delta G^{\ddagger}$ can be used to find the actual/known rate-determining step based on "actual" values. Interestingly, these return negative values for $\Delta\Delta G^{\ddagger}_{\beta H\text{-}OD}$, indicating that the true rate-determining step of Catalyst A is actually olefin dissociation, not β-H elimination as predicted by DFT. The differences in "actual" versus DFT-predicted $\Delta\Delta G^{\ddagger}_{\beta H\text{-}OD}$ values during C1-C2 (which were -4.0 and +1.0 kcal/mol, respectively), amount to a net difference in 5.0 kcal/mol. In turn, this came from a combination of two systematic errors. DFT calculations overestimated the barriers of β-H elimination by 2.0 kcal/mol, while also underestimating the barriers for olefin dissociation by 3.0 kcal/mol, hence yielding the 5.0 kcal/mol difference observed.

Therefore, systematic errors when comparing different transition states could cause erroneous predictions regarding the identity of the rate-determining step. Hence, DFT calculations would be more reliable as a *qualitative* tool for assessing general trends in the energies of each transition state, and not necessarily a *quantitative* measure of the energy of each transition state and/or intermediate.

3.4.5 Using $\Delta\Delta G^{\ddagger}_{\beta H\text{-}OD}$ to understand the rate-determining step

Since systematic errors when comparing different transition states can cause the incorrect rate-determining step to be predicted, comparing the various transition states with the $\Delta\Delta G^{\ddagger}_{\beta H\text{-}OD}$ parameter might be more effective at determining the true rate-determining step.

Before making a full comparison with $\Delta\Delta G^{\ddagger}_{\beta H\text{-}OD}$ between all pincer iridium catalysts, the final catalyst in the sequence (^{iPr4}PCOP)Ir was examined. (Table 3.15) Similarly to (^{tBu4}PCOP)Ir, the identity of the rate-determining step during generation of 1-hexene was unclear.

	C1-C2	C2-C1	C2-C3	C3-C2
[Ir](1-hexene)	0.0	0.0	0.0	0.0
[Ir] + hexane	15.7	15.7	15.7	15.7
σ-complex	21.8	23.9	23.9	23.9
C-H activation	26.6	31.8	30.5	32.8
[Ir](H)(hexyl)	25.3	27.1	30.2	28.2
β-H elimination	31.0	27.8	33.3	32.1
[Ir](H)(H)(hexene)	19.8	19.8	21.4	21.4
olefin dissociation	31.6	31.6	32.3	32.3
[Ir]H_2 + hexene	18.4	18.4	14.7	14.7

Table 3.15 Kinetic barriers to dehydrogenation by (^{iPr4}PCOP)Ir in kcal/mol

Considering the Eyring equation at a reaction temperature of 125 °C, the DFT calculations predict a regioselectivity of approximately 71%. By comparison, the direct determination experiments gave an estimated regioselectivity of 79%.

With the data for (^{iPr4}PCOP)Ir tabulated, the $\Delta\Delta G^{\ddagger}_{\beta H\text{-}OD}$ values for eight different pincer iridium catalysts could be calculated. (Table 3.16) Positive values indicated a β-H elimination rate-determining step whereas negative values indicated an olefin dissociation rate-determining step.

$\Delta\Delta G^{\ddagger}_{\beta H\text{-}OD}$	C1-C2	C2-C1	C2-C3	C3-C2	average
(^{tBu4}PCP)Ir	4.4	3.6	7.2	6.5	5.5
(Me$_2$N-^{tBu4}PCP)Ir	1.9	1.2	7.2	5.8	4.0
(MeO-^{tBu4}PCP)Ir	1.9	0.6	7.8	6.2	4.1
(^{iPr4}PCP)Ir	0.3	-0.7	1.7	2.4	1.0
(^{tBu4}PCOP)Ir	0.4	-2.6	2.2	4.0	1.0
(^{iPr4}PCOP)Ir	-0.6	-3.8	1.0	-0.2	-0.9
(^{tBu4}POCOP)Ir	-1.6	-6.1	-1.3	0.5	-2.1
(^{iPr4}POCOP)Ir	-7.1	-7.7	-5.3	-3.1	-5.8

Table 3.16 $\Delta\Delta G^{\ddagger}_{\beta H\text{-}OD}$ values for several pincer iridium catalysts in kcal/mol

First, the three pincer iridium catalysts with four ^{t}Bu groups and no functionalization in the *para* position were compared. (Table 3.17) Since the average value decreases from 5.5 to 1.0 to -2.1 kcal/mol upon changing from a PCP to PCOP to POCOP framework, then this confirms the effect of the ligand backbone on the rate-determining step. Despite the $\Delta\Delta G^{\ddagger}_{\beta H\text{-}OD}$ value for (^{tBu4}PCOP)Ir being positive at 1.0 kcal/mol, its closeness to zero left open the possibility that systematic error had perturbed the DFT calculations. In fact, if the random error of these calculations was close to 0.5 kcal/mol, then even a small systematic error could have easily pushed the true, negative $\Delta\Delta G^{\ddagger}_{\beta H\text{-}OD}$ value for (^{tBu4}PCOP)Ir erroneously into the positive range.

$\Delta\Delta G^{\ddagger}_{\beta H\text{-}OD}$	C1-C2	C2-C1	C2-C3	C3-C2	average
(^{tBu4}PCP)Ir	4.4	3.6	7.2	6.5	5.5
(^{tBu4}PCOP)Ir	0.4	-2.6	2.2	4.0	1.0
(^{tBu4}POCOP)Ir	-1.6	-6.1	-1.3	0.5	-2.1

Table 3.17 $\Delta\Delta G^{\ddagger}_{\beta H\text{-}OD}$ values for pincer iridium catalysts with four ^{t}Bu groups in kcal/mol

In order to validate the trends observed with (^{tBu4}pincer)Ir catalysts, the preceding analysis was repeated for the three studied catalysts with four ^{i}Pr groups. (Table 3.18) While the numerical values changed, the trends were very similar to those with the ^{t}Bu catalysts. Namely, the average $\Delta\Delta G^{\ddagger}_{\beta H\text{-}OD}$ value decreased significantly upon changing from the PCP to PCOP to

POCOP backbones. Notably, the average value for (^{iPr4}PCOP)Ir was negative, suggesting an olefin dissociation rate-determining step.

$\Delta\Delta G^{\ddagger}_{\beta H\text{-}OD}$	C1-C2	C2-C1	C2-C3	C3-C2	average
(^{iPr4}PCP)Ir	0.3	-0.7	1.7	2.4	1.0
(^{iPr4}PCOP)Ir	-0.6	-3.8	1.0	-0.2	-0.9
(^{iPr4}POCOP)Ir	-7.1	-7.7	-5.3	-3.1	-5.8

Table 3.18 $\Delta\Delta G^{\ddagger}_{\beta H\text{-}OD}$ values for pincer iridium catalysts with four ^{i}Pr groups in kcal/mol

Overall, this analysis showed that since the $\Delta\Delta G^{\ddagger}_{\beta H\text{-}OD}$ value for (PCOP)Ir catalysts was within the random error of zero, then the DFT calculations could not discern the identity of the rate-determining step. Hence, it is very possible that olefin dissociation was the rate-determining step, in agreement with the low regioselectivity observed experimentally.

Moving forward, the $\Delta\Delta G^{\ddagger}_{\beta H\text{-}OD}$ analysis was also used to explore the effects of *para*-functionalizing (^{tBu4}PCP)Ir. (Table 3.19) Although the observed regioselectivity of (Me_2N-^{tBu4}PCP)Ir and (MeO-^{tBu4}PCP)Ir were identical to that of (^{tBu4}PCP)Ir, their behavior during DFT calculations was much different. Namely, both had *much* lower $\Delta\Delta G^{\ddagger}_{\beta H\text{-}OD}$ values (around 1.5 kcal/mol) than (^{tBu4}PCP)Ir (average of 4.0 kcal/mol). Thus, it appeared that the methoxy and dimethylamino groups *did* have an effect on the relative barriers of the transition states. The electronic effects of these groups moved the barriers towards an olefin dissociation rate-determining step, but the *magnitude* of this change was not enough to actually cause a change in rate-determining step. Thus, the DFT calculations predict that (MeO-^{tBu4}PCP)Ir and (Me_2N-^{tBu4}PCP)Ir would retain high regioselectivity, in agreement with experimental observations.

$\Delta\Delta G^{\ddagger}_{\beta H\text{-}OD}$	C1-C2	C2-C1	C2-C3	C3-C2	Overall average	Average for 1-hexene
(^{tBu4}PCP)Ir	4.4	3.6	7.2	6.5	5.5	4.0
(Me$_2$N-^{tBu4}PCP)Ir	1.9	1.2	7.2	5.8	4.0	1.6
(MeO-^{tBu4}PCP)Ir	1.9	0.6	7.8	6.2	4.1	1.3

Table 3.19 $\Delta\Delta G^{\ddagger}$ values for (^{tBu4}PCP)Ir and its *para*-functionalized analogs in kcal/mol

3.5 Identifying how steric and electronic factors determine the rate-determining step

3.5.1 Effect of para-OMe and para-NMe$_2$ groups on the rate-determining step

To further examine the role of aryl electronics, a comparison between four pincer iridium catalysts was made. (Table 3.20) For a proper comparison, the same pathway of C2-C1 was tabulated for each catalyst. In general, C2-C1 seemed to give consistent results from each catalyst, whereas C1-C2 sometimes yielded values which seemed somewhat less consistent.

When viewed in this way, it appears that the *para*-methoxy and *para*-dimethylamino groups have helped the (PCP)Ir catalyst to "look more like (POCOP)Ir." Energetically, these functional groups have caused the catalyst to move towards the energetics of (POCOP)Ir.

	(^{tBu4}PCP)Ir C2-C1	(Me$_2$N-^{tBu4}PCP)Ir C2-C1	(MeO-^{tBu4}PCP)Ir C2-C1	(^{tBu4}POCOP)Ir C2-C1
β-H elimination	26.2	26.5	25.9	16.9
Olefin dissociation	22.6	25.3	25.4	23.0
$\Delta\Delta G^{\ddagger}_{\beta H\text{-}OD}$	3.6	1.2	0.5	-6.1

Table 3.20 $\Delta\Delta G^{\ddagger}$ values of common catalysts in kcal/mol

While the magnitude of this change was not significant enough to alter the rate-determining step, and therefore change the experimentally-observed regioselectivity, the energetic movements nonetheless appear to be very real.

3.5.2 Effect of steric differences between (PCP)Ir and (POCOP)Ir catalysts on the rate-determining step

In order to continue the comparison of (PCP)Ir versus (POCOP)Ir catalysts, the possibility that steric differences were affecting the rate-determining step was explored. In particular, these steric differences included the retraction of the PR_2 groups towards the aryl ring in (POCOP)Ir catalysts,[5] and the more planar conformation of POCOP ligands versus the more twisted geometry of the PCP ligands.

In the process of calculating the energies of the 14 electron complexes of (^{tBu4}PCP)Ir and (^{tBu4}POCOP)Ir, their DFT-optimized structures were also found. These results showed that in (PCP)Ir catalysts (such as (^{tBu4}PCP)Ir) the aryl ring was tilted/twisted slightly relative to the plane defined by the plane of P-Ir-P-C_{ipso}. (Figure 3.13) While 3-dimensional planes are technically defined by three locations (i.e. atoms) and not four, the P-Ir-P connection was found to be very close to linear. In addition, the C_{ipso} atom is hidden directly behind the iridium atom. In contrast, the aryl ring of (POCOP)Ir catalysts (such as (^{tBu4}POCOP)Ir) was very close to coplanar with the plane defined by P-Ir-P-C_{ipso}. In fact, this planarity is why the oxygen linkages in (^{tBu4}POCOP)Ir are almost invisibly hidden directly behind the phosphorous atoms.

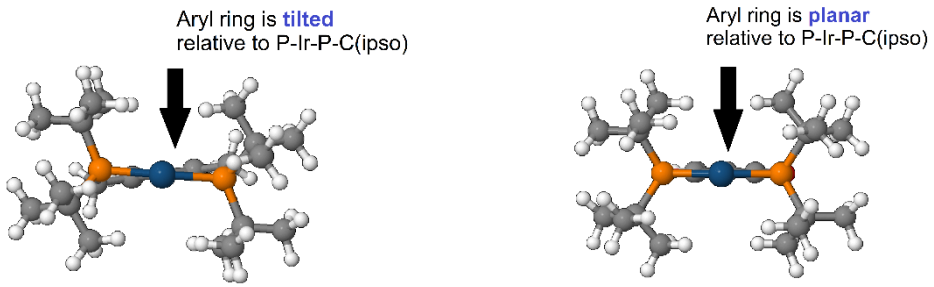

Figure 3.13 DFT-optimized geometries of 14 electron complexes of (^{tBu4}PCP)Ir (left) and (^{tBu4}POCOP)Ir (right)

Presumably, the conjugation of the lone pair on the oxygen atoms in (POCOP)Ir with the π-cloud of the aryl rings locked the POCOP ligand into a particular geometry (which was planar). (Figure 3.14) In contrast, the obvious lack of conjugation between the methylene bridge groups (CH_2) and the aryl ring PCP ligands.

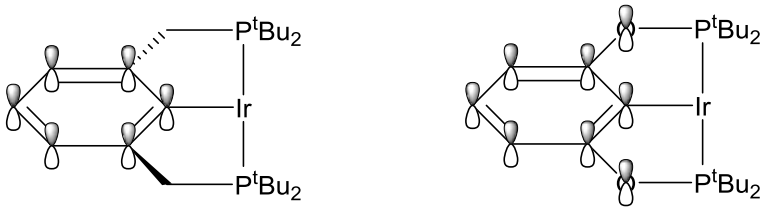

(^{tBu4}PCP)Ir
no conjugation with
CH_2 groups

(^{tBu4}POCOP)Ir
conjugation of aryl ring
with oxygen atoms

Figure 3.14 Conjugation in (^{tBu4}PCP)Ir versus (^{tBu4}POCOP)Ir

Computationally, the role of twisted versus planar ligands was investigated first. While the geometry of the arms would not directly influence sterics, the angle of the P-C or P-O linker between the aryl ring and the PR_2 groups *would* influence the angles of the P-C bonds of the PR_2 groups. (Figure 3.15) In turn, this would change the spatial configuration of the ^{t}Bu and/or ^{i}Pr groups around the iridium center. It is important to recognize that sterics is not a single, linear parameter; instead, it is multifaceted phenomenon.

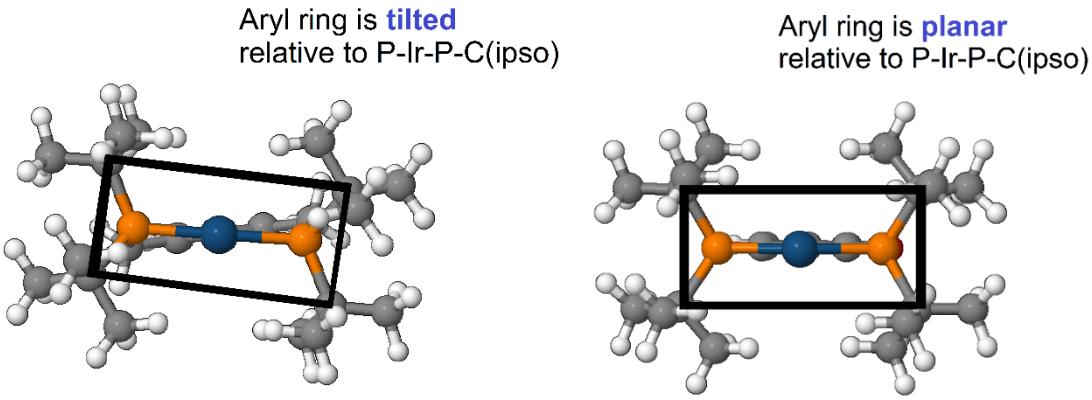

Figure 3.15 Arrangement of ^{t}Bu groups in 14 electron complexes of (^{tBu4}PCP)Ir (left) and (^{tBu4}POCOP)Ir (right)

In order to test this possibility, DFT calculations were conducted where the ligand of the (^{tBu4}PCP)Ir catalyst was locked into a more planar geometry resembling that of (^{tBu4}POCOP)Ir. (Table 3.21) In general, this energies for each intermediate and transition state of this new "catalyst" of (^{tBu4}PCP)Ir-locked appeared to be very similar to its unrestricted cousin (^{tBu4}PCP)Ir. In contrast, (^{tBu4}PCP)Ir-locked had energetic patterns and values that were very different than those of (^{tBu4}POCOP)Ir. (Table 3.22)

	C1-C2	C2-C1	C2-C3	C3-C2
[Ir] + hexane	0.0	0.0	0.0	0.0
σ-complex	8.2	8.9	8.9	5.2
C-H activation	17.0	24.3	23.9	25.9
[Ir](H)(hexyl)	19.5	22.4	19.4	21.9
β-H elimination	25.5	24.1	30.8	32.4
[Ir](H)(H)(hexene)	12.7	12.7	18.8	18.8
olefin dissociation	24.0	24.0	25.0	25.0
[Ir]H_2 + hexene	-0.4	-0.4	-4.0	-4.0

Table 3.21 Kinetic barriers to dehydrogenation by (^{tBu4}PCP)Ir locked into planarity like (^{tBu4}POCOP)Ir in kcal/mol

	(^{tBu4}PCP)Ir	(^{tBu4}PCP)Ir-locked	(^{tBu4}POCOP)Ir
[Ir] + hexane	0.0	0.0	0.0
σ-complex	13.1	8.9	6.5
C-H activation	25.8	24.3	15.5
[Ir](H)(hexyl)	22.2	22.4	10.8
β-H elimination	26.2	24.1	16.9
[Ir](H)(H)(hexene)	11.9	12.7	9.2
olefin dissociation	22.6	24.0	23.0
[Ir]H_2 + hexene	2.4	-0.4	-3.3

Table 3.22 Effects of locking the geometry of (^{tBu4}PCP)Ir during C2-C1 pathway in kcal/mol

Therefore, the DFT calculations regarding (^{tBu4}PCP)Ir-locked strongly suggested that the differences in rate-determining step, and therefore regioselectivity, between (PCP)Ir and (POCOP)Ir catalysts were most likely *not* caused by the twisted versus planar geometries of the corresponding ligands.

Next, attempts were made to examine the other known steric difference between (^{tBu4}PCP)Ir and (^{tBu4}POCOP)Ir. Specifically, using (^{tBu4}PCP)Ir as a reference point, the oxygen linkages in (^{tBu4}POCOP)Ir were known to retract the PR_2 groups backwards towards the aryl ring, creating a less stericly crowded environment around the iridium center.[5] Unfortunately, however, technical difficulties prevented this aspect from being examined with DFT calculations. The DFT calculations failed to converge at a stable complex for the various transition states when the energy of the (^{tBu4}PCP)Ir catalyst with its PR_2 and CH_2 groups retracted backwards was employed. Thus, this possible factor affecting regioselectivity could not be tested directly.

However, on a qualitative level, it did not appear that this movement of the PR_2 groups backwards or forwards had the capability of influencing the transition states enough to change the rate-determining step. In particular, even the substitution of one methylene bridge group in (PCP)Ir for an oxygen atom, forming the corresponding (PCOP)Ir catalyst, was found to drastically

lower regioselectivity. However, the substitution of four ^{t}Bu groups with four ^{i}Pr groups, changing the catalyst from (^{tBu4}PCP)Ir to (^{iPr4}PCP)Ir, drastically reduced steric crowding at the iridium center but only caused a minor decrease in regioselectivity from 96% to 91%. While sterics did influence regioselectivity to a small degree within the (PCP)Ir framework, the massive changes in regioselectivity between (PCP)Ir and (PCOP)Ir/(POCOP)Ir catalysts appeared to originate from a different phenomenon.

3.5.3 Effect of electron density on the phosphorous atoms on the rate-determining step

Moving forward, the possibility that electronic factors originating from the phosphorous atoms was investigated with DFT calculations. Upon initial inspection, it was clear that varying *only* the electron density on phosphorous, without perturbing any other steric or electronic factors, would be difficult. Modification of the methylene bridge group could unintentionally influence the electronics of the aryl ring, while substituting the PR_2 groups with more electron-donating or electron-withdrawing substituents would likely also perturb the steric crowding at the iridium center.

The first calculation attempted was with derivatives of (^{tBu4}PCP)Ir which had perfluoro substituents attached to the carbon atom linking the PR_2 groups with the aryl ring. (Figure 3.16) Many configurations were considered, but all produced anomalous and inconsistent energies for the various transition states. Upon inspection of the DFT-optimized geometries, it was clear that the perfluoro substituents had pushed the $P^{t}Bu_2$ groups forward, making the iridium center much more stericly crowded. Due to these complications, this approach would not be successful at understanding how the electronics on phosphorous influenced the various transition states.

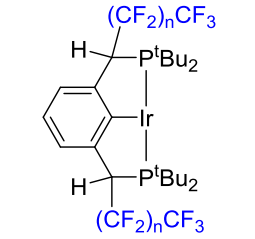

methylene-fluorinated (^{tBu4}PCP)Ir

Figure 3.16 Methylene-fluorinated (^{tBu4}PCP)Ir

Next, modification of the P^{t}Bu$_2$ groups in (^{tBu4}PCP)Ir was conducted and four new catalysts were considered. (Figure 3.17) When calculating the DFT-optimized structures, the CF_3 groups were deliberately pointed away from the iridium center in order to minimize any steric effects.

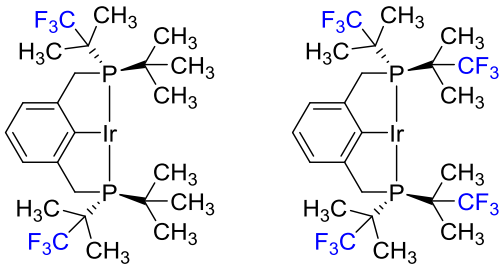

(F_6-^{tBu4}PCP)Ir **(F_{12}-^{tBu4}PCP)Ir**

Figure 3.17 Catalysts with fluorination of PR_2 groups

While all four pathways were calculated for each of the two new catalyst, the raw energies were not meaningful when examining the rate-determining step. Instead, it was the *differences* in energies between the "control group" of (^{tBu4}PCP)Ir and the CF_3-modified catalysts. For simplicity, the average of all four pathways (i.e. C1-C2) for a given catalyst were taken first, and then the differences were calculated and reported as $\Delta\Delta G^{\ddagger}_{catalysts}$. (Equation 3.3) Notably, this $\Delta\Delta G^{\ddagger}_{catalysts}$ represents a separate concept (the difference in a given intermediate's/transition state's energy between two catalysts) than the $\Delta\Delta G^{\ddagger}_{\beta H\text{-}OD}$ used previously (the difference between β-H elimination and olefin dissociation for the *same* catalyst).

$$\Delta\Delta G^{\ddagger}_{\text{catalysts}} = (transition\ state\ energy\ for\ Catalyst\ A) - (transition\ state\ energy\ for\ Catalyst\ B)$$

Equation 3.3 Definition of $\Delta\Delta G^{\ddagger}_{\text{catalysts}}$

First, comparison of (^{tBu4}PCP)Ir with (F_6-^{tBu4}PCP)Ir revealed that the substitution of two methyl groups with two CF_3 groups caused C-H activation, β-H elimination, and olefin dissociation to increase in energy. (Table 3.23) Notably, the increases were larger for C-H activation and β-H elimination (~4 kcal/mol) than for olefin dissociation (2.4 kcal/mol).

	(^{tBu4}PCP)Ir average	(F_6-^{tBu4}PCP)Ir average	$\Delta\Delta G^{\ddagger}_{\text{catalysts}}$
[Ir] + hexane	0.0	0.0	0.0
σ-complex	12.3	9.4	-2.9
C-H activation	25.0	29.0	4.1
[Ir](H)(hexyl)	21.4	26.2	4.8
β-H elimination	29.1	33.5	4.4
[Ir](H)(H)(hexene)	15.2	21.2	6.0
olefin dissociation	23.7	26.1	2.4
[Ir]H_2 + hexene	0.5	2.0	1.4

Table 3.23 Effect of fluorinations with (F_6-^{tBu4}PCP)Ir in kcal/mol

Likewise, the DFT calculations with (F_{12}-^{tBu4}PCP)Ir showed that 12 total fluorine atoms caused an even larger increase in energy (Table 3.24)

	(^{tBu4}PCP)Ir average	(F_{12}-^{tBu4}PCP)Ir average	$\Delta\Delta G^{\ddagger}_{\text{catalysts}}$
[Ir] + hexane	0.0	0.0	0.0
σ-complex	12.3	10.5	-1.8
C-H activation	25.0	30.5	5.6
[Ir](H)(hexyl)	21.4	27.9	6.5
β-H elimination	29.1	38.0	8.9
[Ir](H)(H)(hexene)	15.2	25.3	10.0
olefin dissociation	23.7	27.6	3.9
[Ir]H_2 + hexene	0.5	1.3	0.7

Table 3.24 Effects of fluorination with (F_{12}-^{tBu4}PCP)Ir in kcal/mol

Hence fluorine substitution in (F_6-^{tBu4}PCP)Ir and (F_{12}-^{tBu4}PCP)Ir *did* appear to influence phosphorous electronics in a meaningful way *without* perturbing sterics, allowing for those calculations to become useful in understanding regioselectivity. In particular, this data suggested that electron withdrawing substituents near the phosphorous atoms cause all the transition states to increase in energy. Notably, this increase would be *larger* with C-H activation and β-H elimination than it would be for olefin dissociation. In turn, this would *favor* a β-H elimination rate-determining step and *disfavor* an olefin dissociation rate-determining step.

Notably, this action is *opposite* of what was observed with the changes between (PCP)Ir and (POCOP)Ir catalysts. Both the oxygen atoms in the POCOP ligand and the fluorines in the (F_x-^{tBu4}PCP)Ir catalysts would make the phosphorous atoms less electron rich. However, in (POCOP)Ir catalysts the rate-determining step changed to olefin dissociation, whereas in the (F_x-^{tBu4}PCP)Ir catalysts the energies moved to even more strongly favor β-H elimination as the rate-determining step.

3.5.4 Reexamining the effect of aryl electronics on the rate-determining step with (azaborinine)Ir catalysts

Given the preceding information, it was unclear which steric and/or electronic factor(s) had determined regioselectivity. While the identity of the PR_2 groups did account for the changes in regioselectivity *within* the (PCP)Ir framework, it did *not* explain the fundamental change in rate-determining step experienced by (PCOP)Ir and (POCOP)Ir which caused drastically lower regioselectivity. Of the other four possible factors examined, none seemed to have caused the experimentally-observed trends.

However, it was hypothesized that aryl electronics might actually be the source of the change in rate-determining step and regioselectivity. While the influence of the *para*-methoxy and *para*-dimethylamino groups did not actually alter the experimental regioselectivity of the (MeO-^{tBu4}PCP)Ir and (Me_2N-^{tBu4}PCP)Ir catalysts, the movement of their transition states *did* follow the trends of (PCOP)Ir and (POCOP)Ir. Hence, this suggests that while the modification of aryl electronics by the para substituents was not strong enough to alter regioselectivity, perhaps the oxygen linkages had *stronger* influences on aryl electronics, and those effects *were* powerful enough to change the rate-determining step and thereby regioselectivity.

To investigate this possibility, a class of azaborinine-related catalysts were selected for DFT calculations. (Figure 3.18) In general, the term "azaborinine" refers to six-membered aromatic rings where there are four carbons, one nitrogen, and one boron. In benzene, the 6 π-electrons needed for aromaticity are provided by the 6 carbon atoms (1 electron each). In contrast, in azaborinine compounds each carbon provides 1 electron each (4 electrons total), with the 1 nitrogen giving the remaining 2 electrons, while boron provides no π-electrons.

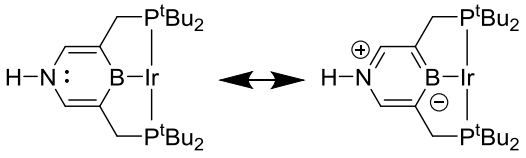

(paraN-^{tBu4}PBP)Ir

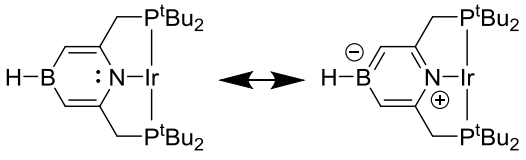

(paraB-^{tBu4}PNP)Ir

Figure 3.18 (paraN-^{tBu4}PBP)Ir and (paraB-^{tBu4}PNP)Ir catalysts

On one hand, these catalysts would have essentially identical steric profiles and phosphorous electronics to (^{tBu4}PCP)Ir. However, their aryl electronic properties would be very different. In particular, aryl electronics can be divided into two distinct effects: σ-donation and π-donation (Figure 3.19). First, the covelant σ-bond of E-Ir (E = C, N, or B) would cause net donation of electron density from the aromatic ring into specific orbitals on the iridium. This property would scale based upon the electronegativity of the E atom as well as inductive effects from neighboring atoms. Notably, σ-donation is closely related to the concept of structural trans influence. Secondly, conjugation of the π-cloud from the aromatic ring would result in a distinct donation of electron density into different orbitals on the iridium. The magnitude of this effect would depend upon the average occupancy of the p-orbital on the E atom.

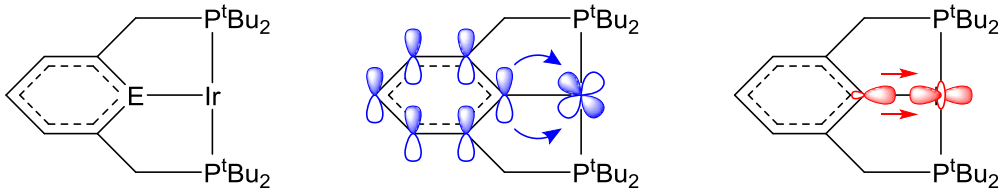

(^{tBu4}PEP)Ir
without any orbitals

(^{tBu4}PEP)Ir
π-donation

(^{tBu4}PEP)Ir
σ-donation

Figure 3.19 σ-donation versus π-donation *via* the C_{ipso}-Ir bond

Since catalytic dehydrogenation proceeds through interactions between the *n*-alkane and *certain* orbitals on iridium, then the σ- and π-donating abilities of different ligands might operate *separately* from one another.

With this groundwork laid, it was necessary to qualitatively predict the σ-donation and π-donation properties of (^{tBu4}PCP)Ir so that the two new catalysts could be compared to it. (Figure 3.20) For (^{tBu4}PCP)Ir, the σ-donation would be defined by the electronegativity of carbon. The

strength of π-donation would reflect the average occupancy of the p-orbital of the ipso carbon, which was 1.0 electron.

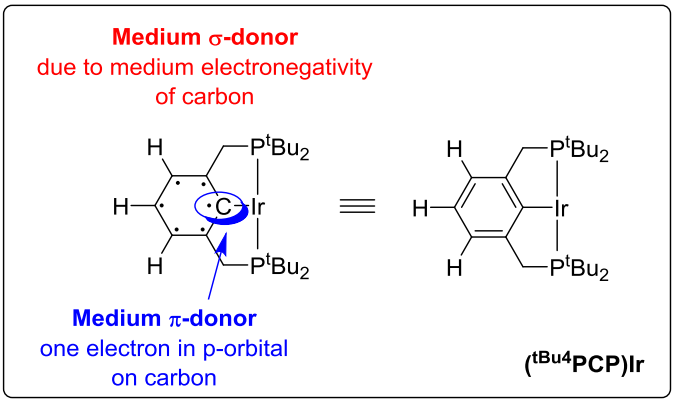

Figure 3.20 Aryl electronics of (^{tBu4}PCP)Ir

For (paraB-^{tBu4}PNP)Ir, the ligand would be a much *weaker* σ-donor than in (^{tBu4}PCP)Ir since the nitrogen atom has a much higher electronegativity than that of carbon. (Figure 3.21) Understanding the strength of π-donation for (paraB-^{tBu4}PNP)Ir is slightly more complex since two valid resonance structures can be drawn, one with 2 electrons in the ipso p-orbital while the other contains only 1 electron in that orbital. Hence, the average occupancy would be between 1.0 and 2.0 electrons, making (paraB-^{tBu4}PNP)Ir a stronger π-donor than (^{tBu4}PCP)Ir.

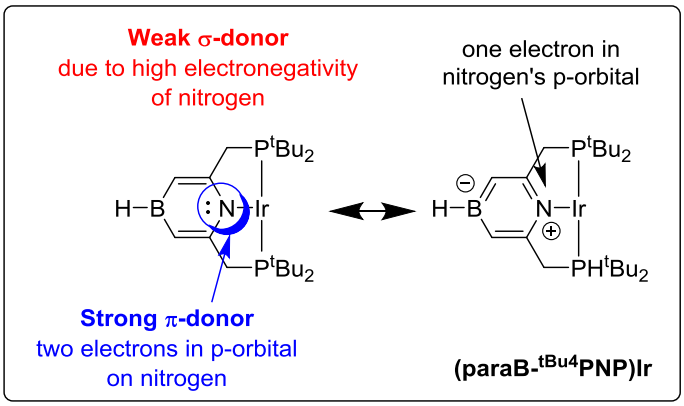

Figure 3.21 Aryl electronics of (paraB-^{tBu4}PNP)Ir

For (paraN-^{tBu4}PBP)Ir, σ-donation would be *stronger* than (^{tBu4}PCP)Ir due to the low electronegativity of boron. (Figure 3.22) Due to the two valid resonance structures for (paraN-^{tBu4}PBP)Ir, the average occupancy of the ipso p-orbital would be between 0 and 1.0 electrons, making it a much weaker π-donor than (^{tBu4}PCP)Ir. In fact, (paraN-^{tBu4}PBP)Ir might even act as a π-acceptor, depending on the particular circumstances.

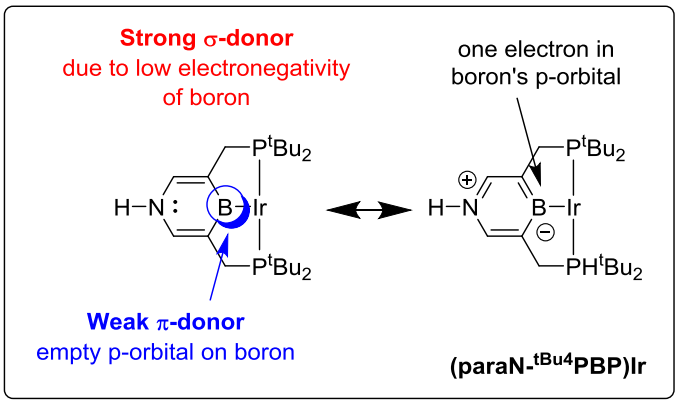

Figure 3.22 Aryl electronics of (paraN-^{tBu4}PBP)Ir

Therefore, the totality of these analyses can be used to rank all of the types of pincer iridium catalysts in terms of the σ-donation and π-donation of their aromatic rings. (Figure 3.23) (PCOP)Ir catalysts would fall between (PCP)Ir and (POCOP)Ir catalysts.

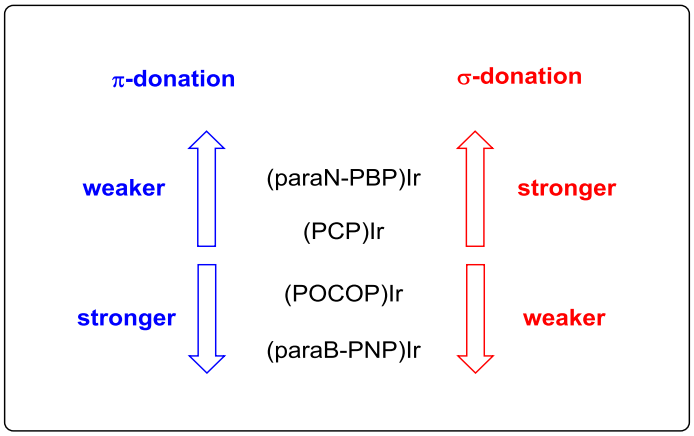

Figure 3.23 Ranking four pincer iridium catalysts by σ-donation and π-donation

With this theoretical foundation firmly established, the actual kinetic barriers to catalytic dehydrogenation were calculated for the two (azaborinine)Ir catalysts. (Tables 3.25 and 2.26) With (paraB-^{tBu4}PNP)Ir, which had aryl electronics similar in the direction of (POCOP)Ir, the rate-determining step became olefin dissociation. In contrast, with (paraN-^{tBu4}PBP)Ir, which had electronics in the opposite direction, olefin dissociation energies were quite low and C-H activation became the rate-determining step. Therefore, aryl electronics appeared to have have massive effects on the energies of each transition state that were consistent with experimental and DFT results from the (PCP)Ir and (POCOP)Ir catalysts.

	C1-C2	C2-C1	C2-C3	C3-C2
[Ir](1-hexene)	0.0	0.0	0.0	0.0
[Ir] + hexane	22.3	22.3	22.3	22.3
σ-complex	24.3	31.4	31.4	31.5
C-H activation	25.4	32.6	31.5	33.6
[Ir](H)(hexyl)	17.7	17.7	21.9	24.5
β-H elimination	33.4	33.4	38.0	36.4
[Ir](H)(H)(hexene)	22.5	22.5	27.6	27.6
olefin dissociation	41.0	41.0	41.0	41.0
[Ir]H_2 + hexene	2.7	2.7	-0.9	-0.9

Table 3.25 Kinetic barriers to dehydrogenation by (paraB-^{tBu4}PNP)Ir in kcal/mol

	C1-C2	C2-C1	C2-C3	C3-C2
[Ir](1-hexene)	12.0	12.0	12.0	12.0
[Ir] + hexane	0.0	0.0	0.0	0.0
σ-complex	9.7	8.7	8.7	7.3
C-H activation	33.5	39.9	37.8	40.5
[Ir](H)(hexyl)	18.5	37.2	35.0	37.8
β-H elimination	33.2	37.1	38.4	38.2
[Ir](H)(H)(hexene)	20.1	20.1	25.0	25.0
olefin dissociation	20.8	20.8	20.7	20.7
[Ir]H_2 + hexene	19.4	19.4	15.7	15.7

Table 3.26 Kinetic barriers to dehydrogenation by (paraN-^{tBu4}PBP)Ir in kcal/mol

Notably, in (paraN-^{tBu4}PBP)Ir the lowest energy intermediate was not the (paraN-^{tBu4}PBP)Ir(1-hexene) complex, but was actually the free 14 electron species (paraN-^{tBu4}PBP)Ir. Presumably, the very strong σ-donation of the paraN-^{tBu4}PCP ligand destabilized the coordination of the 1-hexene through the structural trans effect.

In an effort to more accurately quantify these results, the $\Delta\Delta G^{\ddagger}_{\beta H\text{-}OD}$ values were also calculated for each (azaborinine)Ir catalyst relative to the other R = ^{t}Bu catalysts. (Table 3.27) These results confirmed the analysis above.

$\Delta\Delta G^{\ddagger}_{\beta H\text{-}OD}$	C1-C2	C2-C1	C2-C3	C3-C2	average
(paraB-^{tBu4}PNP)Ir	-7.7	-7.7	-2.9	-4.6	-5.7
(^{tBu4}POCOP)Ir	-1.6	-6.1	-1.3	0.5	-2.1
(^{tBu4}PCOP)Ir	0.4	-2.6	2.2	4.0	1.0
(^{tBu4}PCP)Ir	4.4	3.6	7.2	6.5	5.5
(paraN-^{tBu4}PBP)Ir	12.4	16.3	17.7	17.5	16.0

Table 3.27 Comparing (paraN-^{tBu4}PBP)Ir and (paraB-^{tBu4}PNP)Ir to other catalysts, values in kcal/mol

For (paraN-^{tBu4}PBP)Ir, the average $\Delta\Delta G^{\ddagger}_{\beta H\text{-}OD}$ value was very large at 16.0 kcal/mol. Therefore, (paraN-^{tBu4}PBP)Ir favored β-H elimination as its rate-determining step even more strongly than (^{tBu4}PCP)Ir did (at 5.5 kcal/mol)! Comparing (paraN-^{tBu4}PBP)Ir to (^{tBu4}PCP)Ir directly gave a $\Delta\Delta\Delta G^{\ddagger}_{\beta H\text{-}OD}$ value of 10.5 kcal/mol. Hence, the changes in aryl electronics caused the β-H elimination and olefin dissociation transition states to shift by 10.5 kcal/mol relative to one another.

Comparing (paraB-^{tBu4}PNP)Ir to (^{tBu4}PCP)Ir revealed an even more massive change: average $\Delta\Delta G^{\ddagger}_{\beta H\text{-}OD}$ values of *negative* 5.7 versus *positive* 5.5 kcal/mol, yielding a $\Delta\Delta\Delta G^{\ddagger}_{\beta H\text{-}OD}$ value of 11.2 kcal/mol! Thus, changing the electronic properties of the aromatic ring caused the β-H

elimination and olefin dissociation transition states to move 11.2 kcal/mol relative to one another! Clearly, this is an enormous difference.

Therefore, the DFT calculations with (paraB-^{tBu4}PNP)Ir and (paraN-^{tBu4}PBP)Ir demonstrated that aryl electronics are capable of changing the rate-determining step by themselves, without assistance from any other steric or electronic effects. And, by extension, this suggests that the differences in rate-determining step between (PCP)Ir and (PCOP)Ir/(POCOP)Ir catalysts might in actuality have been caused by differences in aryl electronics.

3.6 Elucidating how aryl electronics affects the barriers for olefin dissociation versus insertion

Before declaring that aryl electronics was the major factor causing the rate-determining step to change within pincer iridium catalysts, a plausible mechanism must be postulated. In particular, orbital theories were constructed which rationalize how these specific σ- and π-effects caused the observed change in rate-determining step.

Early attempts at rationalizing the importance of aryl electronics were made by comparing the 14 electron complex to the two rate-determining steps (β-H elimination and olefin dissociation). However, these comparisons proved difficult to make, since the steric and coordination situation between the 14 electron complex and the two transition states were very different. Hence, no viable mechanistic interpretations were generated. Next, the two transition states were compared to the (pincer)Ir(1-olefin) resting state, but this strategy proved to be difficult as well.

Fortunately, comparison of the transition states with the (pincer)Ir(H)(H)(olefin) intermediate *did* provide a seemingly valid mechanistic explanation for why aryl electronics could alter the rate-determining step. To understand why, the differences between reversible and irreversible elementary reaction steps must be understood. (Scheme 3.3) Depending on the rate-determining step, β-H elimination/insertion changed from reversible to irreversible, thereby determining the rate-determining step and therefore regioselectivity. In fact, all elementary reaction steps *before* the rate-determining step can be considered reversible, whereas the rate-determining step and all elementary reaction steps *after* it will be irreversible.

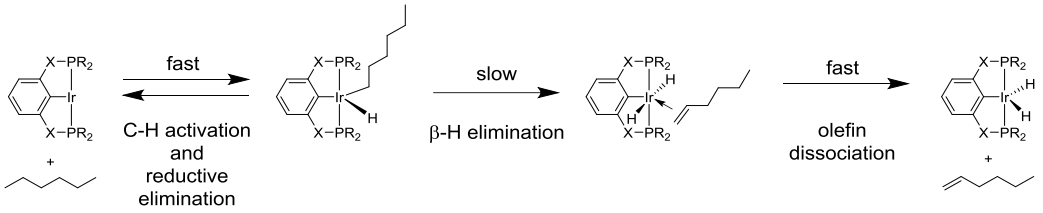

Scheme 3.3 Dehydrogenation when β-H elimination is the rate-determining step

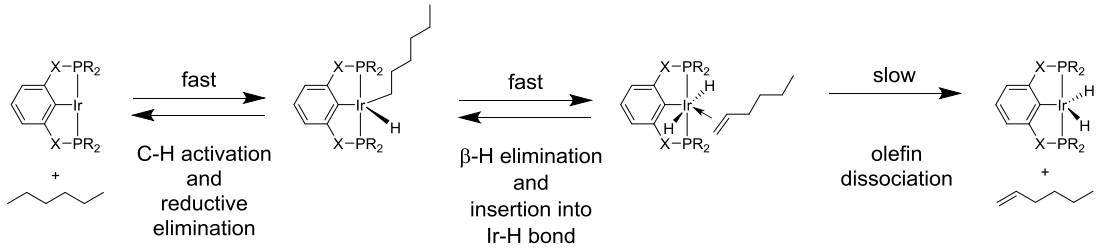

Scheme 3.4 Dehydrogenation when olefin dissociation is the rate-determining step

Hence, the determination of regioselectivity through the rate-determining step could be reframed as the difference in kinetic barrier to insertion (reverse of β-H elimination) versus olefin dissociation when beginning at the (pincer)Ir(H)(H)(olefin) complex.

However, analyzing the effects of σ-donation and π-donation would be difficult if the two geometries being compared were an intermediate, the (pincer)Ir(H)(H)(olefin) complex, and a

transition state, either β-H elimination or olefin dissociation. It would be much more intuitive to compare the geometries and sterics of two intermediates.

Fortunately, Hammond's postulate allows qualitative comparisons between the thermodynamics of a transition (i.e. ΔG of insertion) with the barrier to the transition (i.e. $\Delta G^{\ddagger}$ of insertion). (Figure 3.24) Therefore, it might be possible to understand the rate-determining step and regioselectivity by comparing the *thermodynamics* (ΔG) of insertion versus olefin dissociation.

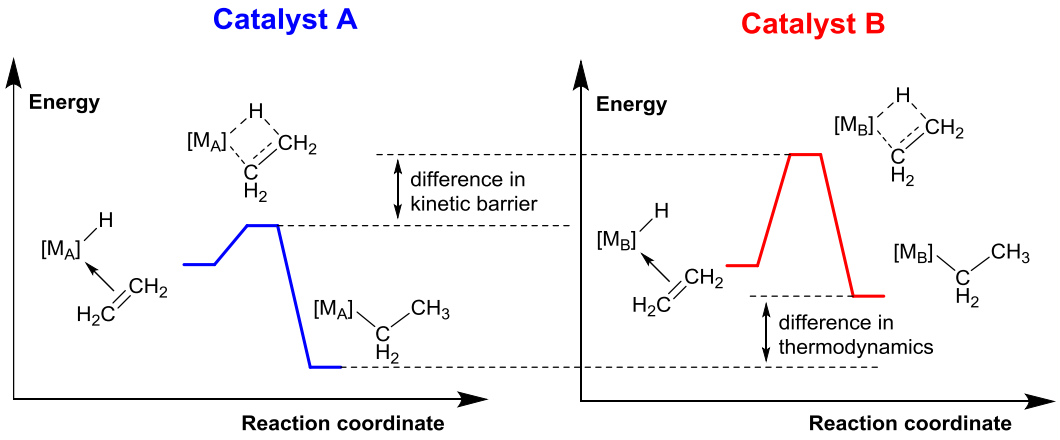

Figure 3.24 Hypothetical examples illustrating Hammond's postulate

In Figure 3.24 the energetics of two hypothetical catalysts are shown. Catalyst A was used as the point of reference. With this in mind, if the thermodynamics of insertion with Catalyst B were to be *less* exergonic than with Catalyst A ($\Delta G_B > \Delta G_A$), then the barrier for insertion with Catalyst B would be *greater* than the barrier with Catalyst A ($\Delta G^{\ddagger}_B > \Delta G^{\ddagger}_A$).

Therefore, if insertion and olefin dissociation from the (pincer)Ir(H)(H)(olefin) complexes follow Hammond's postulate, then the thermodynamic change (ΔG) could be used to qualitatively estimate the kinetic barrier ($\Delta G^{\ddagger}$), and therefore the rate-determining step. And by extension, the σ-donation and π-donation effects on each *intermediate* could be linked to the rate-determining step.

3.6.1 Examining the effect of π-donation on insertion

The energetics of insertion were plotted while using the (pincer)Ir(H)(H)(olefin) complex as the energetic zero point. (Figure 3.25) (Table 3.28) Average values for all four pathways (i.e. C1-C2) were used to minimize random error. With one minor exception (abnormally high insertion $\Delta G^{\ddagger}$ for (paraN-^{tBu4}PBP)Ir), the results showed perfect agreement with Hammond's postulate. Lower thermodynamic values of ΔG correlated qualitatively and semi-quantitatively with lower kinetic barriers of $\Delta G^{\ddagger}$.

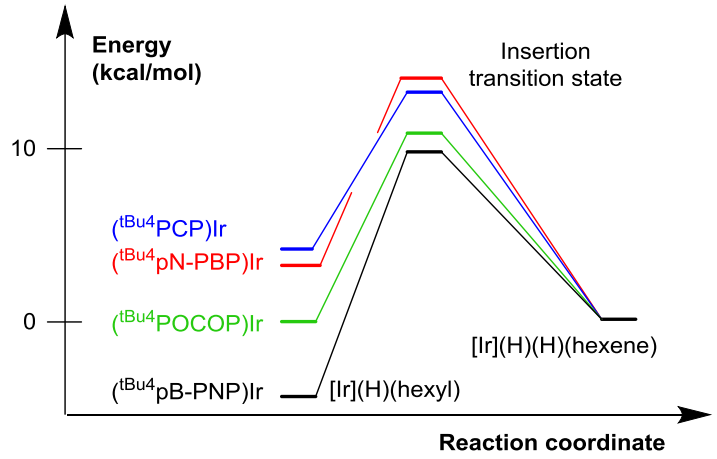

Figure 3.25 Insertion follows Hammond's postulate

Insertion step	(^{tBu4}PBP-pN)Ir	(^{tBu4}PCP)Ir	(^{tBu4}POCOP)Ir	(^{tBu4}PNP-pB)Ir
[Ir](H)(hexyl)	4.2	6.2	0.1	-4.6
β-H elimination	14.4	13.9	10.7	10.2
[Ir](H)(H)(hexene)	0.0	0.0	0.0	0.0

Table 3.28 Insertion follows Hammond's postulate

Thus, since insertion was found to follow Hammond's postulate, the next step of proposing how aryl electronics affected the thermodynamic ΔG of the elementary reaction steps was begun. The mechanism can be divided into the effects of σ-donation and π-donation.

The main effect of σ-donation on the energetics of each species would happen through the trans influence. Namely, a strongly σ-donating ligand will destabilize the bond or coordination trans to it. If two ligands which are trans to one another are both strong trans influences, then they will destabilize each other, and thereby raise the overall thermodynamic energy of the whole complex.

In the case of insertion by (pincer)Ir(H)(H)(olefin), the starting complex has an iridium-olefin coordination that is trans to the C_{ipso} of the pincer ligand, whereas the final complex of (pincer)Ir(H)(R) has an Ir-C bond trans to the C_{ipso}. Since both an olefin and an alkyl group are both strong trans influencing ligands, then the net change in energy due to σ-donation upon insertion will be very small. The weaker trans influence of the C_{ipso} in (POCOP)Ir(H)(H)(olefin) will only destabilize that complex by a small amount, but it will also only destabilize the (POCOP)Ir(H)(R) by a small amount. Similarly, the stronger trans influence of the C_{ipso} in (PCP)Ir(H)(H)(olefin) will destabilize that complex by a large amount, but that same large destabilization will also occur in (PCP)Ir(H)(R) by a similar amount. Hence, because σ-donation appears to have little effect on ΔG of insertion, it would also have a minimal effect on the $\Delta G^{\ddagger}$ of insertion.

In contrast, the magnitude of π-donation by the pincer ligand *could* cause the differences in kinetic barrier to insertion seen above. Namely, complexes with hydrides in the position *cis* to the C_{ipso} of the pincer ligand would be destabilized by strong π-donation of the C_{ipso} atom.[8,9] When considering the position cis to C_{ipso} during insertion, the starting complex (pincer)Ir(H)(H)(olefin) has *both* cis positions occupied by hydrides, and therefore strong π-donation would cause large thermodynamic destabilization. (Figure 3.26) In contrast, in the product of insertion, (pincer)Ir(H)(R), only one of the cis positions is occupied by an atom (a hydride) while the other is empty. Hence, in (pincer)Ir(H)(R) the destabilization due to π-donation will be less because only

one of the two possible sites are involved. Overall, this indicates that with a π-neutral ligand the ΔG of insertion will be closer to thermoneutral, whereas with a strongly π-donating ligand the ΔG of insertion will be much more exothermic (more negative).

(pincer)Ir(H)(R)
only one cis-hydride
π-donation causes **minor** destabilization

(pincer)Ir(H)(H)(olefin)
two cis-hydrides
π-donation causes **large** destabilization

Figure 3.26 Effect of π-donation and location of hydrides on thermodynamics

Hence, this analysis regarding π-donation explains the DFT calculations discussed above. Namely, in a strongly π-donating complex such as (^{tBu4}POCOP)Ir or (paraB-^{tBu4}PNP)Ir, insertion greatly reduces the thermodynamic destabilization caused by π-donation, giving a very negative ΔG and a therefore smaller $\Delta G^{‡}$ kinetic barrier to insertion/β-H elimination. In contrast, with the weaker π-donating complexes of (^{tBu4}PCP)Ir and (paraN-^{tBu4}PBP)Ir, there was no much destabilization which could be released, and so ΔG is more positive and the kinetic barrier of $\Delta G^{‡}$ is much higher.

3.6.2 Examining the effect of σ-donation on olefin dissociation

Thus, with a hypothesis relating aryl electronics with the kinetic barrier of insertion in hand, focus was turned towards the olefin dissociation barrier. Following the procedure with insertion, the first step was to establish whether olefin dissociation followed Hammond's postulate. In contrast to expectations, however, it appeared that the actual relationship between

the kinetic barrier ($\Delta G^{\ddagger}$) and thermodynamics (ΔG) was *opposite* of what would be predicted by Hammond's postulate. (Figure 3.27) (Table 3.29) Although not shown in Figure 3.27, this analysis was repeated with other catalysts, but those analyses also confirmed this phenomenon: the olefin dissociation elementary reaction step behaved in the exact *opposite* manner that would be expected from Hammond's postulate. If the transition became *more* exothermic then the kinetic barrier actually *increased*, instead of decreasing.

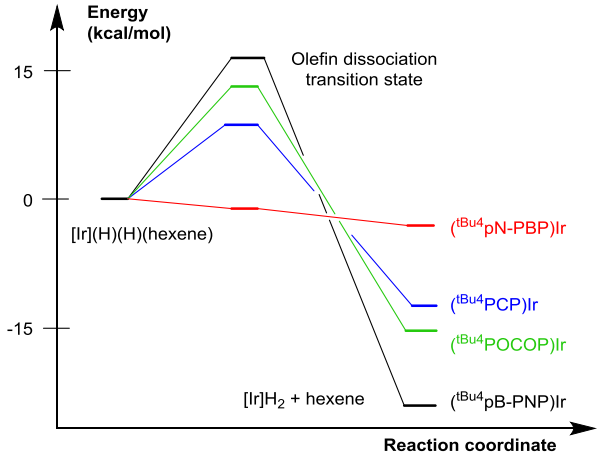

Figure 3.27 Olefin dissociation does not follow Hammond's postulate

Olefin dissociation	(^{tBu4}PBP-pN)Ir	(^{tBu4}PCP)Ir	(^{tBu4}POCOP)Ir	(^{tBu4}PNP-pB)Ir
[Ir](H)(H)(hexene)	0.0	0.0	0.0	0.0
olefin dissociation	-1.8	8.5	12.8	15.9
[Ir]H_2 + hexene	-5.0	-14.7	-15.4	-24.1

Table 3.29 Olefin dissociation does not follow Hammond's postulate

Superficially, this suggested that the analysis of aryl electronics during the olefin dissociation transition state would not succeed, and should therefore be abandoned. However, it was decided to investigate *why* olefin dissociation behaved anti-Hammond. After much consideration, it was determined that the olefin dissociation barrier had *not* violated Hammond's postulate. Instead, olefin dissociation represented an abnormal situation where Hammond's

postulate did not apply. And, upon adjusting for this abnormality, analysis of the effect of aryl electronics on the olefin dissociation barrier *could* be successfully completed.

Critically, Hammond's postulate assumes that the geometric movement of all atoms during a reaction happen at a relatively constant rate over the entire course of the reaction. For example, during a S_N2 reaction the nucleophile is continuously approaching the central atom, eventually forming a covelant bond to it. Likewise, the leaving group is continuously moving away from the central atom, until it has completely left. Thus, a typical S_N2 reaction would always follow Hammond's postulate.

However, close inspection of the olefin dissociation transition state showed that the movement of the hydrides and olefin were *not* constant over the course of the elementary reaction step, causing the observed anti-Hammond behavior. Namely, when DFT calculations find the energy of a transition state or an intermediate, they do so by determining the geometry which gives the lowest energy. Hence, these DFT-optimized geometries can be viewed in three dimensions using certain software packages. In this case, the DFT results for olefin dissociation were examined using computer program GaussView. Upon inspection using GaussView, it became clear the "olefin dissociation" was essentially two distinct steps without a kinetic barrier between them. (Scheme 3.5) First, it was observed that the in the olefin dissociation transition state the olefin was the only group which moved, and it moved considerably further away from the iridium center. Hence, this aspect will be referred to as "olefin loss." Noticeably, however, the product of (pincer)IrH_2 almost always showed that hydrides had moved considerably. (footnote) Whereas in the (pincer)Ir(H)(H)(olefin) complex the angle defined by H-Ir-H was always 180°, the angles in the (pincer)IrH_2 complexes were typically around 60°. And, since the H-Ir-H angles in the olefin dissociation transition state were also 180°, then then the entire process of

"hydride bending" occurred *after* the transition state! (paraN-^{tBu4}PBP)Ir was the only exception, where the hydrides did not move and remained at 180° to one another.

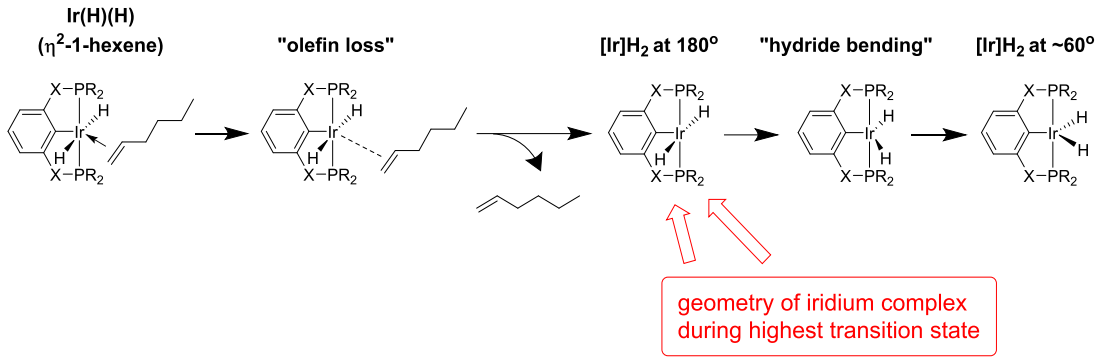

Scheme 3.5 Olefin dissociation is actually two separate transformations

Therefore, olefin dissociation transition state might be more accurately referred to as two distinct elementary reaction steps ("olefin loss" and "hydride bending") that occurred sequentially and without a barrier between them. Presumably, the presence of the olefin made the iridium center too crowded to allow the hydrides to bend towards their thermodynamically most favorable angle of approximately 55.6° for (^{tBu4}PCP)Ir and 60.0° for (^{tBu4}POCOP)Ir. It was only until *after* the olefin departed from the iridium center (and until after the transition state) that the hydrides could move an appreciable amount. During the olefin dissociation transition state the hydrides were found to be approximately 177° to one another.

The origins of this high barrier to olefin loss in (pincer)Ir(H)(H)(olefin) complexes, which is typically small in most organometallic species, can be explained by the work of Eisenstein on *trans*-L_2IrXH_2 complexes.[8,9] In those studies, the thermodynamic energy of a variety of complexes were calculated with various H-H angles. (Figure 3.28) In particular, it was found that the electronic properties of the X ligand significantly affected the more energetically stable configuration of the two hydride ligands. In particular, if X = Cl^-, a strong π-donor, then the most

stable complexes would have an H-H angle of approximately 70°. In contrast, if X = CO, a strong π-*acceptor*, then the most favorable H-H angle was found to be 180°.

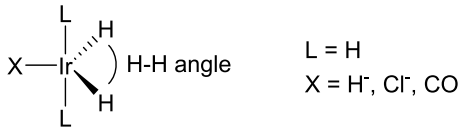

Figure 3.28 Complexes studied by Eisenstein

Returning to the current examination of (pincer)Ir(H)(H)(olefin) complexes, this work by Eisenstein helps to explain the relative barriers to olefin dissociation of (PCP)Ir versus (POCOP)Ir catalysts. In the olefin dissociation transition state the (pincer)Ir(H)(H) complex has an H-H angle of 177°. Since PCP ligand can be considered a "medium strength" π-donor, then the two hydrides at 177° cause a fair amount of destabilization, leading to a significant olefin dissociation barrier. However, the POCOP ligand is a *very* strong π-donor, and thus the two hydrides at 177° make the transition state *very* unstable, and even higher in energy than that of (PCP)Ir catalysts.

In addition to the π-donation, effects of σ-donation on the barrier to "olefin loss" can also be assessed. In the studies by Eisenstein, σ-donation by the X ligand appeared to have a small or insignificant effect on which H-H angle was most stable. [8,9] Therefore, the effect of σ-donation would only apply to the loss of the olefin, and not to any actions regarding the hydrides.

Due to the concept of trans influence it is known that a σ-donor, such as the C_{ipso} of the aryl ring, will weaken and lengthen the bond *trans* to it. In this case, this suggests that the pincer ligand's σ-donation will weaken the iridium-olefin coordination. (Figure 3.29) Hence, in a strong σ-donor like the PCP ligand, then the Ir-olefin coordination will be relatively weak. Therefore, effecting "olefin loss" from (PCP)Ir(H)(H)(olefin) would be relatively easy. In contrast, the POCOP ligand is a weaker σ-donor than PCP, and therefore does not cause as much pre-weakening of the

iridium-olefin coordination. Hence, "ligand loss" in (POCOP)Ir(H)(H)(olefin) would be more difficult than with a PCP ligand.

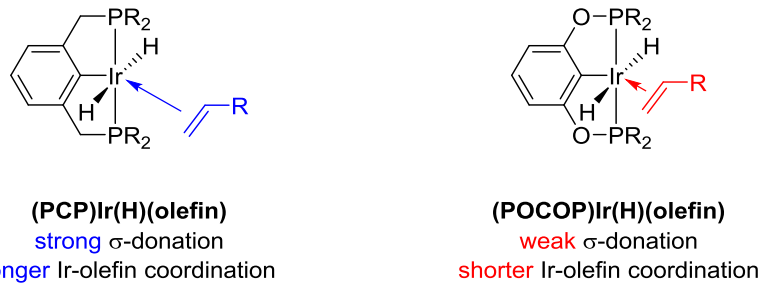

(PCP)Ir(H)(olefin)
strong σ-donation
longer Ir-olefin coordination

(POCOP)Ir(H)(olefin)
weak σ-donation
shorter Ir-olefin coordination

Figure 3.29 Strong σ-donation makes olefin loss easier

Similarly, the apparently "anti-Hammond" behavior of the olefin dissociation step can be attributed to π-donation. Regardless of the transition state, olefin dissociation allows the hydrides at 177° to each other in the (pincer)Ir(H)(H)(olefin) complexes to bend towards the approximately 60° configuration in the final (pincer)IrH_2 complex. Thus, the release of energy upon "hydride bending" is more exothermic with the strongly π-donating POCOP ligand that it is with the weaker π-donating PCP ligand.

Therefore, analysis of σ-donation and π-donation gives a plausible explanation for why the olefin dissociation barrier is relatively high for (POCOP)Ir(H)(H)(olefin) complexes but lower in (PCP)Ir(H)(H)(olefin) species. (Figure 3.30) The strong π-donation of the POCOP ligand makes the olefin dissociation transition state very high in energy due to the 177° angle between the hydrides, while the weak σ-donation of the POCOP ligand does not help with weakening the iridium-olefin coordination. Conversely, the weak π-donation of the PCP ligand does not significantly disfavor the hydrides at 177° relative to one another, while its strong σ-donation *does* help with olefin loss by weakening the iridium-olefin bond *via* the trans influence.

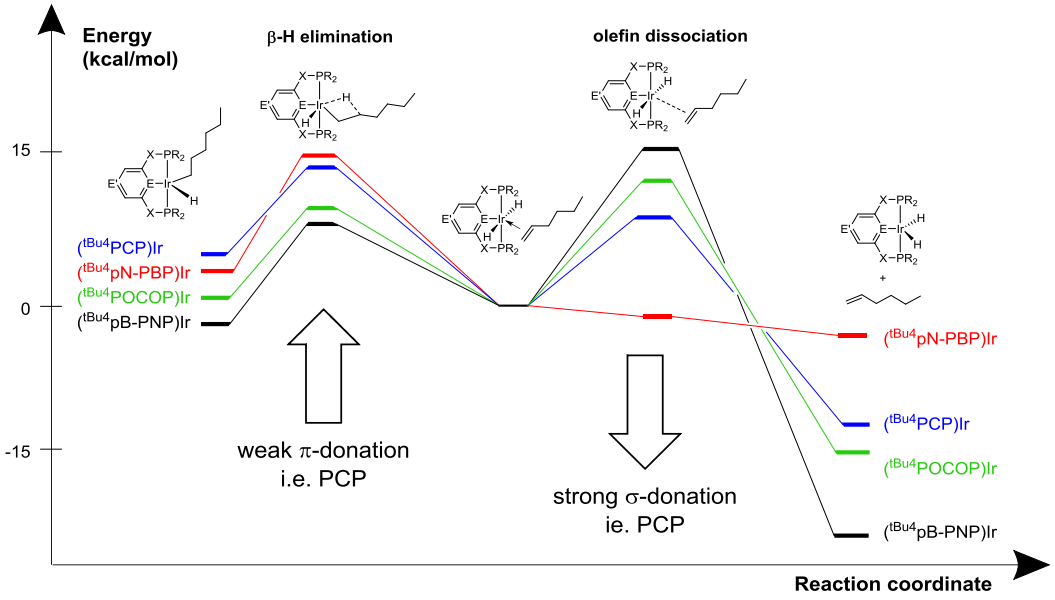

Figure 3.30 Energetics of insertion versus olefin dissociation

3.7 Summary

Overall, DFT calculations were used to elucidate the mechanistic reasons why certain catalysts gave experimentally high regioselectivities, whereas others displayed lower regioselectivities. First, it was shown that considerable steric crowding during C-H activation and β-H elimination caused the 1-olefin pathways to have much lower barriers than their corresponding 2-olefin (or other internal olefin) pathways. Hence, catalysts with C-H activation or β-H elimination rate-determining steps (i.e. (PCP)Ir catalysts) would have high regioselectivity for generating 1-olefins. In addition, catalysts with bulky PR_2 groups would have the greatest steric crowding and therefore the highest regioselectivity (i.e. (^{tBu4}PCP)Ir at 96%), whereas less bulky PR_2 groups would cause less steric crowding and therefore slightly lower regioselectivity (i.e. (^{iPr4}PCP)Ir at 91%). All of these predictions by DFT were in excellent agreement with the experimental evidence reported in Chapter 2.

In contrast, steric crowding during olefin dissociation was much lower, and therefore the 1-olefin and 2-olefin pathways had similar kinetic barriers. Hence, catalysts with an olefin dissociation rate-determining step (i.e. (PCOP)Ir and (POCOP)Ir catalysts) would have much lower regioselectivity for producing 1-olefins, also in excellent agreement with the experimental results presented in Chapter 2.

Lastly, the steric and electronic factors which caused the change in rate-determining step between (PCP)Ir catalysts and (PCOP)Ir/(POCOP)Ir catalysts was investigated. (Table 3.30)

Possible factors affecting regioselectivity	**Results from DFT calculations**
Sterics: identity of PR_2 groups	Probably responsible for small changes in regioselectivity, such as 96% to 91% for (^{tBu4}PCP)Ir to (^{iPr4}PCP)Ir
Sterics: planar versus twisted ligand	Unlikely to have caused any noticeable changes
Sterics: retraction of PR_2 groups back towards aryl ring	Not directly testable with current DFT capabilities, but did not appear to be a major factor determining regioselectivity
Electronics: phosphorous atoms	Electron withdrawing groups appear to disfavor olefin dissociation being the rate-determining step, in direct contradiction to the trends observed with (POCOP)Ir
Electronics: aryl ring	*Para*-MeO/NMe_2 groups seemed to encourage an olefin dissociation rate-determining step, but were not strong enough to actually change the rate-determining step However, (PCOP)Ir/(POCOP)Ir catalysts did have olefin dissociation rate-determining steps due to changes in aryl electronics

Table 3.30 Summary of possible factors influencing regioselectivity

Namely, six parameters (three steric and three electronic) were examined. Overall, the steric factors appeared to have very minimal effects on the identity of the rate-determining step. However, it was found that the electronics of the phosphorous atoms *could* influence the

rate-determining step, but that it caused changes which were *opposite* of what was observed when comparing (PCP)Ir to (PCOP)Ir/(POCOP)Ir.

Finally, the electronics of the aryl ring were examined, showing that an interplay between σ-donation and π-donation most likely caused the observed change in rate-determining step. Namely, strong σ-donation disfavors an olefin dissociation rate-determining step whereas weak π-donation favors a β-H elimination rate-determining step.

3.8 Experimental

All electronic structure calculations employed the DFT method[10] and the PBE[11] exchange-correlation functional. A relativistic, small-core ECP and corresponding basis set were used for the Ir atom (LANL2TZ model);[12,13] all-electron 6-311G(d) basis sets were applied to all P, N, C and B atoms; 311G basis sets were applied to all H atoms and, in addition, a set of diffuse p-type functions (exponent = 0.75) were placed on all hexane H atoms involved in C-H activation.[14-16] Reactant, transition state and product geometries were fully optimized, and the stationary points were characterized further by normal mode analysis. Expanded integration grid sizes (pruned (99,590) atomic grids invoked using the integral=ultrafine keyword) were applied to increase numerical accuracy and stability in both geometry optimizations and normal mode analyses.[17] The (unscaled) vibrational frequencies formed the basis for the calculation of vibrational zero-point energy (ZPE) corrections; standard thermodynamic corrections (based on the harmonic oscillator/rigid rotor approximations and ideal gas behavior) were made to convert from purely electronic (reaction or activation) energies to (standard) enthalpies (H) and Gibbs free energies (G; P = 1 atm).[18] H, entropy (S), and G were evaluated at two temperatures, T = 25 °C (= 298 K) and T = 125 °C (= 398 K). All energy values quoted in the principal text refer to T = 25 °C. In Supporting Information, we tabulate enthalpies, entropies, and free energies at T = 298 K (P = 1

atm) as well as free energies at T = 398 K (P = 1 atm). The latter T (125 °C, 398 K) approximates the temperature used in the experimental work. All calculations were executed using the GAUSSIAN 09 series of computer programs.[19]

3.9 References

(1) Kundu, S.; Choliy, Y.; Zhuo, G.; Ahuja, R.; Emge, T. J.; Warmuth, R.; Brookhart, M.; Krogh-Jespersen, K.; Goldman, A. S. *Organometallics* **2009**, *28*, 5432.

(2) Allen, K. E.; Heinekey, D. M.; Goldman, A. S.; Goldberg, K. I. *Organometallics* **2013**, *32*, 1579.

(3) Allen, K. E.; Heinekey, D. M.; Goldman, A. S.; Goldberg, K. I. *Organometallics* **2014**, *33*, 1337.

(4) Pahls, D. R.; Allen, K. E.; Goldberg, K. I.; Cundari, T. R. *Organometallics* **2014**, *33*, 6413.

(5) Biswas, S. *Doctoral Thesis, Rutgers, The State University of New Jersey* **2010**.

(6) Zhu, K.; Achord, P. D.; Zhang, X.; Krogh-Jespersen, K.; Goldman, A. S. *J. Am. Chem. Soc.* **2004**, *126*, 13044.

(7) Renkema, K. B.; Kissin, Y. V.; Goldman, A. S. *J. Am. Chem. Soc.* **2003**, *125*, 7770.

(8) Jean, Y.; Eisenstein, O. *Polyhedron* **1988**, *7*, 405.

(9) Rachidi, I. E. I.; Eisenstein, O.; Jean, Y. *New J. Chem.* **1990**, *14*, 671.

(10) Koch, W.; Holthausen, M. C. *A Chemist's Guide to Density Functional Theory*; Wiley: New York, 2001.

(11) Perdew, J. P.; Burke, K.; Ernzerhof, M. *Phys Rev. Lett.* **1996**, *77*, 3865.

(12) Hay, P. J.; Wadt, W. R. *J. Chem. Phys.* **1985**, *82*, 299.

(13) Roy, L. E.; Hay, P. J.; Martin, R. L. *J. Chem. Theory Comput.* **2008**, *4*.

(14) Ditchfield, R.; Hehre, W. J.; Pople, J. A. *J. Chem. Phys.* **1971**, *54*, 724.

(15) Hariharan, P. C.; Pople, J. A. *Mol. Phys.* **1974**, *27*, 209.

(16) McLean, A. D.; Chandler, G. S. *J. Chem. Phys.* **1980**, *72*, 5639.

(17) Frisch, Æ.; Frisch, M. J.; Clemente, F. R.; G. W. Trucks *Gaussian 09 User's Reference*, 147.

(18) McQuarrie, D. A. *Statistical Thermodynamics*; Harper and Row: New York, 1973.

(19) Frisch, M. J.; Trucks, G. W.; Schlegel, H. B.; Scuseria, G. E.; Robb, M. A.; Cheeseman, J. R.; Scalmani, G.; Barone, V.; Mennucci, B.; Petersson, G. A.; Nakatsuji, H.; Caricato, M.; Li, X.; Hratchian, H. P.; Izmaylov, A. F.; Bloino, J.; Zheng, G.; Sonnenberg, J. L.; Hada, M.; Ehara, M.; Toyota, K.; Fukuda, R.; Hasegawa, J.; Ishida, M.; Nakajima, T.; Honda, Y.; Kitao, O.; Nakai, H.; Vreven, T.; Montgomery, J. J. A.; Peralta, J. E. O., F.; Bearpark, M.; Heyd, J. J.; Brothers, E.; Kudin, K. N.; Staroverov, V. N.; Kobayashi, R.; Normand, J.; Raghavachari, K.; Rendell, A.; Burant, J. C.; Iyengar, S. S.; Tomasi, J.; Cossi, M.; Rega, N.; Millam, N. J.; Klene, M.; Knox, J. E.; Cross, J. B.; Bakken, V.; Adamo, C.; Jaramillo, J.; Gomperts, R.; Stratmann, R. E.; Yazyev, O.; Austin, A. J.; Cammi, R.; Pomelli, C.; Ochterski, J. W.; Martin, R. L.; Morokuma, K.; Zakrzewski, V. G.; Voth, G. A.; Salvador, P.; Dannenberg, J. J.; Dapprich, S.; Daniels, A. D.; Farkas, Ö.; Foresman, J. B.; Ortiz, J. V.; Cioslowski, J.; Fox, D. J., Gaussian 09.

Chapter 4

Rational design of new transfer dehydrogenation catalysts by DFT calculations

Abstract

Computational studies were used to elucidate the fundamental factors which govern the activity of pincer iridium catalysts for dehydrogenation, and to use these findings to predict new and synthesizable catalysts. First, the DFT-predicted energy barriers of known catalysts were compared to their experimentally-observed reaction rates. It was found that our initial measurement of the DFT energy barriers, from the 14 electron species to the highest transition state, was in extremely poor agreement with experiment. To remedy this issue, the 14 electron species was replaced with the (pincer)Ir(1-hexene) complex as the lower end of the energy barrier, leading to excellent agreement between experiment and DFT. With this calibration complete, we hypothesized that the magnitude of σ- and π-donation from the aryl ring of the pincer ligand was the main factor influencing the magnitude of the barrier. Comparisons between catalysts suggested that π-donation was the main determinant of the energy barrier, and that a slightly weaker π-donor should be a more active catalyst. Screening of new catalysts was conducted by DFT, predicting that (PCP-pyridinium)Ir^{+} catalysts should be exceedingly more active than the best currently known catalyst (ca. 3,000 fold), and also highly selective for generating 1-olefins.

4.1 Introduction

After the experimental regioselectivities of several pincer iridium catalysts were determined in Chapter 2, a new project involving DFT calculations was launched to investigate the *mechanism* by which regioselectivity was determined. That study, detailed in Chapter 3, found that high regioselectivity would be obtained if the rate-determining step was C-H activation or β-H elimination, but low regioselectivity would result if olefin dissociation was the rate-determining step. In turn, the identity of the rate-determining step was determined by a complex interplay between the σ-donation and π-donation from the ipso carbon of the aryl ring.

Thus, if a given catalyst had high activity but low regioselectivity (due to an olefin dissociation rate-determining step), then carefully modifying the σ-donation and π-donation parameters of the ligand might allow for high activity to be maintained while achieving high regioselectivity (*via* a C-H activation or β-H elimination rate-determining step). Then, this new catalyst with both high activity and selectivity could be employed in alkane metathesis, dehydroaromatization, or other processes to obtain valuable products such as diesel fuel,[1] benzene,[2,3] xylenes,[2,3] α-olefins,[4] or dimethylnapthalene.[2,3]

Notably, however, there are two issues with this theoretical plan. First, starting with a highly-active catalyst with low regioselectivity, and modifying its electronic properties to achieve higher regioselectivity, presumes that those electronic changes will not influence activity. In fact, it is possible that those electronic modifications will actually *reduce* catalytic activity, preventing the desired catalyst from being obtained. Secondly, this also presumes that the starting catalyst has high enough activity for the intended application. Notably, the current pincer iridium transfer dehydrogenation catalysts are *several orders of magnitude* less active than would be desired for commercial or practical applications. In alkane metathesis, the most selectivity catalyst,

(^{tBu4}PCP)Ir, achieves only a few dozen turnovers before decomposition of the olefin metathesis catalyst causes the reaction to terminate.[1] Similarly, full conversion in dehydroaromatization (measured as full consumption of the hydrogen acceptor) requires several hours or days to complete with catalyst loadings of around 10 mM.[2] Notably, commercial applications of these processes will employ very different reaction conditions, such as flow reactors instead of batch reactors, which could either increase or decrease catalytic activity and selectivity. Regardless, however, it appears that the activity of current pincer iridium catalysts is still several orders of magnitude slower than would be necessary for practical or commercial applications.

Therefore, this Chapter describes how a new DFT study was conducted to elucidate the electronic factors which determine the *activity* of pincer iridium catalysts. Hence, this plan would solve the issues described in the preceding paragraph. If a catalyst with high activity but low regioselectivity (such as a (PCOP)Ir catalysts during alkane metathesis[5]) was modified in an attempt to increase regioselectivity, then the effect of those changes on catalytic *activity* could also be estimated in advance, before expending the time and effort to synthesize and test the new catalyst. Similarly, a catalyst with high regioselectivity but lower activity (i.e. (^{tBu4}PCP)Ir) could be modified so that its catalytic activity increases (based upon results in this Chapter), but only if its high regioselectivity is not negatively affected (as analyzed by results from Chapter 2).

Notably, this Chapter will not examine the effect of steric crowding on catalytic activity because that study has already been conducted. In 2009 Goldman reported DFT calculations which predicted that (^{tBu3Me}PCP)Ir, a new catalyst, should have higher catalytic activity than (^{iPr4}PCP)Ir, which was the currently fastest catalyst for transfer dehydrogenation of *n*-alkanes.[6] Upon synthesizing (^{tBu3Me}PCP)Ir, Goldman found that it was indeed more active for a variety of transfer dehydrogenation reactions than all previous catalysts. However, it is unlikely that any further study of steric crowding would yield a better catalyst, simply because there are a limited

number of steric permutations which are possible. In contrast, a vast array of pincer ligands have been synthesized, (Section 1.3) providing a wealth of electronic possibilities which could be employed.

Before describing the efforts to design a more active pincer iridium dehydrogenation catalyst, it is noteworthy that "dehydrogenation" reactions take many forms, and it is prudent to define which type of catalyst is sought. In both acceptorless dehydrogenation and transfer dehydrogenation, the reaction begins with dehydrogenation of the alkane to give an olefin and the (pincer)IrH_2 complex.[7,8] However, the difference between these reactions arises in where the two hydrides are ultimately placed. In acceptorless dehydrogenation, the hydrides are reductively eliminated as H_2 gas which evolves out of the solution, whereas in transfer dehydrogenation they hydrides are transferred to an olefin (the "sacrificial hydrogen acceptor"), thereby converting the olefin into an alkane. Mechanistically, transfer dehydrogenation simply involves a reversal of the dehydrogenation sequence, but acceptorless dehydrogenation requires loss of H_2 gas in a completely different transformation.

Furthermore, even within the transfer dehydrogenation reaction, varying the alkanes and olefins involved can change which catalyst is most active. For example, (^{R4}POCOP)Ir catalysts are significantly faster than their (^{R4}PCP)Ir counterparts for the cyclooctane/*tert*-butylethylene (COA/TBE) transfer dehydrogenation,[9,10] but switching to 1-hexene/*n*-octane inverts the relative activities and the (PCP)Ir catalysts become much faster than their (POCOP)Ir analogs.

Thus, the current endeavor sought to design the most active transfer dehydrogenation catalyst for linear 1-olefin/linear alkane reactions since this is what transpires in alkane metathesis and dehydroaromatization. In addition, a secondary goal was also established: a dehydrogenation catalyst which selectively produces 1-olefins. Although the 1-olefin selectivity would have little

to no effect on dehydroaromatization, it was predicted to cause large increases in selectivity for the desired/longest alkane (i.e. *n*-decane from *n*-hexane) in alkane metathesis.

During the course of this study, the first objective achieved was elucidating how electronics affect the overall kinetic barrier to dehydrogenation. Next, DFT-assisted screening was performed in order to find a more active pincer iridium catalyst for dehydrogenation. While most of the complexes screened followed the traditional format of a single pincer ligand attached to iridium, some of the complexes examined were heterodinuclear complexes.

By definition, a heterodinuclear complex is a species which contains two different metals (transition metals or main group metals). These were considered because adding the second metal-containing moiety is a known method for adjusting the electronic properties of the primary metal. In particular, the electrochemical behavior of certain naphthoresorcinate POCOP compounds was found to be influenced by the attachment of Fe/Ru/Cr moieties to the backbone of the POCOP ligand.[11] (Figure 4.1) In addition, the catalytic activity of (^{tBu4}PCP)Ir was modified by attaching CpFe or CpRu moieties to the benzene backbone of the catalyst.[12] (Figure 4.1) In particular, these heterodinuclear catalysts were found to be *more* active than both (^{tBu4}PCP)Ir and (^{tBu4}POCOP)Ir during COA/TBE transfer dehydrogenation. Therefore, the investigations into new possibilities for transfer dehydrogenation catalysts involved both traditional and heterodinuclear catalysts.

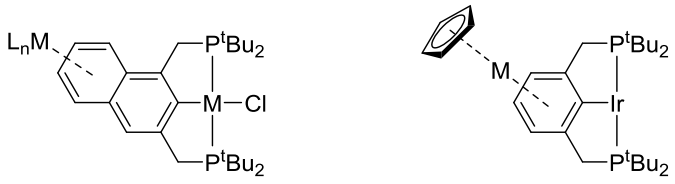

(L_nM-naphthoresorcinate-POCOP)M'Cl
M' = Ni, Pd, Pt
L_nM = Cp^*Ru, CpRu, CpFe, $Cr(CO)_3$

(CpM-^{tBu4}PCP)Ir
M = Fe, Ru

Figure 4.1 Examples of heterodinuclear compounds

Tian Zhou, another member of Professor Goldman's research group, performed the actual DFT calculations and reported the calculated energies. Planning which DFT calculations to conduct, and interpreting the results of those calculations, was a collaboration between myself and Professor Goldman.

4.2 Calibrating DFT predictions to experimental observations

4.2.1 Correlations between experimentally observed catalytic activity and molecular structure

Before making DFT-assisted predictions about new catalysts, it was necessary to assess any experimentally-observed trends in catalytic activity for existing catalysts. Thus, experimental data for the 9 catalysts studied during the selectivity project was used to tabulate approximate rates of 1-hexene/*n*-octane transfer dehydrogenation. Although not examined in the selectivity project, the transfer dehydrogenation abilities of many other pincer catalysts have been studied previously, albeit under different reaction conditions. Using comparisons from these other reports, a semi-quantitative comparison of several pincer catalysts can be made.[6,13] (Table 4.1)

Catalyst	Rate (hr^{-1})	Comparative Rate
(^{tBu4}PCP)Ir	68	-
(MeO-^{tBu4}PCP)Ir	13	-
(Me_2N-^{tBu4}PCP)Ir	5	-
(MeO_2C-^{tBu4}PCP)Ir	-	20% faster than (^{tBu4}PCP)Ir before decomposition
(^{tBu3Me}PCP)Ir	-	70% faster than (^{iPr4}PCP)Ir
(^{tBuMe}PCP^{tBuMe})Ir	-	11% faster than (^{iPr4}PCP)Ir
(^{tBu2}PCP^{iPr2})Ir	78	-
(^{iPr4}PCP)Ir	89	-
(^{tBu4}PCOP)Ir	7	-
(^{iPr4}PCOP)Ir	16	-
(^{tBu4}POCOP)Ir	0.2	-
(MeO-^{iPr4}POCOP)Ir	< 0.01	-
(^{iPr4}anthraphos)Ir	39	-

Table 4.1 Turnover frequency of pincer iridium catalysts for 1-hexene/*n*-octane transfer dehydrogenation using conditions specified in Scheme 2.10

This data demonstrates that various ligand modifications can play a significant role in determining catalytic activity. For (PCP)Ir catalysts without electronic substituents on the aryl backbone, modifications to the steric environment (by changing the PR_2 groups) from the slowest catalyst (^{tBu4}PCP)Ir to the fastest catalyst (^{tBu3Me}PCP)Ir leads to a 55% increase in activity. Attaching electronic substituents to the aryl backbone's para position also causes activity to change. Employing the CO_2Me group increases activity by ~20% (before catalyst decomposition), whereas the NMe_2 and OMe groups reduce activity by 93% and 81% respectively. In addition, substituting one or both methine linkages in (PCP)Ir for an oxygen has massive effects on activity. (PCOP)Ir catalysts (one methine substitution) were found to be 82% to 90% slower than their (PCP)Ir counterparts, whereas (POCOP)Ir catalysts (two substitutions) were 99.7% to >99.9% slower than their (PCP)Ir analogs.

As discussed in detail in the regioselectivity section, these ligand modifications can alter the energy of each transition state through four main routes: σ- and π-donation from the aryl ring, electron donation from the phosphorous atoms, and the steric environment around iridium.

Although completely isolating each of these routes is technically impossible, the regioselectivity studies demonstrated that σ- and π-donation from the aryl ring was the main route by which the *relative* height of β-H elimination and olefin dissociation (relative to one another) and therefore regioselectivity was determined. Thus, we hypothesized that the *absolute* height (and therefore overall barrier to dehydrogenation) was also mostly determined by σ- and π-donation from the aryl ring. The data from Table 4.1 seems to reinforce this hypothesis, since the substitution of methines (PCP vs. PCOP vs. POCOP) had the most profound effect on reaction rate, and since the regioselectivity studies showed the methylene-for-oxygen switch mainly effected regioselectivity through the aryl ring's electronics. In addition, the attachment of various electronic moieties to the para position of the ring, which could not influence sterics or phosphorous electronics to any significant extent,[14] caused changes in activity larger than any steric modification.

Thus, DFT calculations for designing more active catalysts focused on modifying the aryl ring's electronics. Even if sterics had been determined to be significant, the possibilities for modifying and therefore optimizing the steric environment would be synthetically limited. In contrast, the electronic aspects of the aryl ring (or phosphorous atoms) could be modified by numerous synthetic methods, and were therefore a more worthwhile target for DFT analysis.

Before predicting new catalysts, the agreement between DFT calculations and experimental observations with existing catalysts was assessed. In particular, two different approaches to DFT analysis could be used: either the calculation of one piece of the dehydrogenation sequence, or a full calculation of all transition states and intermediates along the sequence. In the first approach, which was the basis for synthesis of the (POP)Rh complexes, that segment would be used as a "model" of the overall sequence.[15] If the model section showed a lower barrier, then the overall reaction barrier might also be lower. Although less complete

than a full analysis, the "model section" approach would allow for quicker analysis and screening of more catalysts than the complete approach.

4.2.2 Early DFT models of catalytic activity

The agreement between experiment and DFT was first examined by using C-H activation at the terminal carbon of n-hexane as a "model" for the overall dehydrogenation rate. (Tables 4.2 and 4.3) After obtaining the $\Delta G^{\ddagger}$ of C-H activation, the Eyring equation (Equation 2.3) was used to predict the relative reaction rate (at 125 ^{o}C) for six pincer iridium catalysts. (Table 4.2) Notably, the trends from the DFT "model" approach were in extremely poor agreement with experiment. First, DFT predicted an enormous increase in catalytic activity when changing the $_{PR2}$ groups from ^{t}Bu to ^{i}Pr (i.e. from (^{tBu4}PCP)Ir to (^{iPr4}PCP)Ir). This increase ranged from ~2,500 *fold* (or 250,000%) for POCOP and ~2,900 fold for (PCOP)Ir to ~7,900 fold for (PCP)Ir. In stark contrast, substituting ^{t}Bu with ^{i}Pr experimentally caused either a minor increase (10% or 124%) or a *decrease* (>95%) in rate. In addition, the effect of the methine-for-oxygen substitution in the DFT analysis was also in extremely poor agreement with experiment. Whereas DFT analysis predicted that each substitution would increase catalytic activity between ~40 and ~1,000 *fold* (or 100,000%), experiment showed that each substitution actually caused a *decrease* in activity of at least 78%.

	(^{tBu4}PCP)Ir	(^{tBu4}PCOP)Ir	(^{tBu4}POCOP)Ir	(^{iPr4}PCP)Ir	(^{iPr4}PCOP)Ir	(^{iPr4}POCOP)Ir
[Ir] + hexane	0.0	0.0	0.0	0.0	0.0	0.0
C-H activation	20.8	17.2	11.7	13.7	10.9	5.5
[Ir](H)(hexyl)	18.2	14.6	8.8	11.7	9.6	3.6

Table 4.2 Kinetic barriers to and thermodynamics of C-H activation

Catalyst	Experimental: rate (h^{-1})	Experimental: relative rate	DFT: C-H activation $\Delta G^{\ddagger}$	DFT: C-H activation relative rate
(^{tBu4}PCP)Ir	68	(defined) 1	20.8	(defined) 1
(^{tBu4}PCOP)Ir	7	0.10	17.2	95
(^{tBu4}POCOP)Ir	0.2	0.003	11.7	99,624
(^{iPr4}PCP)Ir	78	1.1	13.7	7,940
(^{iPr4}PCOP)Ir	16	0.24	10.9	274,021
(^{iPr4}POCOP)Ir	<0.01	< 0.0002	5.5	253,424,356

Table 4.3 Catalytic activity: comparison between experiment and DFT-predicted rates using the 14 electron complex and the C-H activation barrier. Experiments were based upon conditions in Scheme 2.10. DFT energies expressed in kcal/mol and relative rates at 125 °C.

Since the "model" approach failed to reproduce the experimentally observed trends in catalytic activity, the full dehydrogenation sequence (to give 1-hexene) was calculated for each catalyst (Table 4.4). Notably, the lowest overall barrier (either C1-C2 or C2-C1) was included in Table 4.4.

	^{tBu4}PCP C1-C2	^{tBu4}PCOP C2-C1	^{tBu4}POCOP C1-C2	^{iPr4}PCP C1-C2	^{iPr4}PCOP C1-C2	^{iPr4}POCOP C1-C2
[Ir] + hexane	0.0	0.0	0.0	0.0	0.0	0.0
σ-complex	9.9	9.6	5.4	4.7	6.1	0.2
C-H activation	20.8	21.2	11.7	13.7	10.9	5.5
[Ir](H)(hexyl)	18.2	17.0	8.8	11.7	9.6	3.6
β-H elimination	26.9	22.3	21.3	14.0	15.3	5.1
[Ir](H)(H)(hexene)	11.9	11.5	9.2	0.1	4.1	-3.9
olefin dissociation	22.6	24.8	23.0	13.7	15.9	12.1
[Ir]H_2 + hexene	2.4	0.3	-3.3	-0.9	2.7	-6.3

Table 4.4 DFT-predicted kinetic barriers to dehydrogenation using the (pincer)Ir 14 electron complex as the zero point, in kcal/mol. All are iridium pincer complexes.

Inspection of Table 4.4 demonstrates that the DFT-predicted barrier for C-H activation (highlighted: orange) does not correlate with the DFT-predicted overall barrier (highlighted: green). Comparing (^{iPr4}PCP)Ir and (^{iPr4}PCOP)Ir, the overall barrier increases from 14.0 to 15.9 upon

the methine-for-oxygen substitution even though the C-H activation barrier decreased from 13.7 to 10.9.

Despite this, the relative rates predicted by the full dehydrogenation sequence were also in extremely poor agreement with experiment. The "full" approach correctly predicted that changing the ^{t}Bu groups to ^{i}Pr groups in PCP and PCOP catalysts would lead to higher activity, but the magnitude of those changes was incorrect by over eight orders of magnitude! For the PCP catalysts, the full approach predicted an increase of ~12,000,000 *fold* (1,200,000,000%), whereas experiment only showed a 10% increase. In addition, the full approach predicted that changing methines into oxygens would increase activity by ~10 fold or 1,000% for each oxygen, whereas experiment showed that the oxygens actually caused activity to *decrease*. (Table 4.5)

Catalyst	Experimental: rate (h^{-1})	Experimental: relative rate	DFT: overall barrier	DFT overall barrier: relative rate
(^{tBu4}PCP)Ir	68	(defined) 1	26.9	(defined) 1
(^{tBu4}PCOP)Ir	7	0.10	24.8	14
(^{tBu4}POCOP)Ir	0.2	0.003	23.0	138
(^{iPr4}PCP)Ir	78	1.1	14.0	12,178,607
(^{iPr4}PCOP)Ir	16	0.24	15.9	1,101,494
(^{iPr4}POCOP)Ir	<0.01	< 0.002	12.1	134,651,992

Table 4.5 Catalytic activity: comparison between experiment and DFT-predicted rates using the 14 electron complex and highest transition state. Experiments were based upon conditions in Scheme 2.10. DFT energies expressed in kcal/mol and relative rates at 125 °C.

4.2.3 Importance of the (pincer)Ir(1-olefin) resting state

Because of the extremely poor agreement between DFT and experiment, it was apparent that random error could not be the source of this vast disagreement. Instead, a fundamental aspect of how DFT and experiment were being compared must have been overlooked. Thus, it

was hypothesized that adding the (pincer)Ir(olefin) 4-coordinate complexes to the DFT analysis might reconcile this discrepancy. Although the 4-coordinate olefin complexes do not participate in the dehydrogenation sequence, NMR studies of COA/TBE transfer dehydrogenation reactions with (^{tBu4}PCP)Ir have shown that the catalytic resting state was an equilibrium between the (^{tBu4}PCP)IrH_2 and (^{tBu4}PCP)Ir(olefin) complexes.[6] (Figure 4.2) Thus, if DFT were to find that the 4-coordinate olefin complexes were lower in energy than the intermediates along the dehydrogenation sequence, then the overall barrier would be recalibrated in a manner which might reconcile DFT with experiment.

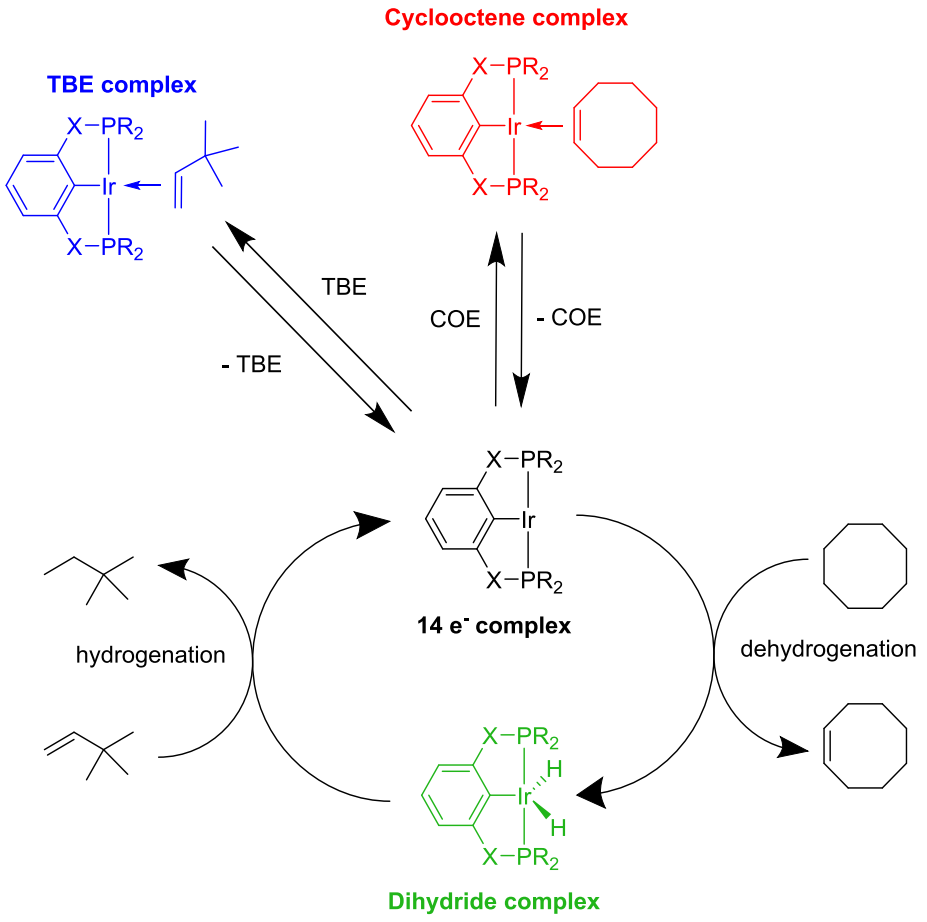

Figure 4.2 Explanation of catalytic resting states during transfer dehydrogenation using COA/TBE example

DFT calculations explored the coordination of 1-hexene and 2-hexenes as a model for the 1-olefins and 2-olefins present during 1-hexene/*n*-octane reactions. Initial calculations found that olefins coordinated *trans* to the aryl ring (giving a square planar 4-coordinate complex) were more stable than 4-coordinate complexes with the olefin *cis* to the aryl ring.

Using the 14 electron complex as the reference point, these calculations demonstrated that each of the 1-hexene complexes was significantly more stable (by 3.1 to 10.0 kcal/mol) than the (E)-2-hexene adducts, which themselves were always most stable than the (Z)-2-hexene complexes (Table 4.6). Since each of the 1- and 2-hexenes would have similar electronic interactions with iridium, this large difference is presumably due to steric crowding at the iridium center. In fact, the difference is more pronounced with bulky ^{t}Bu groups than with less sterically encumbering ^{i}Pr groups. Likewise, the effect is larger with (PCP)Ir complexes, which are known to be more sterically crowded than (POCOP)Ir complexes.[16]

	^{tBu4}PCP	^{tBu4}PCOP	^{tBu4}POCOP	^{iPr4}PCP	^{iPr4}PCOP	^{iPr4}POCOP
[Ir]	0.0	0.0	0.0	0.0	0.0	0.0
[Ir](1-hexene)	-2.4	-6.3	-13.3	-14.7	-15.7	-20.5
[Ir](E-2-hexene)	7.6	1.7	-6.2	-9.1	-10.5	-17.4
[Ir](Z-2-hexene)	8.8	3.9	-3.9	-7.9	-9.1	-15.1

Table 4.6 Energies of (pincer)Ir(olefin) 4-coordinate complexes compared to the 14 electron complex in kcal/mol. All species are pincer iridium complexes.

In addition, the 1-hexene adducts are significantly lower in energy than the 14 electron complexes and, therefore, the comparisons between DFT and experimental results should be recalibrated. Thus, including the (pincer)Ir(1-hexene) adducts in the DFT estimates causes those estimates to change significantly, both in their absolute values *and* in the relative ranking of each catalyst. For example, in the previous estimates in Tables 4.3 and 4.5, the (PCOP)Ir catalysts were always predicted to be faster than their (PCP)Ir analogs, in stark contrast to experiment. (Table

4.1) However, after adjusting for the 1-olefin catalytic resting states, the DFT barriers now *correctly* predict that (PCOP)Ir catalysts will be slower than their (PCP)Ir counterparts. Moreover, the resting-state-adjusted DFT calculations also more accurately estimate the approximate *magnitudes* for these changes. For example, resting-state-adjusted DFT calculations predict that (^{tBu4}PCP)Ir will be approximately 24 times more active than (^{tBu4}PCOP)Ir, while experiment shows it to be about 9 times more active. Likewise, (^{iPr4}PCP)Ir is estimated to be 38 times more active than (^{iPr4}PCOP)Ir by DFT, whereas experiment showed (^{iPr4}PCP)Ir is about 5 times more active. (Table 4.7)

Catalyst	Experimental: rate (h^{-1})	Experimental: relative rate	DFT: overall barrier	DFT overall barrier: relative rate
(^{tBu4}PCP)Ir	68	(defined) 1	28.6	(defined) 1
(^{tBu4}PCOP)Ir	7	0.10	31.2	0.041
(^{tBu4}POCOP)Ir	0.2	0.003	36.3	0.00006
(^{iPr4}PCP)Ir	78	1.1	28.7	0.88
(^{iPr4}PCOP)Ir	16	0.24	31.6	0.023
(^{iPr4}POCOP)Ir	<0.01	< 0.002	32.4	0.0083

Table 4.7 Catalytic activity: comparison between experiment and DFT-predicted rates using (pincer)Ir(1-hexene) complex and highest transition state. Experiments were based upon conditions in Scheme 2.10. DFT energies expressed in kcal/mol and relative rates at 125 °C.

In addition, the resting-state-adjusted DFT calculations also showed good agreement with experiment when comparing the activity of R = ^{t}Bu versus R = ^{i}Pr catalysts. DFT analysis predicted that (^{iPr4}PCP)Ir would be 12% slower than (^{tBu4}PCP)Ir, whereas experiment found it to be 10% faster, giving the closest agreement in the data set. Likewise, DFT analysis suggested that (^{iPr4}PCOP)Ir would be 44% slower than (^{tBu4}PCOP)Ir , whereas it was experimentally found to be 129% more active. Compared to the previous DFT estimates in Tables 4.3 and 4.5, the current data is in very good agreement with experiment.

4.3 Understanding the effects of aryl electronics on catalytic activity *via* the ΔG_{HH1hex} parameter

With strong agreement between DFT calculations and experimental observations in hand, steps towards predicting more active and selective catalysts were begun. Namely, correlations between catalyst structure and activity would need to be strengthened into hypotheses about *causation*. Since the electronic structure of (pincer)Ir catalysts could be modified more extensively than their steric environments, DFT calculations were undertaken in order to understand how electronic factors affected the overall kinetic barrier.

Initially, many comparisons between the (pincer)Ir(1-hexene) resting state and the β-H elimination transition state were made since β-H elimination was the rate-determining step with (^{tBu4}PCP)Ir, (^{iPr4}PCP)Ir, (MeO-^{tBu4}PCP)Ir, and (Me_2N-^{tBu4}PCP)Ir. Ideally, deducing the σ- and π-effects which governed this energy gap would allow the design of catalysts with lower $\Delta G^{\ddagger}_{\beta\text{-H}}$ and therefore faster activity.

However, this approach does not account for the possibility that C-H activation or olefin dissociation would rise in energy and become the rate-determining step, thus obviating any gains from lowering the β-H elimination barrier. This is an especially important concern since the three transition states moved to very different degrees depending on the type of ligand modification. Comparing the same C1-C2 pathway for (^{tBu4}PCP)Ir and (^{tBu4}PCOP)Ir, which only differ by a single methylene/oxygen unit, C-H activation and olefin dissociation increased by 3.1 and 3.5 kcal/mol, whereas β-H elimination increased by only 0.3 kcal/mol. (Table 4.8)

	(^{tBu4}PCP)Ir C1-C2	(^{tBu4}PCOP)Ir C1-C2	Difference
[Ir](1-hexene)	0.0	0.0	0.0
[Ir] + hexane	2.4	6.3	3.9
C-H activation	23.1	23.5	0.3
[Ir](H)(hexyl)	20.6	20.9	0.3
β-H elimination	29.3	31.5	2.2
[Ir](H)(H)(hexene)	14.3	17.8	3.5
olefin dissociation	24.9	31.2	6.2
[Ir]H_2 + hexene	4.7	6.6	1.9

Table 4.8 DFT predicts that changes in catalyst structure cause each transition state to move in energy by a different amount during C1-C2 pathway, in kcal/mol

In order to avoid the effects of random error, the differences between (^{tBu4}PCP)Ir and (^{tBu4}PCOP)Ir were compared again by averaging the energies of all four pathways (two for generating 1-hexene, and two for giving (E)-2-hexene) (Table 4.9). The energy of C-H activation decreased by 0.3 kcal/mol, whereas β-H elimination increased by 0.6 kcal/mol. Oefin dissociation increased drastically at 5.0 kcal/mol. Thus, modifying the ligand could easily cause different changes in each transition state, which is why olefin dissociation is the rate-determining step with (POCOP)Ir catalysts, whereas β-H elimination is the rate-determining step with (PCP)Ir catalysts.

	(^{tBu4}PCP)Ir average	(^{tBu4}PCOP)Ir average	Difference
[Ir](1-hexene)	0.0	0.0	0.0
[Ir] + hexane	2.4	6.3	3.9
C-H activation	27.3	27.0	-0.3
[Ir](H)(hexyl)	23.8	22.9	-0.8
β-H elimination	31.5	32.1	0.6
[Ir](H)(H)(hexene)	17.6	19.9	2.3
olefin dissociation	26.1	31.1	5.0
[Ir]H_2 + hexene	2.9	4.8	1.9

Table 4.9 DFT predicts that changes in catalyst structure cause each transition state to move in energy by a different amount on average, in kcal/mol

Therefore, simply examining the energy gap between the (pincer)Ir(1-hexene) complex and the β-H elimination transition state would be insufficient for understanding the electronic factors which determine catalytic activity. Although much more complex, three separate comparisons could have been undertaken: between the resting state and each of the transition states independently. However, this would not avoid another complicating factor: sterics. By inspection, it is apparent that the geometric configuration of the resting state is very different than that of the three transition states. So, if the energy gap between the resting state and the C-H activation transition state ($\Delta G^{\ddagger}_{C\text{-}H}$) of a new catalyst (i.e. L_1Ir) was calculated, then that value ($\Delta G^{\ddagger}_{C\text{-}H}$-$L_1$) would be influence by both electronics *and* sterics. If a second catalyst (i.e. L_2Ir) with different electronic and steric properties was considered, and its $\Delta G^{\ddagger}_{C\text{-}H}$ was calculated, then $\Delta\Delta G^{\ddagger}_{C\text{-}H} = \Delta G^{\ddagger}_{C\text{-}H}$-$L_1$ - $\Delta G^{\ddagger}_{C\text{-}H}L_2$ could be determined in an attempt to observe how the *electronic* differences between L_1 and L_2 affected their C-H activation barriers. However, $\Delta\Delta G^{\ddagger}_{C\text{-}H}$ would have *also* been influenced by any steric differences between L_1Ir and L_2Ir. For example, if L_1Ir was more crowded at the iridium center than L_2Ir, then the calculated value for $\Delta G^{\ddagger}_{C\text{-}H}$-$L_1$ would be larger than electronics alone would have caused it to be. Hence, the effects of electronics could not be isolated from the effects of sterics if the upper energy level (i.e. C-H activation) had a different geometric configuration than the resting state (i.e. (pincer)Ir(1-hexene)).

To avoid the complicating factors associated with sterics, a new model transformation was selected: between the (pincer)Ir(1-hexene) resting state and the (pincer)Ir(H)(H)(1-hexene) *intermediate* (ΔG_{HH1hex}). Examination of DFT-optimized structures revealed that the geometric configuration of these two species for common (PCP)Ir and (POCOP)Ir complexes were extremely similar. In addition, the only formal difference between these two species was the addition of two hydrides, which were small enough that any steric interactions would be minimal. Moreover, the (pincer)Ir(H)(H)(1-hexene) intermediate was located at an optimal place along the reaction

coordinate: immediately adjacent to and between β-H elimination and olefin dissociation, the two rate-determining steps for known catalysts. If that intermediate increased or decreased, then the energy of the two transition states might also increase or decrease in a similar way.

Before attempting to examine new catalysts, ΔG_{HH1hex} values were compared to the DFT-calculated overall barriers ($\Delta G^{\ddagger}_{overall}$) and experimental reaction rates of known catalysts (Table 4.10). The trends in ΔG_{HH1hex} for the six examined catalysts were in strong agreement with both the DFT-estimations for the overall barriers ($\Delta G^{\ddagger}_{overall}$) and with experimental observations. In all three cases, switching between R = ^{t}Bu and R = ^{i}Pr for (^{R4}pincer)Ir catalysts made only small differences in the observed rates or predicted energies. Likewise, changing the methine linkers to oxygens lead to significant increases in the predicted energies and to slower experimental rates. These very strong agreements suggested that it would be worthwhile to use the ΔG_{HH1hex}-based model for attempting to understand how electronics affected the rates/barriers to pincer iridium dehydrogenation.

Catalyst	Experimental: relative rate	DFT $\Delta G^{\ddagger}_{overall}$: relative rate	DFT $\Delta G^{\ddagger}_{overall}$	DFT: ΔG_{HH1hex}
(^{tBu4}PCP)Ir	(defined) 1	(defined) 1	28.6	14.3
(^{tBu4}PCOP)Ir	0.10	0.041	31.2	17.8
(^{tBu4}POCOP)Ir	0.003	0.00006	36.3	22.5
(^{iPr4}PCP)Ir	1.1	0.88	28.7	14.8
(^{iPr4}PCOP)Ir	0.24	0.023	31.6	19.8
(^{iPr4}POCOP)Ir	< 0.002	0.0083	32.4	24.4

Table 4.10 The parameter ΔG_{HH1hex} strongly correlates with experimental observations and the overall barrier predicted by DFT. Experiments were based upon conditions in Scheme 2.10. DFT energies expressed in kcal/mol and relative rates at 125 °C.

Since electronic effects had been isolated from those of sterics using the ΔG_{HH1hex} model, judicious selection of catalyst structure was employed to separate the three possible electronic effects from one another: σ-donation from the aryl ring, π-donation from the aryl ring, and

donation of electron density from the phosphorous. Using (PCP)Ir catalysts as the reference point, (POCOP)Ir catalysts are known to have less electron density on the phosphorous atoms,[14] which suggests that they would donate less electron density to the iridium. In addition, chemical intuition suggests that (POCOP)Ir catalysts would also be weaker σ-donors due to inductive effects of the oxygens, but stronger π-donors due to resonance effects. (Figure 4.3) As detailed in the regioselectivity section of this thesis, computational methods were used to investigate the σ- and π-donating capabilities of these ligands, and confirmed that they hypotheses listed above were true.

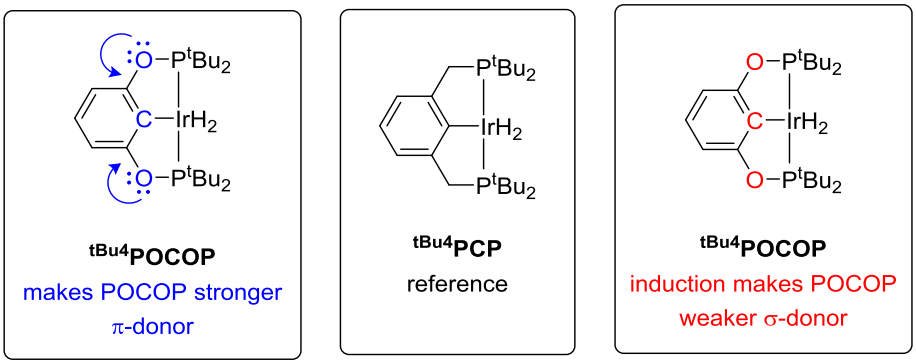

Figure 4.3 σ-donation and π-donation *via* the C_{ipso}-Ir bond

In addition to the five main catalysts studied for the regioselectivity project, (^{tBu4}PCP)Ir, (^{tBu4}PCOP)Ir, (^{tBu4}POCOP)Ir, (paraB-^{tBu4}PNP)Ir, and (paraN-^{tBu4}PBP)Ir, the current study also examined the (^{tBu4}PPP)Ir catalyst. (Figure 4.4) Together, these six complexes allowed each of the three electronic effects to be isolated. Namely, the electronics of the phosphorous atoms in (^{tBu4}PNP-pB)Ir and (^{tBu4}PBP-pN)Ir should be nearly identical to those in (^{tBu4}PCP)Ir since all three catalysts contain two methine linkers, prohibiting the movement of π-electrons between the aryl ring and the phosphorous atoms. However, isolating the two components of aryl electronics (σ and π) would be more difficult.

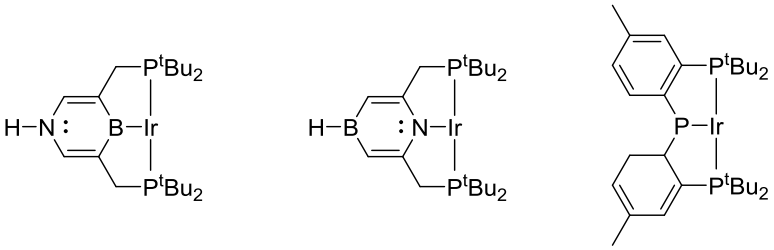

(paraN-^{tBu4}PBP)Ir **(paraB-^{tBu4}PNP)Ir** **(^{tBu4}PPP)Ir**

Figure 4.4 Three catalysts examined with DFT calculations

The first five catalysts (excluding (^{tBu4}PPP)Ir) can be plotted on a spectrum where both σ- and π-donation change concurrently, which would make resolving the effects of σ- versus π-donation impossible. (Figure 4.5) However, the (^{tBu4}PPP)Ir catalyst is both a strong σ-donor *and* a strong π-donor, which would allow the effects of σ- and π-donation to be compared.

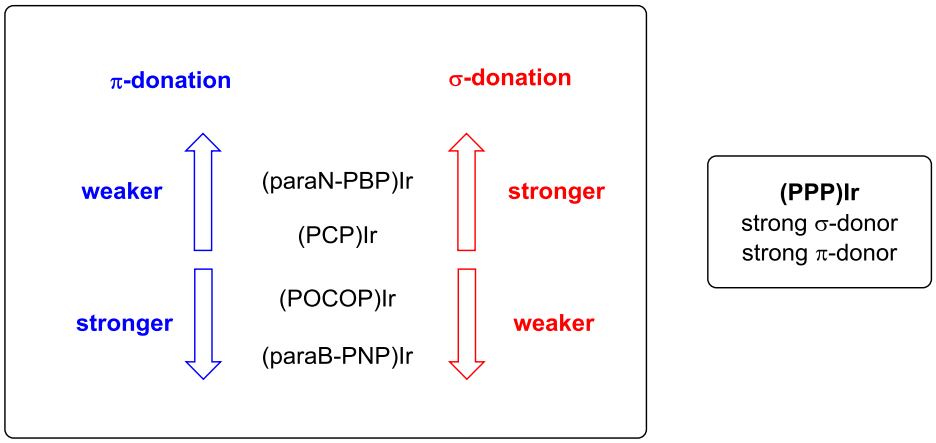

Figure 4.5 Relative σ-donation and π-donation of catalysts examined by DFT

Comparing the ΔG energy gaps and σ/π parameters for each of the six catalysts with their $\Delta G^{\ddagger}_{overall}$ values gave useful insight into how each of the electronic effects influence catalytic activity. (Table 4.11) To reduce random error in the DFT calculations, the values of ΔG_{HH1hex} were averaged with those of $\Delta G_{HH\text{-}E2hex}$ to give $\Delta G_{HH\text{-}hexene}$.

For five of the catalysts (excluding (^{tBu4}PPP)Ir) there was a perfect qualitative correlation between σ-donation and $\Delta G_{HH\text{-}hexene}$ and $\Delta G^{\ddagger}_{overall}$: stronger σ-donation lead to lower ΔG_{HH1hex} and lower $\Delta G^{\ddagger}_{overall}$ in all cases. Likewise, a perfect qualitative correlation with the five catalysts also existed between π-donation and the two ΔG values: stronger π-donation always caused the two ΔG values to *increase*. Although the role of phosphorous electronics cannot be *disproven*, the massive changes seen with (^{tBu4}PBP-pN)Ir and (^{tBu4}PNP-pB)Ir suggest that aryl electronics are the dominant factor. Next, the (^{tBu4}PPP)Ir catalyst was used to investigate these aryl electronics and to identify whether σ-donation or π-donation (or both) played a significant role in determining the two ΔG values. If σ-donation was the determining factor, then the strongly σ-donating (^{tBu4}PPP)Ir should have relatively *low* ΔG values like the strongly σ-donating (^{tBu4}PBP-pN)Ir catalyst. On the other hand, if π-donation was an important factor, then strongly π-donating (^{tBu4}PPP)Ir should have relatively *high* ΔG values like the strongly π-donating (^{tBu4}PNP-pB)Ir catalyst. Upon completion of the DFT calculations, (^{tBu4}PPP)Ir was found to have a relatively high value of 22.1 kcal/mol for $\Delta G_{HH\text{-}hexene}$. Since that value was only 3.0 kcal/mol lower than that of strongly π-donating (^{tBu4}PNP-pB)Ir (25.1 kcal/mol), but 11.5 kcal/mol higher than that of strongly σ-donating (^{tBu4}PBP-pN)Ir (10.6 kcal/mol), this suggests that the value of $\Delta G_{HH\text{-}hexene}$ is mainly dependent on π-donation!

Catalyst	σ-donation	π-donation	$\Delta G_{HH\text{-}hexene}$	$\Delta G^{\ddagger}_{overall}$
(^{tBu4}PNP-pB)Ir	Extremely weak	Extremely strong	25.1	41.0
(^{tBu4}POCOP)Ir	Very weak	Very strong	23.6	36.3
(^{tBu4}PPP)Ir	Strong	Strong	22.1	36.5*
(^{tBu4}PCOP)Ir	Weak	Somewhat strong	19.9	31.2
(^{tBu4}PCP)Ir	Reference	Reference	17.6	28.6
(^{tBu4}PBP-pN)Ir	Strong	Weak	10.6	33.5*

Table 4.11 Strong correlation between π-donation and both ΔG_{HH1hex} and $\Delta G^{\ddagger}_{overall}$, in kcal/mol

It is noteworthy that the (^{tBu4}PPP)Ir and (^{tBu4}PBP-pN)Ir catalysts were calculated to have 1-hexene resting states that were *higher* in energy than their 14 electron complexes. Therefore,

the $\Delta G^{\ddagger}_{overall}$ values reported in Table 4.11 represent the energy difference between the 14 electron complexes and the corresponding highest transition states. The energy differences between the 1-hexene complexes and the highest transition states were 21.3 kcal/mol for (^{tBu4}PBP-pN)Ir and 27.4 kcal/mol for (^{tBu4}PPP)Ir.

With a hypothesis regarding possible causation between π-donation and $\Delta G_{HH\text{-}hexene}$ in hand, a possible relationship between π-donation and $\Delta G^{\ddagger}_{overall}$ was investigated. Examination of the $\Delta G_{HH\text{-}hexene}$ and $\Delta G^{\ddagger}_{overall}$ data in Table 4.11 shows that as $\Delta G_{HH\text{-}hexene}$ decreases from its highest value to its second-lowest (25.1 to 17.6 kcal/mol), $\Delta G^{\ddagger}_{overall}$ also decreases (41.0 to 28.6 kcal/mol) in a remarkably linear fashion. By itself, this suggests that increasingly weak π-donating catalysts would also have increasingly small $\Delta G^{\ddagger}_{overall}$ barriers, and would therefore be increasingly more active experimentally. However, even though the (^{tBu4}PBP-pN)Ir catalyst has the smallest value of $\Delta G_{HH\text{-}hexene}$ of all catalysts, the decrease in $\Delta G_{HH\text{-}hexene}$ between (^{tBu4}PCP)Ir and (^{tBu4}PBP-pN)Ir actually lead to an *increase* in $\Delta G^{\ddagger}_{overall}$ from 28.6 to 33.5 kcal/mol. Presumably, the extremely weak π-donation (or extremely strong σ-donation) of (^{tBu4}PBP-pN)Ir crossed a threshold that caused the previous correlation between π-donation and $\Delta G^{\ddagger}_{overall}$ to no longer apply.

Thus, the totality of these investigations suggested that examining catalysts which are slightly weaker π-donors than (^{tBu4}PCP)Ir would be the most effective method for discovering more active transfer dehydrogenation catalysts.

4.4 Screening heterodinuclear catalysts by DFT calculations

The next step in designing more active catalysts was to take the theoretical hypothesis regarding catalytic activity and convert it into an actual catalyst structure that could be

synthesized. Namely, it was necessary to brainstorm molecular structures that would be slightly less π-donating than the (PCP)Ir catalysts. The first class of catalyst candidates to be examined were heterodinuclear complexes.

Design of actual heterodinuclear complexes began by considering the 18 electron rule. In order to obtain a thermodynamically stable complex, it was hypothesized that the secondary transition metal (i.e. chromium) should follow the 18 electron rule. This rule states that transition metal complexes with 18 electrons in their valence shell, which completely fills the valence shell, are the most stable and therefore the most resistant towards chemical reactions. Due to the design of these complexes, the secondary metal (i.e. chromium) should be completely inert to any chemical reactions, leaving that purpose to the iridium center.

In order to obtain this 18 electron count, the first aspect of the secondary transition coordination sphere of the metal will be the aryl ring from the pincer ligand. For maximum stability, this can safely be assumed to be an η^6-benzene moiety, adding 6 electrons to the secondary metal. Hence, another 18 – 6 = 12 electrons would need to be added through a combination of the valence electrons of the secondary metal and the other ligand(s) coordinating to it.

Several combinations were brainstormed in order to achieve the additional 12 electrons. First, the benzene-chromium moiety was considered, as a neutral chromium atom has 6 valence electrons from its electron configuration of [Ar] $3d^5\ 4s^1$. In addition, the benzene ring coordinated to chromium would add another 6 electrons through an η^6 coordination mode, bringing the total electron count to the desired 18 electrons. The barriers to dehydrogenation were calculated for the (η^6-benzene-Cr-^{tBu4}PCP)Ir and (η^6-benzene-Cr-^{tBu4}POCOP)Ir complexes. (Figure 4.6)

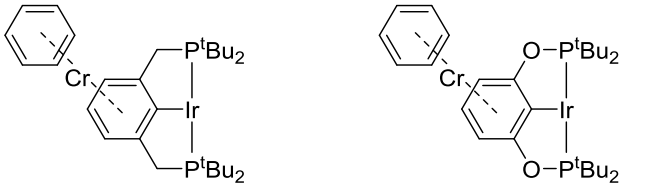

(η^6-benzene-Cr-^{tBu4}PCP)Ir **(η^6-benzene-Cr-^{tBu4}POCOP)Ir**

Figure 4.6 The two heterodinuclear complexes studied by DFT

The effects of attaching the benzene-chromium adduct to (^{tBu4}PCP)Ir were found to be quite significant. (Table 4.12) Most notably, the catalytic resting state changed from the (pincer)Ir(1-hexene) complex with (^{tBu4}PCP)Ir to the (pincer)IrH_2 complex with (η^6-benzene-Cr-^{tBu4}PCP)Ir. After recalibrating the zero-point for this difference, it is clear that although (η^6-benzene-Cr-^{tBu4}PCP)Ir would be very selective for producing 1-olefins over 2-olefins, it would also be a slower catalyst than the monometallic (^{tBu4}PCP)Ir (28.6 versus 31.8 kcal/mol).

	(^{tBu4}PCP)Ir (C2-C1)	(η^6-benzene-Cr-^{tBu4}PCP)Ir (C2-C1)	(η^6-benzene-Cr-^{tBu4}PCP)Ir (C2-C3)
[Ir](1-hexene)	0.0	5.0	5.0
[Ir] + hexane	2.4	0.3	0.3
C-H activation	28.2	31.8	32.7
[Ir](H)(hexyl)	24.6	22.5	20.7
β-H elimination	28.6	27.4	40.2
[Ir](H)(H)(hexene)	14.3	22.1	27.6
olefin dissociation	24.9	27.9	36.9
[Ir]H_2 + hexene	4.7	3.6	0.0

Table 4.12 Kinetic barriers to dehydrogenation by (η^6-benzene-Cr-^{tBu4}PCP)Ir, in kcal/mol

Examination of (η^6-benzene-Cr-^{tBu4}POCOP)Ir showed that, unlike in the (PCP)Ir case, its catalytic resting state is still the (pincer)Ir(1-hexene) complex. (Table 4.13) In contrast to the (PCP)Ir situation, attaching the benzene-chromium adduct to (^{tBu4}POCOP)Ir actually *decreased* the barrier to dehydrogenation (30.4 versus 36.3 kcal/mol). However, the barrier with (η^6-benzene-Cr-^{tBu4}POCOP)Ir is still higher than that of traditional (^{tBu4}PCP)Ir and, therefore, attempts to synthesize and test (η^6-benzene-Cr-^{tBu4}POCOP)Ir would not be warranted.

	(^{tBu4}POCOP)Ir (C2-C1)	(η^6-benzene-Cr-^{tBu4}POCOP)Ir (C2-C1)	(η^6-benzene-Cr-^{tBu4}POCOP)Ir (C2-C3)
[Ir](1-hexene)	0.0	0.0	0.0
[Ir] + hexane	19.8	7.2	7.2
C-H activation	28.8	30.4	31.4
[Ir](H)(hexyl)	24.2	22.4	20.8
β-H elimination	30.2	29.0	37.5
[Ir](H)(H)(hexene)	22.5	19.7	25.9
olefin dissociation	36.3	30.4	37.0
[Ir]H_2 + hexene	10.1	9.3	5.6

Table 4.13 Kinetic barriers to dehydrogenation by (η^6-benzene-Cr-^{tBu4}POCOP)Ir, in kcal/mol

Despite the failure to predict more active catalysts, a mechanistic analysis of these results might help determine whether it would be worthwhile to consider and screen other heterodinuclear complexes. To this end, the differences in energy between (η^6-benzene-Cr-^{tBu4}POCOP)Ir and (^{tBu4}POCOP)Ir for each species along the four dehydrogenation pathways were calculated (Table 4.14). For example, the C-H activation difference for the C2-C1 pathway was found to be 1.6 kcal/mol by subtracting the corresponding value of 28.8 kcal/mol from 30.4 and kcal/mol in Table 4.12 above. This parameter was represented by the variable $\Delta\Delta G^{\ddagger}_{catalysts}$. (Equation 3.3)

$\Delta\Delta G^{\ddagger}_{catalysts}$	C1-C2	C2-C1	C2-C3	C3-C2
[Ir](1-hexene)	0.0	0.0	0.0	0.0
C-H activation	0.5	1.6	2.0	1.9
β-H elimination	-0.1	-1.2	2.3	-3.0
olefin dissociation	-5.9	-5.9	0.4	0.4
[Ir]H_2 + hexane	-0.8	-0.8	-0.8	-0.8

Table 4.14 $\Delta\Delta G^{\ddagger}_{catalysts}$ for (η^6-benzene-Cr-^{tBu4}POCOP)Ir versus (^{tBu4}POCOP)Ir in kcal/mol. Zero point was (pincer)Ir(1-hexene) complex.

Overall, the effect of the benzene-chromium adduct on C-H activation and β-H elimination was found to be small and relatively inconsequential. In addition, the adduct only lowered the energy of the (pincer)IrH_2 complex by 0.8 kcal/mol (relative to the 1-hexene resting state), which

also proved inconsequential. However, there was a large decrease in the olefin dissociation barrier for the (pincer)Ir(H)(H)(1-hexene) species (5.9 kcal/mol) despite an *increase* in the corresponding olefin dissociation barrier for the 2-hexene analog.

To determine whether these trends were caused by random error, or whether they represented a true mechanistic effect, an identical analysis was repeated for the PCP case. To keep all comparisons valid, the (pincer)Ir(1-hexene) complex was set as the zero-point in all cases. The trends seen in C-H activation and β-H elimination in the (PCP)Ir case were very similar to those of the (POCOP)Ir case: attaching the benzene-chromium adduct made little difference to energetic barriers. Likewise, the (PCP)Ir comparison also seemed to corroborate another observation made with (POCOP)Ir: the benzene-chromium adduct stabilizes olefin dissociation with (pincer)Ir(H)(H)(1-hexene), but *destabilizes* it from (pincer)Ir(H)(H)(2-hexene).

These changes were very large, and would significantly impact experimental performance. In fact, if the DFT-calculated barriers for (η^6-benzene-Cr-^{tBu4}POCOP)Ir were taken at face-value, then the benzene-chromium adduct could transform a catalyst with low regioselectivity for producing 1-olefins ((^{tBu4}POCOP)Ir) into one with very high selectivity ((η^6-benzene-Cr-^{tBu4}POCOP)Ir)! As seen in (Table 4.15), the C2-C1 pathway (which produces 1-hexene) has a much lower overall $\Delta G^{\ddagger}$ (30.4 kcal/mol) than the pathways to 2-hexene (37.5 kcal/mol for C2-C3 and 37.0 kcal/mol for C3-C2, not shown).

$\Delta\Delta G^{\ddagger}_{catalysts}$	C1-C2	C2-C1	C2-C3	C3-C2
[Ir](1-hexene)	0.0	0.0	0.0	0.0
C-H activation	-2.3	-1.4	-0.4	-0.6
β-H elimination	1.0	-6.2	0.7	-3.5
olefin dissociation	-2.1	-2.1	4.7	4.7
[Ir]H_2 + hexene	-6.1	-6.1	-6.1	-6.1

Table 4.15 $\Delta\Delta G^{\ddagger}_{catalysts}$ for (η^6-benzene-Cr-^{tBu4}PCP)Ir versus (^{tBu4}PCP)Ir in kcal/mol. Zero point was (pincer)Ir(1-hexene) complex.

Overall, investigations into (η^6-benzene-Cr-pincer)Ir catalysts by DFT calculations showed that the benzene-chromium adduct can significantly affect the behavior of these catalysts. For the specific cases examined, the adducts did not significantly affect C-H activation or β-H elimination, but they did stabilize the dissociation of 1-hexene while destabilizing the dissociation of 2-hexene. Although it has not been determined whether sterics or electronics are the root cause of these changes, it suggests that employing these types of adducts might increase catalytic activity or selectivity under the correct circumstances.

4.5 Screening PCP-pyridinium catalysts by DFT calculations

Since the heterodinuclear catalyst study failed to produce a viable lead, it was decided that examining catalysts with more easily predictable σ- and π-donation parameters would be prudent. In fact, the previous analyses with ΔG_{HH1hex} suggested that optimizing the electronic factors would be a delicate operation – possibly too nuanced for a heterodinuclear catalyst.

It was hypothesized that slightly weaker π-donation (the objective derived from the ΔG_{HH1hex} study) could be achieved if one resonance form of the catalyst contained an empty p-orbital on the ipso-carbon of the aryl ring. Since the electronic structure of the real catalyst will be the weighted average of its "on paper" resonance forms, then a formally empty p-orbital in one resonance form will give a "real life" occupancy of less than one electron but more than zero electrons. For comparison, all (PCP)Ir catalysts would formally have an average occupancy on their ipso carbons of exactly one electron, whereas (PCOP)Ir and (POCOP)Ir catalysts would have an occupancy greater than one.

Although many structures were brainstormed which met the requirement of an empty-p resonance form, additional issues were also considered. First, the ligand would need to be synthesized, metalated onto iridium, and then converted to an active catalyst. Secondly, intermolecular decomposition would need to be avoided. One of the most active pincer iridium catalysts reported to date, (MeO_2C-^{tBu4}PCP)Ir, was found to decompose intermolecularly within only minutes at reaction conditions.[13] Presumably the ester group on the back of the aryl ring, which gave the catalyst its notably high activity, was also the cause of its decomposition.

Careful consideration of these factors lead to the (PCP-pyridinium)Ir^+ family of catalysts. By replacing the para C-H group with a nitrogen, and then bonding a third atom to the nitrogen, the one of the resonance forms created contained an empty p-orbital on the C_{ipso}! (Figure 4.7) This should, in turn, create a slightly weaker π-donating catalyst which would also have a lower ΔG_{HH1hex}, a lower $\Delta G^{\ddagger}$, and a faster experimental reaction rate. With the theoretical groundwork laid, DFT calculations were conducted to estimate whether (PCP-pyridinium)Ir^+ catalysts were more active or selective than their (PCP)Ir parents.

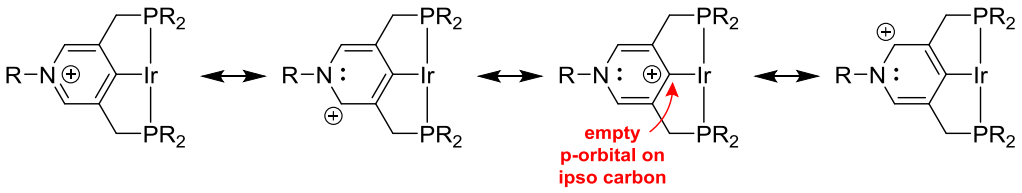

Figure 4.7 Resonance forms of (PCP-pyridinium)Ir^+ complexes

Initial DFT studies were conducted on (HN-^{tBu4}PCP)Ir^+ and (MeN-^{tBu4}PCP)Ir^+ since the proton and methyl groups would be computationally simpler than larger alkyl or aryl groups. (Figure 4.8) In addition, (H_3BN-^{tBu4}PCP)Ir was also examined to test whether a Lewis acid could have the same effect as the covalently bonded proton and methyl groups.

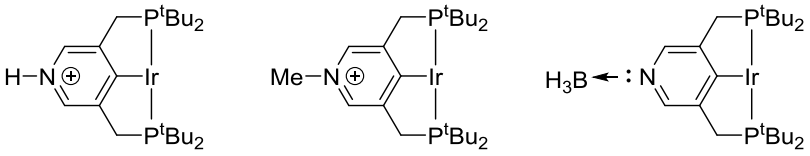

(HN-^{tBu4}PCP)Ir$^+$ **(MeN-^{tBu4}PCP)Ir$^+$** **(H$_3$BN-^{tBu4}PCP)Ir**

Figure 4.8 (PCP-pyridinium)Ir$^+$ complexes studied by DFT

These DFT calculations predicted that the cationic (PCP-pyridinium)Ir$^+$ catalysts would have *much* lower barriers to dehydrogenation than the parent catalyst (^{tBu4}PCP)Ir. (Table 4.16) Quantitatively, the barriers for the C1-C2 pathway were found to be 6.1 and 6.5 kcal/mol lower for the methylated and protonated catalysts, respectively. Using the Eyring equation and a reaction temperature of 125 °C, which is the most common temperature for alkane metathesis,[1] the Eyring equation predicts that the cationic (PCP-pyridinium)Ir catalysts would be ca. 2,000- to 4,000-fold more active than (^{tBu4}PCP)Ir!

A related catalyst, (H$_3$BN-^{tBu4}PCP)Ir, was also examined by DFT and was found to also have a lower barrier to dehydrogenation than (^{tBu4}PCP)Ir (1.9 kcal/mol for the C1-C2 pathway). This demonstrates that the Lewis acid catalyst might also be more effective than (^{tBu4}PCP)Ir.

	(^{tBu4}PCP)Ir (C1-C2)	(H$_3$BN-^{tBu4}PCP)Ir (C1-C2)	(HN-^{tBu4}PCP)Ir$^+$ (C1-C2)	(MeN-^{tBu4}PCP)Ir$^+$ (C1-C2)
[Ir](1-hexene)	0.0	0.0	0.0	0.0
[Ir] + hexane	2.4	0.4	-2.6	-2.0
C-H activation	23.1	23.3	21.0	21.7
[Ir](H)(hexyl)	20.6	17.7	17.5	17.4
β-H elimination	29.3	27.4	22.8	23.2
[Ir](H)(H)(hexene)	14.3	15.5	15.9	15.7
olefin dissociation	24.9	23.4	19.2	19.9
[Ir]H$_2$ + hexene	4.7	7.1	8.5	8.8

Table 4.16 Kinetic barriers to dehydrogenation for (PCP-pyridinium)Ir$^+$ catalysts, in kcal/mol

To verify these trends, DFT calculations on the PCOP and POCOP catalysts with nitrogen in the para position were also conducted. (Tables 4.17 and 4.18) (Figure 4.9)

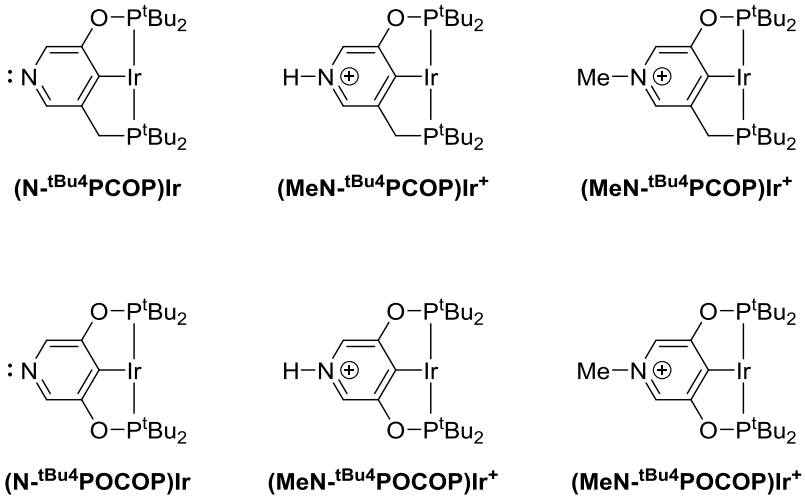

Figure 4.9 (PCOP-pyridinium)Ir^+ and (POCOP-pyridinium)Ir^+ complexes studied by DFT

First, (^{tBu4}PCOP)Ir can be compared with the neutral complex (N-^{tBu4}PCOP)Ir where the para C-H bond is replaced with a nitrogen, but where the complex is still neutral because no third atom is bonded to the nitrogen. The cationic protonated and methylated PCOP complexes were also examined. Overall, the substitution of the para C-H group for a nitrogen caused noticeable changes in the energy of each species, but the "cationization" with a proton or methyl group caused more massive changes. For example, the energy of olefin dissociation decreased from 31.2 to 29.9 kcal/mol between (^{tBu4}PCOP)Ir and (N-^{tBu4}PCOP)Ir, a difference of 1.3 kcal/mol. However, "cationization" with a proton or methyl group caused the olefin dissociation energy to decrease an additional 3.0 to 3.3 kcal/mol.

	(^{tBu4}PCOP)Ir (C1-C2)	(N-^{tBu4}PCOP)Ir (C1-C2)	(HN-^{tBu4}PCOP)Ir^+ (C1-C2)	(MeN-^{tBu4}PCOP)Ir^+ (C1-C2)
[Ir](1-hexene)	0.0	0.0	0.0	0.0
[Ir] + hexane	6.3	5.2	3.6	3.7
C-H activation	23.5	22.6	22.4	22.0
[Ir](H)(hexyl)	20.9	19.6	20.5	20.6
β-H elimination	31.5	26.7	23.9	22.9
[Ir](H)(H)(hexene)	17.8	15.8	17.4	17.0
olefin dissociation	31.2	29.9	26.3	26.9
[Ir]H_2 + hexene	6.6	7.8	13.0	12.5

Table 4.17 Kinetic barriers to dehydrogenation for (PCOP-pyridinium)Ir^+ catalysts in kcal/mol

Thus, these results with PCOP catalysts show that both the substitution of the para C-H group for a nitrogen, as well as "cationization" of the resulting nitrogen, significantly reduced the kinetic barrier to dehydrogenation. Performing the analogous analysis with POCOP catalysts revealed while the C-H for N substitution had negligible (or even detrimental) effects on the kinetic barrier, cationization with a proton or methyl group once again lead to large decreases in the barriers of all transition states. (Table 4.18)

	(^{tBu4}POCOP)Ir C1-C2	(N-^{tBu4}POCOP)Ir C1-C2	(HN-^{tBu4}POCOP)Ir$^+$ C1-C2	(MeN-^{tBu4}POCOP)Ir$^+$ C1-C2
[Ir](1-hexene)	0.0	0.0	0.0	0.0
[Ir] + hexane	13.3	11.8	9.6	9.2
C-H activation	25.0	25.3	24.5	23.8
[Ir](H)(hexyl)	22.1	22.0	21.2	21.2
β-H elimination	34.6	30.1	25.6	25.3
[Ir](H)(H)(hexene)	22.5	20.5	20.4	20.4
olefin dissociation	36.3	38.4	31.0	30.4
[Ir]H_2 + hexene	10.1	11.8	17.4	17.3

Table 4.18 Kinetic barriers to dehydrogenation for (POCOP-pyridinium)Ir$^+$ catalysts in kcal/mol.

Thus, from the perspective of designing more active catalysts, any synthetic attempts should focus on the cationic versions of each catalyst. In addition, the DFT results could also be used to predict the regioselectivity of each catalyst. Since the rate-determining step of each of the newly-examined (PCOP)Ir and (POCOP)Ir catalyst was still olefin dissociation, they would likely have low regioselectivity for producing 1-olefins. In contrast, the rate-determining step for (PCP-pyridinium)Ir$^+$ catalysts was found to be β-H elimination, suggesting high regioselectivity. In addition, the actual kinetic barrier for the (PCP-pyridinium)Ir$^+$ catalysts (~ 23 kcal/mol) was found to be much lower than those of the (PCOP-pyridinium)Ir$^+$ (~26 kcal/mol) or (POCOP-pyridinium)Ir$^+$ (~31 kcal/mol) catalysts.

4.6 **Summary**

Therefore, the final conclusion of these DFT investigations is that the (HN-^{tBu4}PCP)Ir^{+} and (MeN-^{tBu4}PCP)Ir^{+} catalysts would be the most promising targets if more active and selective dehydrogenation catalysts were to be synthesized. Since both catalysts showed nearly identical energies for each species within the random error of DFT calculations, then the identity of the third group bonded to nitrogen may not significantly affect activity or selectivity. Therefore, other functional groups could be bonded to the nitrogen for the purpose of increasing solubility or attaching the catalyst to a heterogeneous support.

4.7 Experimental

All electronic structure calculations employed the DFT method[17] and the PBE[18] exchange-correlation functional. A relativistic, small-core ECP and corresponding basis set were used for the Ir atom (LANL2TZ model);[19,20] all-electron 6-311G(d) basis sets were applied to all P, N, C and B atoms; 311G basis sets were applied to all H atoms and, in addition, a set of diffuse p-type functions (exponent = 0.75) were placed on all hexane H atoms involved in C-H activation.[21-23] Reactant, transition state and product geometries were fully optimized, and the stationary points were characterized further by normal mode analysis. Expanded integration grid sizes (pruned (99,590) atomic grids invoked using the integral=ultrafine keyword) were applied to increase numerical accuracy and stability in both geometry optimizations and normal mode analyses.[24] The (unscaled) vibrational frequencies formed the basis for the calculation of vibrational zero-point energy (ZPE) corrections; standard thermodynamic corrections (based on the harmonic oscillator/rigid rotor approximations and ideal gas behavior) were made to convert from purely electronic (reaction or activation) energies to (standard) enthalpies (H) and Gibbs free energies (G; P = 1 atm).[25] H, entropy (S), and G were evaluated at two temperatures, T = 25 °C (= 298 K)

and T = 125 °C (= 398 K). All energy values quoted in the principal text refer to T = 25 °C. In Supporting Information, we tabulate enthalpies, entropies, and free energies at T = 298 K (P = 1 atm) as well as free energies at T = 398 K (P = 1 atm). The latter T (125 °C, 398 K) approximates the temperature used in the experimental work. All calculations were executed using the GAUSSIAN 09 series of computer programs.[26]

4.8 **References**

(1) Goldman, A. S.; Roy, A. H.; Huang, Z.; Ahuja, R.; Schinski, W.; Brookhart, M. *Science* **2006**, *312*, 257.

(2) Ahuja, R.; Punji, B.; Findlater, M.; Supplee, C.; Schinski, W.; Brookhart, M.; Goldman, A. S. *Nature Chem.* **2011**, *3*, 167.

(3) Steffens, A. M., Rutgers, The State University of New Jersey, 2015.

(4) Kumar, A.; Zhou, T.; Emge, T. J.; Mironov, O.; Saxon, R.; Krogh-Jespersen, K.; Goldman, A. S. *J. Am. Chem. Soc.* **2015**, *137*, 9894.

(5) Nawara-Hultzsch, A. J.; Hackenberg, J. D.; Punji, B.; Supplee, C.; Emge, T. J.; Bailey, B. C.; Schrock, R. R.; Brookhart, M.; Goldman, A. S. *ACS Catal.* **2013**, *3*, 2505.

(6) Kundu, S.; Choliy, Y.; Zhuo, G.; Ahuja, R.; Emge, T. J.; Warmuth, R.; Brookhart, M.; Krogh-Jespersen, K.; Goldman, A. S. *Organometallics* **2009**, *28*, 5432.

(7) Krogh-Jespersen, K.; Czerw, M.; Summa, N.; Renkema, K. B.; Achord, P. D.; Goldman, A. S. *J. Am. Chem. Soc.* **2002**, *124*, 11404.

(8) Renkema, K. B.; Kissin, Y. V.; Goldman, A. S. *J. Am. Chem. Soc.* **2003**, *125*, 7770.

(9) Göttker-Schnetmann, I.; White, P.; Brookhart, M. *J. Am. Chem. Soc.* **2004**, *126*, 1804

(10) Gupta, M.; Hagen, C.; Flesher, R. J.; Kaska, W. C.; Jensen, C. M. *Chem. Commun.* **1996**, 2083.

(11) Espinosa-Jalapa, N. A.; Hernandez-Ortega, S.; Le Goff, X.; Morales-Morales, D.; Djukic, J.; Lagadec, R. L. *organometallics* **2013**, *32*, 2661.

(12) Kuklin, S. A.; Sheloumov, A. M.; Dolgushin, F. M.; Ezernitskaya, M. G.; Peregudov, A. S.; Petrovskii, P. V.; Koridze, A. A. *Organometallics* **2006**, *25*, 5466.

(13) Huang, Z.; Brookhart, M.; Goldman, A. S.; Kundu, S.; Ray, A.; Scott, S. L.; Vicente, B. C. *Adv. Synth. Catal.* **2009**, *351*, 188.

(14) Zhu, K.; Achord, P. D.; Zhang, X.; Krogh-Jespersen, K.; Goldman, A. S. *J. Am. Chem. Soc.* **2004**, *126*, 13044.

(15) Haibach, M. C.; Wang, D. Y.; Emge, T. J.; Krogh-Jespersen, K.; Goldman, A. S. *Chem. Sci.* **2013**, *4*, 3683.

(16) Biswas, S. *Doctoral Thesis, Rutgers, The State University of New Jersey* **2010**.

(17) Koch, W.; Holthausen, M. C. *A Chemist's Guide to Density Functional Theory*; Wiley: New York, 2001.

(18) Perdew, J. P.; Burke, K.; Ernzerhof, M. *Phys Rev. Lett.* **1996**, *77*, 3865.

(19) Hay, P. J.; Wadt, W. R. *J. Chem. Phys.* **1985**, *82*, 299.

(20) Roy, L. E.; Hay, P. J.; Martin, R. L. *J. Chem. Theory Comput.* **2008**, *4*.

(21) Ditchfield, R.; Hehre, W. J.; Pople, J. A. *J. Chem. Phys.* **1971**, *54*, 724.

(22) Hariharan, P. C.; Pople, J. A. *Mol. Phys.* **1974**, *27*, 209.

(23) McLean, A. D.; Chandler, G. S. *J. Chem. Phys.* **1980**, *72*, 5639.

(24) Frisch, Æ.; Frisch, M. J.; Clemente, F. R.; G. W. Trucks *Gaussian 09 User's Reference*, 147.

(25) McQuarrie, D. A. *Statistical Thermodynamics*; Harper and Row: New York, 1973.

(26) Frisch, M. J.; Trucks, G. W.; Schlegel, H. B.; Scuseria, G. E.; Robb, M. A.; Cheeseman, J. R.; Scalmani, G.; Barone, V.; Mennucci, B.; Petersson, G. A.; Nakatsuji, H.; Caricato, M.; Li, X.; Hratchian, H. P.; Izmaylov, A. F.; Bloino, J.; Zheng, G.; Sonnenberg, J. L.; Hada, M.; Ehara, M.; Toyota, K.; Fukuda, R.; Hasegawa, J.; Ishida, M.; Nakajima, T.; Honda, Y.; Kitao, O.; Nakai, H.; Vreven, T.; Montgomery, J. J. A.; Peralta, J. E. O., F.; Bearpark, M.; Heyd, J. J.; Brothers, E.; Kudin, K. N.; Staroverov, V. N.; Kobayashi, R.; Normand, J.; Raghavachari, K.; Rendell, A.;

Burant, J. C.; Iyengar, S. S.; Tomasi, J.; Cossi, M.; Rega, N.; Millam, N. J.; Klene, M.; Knox, J. E.; Cross, J. B.; Bakken, V.; Adamo, C.; Jaramillo, J.; Gomperts, R.; Stratmann, R. E.; Yazyev, O.; Austin, A. J.; Cammi, R.; Pomelli, C.; Ochterski, J. W.; Martin, R. L.; Morokuma, K.; Zakrzewski, V. G.; Voth, G. A.; Salvador, P.; Dannenberg, J. J.; Dapprich, S.; Daniels, A. D.; Farkas, Ö.; Foresman, J. B.; Ortiz, J. V.; Cioslowski, J.; Fox, D. J., Gaussian 09.

Chapter 5

Attempting to improve the activity of alkane metathesis through process chemistry

Abstract

In addition designing better catalysts, the rate of a reaction can also be increased by optimizing the reaction conditions. Therefore, the reaction conditions of alkane metathesis were varied in an attempt to increase its activity. Namely, it was found that the optimal concentration of the TBE hydrogen acceptor was approximately 200 mM when using (^{tBu4}PCP)Ir as the catalyst, providing about double the concentration of products than obtained with the traditional TBE concentration of 10 mM. Similarly, alkane metathesis reactions with *two* pincer iridium catalysts, but the same total catalyst concentration as with one pincer iridium catalyst, were performed in an attempt to balance the dehydrogenation and hydrogenation halves of the transfer dehydrogenation cycle. Interestingly, these two-catalyst studies showed a non-linear relationship between the concentration of each catalyst and the quantity of products generated. This suggests a complex balance between dehydrogenation and hydrogenation during alkane metathesis. Unfortunately, however, no combination of two catalysts was found which gave more activity than using a full concentration of the more active catalyst by itself.

5.1 Introduction

In addition to designing more active and selectivity catalysts, modifying the reaction conditions during catalysis can also affect the performance of the catalyst. Notably, alkane metathesis can produce many valuable products such as diesel fuel[1-5] and *n*-alkyl arenes,[6] and therefore improvement of its reaction conditions might lead to increases in activity or selectivity. Since the initial report of alkane metathesis, no systematic study of reaction conditions had been conducted.

Notably, however, studies had been performed regarding the optimal conditions for transfer dehydrogenation, one half of the alkane metathesis cycle. Olefin metathesis, the other half of alkane metathesis, would not affect either the overall activity of alkane metathesis because the olefin metathesis catalysts are orders of magnitude faster than the transfer dehydrogenation ones.[7,8] Specifically, it was also found that the rate of transfer dehydrogenation varied considerably with the concentration of hydrogen acceptor.[9] In particular, the rate of transfer dehydrogenation with variable concentrations of TBE (20 to 750 mM) in neat cyclooctane was measured. (Scheme 5.1) (Figure 5.1) At low concentrations of TBE (< 300 mM), increasing [TBE] led to higher rates of transfer dehydrogenation (as measured by changes in [cyclooctene] over time). In contrast, if [TBE] was greater than 500 mM then further increasing [TBE] actually led to a slight decline in the rate of transfer dehydrogenation.

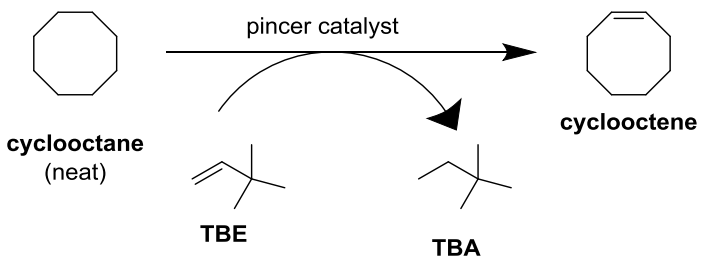

Scheme 5.1 COA/TBE transfer dehydrogenation by a pincer catalyst

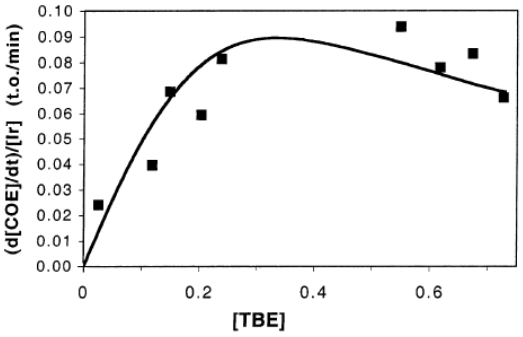

Figure 5.1 Catalytic activity of (^{tBu4}PCP)Ir during COA/TBE transfer dehydrogenation as a function of [TBE]

The authors hypothesized that the rate of the full transfer dehydrogenation cycle was limited either by the dehydrogenation half-cycle or by the hydrogenation half-cycle. (Figure 5.2) Notably, the parameter [total olefin] = [COE] + [TBE] was believed to be important.

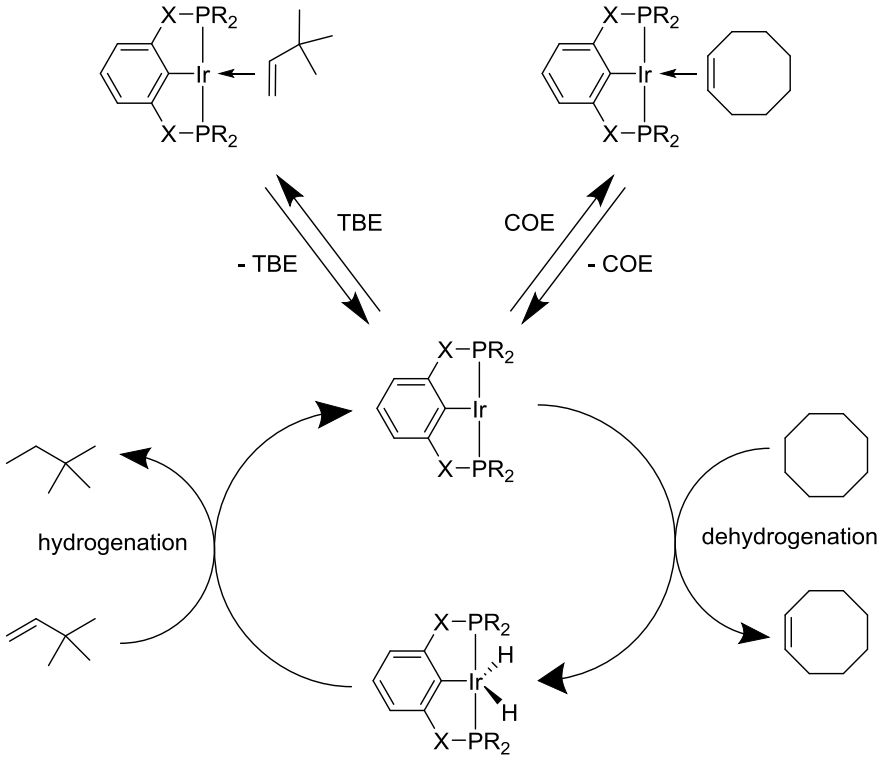

Figure 5.2 Catalytic cycle during COA/TBE transfer dehydrogenation

In experiments with low [total olefin], the authors postulated that olefin hydrogenation was the rate-limiting half of the cycle. After dehydrogenating an alkane into an olefin, the resulting (pincer)IrH_2 complex would need hydrogenate another olefin in order to continue with the cycle. Hence, the hydrogenation half-cycle would likely be first-order in olefin. With low [total olefin] then the hydrogenation half-cycle would be relatively slow.

In contrast, at high [total olefin] the overall transfer dehydrogenation was rate-limited by alkane dehydrogenation. In essence, the dehydrogenation half-cycle would be first-order in alkane. More importantly, however, is that dehydrogenation would be *inverse order* in olefin due to binding of an olefin to the 14 electron species, removing it from the catalytic cycle. Hence, high [total olefin] would reduce the concentration of the 14 electron species, slowing the overall cycle.

Hence, this study showed that in a COA/TBE transfer dehydrogenation with (^{tBu4}PCP)Ir, and most likely any transfer dehydrogenation with any catalyst, there existed an optimal [total olefin] value where the reaction rate was at its maximum.

Notably, the alkane metathesis reaction is a tandem reaction involving both transfer dehydrogenation and olefin metathesis. Importantly, the rate of alkane metathesis only depends upon the catalytic activity of the transfer dehydrogenation catalyst and *not* on the speed of the olefin metathesis catalyst. This is because the olefin metathesis catalysts used are orders of magnitude faster than the transfer dehydrogenation catalysts.[7,8] Hence, determining the optimal [total olefin] during alkane metathesis might significantly increase the rate of that reaction.

In addition, employing two different transfer dehydrogenation catalysts might also increase catalytic activity during alkane metathesis. (Figure 5.4, further below) Hypothetically, one catalyst could perform the dehydrogenation half-cycle while the other accomplished the

hydrogenation half-cycle. Obviously, a method of shuttling hydrogens between them would also be required.

Although no mechanism for moving the hydrogens was known to exist (besides extremely slow acceptorless dehydrogenation), previous experimental results raised the possibility that a new pathway could be designed. Notably, whereas (^{tBu4}PCOP)Ir is nearly 4 times as active as (^{tBu4}PCP)Ir during alkane metathesis, it is about 10 times *slower* during 1-hexene/*n*-octane transfer dehydrogenations.[10] (Figure 4.1) Therefore, some undiscovered mechanistic detail must be able to account for this seemingly counterintuitive behavior. And, that mechanism might allow for faster alkane metathesis reactions through dual-catalyst transfer dehydrogenation.

5.2 Optimization of total olefin concentration during alkane metathesis

The attempt to optimize [total olefin] was done in a single day, with the same batch of stock solutions, in order to minimize random errors. (Scheme 5.2) Alkane metathesis is known to be a very sensitive reaction where trace impurities can easily poison the Schrock-type olefin metathesis catalysts.

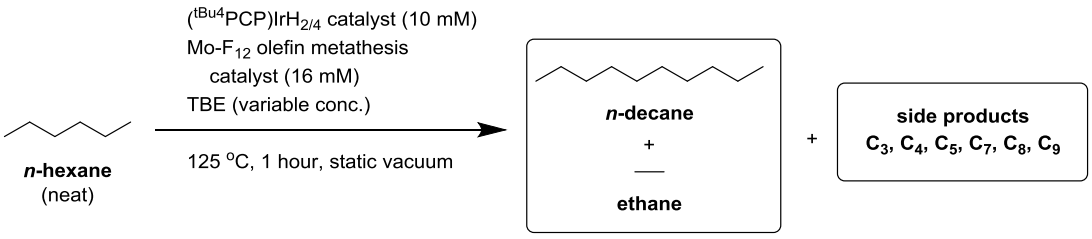

Scheme 5.2 Experimental conditions for optimizing [total olefin] during alkane metathesis

Since initiation of the catalytic cycle would require the removal of the hydrides on the pincer iridium catalyst, the concentration of TBE added was scaled appropriately. For example,

since the (^{tBu4}PCP)Ir was found to be a roughly 50:50 mixture of dihydride and tetrahydride complexes, then approximately 15 mM of TBE would be required to remove those hydrides from the pincer iridium species. Therefore, 35 mM of TBE was added to the sample targeting 20 mM of [total olefin].

Due to the volatility of the light products (lighter than the hexane starting material), conversion and selectivity were assessed by looking at the heavier products of *n*-heptane through *n*-decane. (Figure 5.3) This showed that the greatest conversion after one hour occurred in the sample with [total olefin] = 250 mM. Thus, the optimal [total olefin] would be somewhere between approximately 100 mM and 400 mM, based on the curvature of the data points.

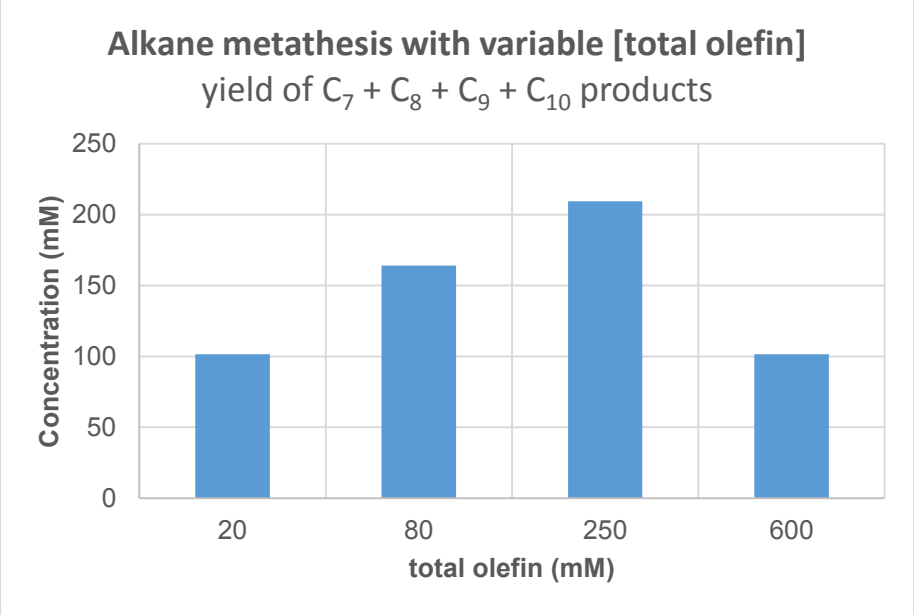

Figure 5.3 Yields of C_7 through C_{10} with variable total olefin concentrations

Notably, conversion in the two samples with 250 and 600 mM of total olefins was less than the amount of TBE added, proving that some TBE was still present and had not been hydrogenated to TBA. Unfortunately, experimental issues prevented this problem from being rectified. If the samples were heated longer, then the known thermal decomposition of the olefin

metathesis catalyst would complicate kinetic analysis. Likewise, if the added olefin was a linear olefin like 1-hexene instead of TBE, then the extremely active (even at 20 °C) olefin metathesis catalyst would have caused the 1-hexene to immediately metathesize upon mixing.[7] This would have caused have the steady-state olefin concentration to be lost to the glovebox atmosphere as ethylene. If an internal olefin like *trans*-5-decene had been used instead, then that very large concentration of C_{10} would have obscured the *n*-decane produced by alkane metathesis of the *n*-hexane starting material.

5.3 Explaining counterintuitive observations regarding the catalytic activity of (PCP)Ir and (PCOP)Ir catalysts

As described in Section 5.1, (PCP)Ir catalysts are more active than (PCOP)Ir catalysts for 1-hexene/*n*-octane transfer dehydrogenation reactions, but they are also *less* active for alkane metathesis reactions. Based upon the DFT calculations described in Chapter 3, this is actually unsurprising. (Schemes 5.3 and 5.4) (Table 5.1)

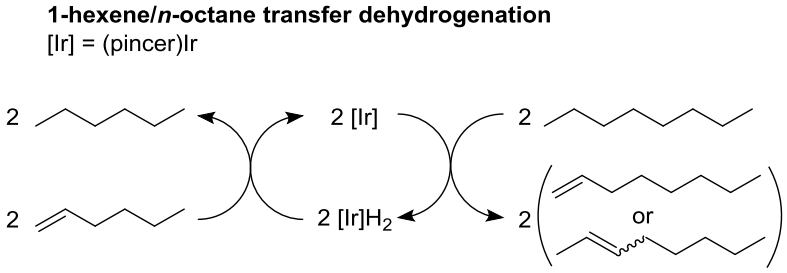

Scheme 5.3 1-hexene/*n*-octane transfer dehydrogenation cycle

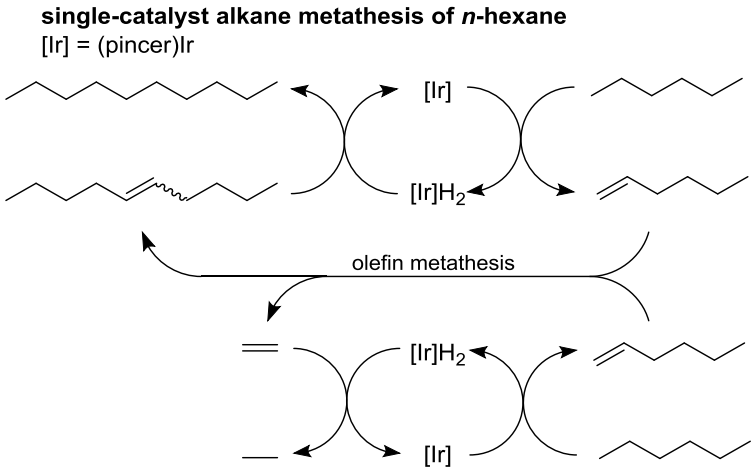

Scheme 5.4 Single-catalyst transfer dehydrogenation cycle during alkane metathesis of *n*-hexane

Catalyst	Terminal 1-olefin	Internal 2-olefin
(PCP)Ir	29	34
(PCOP)Ir	31	31
(POCOP)Ir	35	35

Table 5.1 Kinetic barriers to dehydrogenation, by ligand framework, in kcal/mol

In both 1-hexene/*n*-octane and alkane metathesis, dehydrogenation can happen at either the terminal position or the internal position. Accordingly, the barriers to dehydrogenation will be ~29 kcal/mol for (PCP)Ir catalysts, and ~31 kcal/mol (either terminal or internal) for (PCOP)Ir catalysts. (Table 5.2)

Catalyst	Terminal 1-olefin	Internal 2-olefin	1-Olefin/*n*-alkane: overall barrier	Alkane metathesis overall barrier
(PCP)Ir	29	34	29	34
(PCOP)Ir	31	31	31	31
(POCOP)Ir	35	35	35	35

Table 5.2 Kinetic barriers for different reaction types, by ligand framework, in kcal/mol

During the hydrogenation half-cycle of 1-hexene/*n*-octane, the catalysts will hydrogenate the abundant 1-hexene with a barrier of 29 kcal/mol for (PCP)Ir catalysts and 31 kcal/mol for (PCOP)Ir catalysts. Hence, (PCP)Ir catalysts have lower barriers (~29 kcal/mol) than (PCOP)Ir catalysts (~31 kcal/mol) during 1-hexene/*n*-octane.

However, alkane metathesis puts more restrictions on the catalysts during the hydrogenation half-cycle. Namely, the catalysts must hydrogenation both ethylene *and trans*-5-decene (assuming selective metathesis of *n*-hexane). Hence, the catalysts must also perform *internal* hydrogenations, which are notably easier for (PCOP)Ir catalysts (~31 kcal/mol) than for (PCP)Ir catalysts (~34 kcal/mol). Hence, DFT calculations actually predict that (PCOP)Ir catalysts should be more active for alkane metathesis.

5.4 Alkane metathesis using two transfer dehydrogenation catalysts

Hence, it was hypothesized that a more active alkane metathesis reaction could be achieved by employing both (PCP)Ir and (PCOP)Ir catalysts. (Figure 5.4) In particular, the (PCP)Ir catalyst would perform the dehydrogenation of *n*-hexane, which it could accomplish faster than (PCOP)Ir catalysts. In addition, the (PCOP)Ir catalyst would hydrogenate *trans*-5-decene, or other internal olefins, since it was more active for that transformation than (PCP)Ir catalysts. Lastly, a hydrogen shuttle that both catalysts could readily dehydrogenation/hydrogenate, such as ethylene, would complete the cycle.

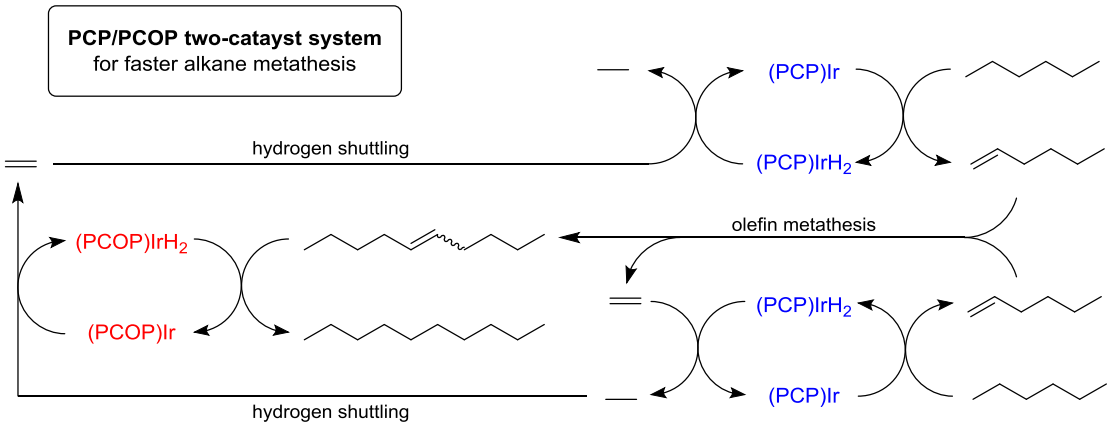

Figure 5.4 Proposed cooperation of two transfer dehydrogenation catalysts during alkane metathesis

The standard conditions used in previous alkane metathesis reactions were also employed in the current study,[1] with the exception of the pincer iridium catalyst. Namely, the total concentration of pincer iridium catalysts was set to be 10 mM for all reactions. However, the combination of (^{tBu2}PCOP^{iPr2})Ir(C_2H_4) and (^{tBu4}PCP)Ir$H_{2/4}$ used to obtained that 10 mM was varied between samples. (Scheme 5.5) Notably, all of the samples in a given experiment were made on the same day from the same batch of stock solutions.

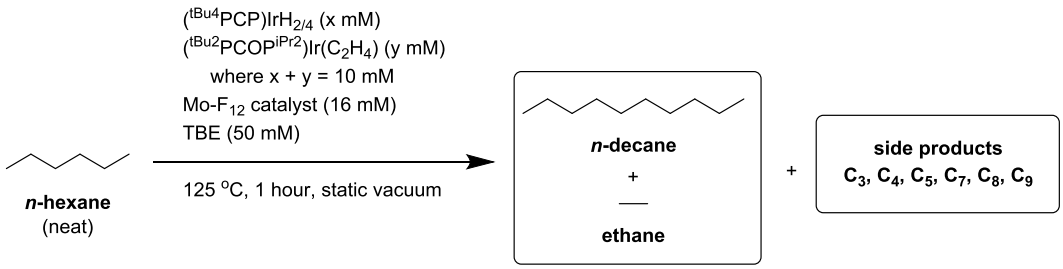

Scheme 5.5 Experimental conditions used for studying alkane metathesis with two transfer dehydrogenation catalysts

The first experiment was conducted with five samples. The one-catalyst sample with 10 mM of (^{tBu2}PCOP^{iPr2})Ir and 0 mM of (^{tBu4}PCP)Ir gave 401 mM of products in the C_8 to C_{10} range, in good agreement with previous studies.[5] (Figure 5.5) Likewise, the one-catalyst sample with no (^{tBu2}PCOP^{iPr2})Ir but 10 mM (^{tBu4}PCP)Ir produced approximately 27 mM of products in the in the C_8 to C_{10} range, also in good agreement with previous results.[5]

Interestingly, the dual-catalyst reactions showed conversions that were greater than the amount predicted by simply performing a weighted average of the one-catalyst reactions. For example, the sample with 5 mM of both (^{tBu2}PCOP^{iPr2})Ir and (^{tBu4}PCP)Ir would theoretically give 214 mM of products (halfway between 27 and 401 mM). However, it actually produced 505 mM of products, slightly greater than the 10 mM (^{tBu2}PCOP^{iPr2})Ir reaction.

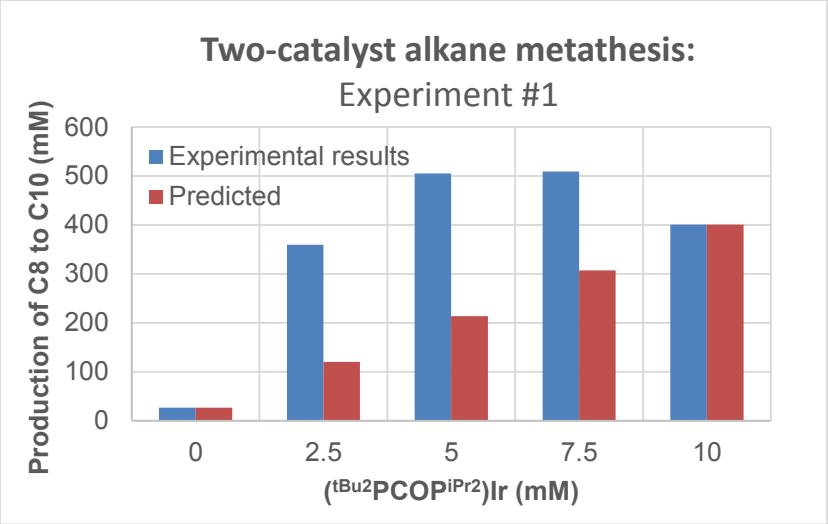

Figure 5.5 First study of cooperativity between two transfer dehydrogenation catalysts during alkane metathesis

To verify these results, a second dual-catalyst alkane metathesis reaction was performed. (Figure 5.6) Interestingly, the conversions observed for the dual-catalyst samples were significantly higher than what would be predicted by simply averaging the concentrations of both catalysts.

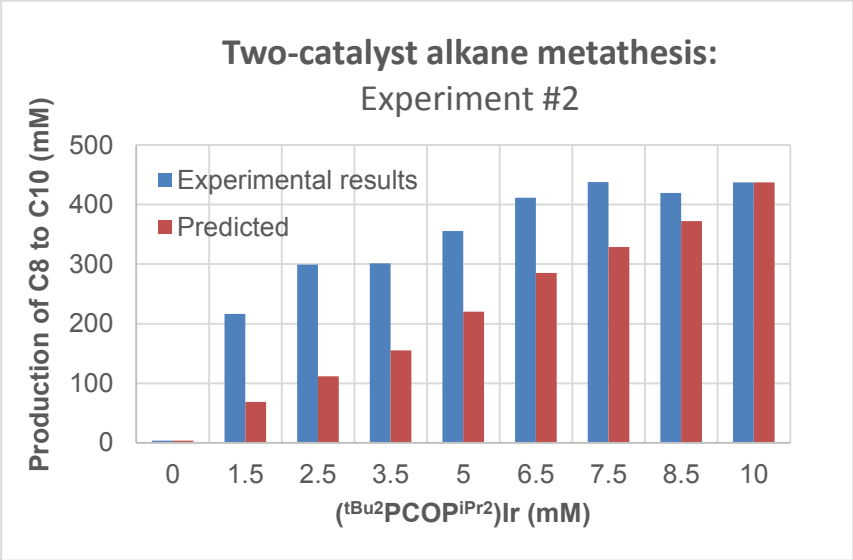

Figure 5.6 Second study of cooperativity between two transfer dehydrogenation catalysts during alkane metathesis

Despite these intriguing results, no dual-catalyst system was found which reliably gave more conversion than (^{tBu2}PCOP^{iPr2})Ir by itself. Presumably, the non-linear relationship between conversion and the concentration of each catalyst might have been caused by some degree of hydrogen shuttling or cooperation between the two pincer iridium catalysts. However, this cooperativity, if present, was not sufficient to significantly increase catalytic activity. Possibly, the dehydrogenation/hydrogenation of the hydrogen shuttles available in these reactions was too difficult to allow for efficient cooperation between the two catalysts.

5.5 Summary

Alkane metathesis reactions with different concentrations of added *tert*-butyl ethylene, and therefore different total olefin concentrations, showed dissimilar levels of catalytic activity. In particular, catalytic activity appeared to increase from 10 mM to 200 mM, but then decreased at 600 mM. Therefore, optimizing the total olefin concentration during alkane metathesis allows for modest increases in catalytic activity.

In addition, alkane metathesis reactions with two transfer dehydrogenation catalysts operating in tandem were investigated. Specifically, it appeared that some type of cooperation existed between (^{tBu4}PCP)Ir and (^{tBu2}PCOP^{iPr2})Ir during alkane metathesis. However, the increases in catalytic activity were relatively small. In the future, adding a dedicated hydrogen shuttle to the dual-catalyst reactions might allow for stronger cooperativity and higher catalytic activity. In particular, an optimal hydrogen shuttle would have high solubility even at reaction temperatures, and low kinetic barriers to dehydrogenation and hydrogenation.

5.6 Experimental

All manipulations were performed either in a glovebox or on a Schlenk line under an inert atmosphere of dry argon. All reagents and solvents were obtained from Aldrich. For catalytic experiments, all solvents and liquid reagents were degassed by three freeze-pump-thaw cycles, dried by stirring over activated alumina for 12 h, and finally distilled under vacuum using Schlenk techniques. (^{tBu4}PCP)Ir$H_{2/4}$[8] and (^{tBu2}PCOP^{iPr2})Ir[11] were synthesized according to literature methods. NMR spectra were recorded on either a Bruker DRX-400, Bruker Avance-400, or Bruker DRX-500 spectrometer at 298 K.

Gas chromatography: Gas chromatography was performed with a Varian 430 gas chromatograph that was equipped with a Supelco column (100 m x 0.25 mm) using the following parameters:

- Starting temperature: 40 ^{o}C
- Time at starting temperature: 1.4 min
- Ramp: 20 ^{o}C/min to 260 ^{o}C, hold for 50 min
- Flow rate: 1.4 mL/min of N_2
- Split ratio: 25
- Injector temperature: 250 ^{o}C
- Detector temperature: 260 ^{o}C
- Detector: flame ionization

Response factors: GC response factors for some of alkanes (*n*-pentane, *n*-hexane, *n*-octane, and *n*-decane) were obtained experimentally by injecting known concentrations of the *n*-alkane, along with mesitylene, into the GC. Each response factor was calculated as the average of three independent runs. The response factors for the other *n*-alkanes were extrapolated based on the

relationship between carbon number and response factor for the *n*-alkanes which were examined experimentally.

Alkane metathesis with variable TBE concentrations: A 4-mL vial was charged with 5.8 mg of (^{tBu4}PCP)Ir$H_{2/4}$ (10 mM), 12.3 mg of Schrock's Mo-F_{12} catalyst (16 mM, CAS 139220-25-0, Mo($C_{10}H_{12}$)($C_{12}H_{17}N$)[OC(CH_3)(CF_3)$_2$]$_2$), 1.0 mL of *n*-hexane, 14 µL of mesitylene (72 mM, as internal standard), and the appropriate amount of *tert*-butyl ethylene (TBE). Since the (^{tBu4}PCP)Ir solid was an approximately 50:50 mixture of the dihydride and tetrahydride complexes (by ^{31}P NMR), 15 mM of TBE (1.9 µL) would be required to remove all the hydrides from the (^{tBu4}PCP)Ir$H_{2/4}$ complex. Thus, for a desired total olefin concentration of 20 mM, then 1.9 µL + 2.6 µL = 4.5 µL of TBE was added to the reaction mixture. Similarly, for desired total olefin concentrations of 80, 200, and 600 mM the volume of TBE added was 12, 28, and 78 µL respectively. Ten aliquots of this stock solution (0.10 mL each) were syringed into glass tubes (5 mm x 140 mm) that had been flame-dried prior to being brought into the glovebox. Vacuum adapters were fitted onto the tubes, and the assemblies were removed from the glovebox. The tubes were then frozen in liquid nitrogen, the headspace was evacuated, and the tubes were flame-sealed to give a headspace:liquid ratio of approximately 1:1. The tubes were immersed into a temperature-calibrated oil bath at the specified temperature. The tubes were then removed at the stated time intervals and cooled with liquid nitrogen. The seal of each tube was carefully broken and capped with a 5 mm septum. Each sample was allowed to return to room temperature and analyzed by GC.

Alkane metathesis with two transfer dehydrogenation catalysts: A stock solution of (^{tBu4}PCP)Ir$H_{2/4}$ (5.8 mg, 10 mM), TBE (4.5 µL, 35 mM), 14 µL of mesitylene (72 mM as internal standard) in 1.0 mL of *n*-hexane was created. Next, a stock solution of (^{tBu2}PCOP^{iPr2})Ir(C_2H_4) (5.8 mg, 10 mM), TBE (1.3 µL, 10 mM), and 14 µL of mesitylene (72 mM as internal standard) in 1.0 mL

of *n*-hexane was also made. Given the presence of either hydrides or ethylene ligands, both stock solutions had total olefin concentrations of 20 mM. Reaction mixtures with the desired (^{tBu4}PCP)Ir/(^{tBu2}PCOP^{iPr2})Ir ratios and volumes of 0.1 mL each were made by combining the appropriate volumes of the two stock solutions. 2.3 mg of Schrock's Mo-F_{12} catalyst (16 mM, CAS 139220-25-0, $Mo(C_{10}H_{12})(C_{12}H_{17}N)[OC(CH_3)(CF_3)_2]_2$) was also added to each reaction mixture. The solutions were then syringed into glass tubes, sealed, heated, and analyzed by GC in the same manner as described during alkane metathesis with variable TBE concentrations.

5.7 References

(1) Goldman, A. S.; Roy, A. H.; Huang, Z.; Ahuja, R.; Schinski, W.; Brookhart, M. *Science* **2006**, *312*, 257.

(2) Bailey, B. C.; Schrock, R. R.; Kundu, S.; Goldman, A. S.; Huang, Z.; Brookhart, M. *Organometallics* **2009**, *28*, 355.

(3) Huang, Z.; Rolfe, E.; Carson, E. C.; Brookhart, M.; Goldman, A. S.; El-Khalafy, S. H.; MacArthur, A. H. R. *Adv. Synth. Catal.* **2010**, *352*, 125.

(4) Haibach, M. C.; Kundu, S.; Brookhart, M.; Goldman, A. S. *Acc. Chem. Res.* **2012**, *45*, 947.

(5) Nawara-Hultzsch, A. J.; Hackenberg, J. D.; Punji, B.; Supplee, C.; Emge, T. J.; Bailey, B. C.; Schrock, R. R.; Brookhart, M.; Goldman, A. S. *ACS Catal.* **2013**, *3*, 2505.

(6) Dobereiner, G. E.; Yuan, J.; Schrock, R. R.; Goldman, A. S.; Hackenberg, J. D. *J. Am. Chem. Soc.* **2013**, *135*, 12572.

(7) Schrock, R. R.; Murdzek, J. S.; Bazan, G. C.; Robbins, J.; DiMare, M.; O'Regan, M. *J. Am. Chem. Soc.* **1990**, *112*, 3875.

(8) Gupta, M.; Hagen, C.; Flesher, R. J.; Kaska, W. C.; Jensen, C. M. *Chem. Commun.* **1996**, 2083.

(9) Renkema, K. B.; Kissin, Y. V.; Goldman, A. S. *J. Am. Chem. Soc.* **2003**, *125*, 7770.

(10) Hackenberg, J., Rutger, the State University of New Jersey, 2014.

(11) Punji, B.; Hackenberg, J.; Supplee, C.; Emge, T. J.; Goldman, A. S. *Abstract of Papers, 238th ACS National Meeting, Washington, DC, United States, August 16-20,* **2009**, INOR.

Chapter 6

Examining the effect of additives on the rate of transfer dehydrogenation

Abstract

Initial observations showed that adding extra sodium *tert*-butoxide to a transfer dehydrogenation reaction mixture, beyond what is required to remove the hydride and chloride ligands from the (pincer)Ir(H)(Cl) complex, led to higher catalytic activity. A series of mechanistic studies were conducted with the aim of elucidating the source of this effect, and to maximize its benefit to transfer dehydrogenation. First, various other Brønsted bases were added to transfer dehydrogenation reaction mixtures in order to test the scope of this effect. However, most of these additives actually reduced catalytic activity, and only lithium *tert*-butoxide and sodium borohydride increased catalytic activity. Additional mechanistic studies suggested that these additives were not simply quenching impurities, but might actually be performing a mechanistic role, such as co-catalyzing dehydrogenation. However, after several months of investigations the effect suddenly stopped happening, and could not be reproduced again. Therefore, the project was concluded without a definitive explanation.

6.1 Introduction

As described in the preceding Chapters, the main focus of the work described in this thesis was to increase the catalytic activity and selectivity of pincer iridium dehydrogenation catalysts. Whereas Chapters 2 through 4 explored the properties of the pincer catalysts themselves, Chapter 5 examined how the reaction conditions during alkane metathesis influenced the activity and selectivity of that reaction. In this Chapter, the role of Brønsted base additives on activity and selectivity was explored.

This project began with an observation by Jaime Flores, a postdoctoral researcher in the Goldman lab, that adding extra sodium *tert*-butoxide (NaO^tBu) to transfer dehydrogenation reaction mixtures seemed to catalytic activity of the new (NCOP)Ir catalysts.[1] (Figure 6.1) After repeating his reactions several times, the effect seemed to be reproducible. Hence, the possibility that an additive could improve a catalytic reaction was raised. Hence, an investigation into "the sodium *tert*-butoxide effect" began.

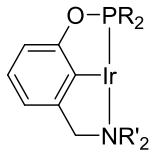

(NCOP)Ir

Figure 6.1 (NCOP)Ir catalyst

However, before discussing the results of these experiments, it is important to consider how the active species for dehydrogenation, the 14 electron complex, is generated from the pre-catalyst.[2] (Figure 6.2) Synthetically, metalation of the pincer ligand with the one of two possible iridium precursors, $[Ir(cyclooctadiene)Cl]_2$ or $[Ir(cyclooctene)_2Cl]_2$, always gives the "hydrido-chloride complex." The name of this species is derived from the two ligands, one chloride from

the iridium species and one hydride from C-H activation of the pincer ligand, which are attached to the iridium. However, the hydrido-chloride complex is very stable, and is remarkably unreactive. Therefore, it must be converted into another species before catalytic transfer dehydrogenation can be performed.

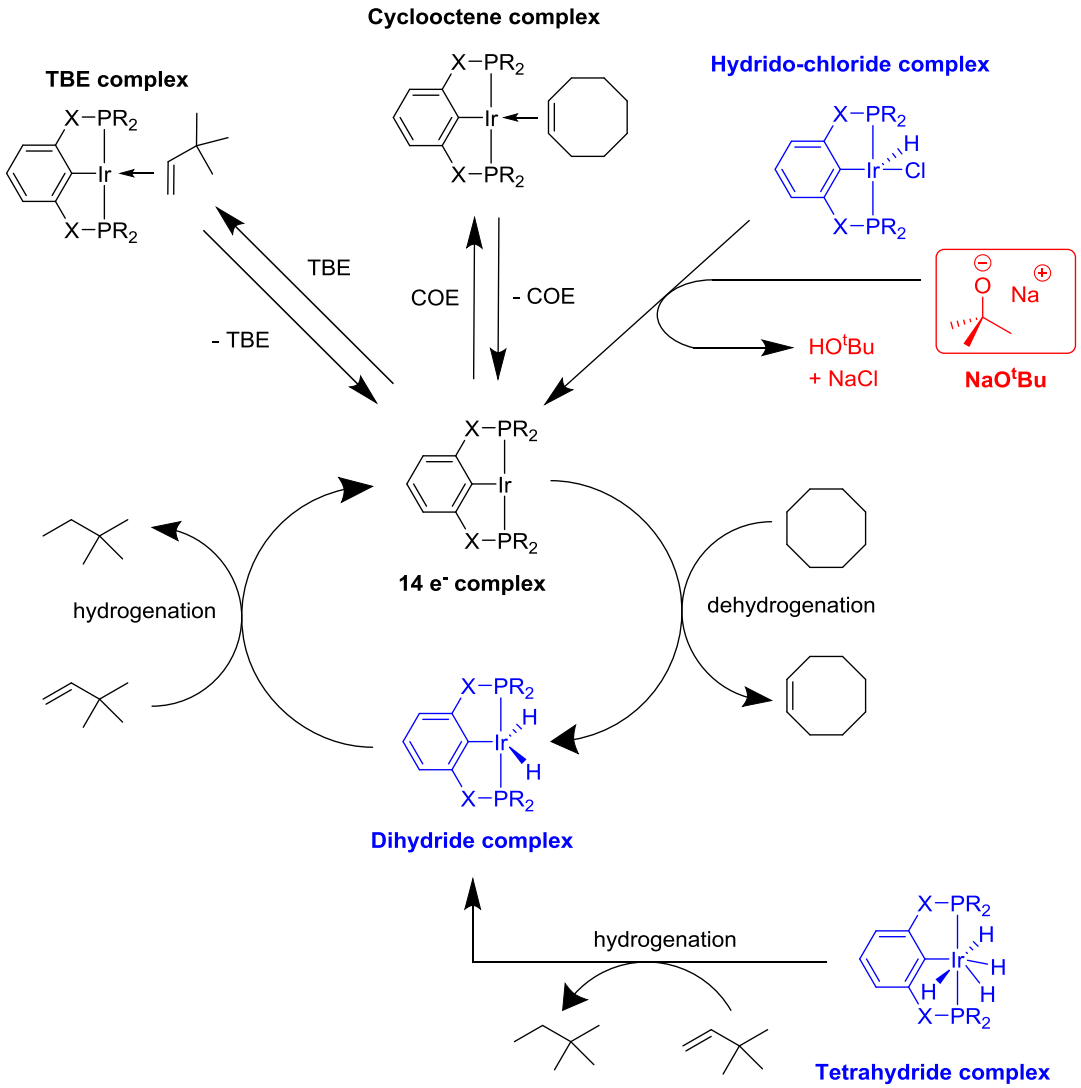

Figure 6.2 Complete COA/TBE transfer dehydrogenation cycle. Starting compounds are shown in blue. Activation of the hydrido-chloride complex by NaO^{t}Bu is shown in red.

The first method of activating the hydrido-chloride complex is the *in-situ* generation of the 14 electron complex. Specifically, the hydrido-chloride complex is added to the reaction mixture along with a Brønsted base, which then removes both the hydride and chloride from the iridium. For example, if the base was sodium *tert*-butoxide then *tert*-butanol and sodium chloride would be produced. (Figure 6.2) However, this method has the distinct disadvantage of being experimentally tedious. If sodium *tert*-butoxide was used as the base, then adding only 1 equivalent of the base requires measuring and transferring only about 1 milligram of the loose, static-prone solid. As will explained later, this experimental annoyance was instrumental in the discovery of the sodium *tert*-butoxide effect.

Alternatively, the hydrido-chloride complex can by synthetically converted into another form that is capable of entering the transfer dehydrogenation cycle directly (i.e. without an additive such as sodium *tert*-butoxide). The first method employed was reducing the hydrido-chloride complex with lithium triethylborohydride ($LiBHEt_3$) in the presence of hydrogen gas.[3] This reaction gives the tertrahydride complex upon the oxidative addition of two equivalents of hydrogen gas (H_2) to the iridium. Interestingly, removal of solvent by vacuum also causes some of the hydrogens to leave the iridium center, yielding a solid which is a mixture of the dihydride and tetrahydride complexes. Hence, adding this "mixed hydride" to the catalytic reaction causes transfer dehydrogenation to begin with the hydrogenation half-cycle. (Figure 6.2) Similarly, the hydrido-chloride complex can be converted to an olefin complex by removing the hydride and chloride ligands in the presence of an *olefin* instead of hydrogen gas. Commonly, the olefin employed is ethylene, giving the 4-coordinate ethylene complex. Hence, if the ethylene complex is added to a transfer dehydrogenation reaction mixture, then dissociation of the ethylene will give the 14 electron complex, which then begins transfer dehydrogenation with the

dehydrogenation half-cycle. Notably, these synthetic reactions can be performed with numerous different Brønsted bases, such as both $LiBHEt_3$ as well as NaO^tBu.

When Jaime was performing his reactions with the new (NCOP)Ir catalyst, his initial studies used the hydrido-chloride complex along with sodium *tert*-butoxide added *in-situ*. However, he did not want to spend the time and effort to accurately measure only 1 equivalent of the Brønsted base, so he added an excess of NaO^tBu. Then, he recorded the reaction rate by GC. Later, he actually synthesized the hydride complexes with hydrogen gas and $LiBHEt_3$, and then tested the mixed-hydride complexes for their transfer dehydrogenation ability. Surprisingly, he found that the (NCOP)$IrH_{2/4}$ complexes performed transfer dehydrogenation *slower* than the (NCOP)Ir(H)(Cl) complex with added NaO^tBu. Upon repeating the reactions several times, it appeared that adding excess NaO^tBu, beyond the one equivalent necessary to remove the hydride and chloride ligand, increased the reaction kinetics by at least 50%.

Thus, it appeared that NaO^tBu was somehow increasing the rate of transfer dehydrogenation by (NCOP)Ir catalysts. Hence, a comprehensive study was began to undercover whether this effect applied to other pincer iridium catalysts besides (NCOP)Ir, and also if other Brønsted bases caused the effect as well. In addition, mechanistic studies were conducted in an attempt to ascertain *why* the NaO^tBu effect was occurring.

6.2 Possible explanations for the NaO^tBu effect

Before conducing any further experiments regarding the NaO^tBu effect, possible explanations for the phenomenon were postulated. With certain mechanisms in mind, further experiments could be conducted in order to test each hypothesis. In particular, four explanations were brainstormed:

1. Catalyst-decomposing impurities – without NaO^tBu, certain impurities in the reaction mixture were reacting with some of the pincer iridium molecules, causing them to decompose and reducing the concentration of active catalyst. For example, if 5 mM of catalyst was added to the reaction but 2 mM of catalyst-decomposing impurities were present, then only 3 mM of the catalyst would be active. Although many possibilities exist, if traces of an alkyl-halide was present in the solvent, then reaction with the 14 electron complex might give an olefin and the (inactive) hydrido-chloride complex. (Scheme 6.1) If NaO^tBu was present, however, then the hydrido-chloride could be converted back into the active 14 electron complex.

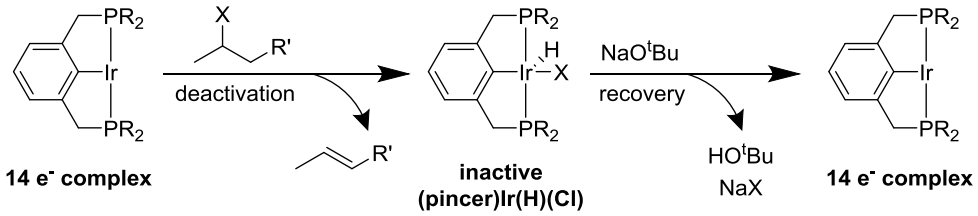

Scheme 6.1 Hypothetical mechanism from NaO^tBu to protect the catalyst from decomposing impurities

2. Catalyst-coordinating impurities – without NaO^tBu, certain impurities might *coordinate* to the 14 electron complex, pushing the iridium complexes into out-of-cycle resting states and reducing catalytic activity. As was discussed in Chapter 4, the presence of olefins not only increases the rate of the hydrogenation half-cycle, but they also *decrease* the rate of the dehydrogenation half-cycle by reducing the concentration of the 14 electron complex.[2] Thus, other Lewis basic species such as ethers, amines, or even water can also reduce the rate of the dehydrogenation half-cycle. (Figure 6.3) Although water actually oxidatively adds to iridium, instead of simply coordinating to it, the effect is the same. However, excess NaO^tBu will react with

the trace water, yielding sodium chloride and (presumably spectating) *tert*-butanol. In effect, the NaO^{t}Bu will "restore" full catalytic activity.

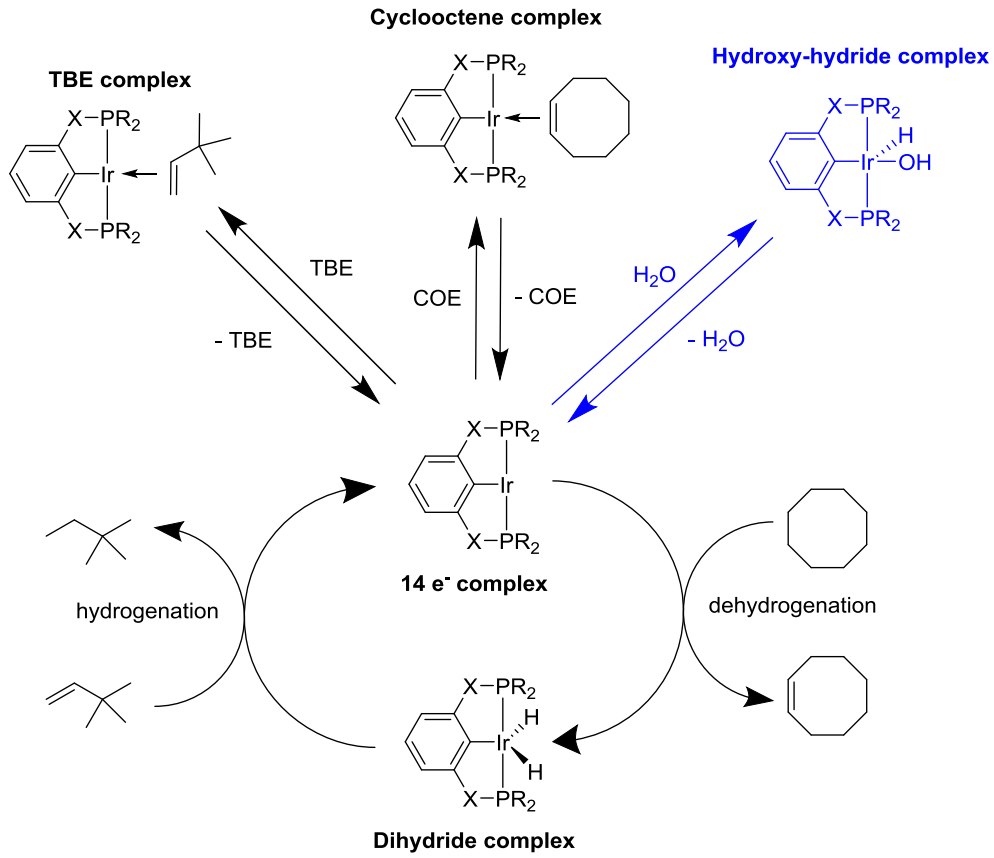

Figure 6.3 COA/TBE transfer dehydrogenation cycle with hydroxy-hydride out-of-cycle resting state

3. Co-catalyzing dehydrogenation – previously, DFT calculations and experimental evidence had shown that transfer (and acceptorless) dehydrogenation can be accomplished by the pincer iridium complexes by themselves, and does not require any additives.[2,4] However, the possibility remains that certain additives, such as NaO^{t}Bu, might allow for a new dehydrogenation pathway that has a lower kinetic barrier, and

would therefore proceed much faster. Based on the DFT results described in Chapter 4, cationic pincer iridium catalysts were predicted to have *much* lower kinetic barriers to dehydrogenation than their neutral counterparts. Thus, *anionic* pincer iridium complexes might also have lower barriers.

In fact, the stoichiometric dehydrogenation of *n*-octane into 1-octene by another pincer iridium complex, (^{dm}phebox)Ir(OAc)$_2$(OH$_2$), was shown to proceed through a concerted metalation-deprotonation mechanism.[5,6] (Scheme 6.2) Of key importance is the *deprotonation* aspect of this mechanism. One of the acetate ligands deprotonated the alkane at the same time that the Ir-alkyl bond was being formed. Thus, with the NaO^{t}Bu effect, the O^{t}Bu$^-$ anion might act as a Brønsted base in a related manner.

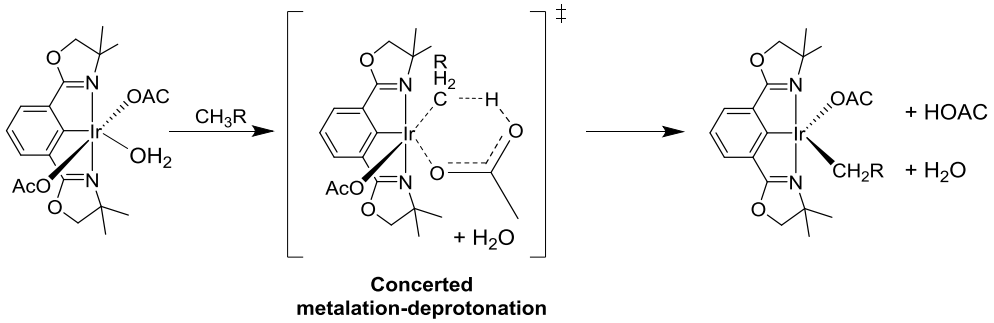

Scheme 6.2 Dehydrogenation of *n*-octane by (^{dm}phebox)Ir(OAc)$_2$(OH$_2$)

4. Co-catalyzing isomerization – lastly, the extra NaO^{t}Bu could also be aiding with the isomerization of 1-olefins to 2-olefins, which is known to influence the catalytic activity of dehydrogenation under certain circumstances.[7] (Figure 6.4) In particular, the mechanism of isomerization by pincer iridium catalysts was shown to proceed through an η^3-allyl pathway which does not require an external additive. However,

as with dehydrogenation, the presence of an appropriate Brønsted base (or Brønsted acid) might allow for a different mechanism with a lower kinetic barrier. Since 1-olefins are known to coordinate more strongly to pincer iridium complexes then 2-olefins, then isomerizing 1-olefins to 2-olefins would allow for a higher steady-state concentration of the 14 electron complex. In turn, this would increase the rate of the dehydrogenation half-cycle, and therefore possibly the whole transfer dehydrogenation cycle.

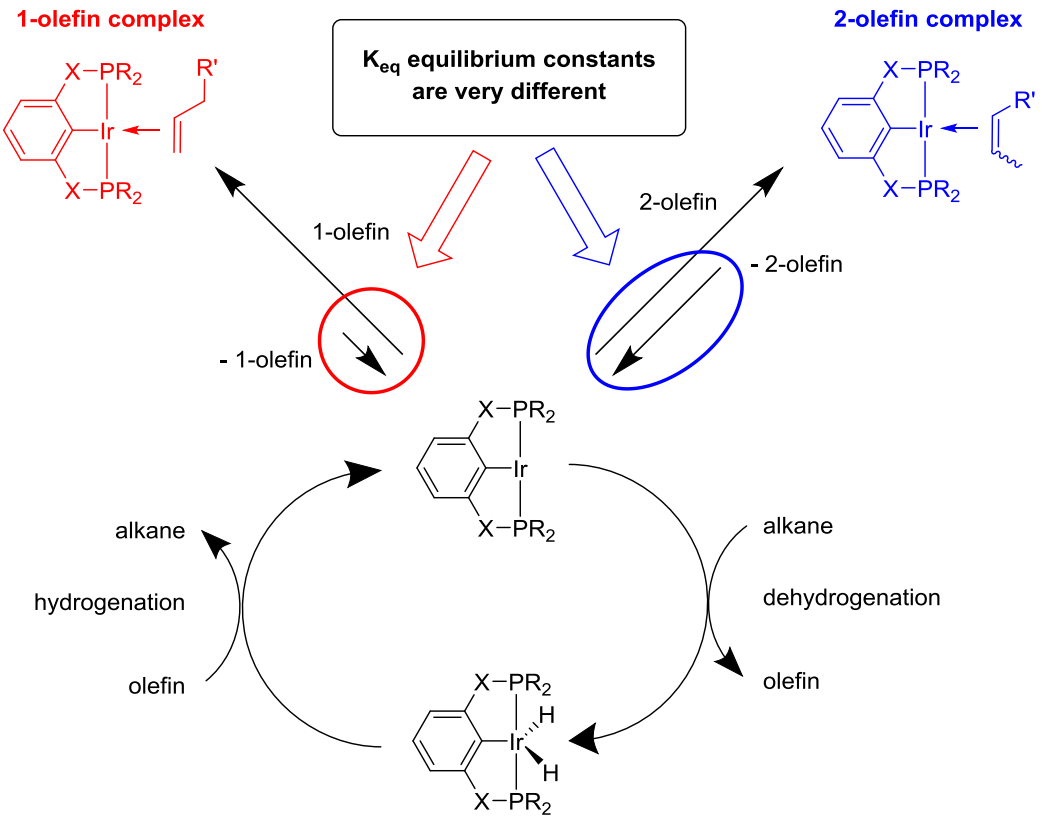

Figure 6.4 Transfer dehydrogenation cycle showing effects of 1-olefins and 2-olefins on catalytic activity

Therefore, four possible mechanistic explanations for the NaO^{t}Bu effect were postulated. Future experiments were designed in order to test each of these hypotheses.

6.3 Confirming the NaO^{t}Bu effect quantitatively

The formal investigation into the NaO^{t}Bu effect began by quantifying conversion during the cyclooctane/*tert*-butyl ethylene (COA/TBE) transfer dehydrogenation. (Scheme 6.3) This reaction had the advantage of isolating one of the possible explanations/variables: co-catalyzing olefin isomerization. Since neither the TBE nor the produced cyclooctene (COE) could be isomerized, then no NaO^{t}Bu effect would be observed if the NaO^{t}Bu was acting only through the isomerization mechanism.

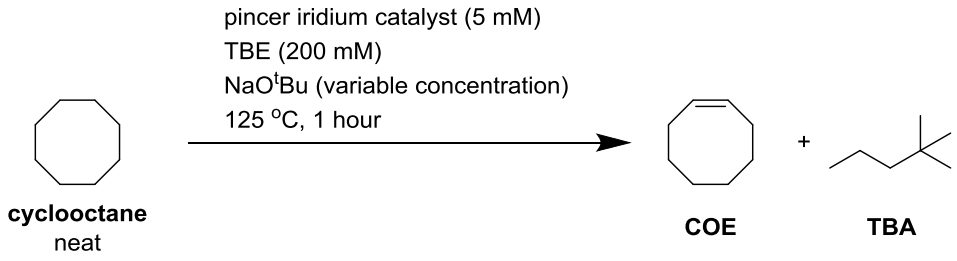

Scheme 6.3 Experimental conditions for initial verification of the NaO^{t}Bu effect

Reactions with (^{tBu4}PCP)Ir, the first catalyst studied, were performed in with NaO^{t}Bu concentrations of 0, 1.25, 5, and 20 mM. (Figure 6.5) The same stock solution was used to make all samples in an effort to minimize any random error. Three samples with each concentration were used, and their conversions were independently quantified by GC. The height of the bar represents the average conversion, while the error bars are equal to plus or minus one standard deviation.

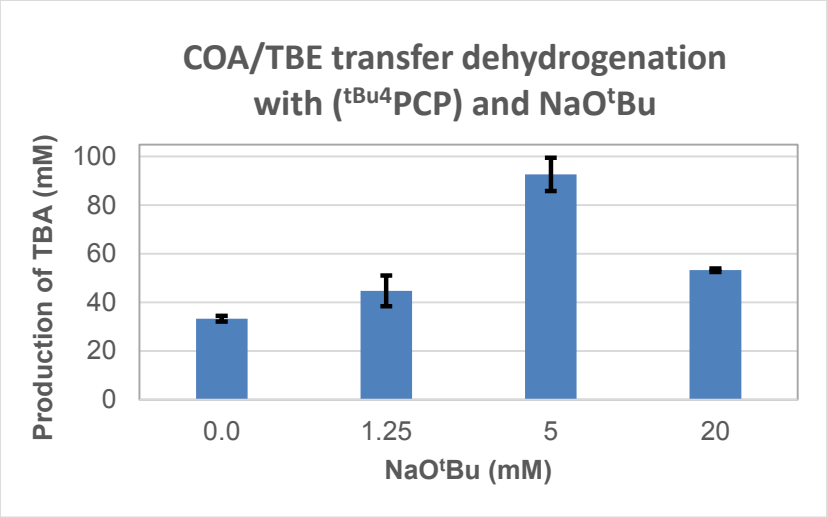

Figure 6.5 Conversion during COA/TBE transfer dehydrogenation reaction with (^{tBu4}PCP)Ir and variable concentrations of NaO^{t}Bu. Error bars are +/- one standard deviation.

The data in Figure 6.5 shows that 1.25 mM of NaO^{t}Bu has a small but seemingly statistically significant effect on conversion. More noticeably, however, is that 5 mM of NaO^{t}Bu resulted in a massive increase in conversion, which was presumably due to a vast increase in catalytic activity. Notably, the 20 mM sample had less conversion than the 5 mM sample, but still more than the 0 mM controls. Thus, this seems to reproduce the NaO^{t}Bu effect, suggesting that it involves more than co-catalyzing isomerization (i.e. impurity quenching or dehydrogenation co-catalyzing).

Notably, the rate of transfer dehydrogenation during COA/TBE has been observed to be very non-linear, being very fast at the beginning and slowing-down as the reaction progresses.[7] Presumably this is because COE binds stronger than TBE, and/or that some back-reaction (hydrogenation of COE instead of TBE) might be occurring. Therefore, the results in Figure 6.5 can only be interpreted qualitatively and not quantitatively

In addition, the same reaction was repeated with (^{tBu4}POCOP)Ir, which also showed a noticeable NaO^{t}Bu effect. (Figure 6.6) In this case, the effect was even more significant, showing

approximately 65 mM of conversion with 20 mM of NaO^{t}Bu but only about 12 mM with the control. Thus, this confirms that the NaO^{t}Bu effect exists, and suggests it is not related to co-catalyzing isomerization.

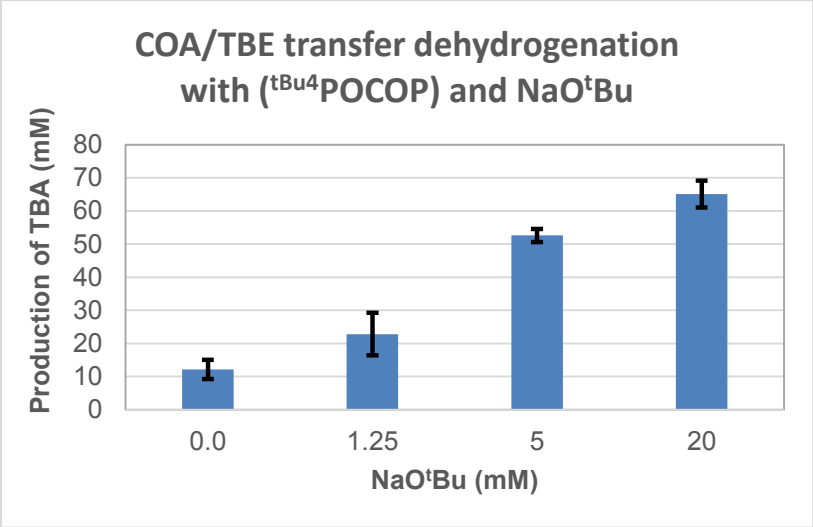

Figure 6.6 Conversion during COA/TBE transfer dehydrogenation reaction with (^{tBu4}POCOP)Ir and variable concentrations of NaO^{t}Bu. Error bars and +/- one standard deviation.

6.4 Screening other additives for their effect on catalytic activity during transfer dehydrogenation

Given the data in the preceding section, the NaO^{t}Bu effect was confirmed to be real. Next, the ability of other Brønsted bases to affect the conversion (as a proxy for rate) in transfer dehydrogenation was assessed. In particular, two different classes of Brønsted bases were considered: ionic bases and neutral bases. The ionic bases had three advantages over neutral bases. First, NaO^{t}Bu was an ionic compound, and therefore other ionic bases would be more similar to it than neutral compounds. Secondly, most of the ionic bases were stronger than their neutral counterparts, which might help increase catalytic activity. Lastly, the ionic bases might

not coordinate to the 14 electron complex very well, since that would generate a (possibly unstable) anionic complex. In contrast, neutral bases such as amines could coordinate to the 14 electron complex, giving a stable 4-coordinate adduct that reduces the rate of the dehydrogenation half-cycle. On the other hand, the ionic Brønsted bases had the disadvantage of having lower solubility in nonpolar alkane solvent than the neutral Brønsted bases.

Experimentally, the screening of Brønsted bases was conducted through a combination of COA/TBE and *n*-octane/1-hexene transfer dehydrogenation reactions with (^{tBu4}PCP)Ir. (Scheme 6.4) In each case, several samples with each reaction were prepared, heated, and analyzed by GC in order to reduce random error. In addition, certain Brønsted bases, such as $NaBH_4$, were analyzed multiple times. Although the results varied slightly from experiment to experiment, the overall trends were relatively consistent. In addition, samples with NaO^tBu were also performed at the same time, using the same stock solutions. Since significant increases in conversion were observed with the NaO^tBu samples, then it was verified that the given reaction mixtures *would* detect the Brønsted base effect if the other bases were capable of causing it.

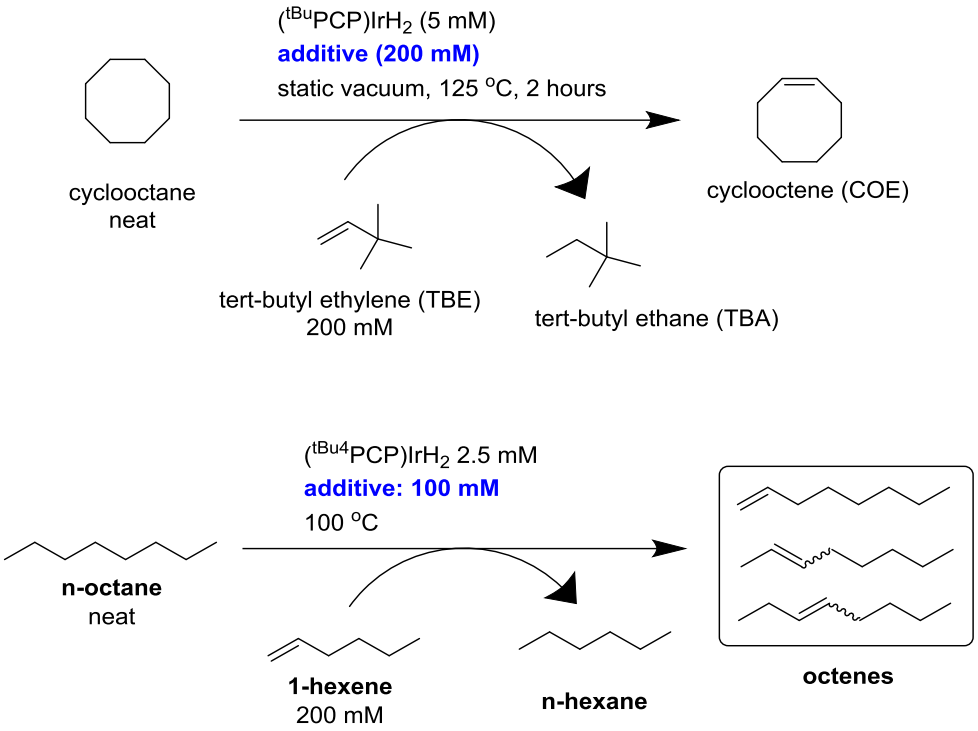

Scheme 6.4 The two experimental conditions used to screen various additives for their effect on transfer dehydrogenation activity

The ionic Brønsted bases were tested first, showing a wide variety of effects. (Figure 6.7) First, the Brønsted bases of lithium dimethylamide ($LiNMe_2$) and lithium methoxide (LiOMe) showed that all catalytic activity was inhibited with these additives. Possibly, their extremely strong basicity caused catalyst decomposition. Similarly, the Brønsted *acid* trifluoro-p-toluic acid was also examined, showing that it inhibited all catalytic activity. Next, the bases of sodium phenoxide (NaOPh) and sodium trimethoxyborohydride ($NaBH(OMe)_3$) were found to reduce catalytic activity relative to the control (no additives), but still allow for some transfer dehydrogenation turnovers. Presumably, these bases might have coordinated to the iridium center, reducing activity. The borohydride was interesting in the sense that it was not a typical (reversible) Brønsted base. If its hydride (H^-) found a proton (H^+), then H_2 would be generated.

Thus, the borohydride might not influence dehydrogenation through the same mechanism as NaO^{t}Bu.

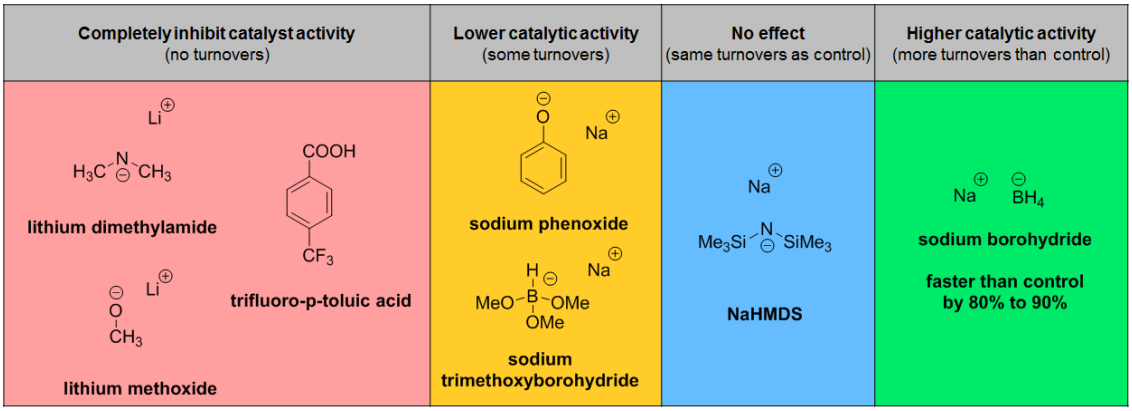

Figure 6.7 Effect of ionic Brønsted bases and one Brønsted acid on transfer dehydrogenation activity

Next, it was found that the sample with sodium bis(trimethylsilyl)amide (NaHMDS) gave almost identical turnovers/conversion as the control (no additives). This result is notable, since it suggests a possible mechanism for the NaO^{t}Bu effect. Whereas the stericly open amide base $LiNMe_2$ caused all catalytic activity to stop, this more crowded base had no effect on catalytic activity. Therefore, NaHMDS might be too crowded (around its nitrogen anion) to interact with and deactivate the pincer iridium catalyst. On the other hand, it did not increase catalytic activity like NaO^{t}Bu did. Thus, if NaO^{t}Bu increased catalytic activity by quenching H_2O, a very small molecule, then presumably NaHMDS would *also* be able to quench water (giving NaOH and the protonated amine) and therefore should *also* have increased catalytic activity. However, since this increase was not observed, then the NaO^{t}Bu effect might involve more than simply quenching water (or, that NaHMDS is actually too crowded to quench water).

Lastly, sodium borohydride ($NaBH_4$) was found to increase conversion by approximately 80% to 90%, noticeably less than NaO^{t}Bu under the same reaction conditions (approximately

150% increase). Again, this is not consistent with NaO^{t}Bu simply quenching water. If the removal of water *was* the mechanism behind the NaO^{t}Bu effect, then both NaO^{t}Bu and $NaBH_4$ would both remove all water completely, and would therefore lead to a very similar increase in conversion. However, because this was not the case, the NaO^{t}Bu effect likely involved more than simply removing water. However, because the borohydride is a different type of Brønsted base (semi-irreversible, generating H_2) than NaO^{t}Bu (simple protonation/deprotonation), then the mechanism behind these effects was not clear.

Moving forward, a variety of nonionic Brønsted bases were also screened for their ability to increase catalytic activity during transfer dehydrogenation. (Figure 6.8) First, two of the benzylidenes, as well as pyridine, all completely inhibited catalytic activity. Presumably, the relatively open environment around their Lewis basic nitrogen atoms allowed them to coordinate to the 14 electron complex, reducing the activity of the dehydrogenation half-cycle. In fact, color changes were observed upon addition of these bases to the reaction mixture (which already contained the pincer iridium complex and an olefin), suggesting coordination of the nitrogen atoms to the iridium centers.

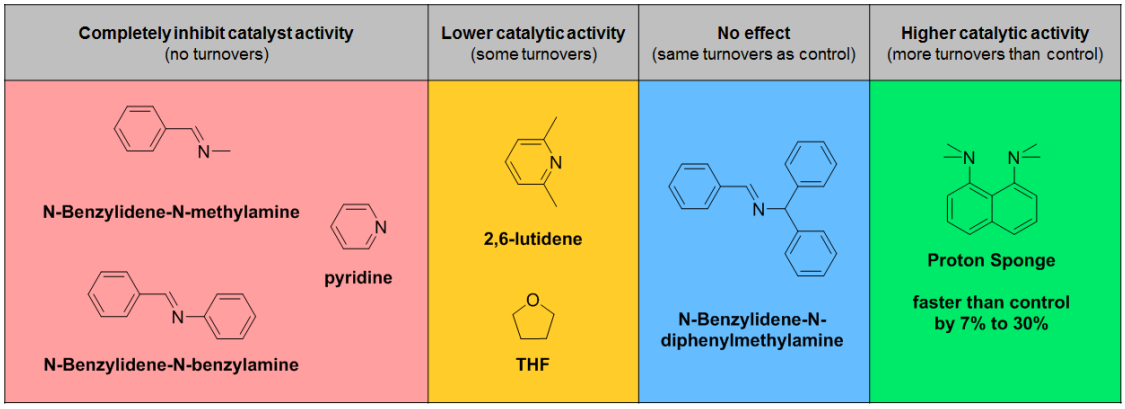

Figure 6.8 Effect of nonionic Brønsted bases on activity transfer dehydrogenation activity

Similarly, it was found that 2,6-lutidene, which is essentially a more stericly crowded analog of pyridine, caused a slight reduction in catalytic activity. Hence, it seems plausible that the two methyl groups made it harder for the nitrogen atom to coordinate to iridium, and therefore 2,6-lutidene inhibited catalytic activity less than pyridine. Likewise, the most stericly crowded benzylidene was found to have no effect on catalytic activity relative to the control (no additives), presumably because it could not coordinate to the iridium. In addition, tetrahydrofuran (THF) was found to have slightly reduced the catalytic activity, presumably due to weak coordination of its oxygen atom to iridium. Lastly, Proton Sponge® was observed to cause a slightly increase in catalytic activity (7% to 30%) relative to the control. After many experiments, this increase was found to be only slightly greater than the random error. Therefore, no meaningful mechanistic insights could be gained from the study of these nonionic Brønsted bases.

In addition, the effect of crown ethers (in conjunction with NaO^tBu) was investigated by examining the 1-hexene/*n*-octane transfer dehydrogenation reaction with (^{tBu4}PCP)Ir. (Scheme 6.5) In particular, four reaction mixtures were examined: no additives, 200 mM of 15-crown-5, 200 mM of NaO^tBu, and 200 mM of both NaO^tBu and 15-crown-5. The hypothesis was that the crown ether would coordinate to and sequester the Na^+ cation, generating a O^tBu^- anion that was more free, and therefore more able to perform its function.

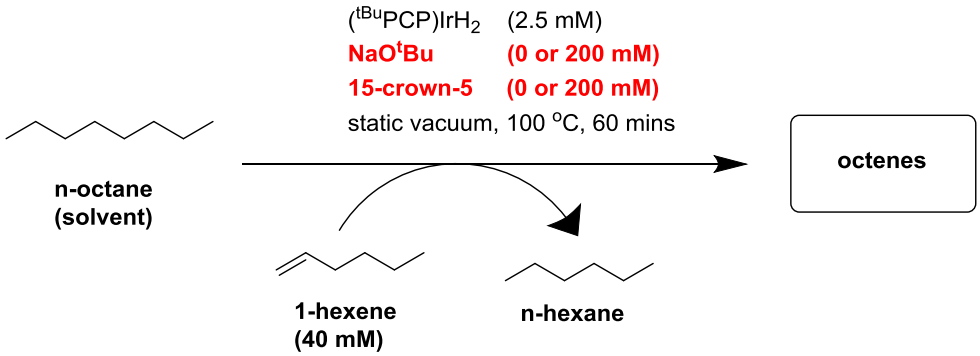

Scheme 6.5 Examining the effect of 15-crown-5 on transfer dehydrogenation activity

When examining the transfer dehydrogenation turnovers during these reactions, more conversion was achieved with NaO^{t}Bu than without NaO^{t}Bu. However, the presence or absence of the crown ether had no meaningful effect on the dehydrogenation turnovers.

6.5 Examining the mechanistic cause of the NaO^{t}Bu effect through kinetic modeling

While the screening of several Brønsted bases gave interesting insights into possible mechanisms for the NaO^{t}Bu effect, none of the experiments provided hard or decisive evidence. Therefore, experiments were conducted in order to more accurately identify the mechanism which caused this effect.

First, catalytic reactions with NaO^{t}Bu and LiO^{t}Bu were conducted at various concentrations. The related complex KO^{t}Bu would have also been tested, but it was found to have very low solubility (<10 mM) in the nonpolar alkane solvents requires for transfer dehydrogenation reactions. Regardless, these experiments allowed two different aspects to be examined simultaneously. First, the influence of the cation on transfer dehydrogenation activity could be inferred by comparing the effects of the sodium additive to that of the lithium additive. Secondly, by varying the concentration of the additives from 0 mM to several hundred mM, then the effect of concentration could also be elucidated.

First, a reaction with NaO^{t}Bu at concentrations up to 200 mM was conducted. (Scheme 6.6) (Figure 6.9) A single stock solution was used in order to reduce random error. Although the data was not completely consistent, it appeared that the effect increased up until approximately 50 mM, but no additional improvements were observed after about 50 mM.

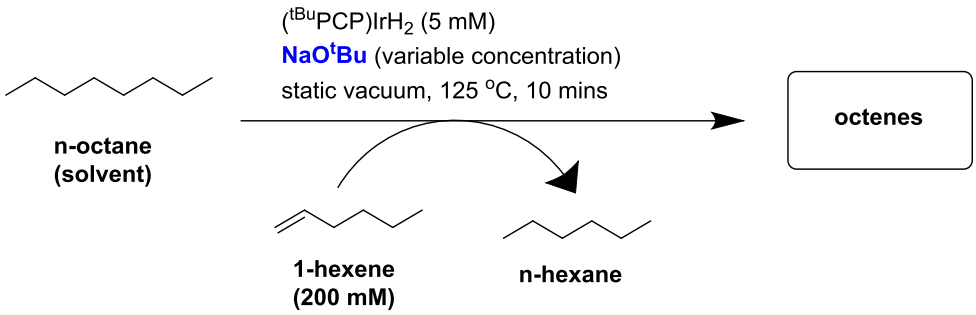

Scheme 6.6 Examining the NaO^{t}Bu effect at various concentrations

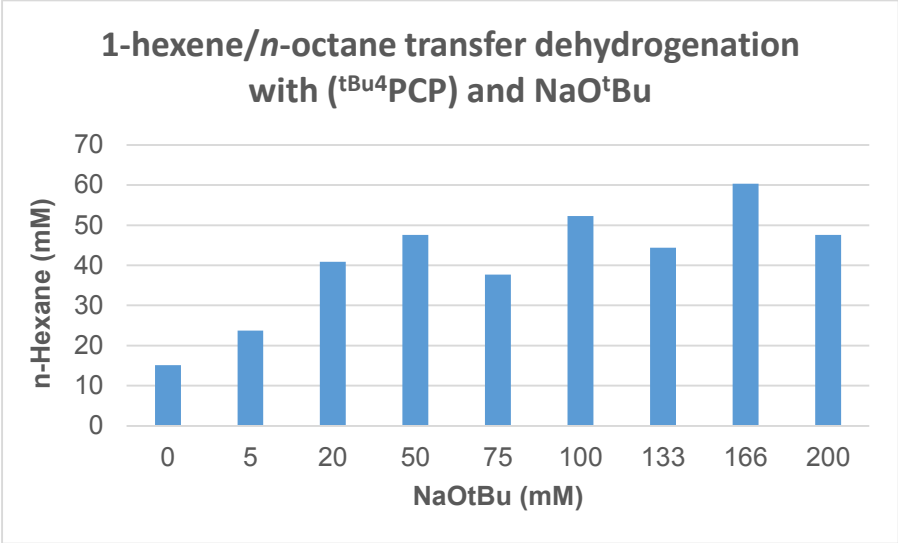

Figure 6.9 Effect of variable concentrations of NaO^{t}Bu on conversion during 1-hexene/*n*-octane transfer dehydrogenation with (^{tBu4}PCP)Ir

Since co-catalyzing isomerization had been fairly rigorously ruled-out previously, this effect could either be caused by quenching impurities or co-catalyzing dehydrogenation. Unfortunately, neither mechanism was a clear fit for the observations. If it had been co-catalyzing dehydrogenation, then a first-order increase would have been expected. However, aggregation of the ionic NaO^{t}Bu molecules in the nonpolar *n*-octane solvent would likely give a partial-order relationship somewhere between zero-order and first-order. On the other hand, if certain impurities were being stoichiometrically quenched by the NaO^{t}Bu, then a *threshold effect* would

be expected. If the stock solution contained, for example, 40 mM of these impurities then catalytic activity would be expected to increase linearly up to 40 mM, after which it would be expected to be the same. Overall, the limited quality of the data did not permit any definitive conclusions to be drawn.

Next, the effect was examined with LiO^{t}Bu. (Scheme 6.7) (Figure 6.10) Notably, the exact same batches of *n*-octane, (^{tBu4}PCP)Ir, and 1-hexene were used to perform these studies with LiO^{t}Bu as with the variable-concentration NaO^{t}Bu reactions above. However, the reaction temperature was lowered from 125 °C (above) to 100 °C (here) in an effort to slow the reaction and permit easier analysis. However, the observations here were very different than in Figure 6.8 above. Catalytic activity increased sharply with only 2.5 mM of added LiO^{t}Bu, which represented a more abrupt increase than in Figure 6.8 above. However, the increases in catalytic activity also stabilized at much lower concentrations of additive. Between 2.5 mM and 50 mM of LiO^{t}Bu, a 20-fold increase in additive, the observed conversion increased only from 25 to 28 mM of *n*-hexane, which was barely a statistically significant difference.

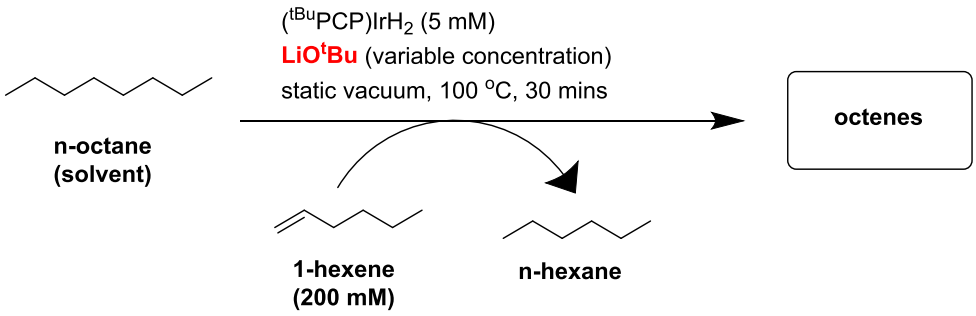

Scheme 6.7 Examining the LiO^{t}Bu effect at various concentrations

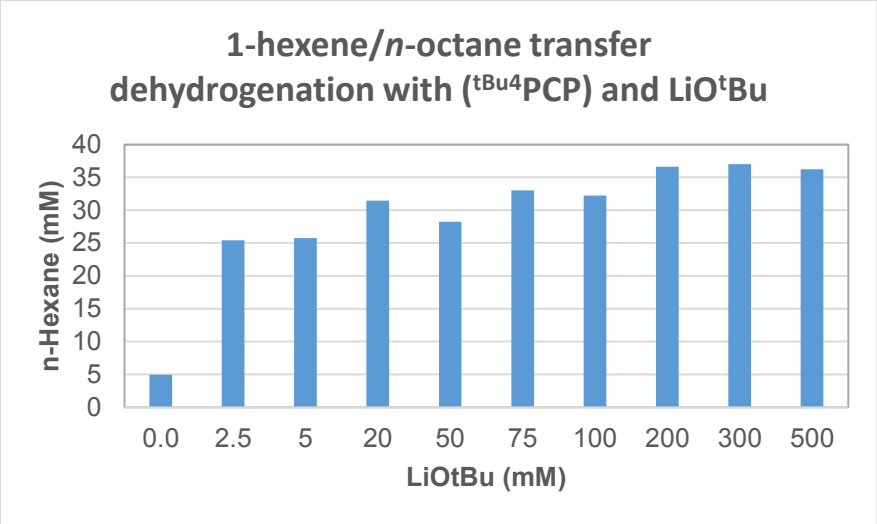

Figure 6.10 Effect of variable concentrations of LiO^{t}Bu on conversion during 1-hexene/*n*-octane transfer dehydrogenation with (^{tBu4}PCP)Ir

Overall, the results of the NaO^{t}Bu and LiO^{t}Bu studies did not allow for any definitive conclusions to be made. Although they once-again confirmed the effects of MO^{t}Bu Brønsted bases, their behavior as a function of additive concentration was not exactly consistent with either co-catalyzing dehydrogenation, nor with stoichiometrically quenching impurities. In addition, the change in temperature between the two reactions prohibited the effect of the cation (Na^+ versus Li^+) from being ascertained.

Next, the ability of NaO^{t}Bu to catalyze olefin isomerization by itself (without any pincer iridium complexes present) was investigated. Although the results from Section 6.3 strong suggested that olefin isomerization was not involved with the NaO^{t}Bu effect, rigorously discrediting this mechanism would still be desirable. In particular, it is known that KO^{t}Bu can by itself catalyze the isomerization of olefins, albeit at a slow rate and only in certain (polar) solvents.[8-10] Hence, the isomerization of 1-hexene by NaO^{t}Bu was examined. (Scheme 6.8) (Figure 6.11) Under conditions very similar to the transfer dehydrogenation reactions conducted previously, it appears that NaO^{t}Bu *can* in fact catalyze the isomerization of 1-hexene to 2-hexenes.

However, this reaction is approximately 1,000 times slower than isomerization by (^{tBu4}PCP)Ir, which itself is the slowest pincer iridium catalyst for olefin isomerization. Therefore, the NaO^{t}Bu effect was not influenced by olefin isomerization.

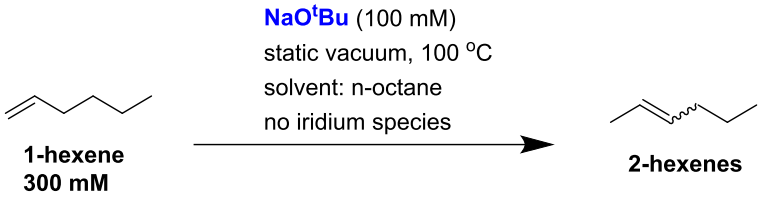

Scheme 6.8 Examining the ability of NaO^{t}Bu to catalyze olefin isomerization without iridium species present

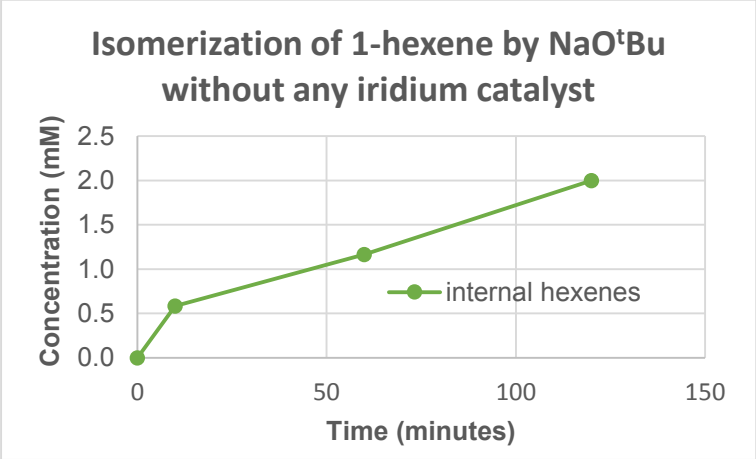

Figure 6.11 Catalytic isomerization of 1-hexene by NaO^{t}Bu without any iridium species

Next, the "pre-treatment" procedure was used to examine whether impurities were responsible for the NaO^{t}Bu effect. Namely, this was investigated by comparing reactions with "NaO^{t}Bu-pretreated" solvent with reactions employing untreated solvent. Traditionally, preparing the reaction solvent involves first degassing the solvent by freeze-pump-thawing, and then "drying" or removing trace amounts of water from the solvent, either by treatment with NaK (sodium-potassium alloy) or activated alumina. Up until this point, all solvents and liquid reagents (such as 1-hexene) used during catalysis had been freeze-pump-thawed and then dried with activated alumina. However, if catalyst-decomposing or catalyst-coordinating impurities were present in the solvent, then the degassing and drying the solvents would most likely not remove

those impurities. On the other hand, if the *in-situ* addition of excess NaO^tBu to the actual reaction mixture caused those impurities to be quenched, then the pre-treatment of the solvent with NaO^tBu should *also* remove/quench those impurities (assuming elevated temperatures were not required to quench the impurities).

Therefore, two batches of *n*-octane were prepared. First, approximately 40 mL of *n*-octane was freeze-pump-thawed and then dried over activated alumina. Next, half of this solution was placed into a new vial inside the glovebox and marked as "traditional *n*-octane." The other half was put inside a separate vial, labeled as "for pretreatment," and 200 mM of NaO^tBu was added to the solution. After 8 hours the "for pretreatment" *n*-octane was placed into a Schlenk bomb and vacuum distilled in order to separate the now-pretreated *n*-octane from the NaO^tBu and (if present) impurities residue.

Afterwards, two 1-hexene/*n*-octane transfer dehydrogenation reaction mixtures were created. (Scheme 6.9) Whereas both mixtures used the same batches of 1-hexene and (^{tBu4}PCP)Ir, one mixture used the "traditional" *n*-octane whereas the other used the "pretreated" *n*-octane. Great care was taken when measuring all volumes and weights. A larger amount of (^{tBu4}PCP)Ir was used than normal, approximately 3.0 mg, which was then diluted to the desired 2.5 mM, in order to reduce the error associated with weighing such a small mass. Overall, the concentration of the (^{tBu4}PCP)Ir and 1-hexene between the two reaction mixtures should have been within 10% of one another. Finally, the two reaction mixtures were heated in parallel next to each other, at the same time, in the same oil bath.

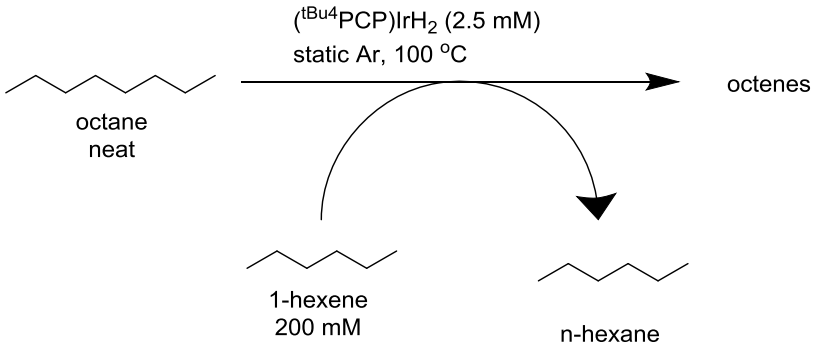

Scheme 6.9 Examining the effect of pre-treating *n*-octane with NaO^{t}Bu

Carefully tracking the kinetics of these reactions showed that both reactions gave statistically identical results. The rates of transfer dehydrogenation, as measured by the production of *n*-hexane, were identical within random error. (Figure 6.12) Similarly, the rate of isomerization, quantified as the production of 2-hexenes, was also essentially identical within expected random error. (Figure 6.13)

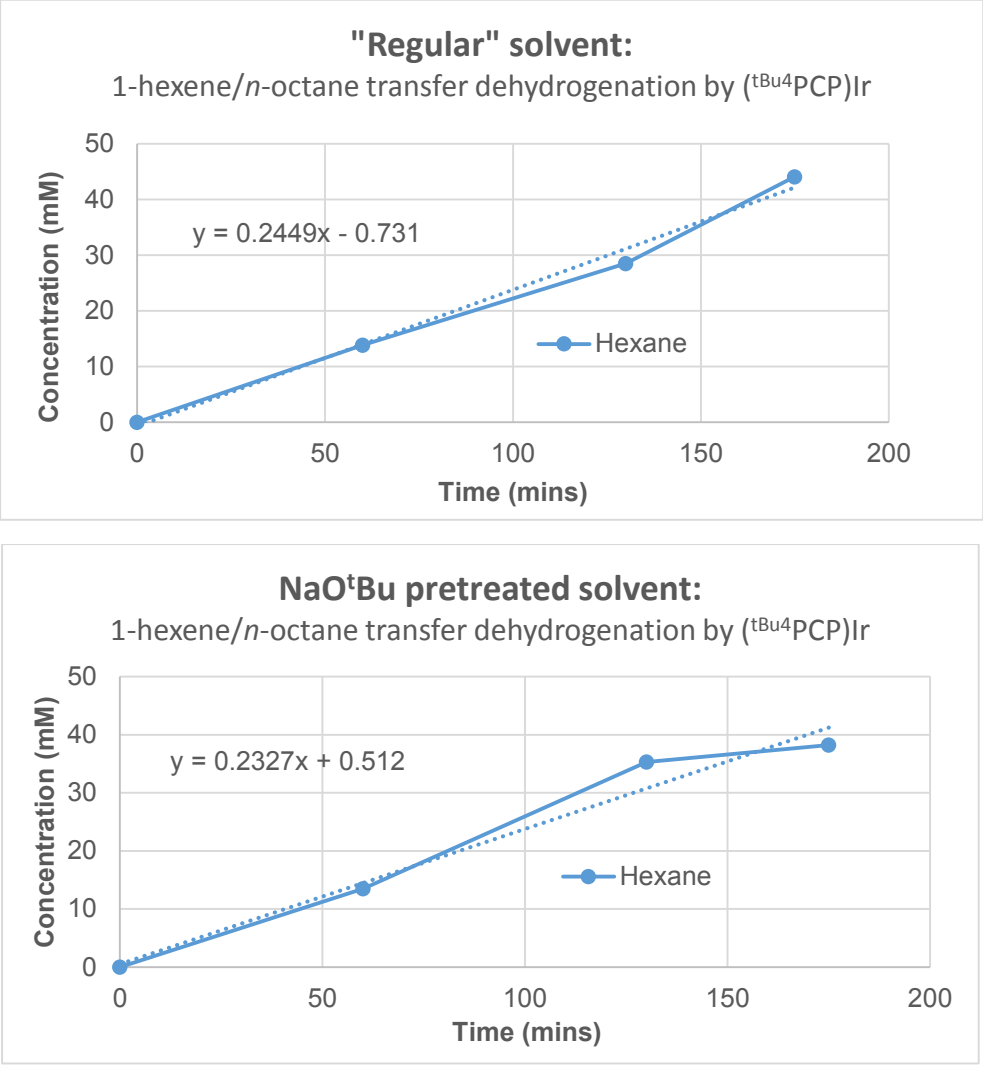

Figure 6.12 Pretreating *n*-octane has no effect on dehydrogenation rate during 1-hexene/*n*-octane transfer dehydrogenation with (^{tBu4}PCP)Ir

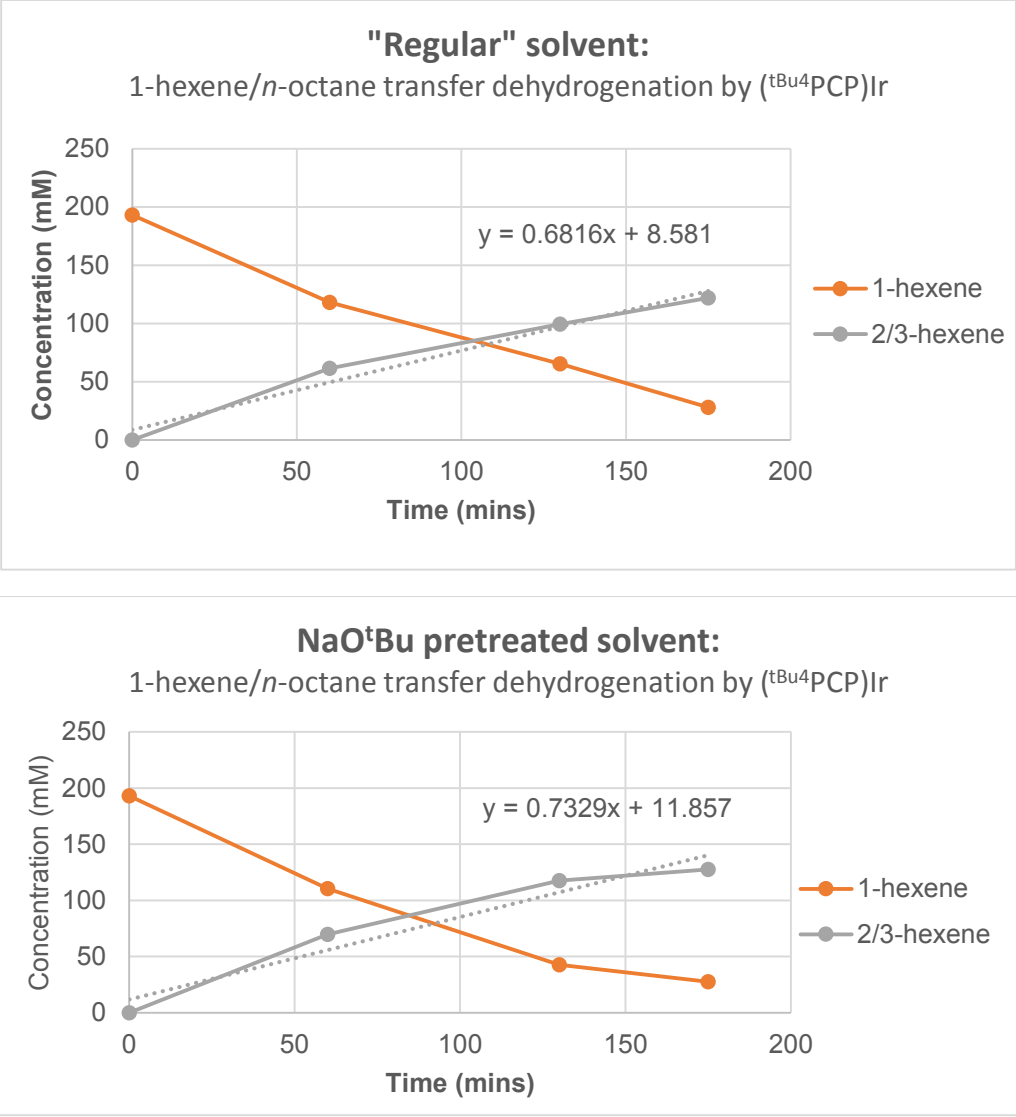

Figure 6.13 Pretreating *n*-octane has no effect on isomerization rate during 1-hexene/*n*-octane transfer dehydrogenation with (^{tBu4}PCP)Ir

Therefore, it appeared that given this particular batch of *n*-octane, the quenching of impurities (either catalyst-decomposing or catalyst-coordinating) was *not* the source of the NaO^{t}Bu effect. Based on the information above in Section 6.3, as well as the identical rates of isomerization in this experiment, it also appeared that co-catalyzing isomerization was also *not* the cause of the NaO^{t}Bu effect. Therefore, by process of elimination, it appeared that NaO^{t}Bu

might be co-catalyzing the transfer dehydrogenation reaction. However, no direct evidence implicating the co-catalyzing of dehydrogenation had been found.

6.6 Examining the mechanistic cause of the NaO^{t}Bu effect through kinetic modeling

In order to gain more evidence that the NaO^{t}Bu effect was not related to impurities, *in-situ* NMR studies were conducted. In general, a single transfer dehydrogenation reaction mixture would be made and then separated into two NMR tubes. One tube would serve as the control, whereas NaO^{t}Bu would be added to the second tube. Heating the tubes in parallel using the same oil bath would cause catalysis to occur, and the conversion in each tube could be quantified by NMR or by GC (taking a sample inside the glovebox).

In addition, the presence of catalyst-coordinating impurities could be detected by ^{31}P NMR. Specifically, the catalytic resting state(s) of the reaction mixture could be ascertained by taking a ^{31}P NMR of each tube, which would indicate which species (i.e. olefin, H_2O, N_2, two hydrides, etc.) was coordinated to the iridium center. Any differences between the control tube and NaO^{t}Bu-tube would indicate that coordination impurities were being quenched by NaO^{t}Bu. Likewise, the *absence* of any differences would suggest that no coordination impurities were being affected by NaO^{t}Bu.

Similarly, the actions of catalyst-decomposing impurities could also be observed with the same ^{31}P NMR scans. Specifically, the peaks for the pincer iridium complexes could be integrated, and those integrations compared an internal standard (in this case, a capillary of trimethylphosphine in toluene-d_8, which also served to lock the NMR). By using internal standards of known concentrations of trimethylphosphine, then the total concentration of "pincer iridium complexes still in solution" could be quantified for each tube. If the concentrations were identical for both the control tube and the NaO^{t}Bu tube, then no catalyst-decomposing impurities were

being quenched by NaO^{t}Bu. In contrast, if the concentration of the NaO^{t}Bu tube was *higher* than that of the control tube, then the NaO^{t}Bu effect would (at least in part) be due to the quenching of catalyst-decomposing impurities.

The first reaction assessed was a 1-octene/*n*-hexane transfer dehydrogenation with (^{tBu4}PCP)Ir. (Scheme 6.10) GC analysis confirmed that adding 20 mM of NaO^{t}Bu increased catalytic activity by approximately 3-fold. Analysis by ^{31}P NMR showed that the sole catalytic resting state, for both tubes, was the 1-octene (or 1-hexene) complex. (Table 6.1) Thus, no coordination impurities were causing the NaO^{t}Bu effect. Although rigorous integrations were not conducted, it appeared that both tubes contained similar concentrations of the 1-olefin complex.

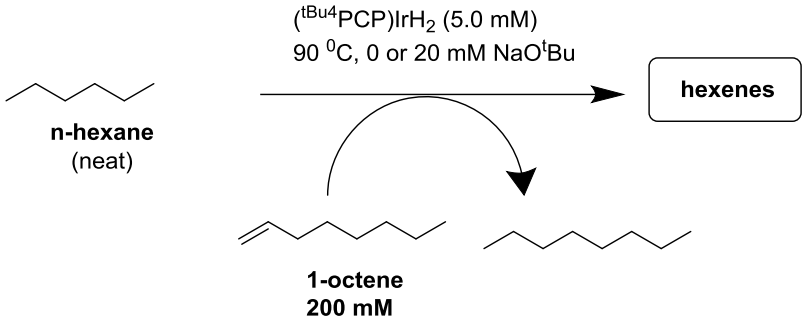

Scheme 6.10 Examining the catalytic resting state during 1-octene/*n*-hexane transfer dehydrogenation by NMR

[NaO^{t}Bu]	Before heating	After heating	Other peaks?
0 mM	1-octene complex	1-octene complex	no
20 mM	1-octene complex	1-octene complex	no

Table 6.1 Catalytic resting state during 1-octene/*n*-hexane transfer dehydrogenation with (^{tBu4}PCP)Ir, both with and without NaO^{t}Bu

Similarly, COA/TBE transfer dehydrogenation reactions were also examined with this process. (Scheme 6.11) Before conversions could be quantified by GC, however, it was noticed that several different complexes were detected by ^{31}P NMR. In addition, the NMR signatures were *different* for the control versus the NaO^{t}Bu tubes.

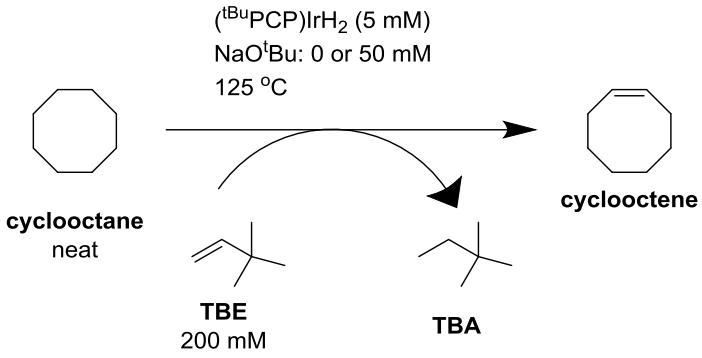

Scheme 6.11 Examining the catalytic resting state during COA/TBE transfer dehydrogenation by NMR

In the control tube, before heating the pincer iridium species included both the (^{tBu4}PCP)Ir(OH)(H) water complex and the [(^{tBu4}PCP)Ir]$_2$(μ^2-N$_2$) nitrogen dimer in a 1:3 ratio. After heating, the equilibrium shifted towards the (^{tBu4}PCP)Ir(COE) COE complex, existing in a 2:2:1 ratio for the COE : water : N$_2$-dimer after 60 minutes. In contrast, the NaO^{t}Bu-containing tube began as only the N$_2$ dimer, but gradually shifted towards an equilibrium with the (^{tBu4}PCP)Ir(COE) complex after heating. No TBE complexes were observed. Hence, catalyst-coordinating impurities *were* present in this reaction mixture, and NaO^{t}Bu was capable of quenching the water. Hence, the NaO^{t}Bu effect observed in (Section 6.3) with the COA/TBE reactions might have actually been due to quenching catalyst-coordinating impurities.

However, this does not explain the observations of the NaO^{t}Bu effect with 1-hexene/*n*-octane reactions in Sections 6.4 and 6.5 above. It appears that given the concentrations each of the species appear at during these reactions, the following order of "coordination strength" can

be described. (Figure 6.14) Hence, presence of H_2O or N_2 will cause those species to out-compete TBE or norbornene (NBE) for the ability to coordinate to iridium. Hence, H_2O and N_2 adducts were observed in the COA/TBE reactions. However, 1-olefins are less stericly bulky than TBE and NBE, and therefore bind stronger than those olefins. Presumably, they also bind stronger to iridium than N_2 and H_2O, which is why only the 1-octene complex was observed during the reaction described in Figure 6.14, despite N_2 and H_2O most likely *also* being in those reaction mixtures.

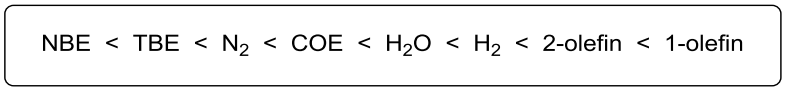

Figure 6.14 Approximate "coordination strength" of various species

Notably, equilibriums are determined by a combination of the relative thermodynamic stability of each species as well as by Le Châtelier's principle. If there was an equal concentration of two different species in solution, such as COE and H_2O, then the equilibrium would be defined by whether (^{tBu4}PCP)Ir(OH)(H) or (^{tBu4}PCP)Ir(COE) was more thermodynamically stable. For example, suppose the (^{tBu4}PCP)Ir(COE) complex was more stable. However, if the concentration of H_2O exceeds that of COE, then the equilibrium will begin to shift towards the H_2O complex. In the above example the concentrations of the various coordinating species are very different, and so precisely estimating the relative thermodynamics was not possible.

6.7 Irreproducibility of the NaO^{t}Bu effect

Therefore, since water appeared to be an issue with the COA/TBE transfer dehydrogenation reactions described in Section 6.6, then additional steps were taken to remove trace quantities of water. Namely, all solvents, which had already been dried once with activated

alumina, were dried a second time with activated alumina. In addition, the glass NMR tubes, which had been pre-dried in an oven to remove water on the surface of the glass, were now dried in a vacuum oven. Lastly, the glovebox was purged for several minutes with argon in an attempt to reduce the gaseous impurities present in the glovebox atmosphere.

After completing these tasks, several transfer dehydrogenation reactions were conducted with (^{tBu4}PCP)Ir and NaO^{t}Bu. Surprisingly, however, the NaO^{t}Bu effect appeared to have disappeared! In the first reaction, a COA/TBE transfer dehydrogenation, the rate and conversion between the control samples and the NaO^{t}Bu-containing samples was statistically identical! To control for the COA solvent, transfer dehydrogenation reactions were performed with 1-hexene/*n*-octane and COE/cyclododecane reaction mixtures as well. However, those tests also no NaO^{t}Bu effect! The only difference observed between the control samples and the NaO^{t}Bu-containing ones was color: in all cases the control solutions were a transparent, bright, clear, and beautiful red. However, the NaO^{t}Bu-containing ones were opaque and reddish-black. Notably, until this most recent set of experiments, none of the NaO^{t}Bu-containing samples were opaque or black, although they did sometimes vary slightly in color from the control samples.

Overall, these results showed that the NaO^{t}Bu effect was beginning to become irreproducible. Even if trace amounts of water had been removed from the solvents and glovebox, the NMR studies of 1-hexene/*n*-octane in Section 6.6 strongly suggested quenching impurities was not the origin of the NaO^{t}Bu effect. In particular, pincer iridium species appeared to bind to 1-olefins stronger than trace amounts of water, and therefore the action of NaO^{t}Bu quenching trace water should *not* affect the rate of transfer dehydrogenation involving 1-olefins.

Therefore, this Chapter gave conflicting accounts of whether the NaO^{t}Bu effect was due to quenching impurities, or due to other mechanisms. And, since the practical improvements in

catalytic activity were relatively limited (≤ 500% increase in rate), continuing with the project was deemed to be an inefficient use of time.

6.8 Summary

Initial investigations into the NaO^{t}Bu effect showed that showed that the effect appeared to be reproducible. In addition, screening of many Brønsted bases showed that while most actually caused catalytic activity to decrease, lithium *tert*-butoxide and sodium borohydride also increased catalytic activity. The results of several mechanistic studies contradicted one another. Namely, some studies suggesting that the quenching of impurities was not the source of the increase in catalytic activity, while other studies indicated that quenching water might have caused the NaO^{t}Bu effect. Due to these inconsistencies, the project was ended without a definitive conclusion regarding the mechanism causing these observations.

6.9 Experimental

All manipulations were performed either in a glovebox or on a Schlenk line under an inert atmosphere of dry argon. All reagents and solvents were obtained from Aldrich. For catalytic experiments, all solvents and liquid reagents were degassed by three freeze-pump-thaw cycles, dried by stirring over activated alumina for 12 h, and finally distilled under vacuum using Schlenk techniques. For synthetic reactions, all solvents and liquid reagents were degassed by bubbling argon through the liquid for 20 min. (^{tBu4}PCP)IrH$_{2/4}$ was synthesized according to literature.[3] NMR spectra were recorded on either a Bruker DRX-400, Bruker Avance-400, or Bruker DRX-500 spectrometer at 298 K.

Catalytic transfer dehydrogenation reactions analyzed by gas chromatography: A 4-mL vial was charged with (^{tBu4}PCP)Ir$H_{2/4}$, the appropriate olefin (1-hexene or *tert*-butyl ethylene), mestitylene (10 μL, 72 mM), NaO^{t}Bu (if appropriate), and 1.0 mL of the alkane. The mixture was shaken until all solids dissolved. Ten aliquots of this stock solution (0.10 mL each) were syringed into glass tubes (5 mm x 140 mm) that had been flame-dried prior to being brought into the glovebox. Vacuum adapters were fitted onto the tubes, and the assemblies were removed from the glovebox. The tubes were then frozen in liquid nitrogen, the headspace was evacuated, and the tubes were flame-sealed to give a headspace:liquid ratio of approximately 1:1. The tubes were immersed into a temperature-calibrated oil bath at the specified temperature. The tubes were then removed at the stated time intervals and cooled with liquid nitrogen. The seal of each tube was carefully broken and capped with a 5 mm septum. Each sample was allowed to return to room temperature and analyzed by GC.

Catalytic transfer dehydrogenation reactions analyzed by NMR: A 4-mL vial was charged with (^{tBu4}PCP)Ir$H_{2/4}$, the appropriate olefin (1-hexene or *tert*-butyl ethylene), NaO^{t}Bu (if appropriate), 350 μL of the alkane, and a capillary of trimethylphosphine in toluene-d_8 (^{31}P NMR reference and for locking the NMR). The mixture was shaken until all solids dissolved. The tubes were heated in a temperature-calibrated oil bath, and analyzed by NMR as described above.

Isomerization of 1-hexene by NaO^{t}Bu without any iridium species: A 4-mL vial was charged with 1-hexene (38 μL, 300 mM), NaO^{t}Bu (9.8 mg, 100 mM), and 1.0 mL of *n*-octane and the reaction mixture was shaken until all solids dissolved. The solution was divided into tubes, sealed, heated, and analyzed by GC in the same manner as described for transfer dehydrogenation catalytic reactions above.

6.10 References

(1) Flores, J. *Unpublished work.*

(2) Renkema, K. B.; Kissin, Y. V.; Goldman, A. S. *J. Am. Chem. Soc.* **2003**, *125*, 7770.

(3) Gupta, M.; Hagen, C.; Flesher, R. J.; Kaska, W. C.; Jensen, C. M. *Chem. Commun.* **1996**, 2083.

(4) Krogh-Jespersen, K.; Czerw, M.; Summa, N.; Renkema, K. B.; Achord, P. D.; Goldman, A. S. *J. Am. Chem. Soc.* **2002**, *124*, 11404.

(5) Pahls, D. R.; Allen, K. E.; Goldberg, K. I.; Cundari, T. R. *Organometallics* **2014**, *33*, 6413.

(6) Allen, K. E.; Heinekey, D. M.; Goldman, A. S.; Goldberg, K. I. *Organometallics* **2013**, *32*, 1579.

(7) Biswas, S. *Doctoral Thesis, Rutgers, The State University of New Jersey* **2010**.

(8) Schriesheim, A.; Hofmann, J. E.; Rowe, C. A. *J. Am. Chem. Soc.* **1961**, *83*, 3731.

(9) Schriesheim, A.; Rowe, C. A. *J. Am. Chem. Soc.* **1962**, *84*, 3160.

(10) Schriesheim, A.; Muller, R. J.; Rowe, C. A. *J. Am. Chem. Soc.* **1962**, *84*, 3164.

Chapter 7

Synthetic progress towards (PONSi)Ir and (PONC)Ir complexes

Abstract

A new type of pincer iridium complex was designed which retained the overall binding mode of existing catalysts (two dative bonds and one covelant bond), but which rearranged the locations of the bond types (the two dative bonds are now *cis* to one another instead of being *trans* to each other). Experimentally, three synthetic targets were selected: (^{tBu2}PONC)Ir, (^{tBu2}PNSi^{iPr2})Ir, and (^{tBu2}PONSi^{iPr2})Ir. Although the construction of the ^{tBu2}PNSi^{iPr2} and ^{tBu2}PONSi^{iPr2} ligands was not completed, the ^{tBu2}PONC ligand was successfully synthesized. Metalation of the ^{tBu2}PONC ligand gave the (^{tBu2}PONC)Ir hydrido-chloride complex, which was then converted to the (^{tBu2}PONC)Ir(ethylene)$_x$ species.

7.1 Introduction

Although many pincer complexes have been synthesized in the hope of creating better dehydrogenation catalysts, (Figure 7.1) most have fallen into a common motif. Namely, an iridium atom which is ligated by a phosphorous atom, an sp^2 carbon, and another phosphorous atom. In essence, a P-C(sp^2)-P framework. (Figure 7.2) This is unsurprising given that the first pincer complex for dehydrogenation, (^{tBu4}PCP)Ir, also followed this motif. Since then, however, the

framework has been retained while modifying other parts of the ligand. (Section 1.3) For example, the *para* position has been functionalized, giving new catalysts such as (MeO-^{tBu4}PCP)Ir,[1] and the linkages between the phosphorous atoms and the aryl rings have been changed into oxygen atoms, giving the (PCOP)Ir and (POCOP)Ir catalysts.[2,3]

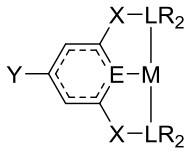

M = Ir, Rh, Ru
L = P, N, carbene
R = ^{t}Bu, ^{i}Pr, Ad, CF_3, Me
X = CH_2, O, S
E = C(sp^2), C(sp^3), Si, O, amine, amido
Y = H, OMe, NMe_2, CO_2Me, Me

Figure 7.1 Scope of pincer complexes for dehydrogenation (Section 1.3 for full description and all references)

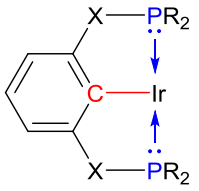

P-C(sp^2)-P ligand
on iridium

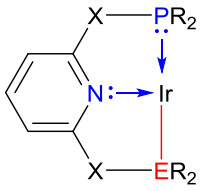

P-N-E ligand
on iridium
where E = C, Si

Figure 7.2 Comparison of how P-C(sp^2)-P and P-N-E ligands bind to a metal center

However, on an electronic level the transformations proceeding at the iridium center are only *directly* influenced by the atoms directly bonded to the iridium. Hence, only mild to moderate changes in the behavior of the catalyst can be achieved by modifying the "secondary groups" which are connected to the "primary" phosphorous and sp^2 carbon attachment points. Therefore, modifying the bonding motif of the pincer ligand might allow for it to become a better dehydrogenation catalyst, or it might create a pincer complex which can catalyze new types of reactions. However, changing the bonding motif by too large of an amount might not allow for successful metalation and reactions.

Hence, this Chapter describes efforts to synthesize (PNC)Ir and (PNSi)Ir complexes which aim to impart novel electronic properties to the iridium center while simultaneously being stable like the traditional P-C(sp^2)-P framework.

In part, the stability of these pincer iridium complexes is determined by the combination of dative bonds and covelant bonds between the ligand and the iridium center. In traditional P-C(sp^2)-P complexes, each phosphorous atom makes a dative bond with the iridium by donating two electrons, yielding a total of two dative bonds. (Figure 7.2) Likewise, the phosphorous and nitrogen atoms of the (PNC)Ir and (PNSi)Ir complexes also make a total of two dative bonds with the iridium center. Next, the Ir-C bond in the traditional P-C(sp^2)-P complexes gives a total of one covelant bond between the ligand and iridium, whereas one Ir-C or Ir-Si fulfills the requirement for one covelant bond in the (PNC)Ir and (PNSi)Ir complexes. Hence, the two new ligand types would have two dative bonds and one covelant one in the same way that traditional P-C(sp^2)-P complexes also do.

Next, switching from P-C(sp^2)-P to (PNC)Ir and (PNSi)Ir complexes involves changing the *locations* of the dative/covelant bonds, which would undoubtedly impart novel electronic properties to these new complexes. As described in Chapter 3, the regioselectivity of pincer iridium catalysts was determined by the electronics of the central Ir-C bond. In addition, Chapter 4 detailed how catalytic activity is *also* highly dependent on the electronics of the central Ir-C covelant bond. Hence, significant differences in reactivity would be expected when the central attachment point of the ligand was changed from a *covelant* Ir-C bond with P-C(sp^2)-P ligands to a *dative* Ir-N bond with PNC and PNSi ligands.

In addition, the presence of a *covelant* Ir-C or Ir-Si bond on the side attachment point of the ligand would likely also impart novel reactivity to (PNSi)Ir and (PNC)Ir complexes. In

traditional P-C(sp^2)-P ligands the two phosphorous atoms are generally considered to be inert towards the substrates interacting with the iridium center. Hence, P-C(sp^2)-P ligands are considered to be "innocent." However, an Ir-C or Ir-Si bond might participate in reactions with the substrate, making the PNC and PNSi ligands "non-innocent."

In particular, a variety of nonclassical interactions have been observed between the metal center and C-H (termed *agostic* interactions) and Si-H bonds.[4,5] For example, classical chemistry would predict that metalation of the pincer ligand PhP{(*o*-$C_6H_4CH_2$)$SiMe_2H$}f_2 onto ruthenium would cause oxidative addition of the Si-H bond. (Scheme 7.1) However, a nonclassical interaction between the Si-H bond and the ruthenium was observed instead.[6]

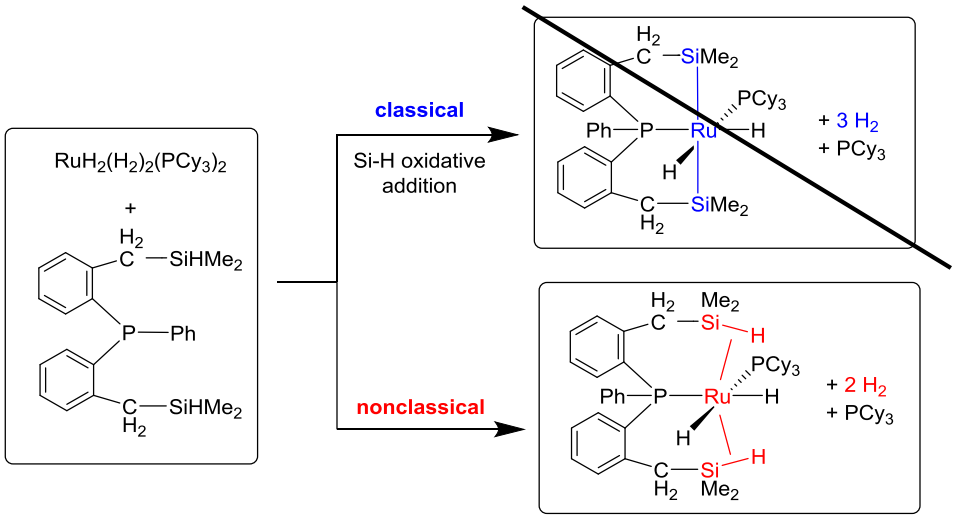

Scheme 7.1 Example of nonclassical Si-H interaction with a metal center

Although the specifics of *metalation* with the PNSi ligand onto iridium are not important, these nonclassical interactions may assist with *catalytic dehydrogenation* by becoming involved during the C-H activation or β-H elimination transition states. Similarly, the presence of a C-Ir bond in the same position may impart novel reactivity to (PNC)Ir complexes. Hypothetically, the (PNC)Ir(H)(R) complex obtained after C-H activation might undergo C(ligand)-H reductive

elimination, opening two coordination sites and allowing for more facile β-H elimination with the R group still attached to the iridium.

Thus, work towards the design and synthesis of (PNSi)Ir and (PNC)Ir complexes was begun. As will be described in the following sections, synthetic work focused on the construction of two PNSi and one PONC ligands, along with their metalation onto iridium. (Figure 7.3)

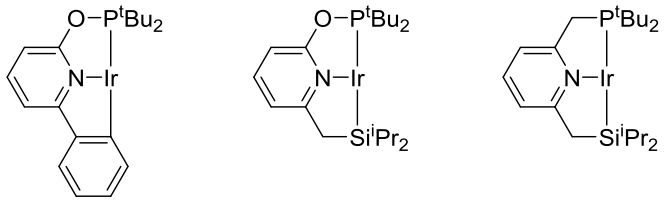

(^{tBu2}PONC)Ir (^{tBu2}PONSi^{iPr2})Ir (^{tBu2}PNSi^{iPr2})Ir

Figure 7.3 Targets for synthesis of (P-N-E)Ir complexes where E = C or Si

7.2 Attempted synthesis of PNSi and PONSi ligands

The first experiments during this project aimed to synthesize the ^{tBu2}PNSi^{iPr} ligand. Michael Haibach, another graduate student in Professor Goldman's lab, performed the first experiment. He found that the "PN precursor" could be obtained by treating 2,6-lutidene with *n*-butyl lithium and then di-*tert*-butylphosphine. However, attempts to convert the PN precursor into the complete ^{tBu2}PNSi^{iPr} ligand proved unsuccessful. (Scheme 7.2) Treating the compound with *n*-butyl lithium and chloro(diisopropyl)silane gave a mixture of products with a ^{31}P NMR shifts of δ = 34.4, 34.8, and 35.4 ppm and a very complex ^{1}H NMR spectrum. Due to the presence of the phosphine group, the compound would decompose in air, and therefore could not be purified by column chromatography.

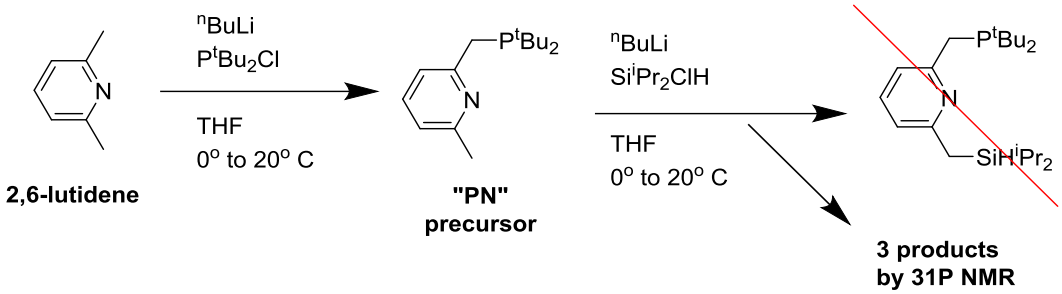

Scheme 7.2 Attempted synthesis of PNSi ligand

Hypothetically, the side products observed in the previous reaction happened due to an unselective deprotonation by the *n*-butyl lithium. In particular, the Ar-CH_2-P^tBu_2 protons could have similar kinetic/thermodynamic acidity to those of the Ar-CH_3 group, which was the desired site for deprotonation. Therefore, a molecule which lacked protons at the Ar-X-P^tBu_2 location might force deprotonation to occur at the desired Ar-CH_3 site, yielding the desired product.

Hence, the ^{tBu2}PONSi^{iPr2} ligand, with an oxygen linker between the phosphine group and the aryl ring, was selected as the new synthetic target. The starting material, 2-hydroxy-6-methylpyridine, exists as a tautomer of two forms. The first synthetic attempt at obtaining the PON precursor employed sodium hydride as the Brønsted base and di-*tert*-butylphosphine. (Scheme 7.3) Upon working-up the reaction, however, no pentane-soluble product was obtained. In addition, no signals in the ^{31}P NMR were obtained by scanning a slurry of the solid residue from the reaction and benzene-d_6. Therefore, it appeared that the reaction had failed and the compound had decomposed.

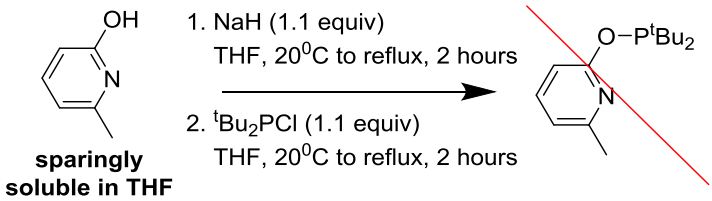

Scheme 7.3 Attempted synthesis of PON precursor using sodium hydride

In order to avoid the apparent decomposition, the phosphination reaction was repeated with different conditions. Without adding a Brønsted base, the pyridine-derivative and phosphine were combined in a flask and refluxed for 6 days. (Scheme 7.4) Then, triethylamine was added and the solution stirred for 2 hours in order to deprotonate the compound which had presumably formed. Taking an NMR of the resulting compounds showed two products at ^{31}P NMR δ = 63.7 and 95.2 ppm. Notably, a nearly identical compound without the methyl group had been reported to have a ^{31}P NMR shift of 153.3 ppm.[7] In addition, the POCOP ligands and pincer iridium complexes also always showed ^{31}P NMR shifts near 150 ppm.[2] Therefore, neither of the two compounds obtained through this reaction appeared to contain the P-O bond which would be present in the desired compound.

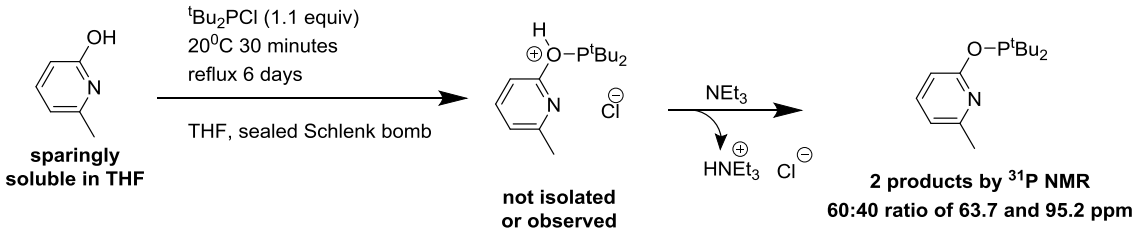

Scheme 7.4 Attempted synthesis of PON precursor using triethylamine

Therefore, due to these synthetic difficulties, attempts at synthesizing the PNSi and PONSi ligands were discontinued.

7.3 Synthesis of (^{tBu2}PONC)Ir hydrido-chloride complex

Due to difficulties with constructing the PNSi and PONSi ligands, attempts at synthesizing the ^{tBu2}PONC ligand were begun. (Scheme 7.5) Based upon the synthesis of a related compound,[8] the pyridone starting material was mixed with triethylamine, tetramethylethylenediamine

(TMEDA), and bistertbutylphosphine in THF. After workup the desired product was obtained in 95% and 35% yield.

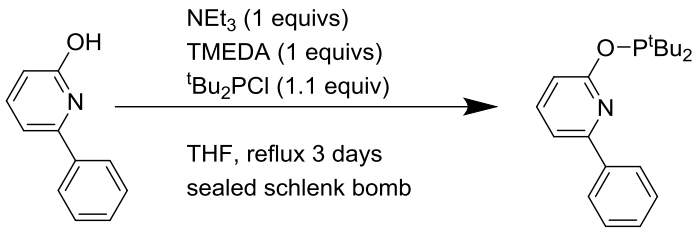

Scheme 7.5 Synthesis of ^{tBu2}PONC ligand

Unfortunately, metalation of the ligand to form the corresponding hydrido-chloride complex encountered more obstacles. (Scheme 7.6) (Table 7.1)

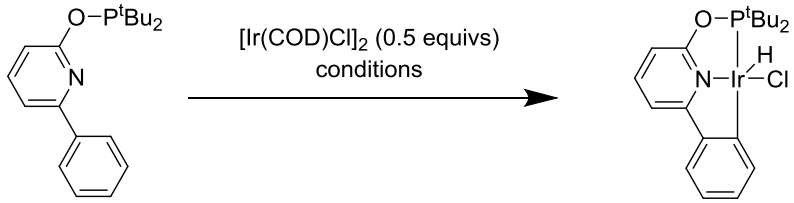

Scheme 7.6 Generalized scheme for synthesizing the (^{tBu2}PONC)Ir(H)(Cl) complex

Metalation attempt	Conditions	Result
First	1) Toluene, argon, 60 °C 2) NaO^{t}Bu, ethylene	Multiple products
Second	1) Toluene, hydrogen atmosphere	Decomposition
Third	1) Toluene, argon, reflux 2 days 2) H_2	Multiple products
Fourth	1) Pyridine, 60 °C 2 days	Major product with small impurities

Table 7.1 Conditions for synthesizing (^{tBu2}PONC)Ir(H)(Cl) complex

During the first attempt, the iridium and then ligand were added to an aliquot of toluene. Approximately 5 seconds after adding the ligand the solution changed from orangeish-red to orangish-yellow, presumably indicating metalation. NMR analysis after 10 minutes shows four products. Upon heating at 60 °C, the integrations and identities of the species continued to change. Eventually, the reaction mixture stabilizes, showing 6 peaks in the ^{31}P NMR. Adding NaO^tBu and ethylene caused decomposition.

Thus, the first attempt showed that metalation happens instantaneously, and multiple products are possible, most likely due to the lack of steric crowding on the Ir-C side.

During the second attempt the ligand and iridium mixture was placed under an atmosphere of hydrogen 15 minutes after mixing. Unexpectedly, black solids precipitated and the solution became colorless within 30 minutes. Presumably, the reactive PONC ligand caused the iridium species to be reduced by hydrogen.

In the third attempt, the ligand and iridium were refluxed in toluene for 2 days under argon, yielding 7 products by ^{31}P NMR (with 2 hydrides). Next, the solution was placed under H_2, causing the ^{31}P NMR spectrum to change to only 4 peaks and two hydrides. Thus, no pure product was obtained.

Finally, in the fourth attempt the ligand and iridium were dissolved in pyridine and heated at 60 °C for 2 days under argon. By NMR there was one major product (140.2 ppm in ^{31}P NMR and -21.5 ppm in ^{1}H NMR) with small impurities. Although the NMR spectra contained too many extraneous peaks for definitive identification, it is hypothesized the product is the 6-coordinate pyridine adduct.

7.4 Purification and reactivity of (^{tBu2}PONC)Ir hydrido-chloride complex

Historically, pincer iridium hydrido-chloride complexes have been purified by recrystalization from hot *n*-hexane. However, attempting to dissolve the crude (^{tBu2}PONC)Ir hydrido-chloride product in *n*-hexane demonstrated that it had much lower solubility (<5 mg per 100 mL) than previous pincer iridium complexes, presumably due to its greater polarity. In contrast, about 1 mL of pyridine will fully dissolve 40 mg of the crude product. Also, 2 mL of toluene will dissolve half of 40 mg of crude product (the other half would not dissolve, even upon additional toluene).

Thus, the crude product was purified by antisolvent crystallization using pyridine and *n*-hexane. First, the reaction mixture (in pyridine) should only be evaporated to a thick gel, and not a dry solid. Redissolving the crude product in pyridine was extremely slow with a dry solid, but was instantaneous with a thick gel. After dissolving approximately 100 mg of crude product in 1 mL of pyridine, 8 mL of *n*-hexane was added in 1 mL aliquots at a rate of 1 aliquot every 5 minutes. The mixture was also shaken periodically. After about 5 mL of *n*-hexane, yellow/brown solids began precipiating on the walls of the vial. The mixture was decanted, and more *n*-hexane was added, multiple times in order to obtain several crops of >95% pure (^{31}P NMR) product.

With pure hydrido-chloride complex obtained, the ability to form (^{tBu2}PONC)IrH_x and (^{tBu2}PONC)Ir(ethylene) complexes was examined. (Scheme 7.7) Upon addition of NaO^{t}Bu and ethylene to the hydrido-chloride complex in an air-free NMR tube, color change from brown to yellow was observed after 30 minutes. NMR analysis showed the disappearance of all hydrides and a single, sharp peak at 142.4 ppm in the ^{31}P NMR spectra, presumably of the (^{tBu2}PONC)Ir(ethylene)$_x$ compound. However, evaporating solvent appeared to cause decomposition.

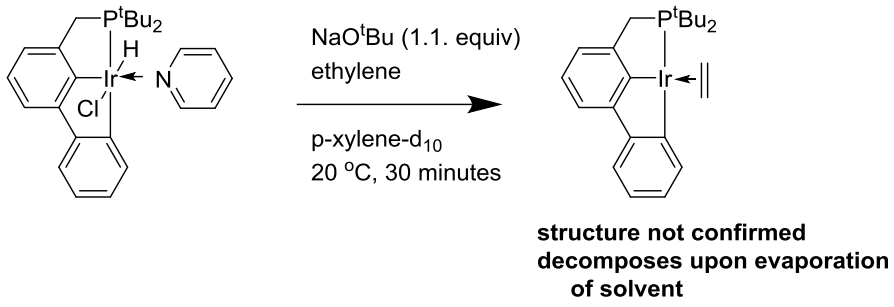

Scheme 7.7 Synthesis of (^{tBu2}PONC)Ir(ethylene)$_x$ complex

Finally, the synthesis of the hydride complex was attempted by adding NaO^{t}Bu and hydrogen gas to a solution containing the hydrido-chloride complex. (Scheme 7.8) However, precipitation of yellow solids, which were also insoluble in more polar solvents such as pyridine, suggested decomposition.

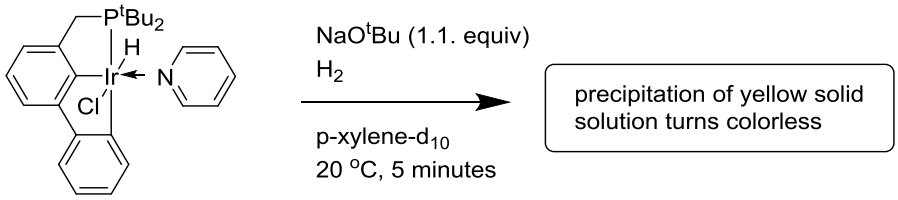

Scheme 7.8 Attempted synthesis of (^{tBu2}PONC)IrH$_x$ complex

7.5 Summary

Synthetic progress was made towards (PONC)Ir and (PONSi)Ir complexes. In particular, the (^{tBu2}PONC)Ir hydrido-chloride complex was synthesized, and its reactivity studied. Although synthesis of the (^{tBu2}PONC)IrH$_x$ complex with H_2 failed due to decomposition, the (^{tBu2}PONC)Ir(ethylene)$_x$ species was successfully observed, although it could not be isolated due to decomposition upon removal of solvent. Lastly, synthetic attempts towards construction of

the PNSi and PONSi ligands were attempted, although attachment of the silane moiety was unsuccessful.

7.6 Experimental

All manipulations were performed either in a glovebox or on a Schlenk line under an inert atmosphere of dry argon. 2-Hydroxy-6-methyl pyridine was obatined from AK Scientific, while 2(1*H*)-pyridinone, 6-phenyl (also known as 2-hydroxy-6-phenyl pyridine) was purchased from Combi-Blocks. All reagents and solvents were obtained from Aldrich. All solvents and liquid reagents were degassed by bubbling argon through the liquid for 20 min. NMR spectra were recorded on either a Bruker DRX-400, Bruker Avance-400, or Bruker DRX-500 spectrometer at 298 K.

7.7 References

(1) Huang, Z.; Brookhart, M.; Goldman, A. S.; Kundu, S.; Ray, A.; Scott, S. L.; Vicente, B. C. *Adv. Synth. Catal.* **2009**, *351*, 188.

(2) Göttker-Schnetmann, I.; White, P.; Brookhart, M. *J. Am. Chem. Soc.* **2004**, *126*, 1804

(3) Nawara-Hultzsch, A. J.; Hackenberg, J. D.; Punji, B.; Supplee, C.; Emge, T. J.; Bailey, B. C.; Schrock, R. R.; Brookhart, M.; Goldman, A. S. *ACS Catalysis* **2013**, *3*, 2505.

(4) Housecraft, C. E.; Sharpe, A. G. *Inorganic Chemistry*; Pearson Education Limited: Essex, England, 2005.

(5) Corey, J. Y. *Chem. Rev.* **2011**, *111*, 863.

(6) Montiel-Palma, V.; Munoz-Hernandez, M. A.; Cuevas-Chavez, C. A.; Vendier, L.; Grellier, M.; Sabo-Etienne, S. *Inorg Chem* **2013**, *52*, 9798.

(7) Scheuermann, M. L.; Grice, K. A.; Ruppel, M. J.; Rosello-Merino, M.; Kaminsky, W.; Goldberg, K. I. *Dalton Trans.* **2014**, *43*, 12018.

(8) Depue, R. T.; Collum, D. B.; Ziller, J. W.; Churchill, M. R. *J Am Chem Soc* **1985**, *107*, 2131.